



Strål  
säkerhets  
myndigheten

Swedish Radiation Safety Authority

Technical Note

**2019:22**

SSM's external experts' reviews of SKB's report on supplementary information on canister integrity issues



## **SSM:s perspektiv**

### **Bakgrund**

Strålsäkerhetsmyndigheten (SSM) granskar Svensk Kärnbränslehantering AB:s (SKB) ansökningar enligt lagen (1984:3) om kärnteknisk verksamhet om uppförande, innehav och drift av ett slutförvar för använt kärnbränsle och av en inkapslingsanläggning. Som en del i granskningen ger SSM konsulter uppdrag för att inhämta information i avgränsade frågor. I SSM:s Technical note-serie rapporteras resultaten från dessa konsultuppdrag.

### **Projektets syfte**

Projektets syfte är att ta fram underlag för SSM:s egen granskning av korrosionsfrågor, korrosionsfrågornas betydelse för kapselns integritet i slutförvarsmiljön, samt konsekvensberäkningar kopplade till dessa frågeställningar.

### **Innehållsförteckning**

1. Review Assignment for the Swedish Radiation Safety Authority: Corrosion of Copper Canister, John R. Scully, Timothy W. Hicks.
2. Review Assignment for the Swedish Radiation Safety Authority: Corrosion of Copper Canister, Peter Szakálos, Christofer Leygraf.
3. Review of Assignment for the Swedish Radiation Safety Authority: Independent Canister Integrity Modelling and Dose Assessment, Osvaldo Pensado, Stuart Stothoff.
4. Review of Assignment for the Swedish Radiation Safety Authority: Biosphere review and independent dose assessment of complementary information relating to spent nuclear fuel canister integrity, Russell Walke, Rebecca Newson.

## **SSM perspective**

### **Background**

The Swedish Radiation Safety Authority (SSM) reviews the Swedish Nuclear Fuel Company's (SKB) applications under the Act on Nuclear Activities (SFS 1984:3) for the construction and operation of a repository for spent nuclear fuel and for an encapsulation facility. As part of the review, SSM commissions consultants to carry out work in order to obtain information on specific issues. The results from the consultants' tasks are reported in SSM's Technical Note series.

### **Objective**

The objectives of the project is to develop a basis for SSM's own review of canister corrosion issues, the significance of corrosion issues in the context of canister integrity in the repository environment, as well as consequence analysis related to those issues.

### **content**

1. Review Assignment for the Swedish Radiation Safety Authority: Corrosion of Copper Canister, John R. Scully, Timothy W. Hicks.
2. Review Assignment for the Swedish Radiation Safety Authority: Corrosion of Copper Canister, Peter Szakálos, Christofer Leygraf.
3. Review of Assignment for the Swedish Radiation Safety Authority: Independent Canister Integrity Modelling and Dose Assessment, Osvaldo Pensado, Stuart Stothoff.
4. Review of Assignment for the Swedish Radiation Safety Authority: Biosphere review and independent dose assessment of complementary information relating to spent nuclear fuel canister integrity, Russell Walke, Rebecca Newson.

### **Project information**

Contact person at SSM: Bo Strömberg



Strål  
säkerhets  
myndigheten

Swedish Radiation Safety Authority

Technical Note

2019:22

SSM's external experts' reviews of SKB's report on supplementary information on canister integrity issues

Date: November 2019

Report number: 2019:22 ISSN: 2000-0456

Available at [www.stralsakerhetsmyndigheten.se](http://www.stralsakerhetsmyndigheten.se)

This report was commissioned by the Swedish Radiation Safety Authority (SSM). The conclusions and viewpoints presented in the report are those of the author(s) and do not necessarily coincide with those of SSM.



Strål  
säkerhets  
myndigheten

Swedish Radiation Safety Authority



**Authors**

John R. Scully<sup>1</sup>  
Timothy W. Hicks<sup>2</sup>

<sup>1</sup>University of Virginia, Charlottesville VA, US

<sup>2</sup>Galson Sciences Ltd, Oakham, UK

# Review Assignment for the Swedish Radiation Safety Authority: Corrosion of Copper Canister

Activity number: 3030016-02

Registration Number: SSM2019-2486

Contact person at SSM: Bo Strömberg



# Summary

SKB's licence application in 2011 to construct a repository for the disposal of spent nuclear fuel in Sweden has been examined by a Swedish Land and Environmental Court. The Court has sought further information on five issues relating to the long-term behaviour of the copper canisters that SKB plans to use for disposal of the spent fuel. On behalf of SSM, this report provides a review of SKB's progress towards resolution of these issues.

The five issues of concern relate to potential copper corrosion mechanisms that may affect the long-term behaviour of the canisters in a repository at Forsmark in Sweden, and thereby the post-closure safety of the repository. The issues are as follows:

- a) Corrosion due to reaction in oxygen-free water.
- b) Pitting due to reaction with sulphide, including the influence of the sauna effect on pitting.
- c) Stress corrosion cracking due to reaction with sulphide, including the influence of the sauna effect on stress corrosion cracking.
- d) Hydrogen embrittlement.
- e) The effect of radioactive radiation on pitting, stress corrosion cracking and hydrogen embrittlement.

SKB's work on these issues has long been in progress, but SKB has intensified its work in these areas through additional theoretical analysis, testing and evaluation. Findings are summarised in SKB's report of supplementary information on canister integrity issues and their importance to repository post-closure safety (SKB Report TR-19-15). SKB's assessment of each issue has been examined in this review with the objective of identifying any unresolved issues or gaps. The review has focused on the supplementary information report, but key supporting documents and the broader literature have been considered in specific instances. This summary highlights the main review findings.

## **Corrosion due to reaction in oxygen-free water**

Copper corrosion due to reaction in oxygen-free water raises a concern over the possibility of a thermodynamically viable and possibly overlooked corrosion process leading to a Cu-O-OH complex, with a finite driving force producing a depth of attack. Recent experiments have considered such anoxic corrosion of copper facilitated by water reduction. Copper corrosion cells coupled to hydrogen permeation membranes and vacuum systems with detectors that sense hydrogen gas could not detect hydrogen above background levels. Flaws in some tests (access to the atmosphere and O<sub>2</sub> leakage into anoxic test cells) corrupted some experiments. However, experimentally obtained pressures above background that were reported in experiments that raised the concern about copper corrosion in oxygen-free water have never been duplicated. Also, theoretical calculations do not support the formation of the CuOH species necessary to obtain high equilibrium H<sub>2</sub> pressures. Existing thermodynamic theory and alternative expected compounds arrived at low H<sub>2</sub> pressures. Although a thorough analysis of hydrogen at all stages was not obtained in the works discussed, the body of experiments does not provide evidence for spontaneous copper corrosion in oxygen-free water that is supported by corroborating diagnostics, nor consensus from multiple investigators. Statistical variations and measurements often are at, or near to, detection limits and this plagues inquiries.

The corrosion depth estimated from copper corrosion in oxygen-free water is 1 mm in  $10^6$  years. While the authors of this review report could recommend alterations and additions or improvements to the methods used, the experiments conducted do serve to provide an upper pessimistic bound for the possible effects of corrosion by this pathway. Consequently, container corrosion will most likely be rate limited by sulphide mass transport to the container, which is a much more viable pathway for copper corrosion than corrosion in oxygen-free water from both thermodynamic driving force and kinetic perspectives. Any copper corrosion by sulphide attack would far exceed the corrosion depths of penetration that have been estimated could occur by anoxic corrosion in pure water in saturated bentonite backfill. Thus, corrosion by sulphide attack is of greater concern in safety assessments than any postulated corrosion in oxygen-free water. In summary, it is the opinion of these reviewers that consideration of corrosion in oxygen-free water by plausible scenarios has been exhausted and is superseded by a more relevant potential mechanism of copper attack.

### **The sauna effect**

Sulphide-induced localised corrosion of copper (pitting and stress corrosion cracking) exacerbated by a 'sauna effect' that is speculated to increase the salt concentration in the vicinity of the canister raises a concern over possible overlooked forms of corrosion attack. In the context of the KBS-3 repository, the sauna effect is the evaporation of water in a deposition hole, where the temperature is high because of the heat from the disposal canister, resulting in the concentration of salt in the remaining water. If groundwater continues to enter the deposition hole and leave as vapour, then salt will accumulate. In aggressive atmospheric corrosion conditions brought about by concentration of species such as sulphides or  $\text{Cl}^-$ , the rate of corrosion attack can increase where there is wetting and drying with water vapourisation to enable salt concentration.

SKB argues that condensation of the vapour largely would occur in the bentonite buffer in the deposition hole as the vapour moves away from the canister, with little water leaving the deposition hole as vapour. On this basis, the amount of groundwater that can enter the deposition hole, and therefore the amount of salt that can be concentrated or precipitated in the deposition hole, is limited by the amount of water that is needed to fully saturate the bentonite in the deposition hole. The diffusivity of water vapour in bentonite decreases as the saturation of the bentonite increases and is zero at full saturation so that vapour transport cannot occur. The argument that vapour condensation will occur close to the canister, thereby limiting the amount of salt that can accumulate while the bentonite saturates, is key to the claim that the sauna effect will have an insignificant impact on the rate of copper corrosion by pitting and stress corrosion cracking.

SKB's arguments are supported by evidence from a number of laboratory experiments and field tests and from modelling analysis, which show that:

- Limited evaporation and concentration of chloride could occur near a canister.
- The evaporation process would be limited by the short transport distance of the water vapour before it condenses in the cooler bentonite, with the process ending when the bentonite becomes fully saturated. There is no viable mechanism for wetting and drying with vapour escape as might occur in an open system.

- The concentration of chloride near the canister would decrease as a result of diffusion (preceding by dissolution of any precipitates) in the saturated bentonite.
- Insufficient chloride could accumulate for supersaturated solutions to develop in the deposition hole bentonite in the 1,000-year thermal period.
- The concentration of chloride is unlikely to increase to as much as one mol/l, which is the minimum chloride concentration that SKB reports would be needed to effect corrosion processes.

These reviewers consider that it is reasonable for SKB to conclude that the sauna effect will be insignificant in the KBS-3 repository, although a clearer explanation of the observations from the FEBEX experiment at Grimsel in Switzerland, where increased chloride concentrations were observed near the surface of a heater in bentonite, would build further confidence in this conclusion.

The arguments above pertain to the behaviour of chloride but the impacts on sulphides should also be considered. When the bentonite is saturated, sulphide arrival at the canister surface cannot exceed the mass transport limited rate. In the unsaturated state, the groundwater is vaporised in the bentonite near the disposal canister as discussed above, with the potential for sulphide concentration in the remaining water. Based on consideration of the arguments relating to chloride behaviour, it is anticipated that no significant sulphide concentrations would occur as a result of the sauna effect, but confirmatory arguments are required to support this expectation.

### **Pitting corrosion**

SKB's recent investigations on pitting corrosion have focused on searching for environmental conditions (i.e., Cl<sup>-</sup> and sulphide combinations in bulk solution combined with applied sulphide fluxes) that produce a physically observed compact corrosion product layer instead of a porous one. A compact layer was assumed to be able to function as a passive film, unlike a porous layer. This assumption was based on the premise that a compact layer would limit dissolution by field driven ionic transport of copper cations, while a porous film would limit dissolution only by sulphide transport in pores. A porous film is subject to limited means to regulate the corrosion rate or produce non-uniform attack, such as could occur at breaks in passive layers. The formation of a compact film (i.e., a passive film) was found to require a high sulphide concentration and a high sulphide flux. The presence of Cl<sup>-</sup> plays several roles which are not really well understood, other than possible competitive adsorption with sulphide.

The reviewers accept SKB's finding that there is a lack of evidence for compact films under disposal conditions that would justify passivity. However, a variety of electrochemical analysis options could have been employed to investigate the most compact and least compact films, providing a number of additional 'easy to obtain' diagnostics. The limitation of copper corrosion by a passive film is just one of many necessary, but not sufficient, conditions required for pitting. That is, pitting of a passive metal requires other conditions such as a specific pit site with a triggering oxide defect that specifically enables breakdown and a theory for formation of a non-protective salt film, harsh chemical conditions and possibly a bare metal surface at the pit site that persists at this anode whilst there is a protective layer that prevails on the rest of the metal surface.

There was an original proposition and a counter view in favour of pitting and Cu<sub>2</sub>S passivity expressed by Macdonald and co-workers. The latter was in response to a discussion article voicing a counter opinion by the Shoemith group. Evidence of

shallow pitting with a low pitting factor was presented in papers by Macdonald. Factors causing pitting, even if shallow, or whether localised attack is alternatively attributed to micro-galvanic corrosion, have not been resolved.

Despite much evidence against pitting, the SKB work overlooks the fact that pitting is sometimes seen in oil and gas applications where FeS films are formed, while under other high H<sub>2</sub>S conditions, more uniform attack occurs. There is the opportunity to learn from this FeS observation and to understand the conditions for localised corrosion. The literature regarding this issue was not explored in the present set of studies.

In summary, it is agreed that there is limited evidence to suggest that a compact film could occur on a copper canister under disposal conditions and act as a passive layer, implying that pitting will not occur. However, there remain unresolved issues regarding the possible occurrence of shallow pitting, which currently is not well explained.

### **Stress corrosion cracking**

SKB's supplementary information report has concluded that anodic dissolution-based Stress Corrosion Cracking (SCC) would be unlikely, and the sauna effect would have little impact on such SCC. A key question is whether various levels of Cl<sup>-</sup> and sulphide can produce cracking with or without a passive film. Many of the arguments against a local SCC site for attack, even at grain boundaries, are the same as those expressed above in the case of pitting. Nevertheless, several SCC studies were reviewed by SKB that mostly utilised the Slow Strain Rate Testing (SSRT) method (involving application of a slow dynamic strain in a potentially corrosive environment). In these studies, various Cl<sup>-</sup> and sulphide levels, types of commercial and pure copper (and related inherent SCC susceptibility), tensile loads, and strain rates were considered. The sulphide concentrations, strain rates and, in most cases, the tensile stresses applied in SSRT were all conservative (i.e., much worse than would be experienced by a canister during and after deployment). There were two studies that mentioned a pre-cracked specimen or long defect. These papers were not clear regarding the extent of SCC observed, if any.

Only two of five studies reviewed showed indication of SCC (alternatively interpreted as sulphide-induced intergranular corrosion) and these studies often only showed evidence of crack length less than a single copper grain length (i.e., ~50 µm). Some authors claimed a drop in load and decrease in elongation to failure, but there was concurrent general dissolution in these tests, and no serious mechanics analysis accompanies these claims. Many arguments exist against an Anodic Dissolution (AD) based SCC mechanism. Primarily, a mass transport controlled argument is made that the interfacial sulphide concentration drops to zero and, therefore, sulphides cannot accumulate (sulphide accumulation is a pre-requisite for crack growth). Lack of detection of sulphur on copper surfaces has been cited as verification of this line of reasoning. Other lines of reasoning include (a) the lack of passivity required for a slip dissolution mechanism, (b) the lack of a trend towards enhanced susceptibility at anodic potentials typical of AD mechanisms of SCC, (c) the low tensile stresses and lack of dynamic plastic strain once stress relaxation lowers creep rates in deployed canisters, and (d) a lack of fractographic evidence of SCC on primary fracture surfaces compared to ductile overload failures.

Evidence of SCC mainly consisted of secondary cracking on the tensile surface of the tensile bar in SSRT. Furthermore, sulphide transport rates required to develop the presence of sulphides at surfaces and subsequently obtain SCC in SSRT are four

orders of magnitude greater in the tests than actually rationalised to be present near disposal canisters, except under eroded and saturated buffer conditions. Also, transport impedances in the crack limit the transport process into these sites. Moreover, vacancies required by one AD mechanism (i.e., the Aaltonen mechanism) are rationalised to be produced at a rate that would be much lower under repository conditions than laboratory test conditions and they are annihilated quickly anyway when anodic dissolution is turned off or suppressed during testing. In other words, vacancies must be created continually by copper dissolution, otherwise vacancy annihilation and/or consumption at sinks occurs. For these reasons, SKB makes the argument that SCC is unlikely.

Considering this information, the following comments can be made:

- SCC requires a tensile stress, susceptible microstructure and a causative environment. All three of these conditions may exist in a repository.
- Both the reviewers and SKB agree that an extremely slow crack growth rate would likely be present, if any, under repository conditions, especially if limited by sulphide transport.
- The issue of SCC incubation time before any crack propagation has not been clarified; an incubation period is often seen in SCC.

These factors indicate that the SSRT is a poor method to assess copper susceptibility to SCC in this system under these circumstances. This is because the tensile specimen will be plastically strained and achieve ductile overload failure prior to sufficient SCC initiation and growth if occurring when it is slow relative to the time duration of the SSRT test. Thus, it is reasonable to assert that SCC cannot be accessed very well by SSRT if the initiation and propagation phenomenon occur extremely slowly. Even if incubation times associated with initiation are short relative to repository lifetimes the same time periods may be long relative the short duration of SSRT meaning that ductile overload could occur before sufficient time for initiation and its transition to propagation. For these reasons and others, SCC should be examined in a pre-cracked specimen conducted over a long period of time under broader exposure conditions. The dissolution, vacancies and hydrogen pickup at the crack tip are also of importance, as discussed below.

The bottom line is that SKB reports cracking that was only seen under laboratory test conditions where the sulphide flux and dissolution rate was four orders of magnitude greater than would be present in the repository. That is, SCC is dismissed on the basis that a critical flux is needed, which could exist but its occurrence remains unproven in a repository environment. However, SSRT would not be capable of detecting very slow environmental cracking which might be supported by slower sulphide fluxes. Fracture mechanics crack studies involving monitoring of extremely slow crack growth rates would provide more convincing evidence that SCC can be ruled out entirely.

### **Hydrogen embrittlement**

SKB considered Hydrogen Embrittlement (HE) in the context of the implications of hydrogen-enhanced vacancy and void formation as a part of the damage process. SKB considered that the main source of hydrogen was O<sub>2</sub>-free cathodic reduction of water, H<sup>+</sup> or HS<sup>-</sup> during sulphide-induced copper corrosion, and that the low permeation rate and extremely low uptake efficiency associated with this form of hydrogen uptake precludes HE. It was argued that the rate of the Open Circuit Potential (OCP) hydrogen generation from HS<sup>-</sup> was extremely low because it is a coupled cathodic reaction that is restricted by the anodic rate of Cu<sub>2</sub>S formation

during OCP corrosion. Therefore, hydrogen production would be limited by the slow rate of mass transport controlled, sulphide-induced corrosion of copper which limits the anodic reaction.

Nine papers were reviewed that discussed various pertinent research studies in this area. A cornerstone of the SKB argument against HE is that deep hydrogen penetration was not observed in the experiments reviewed, and that voids trapped and essentially sequestered most of the hydrogen in a surface layer without further penetration. SKB also argues that as-received hydrogen levels in the test materials are often almost as large as those seen in testing. The suggestion is that hydrogen uptake over various locations in copper is limited.

SKB relies on an assumption that deep penetration of hydrogen is required in order for there to be a risk of HE, although this is not certain. Hydrogen penetration beyond near surface voids is mainly a concern in non-pre-cracked SSRT tests where a tensile bar is utilised and damage is mainly detected by a change in global mechanical properties. In order for this to be observed in a typical SSRT, HE or SCC must penetrate into the tensile bar over tens or hundreds of micrometres, ideally some substantial fraction of the tensile diameter. This requires relatively fast cracking given the short time frame of the test method. Consequently, SSRT is not a suitable method for assessing HE susceptibility for slow environmental cracking that requires decades or hundreds of years to occur. Alternatively, observation of surface cracking of shallow cracks may be one of the only viable ways to detect SCC or HE susceptibility by this method when the crack growth rate is slow. Consideration of a slowly moving crack tip under conditions where hydrogen uptake is local to the crack tip is warranted. An argument can be made that shallow hydrogen penetration can support slow crack rates in small fracture process zones a short distance ahead of crack surfaces and that this typically is not detected in SSRT tests of less than one hundred hours duration. Moreover, uncertain incubation times further exacerbate the ability of a short-term test to detect HE. This argument is similar to that expressed above in the case of SCC.

If vacancies or clusters of voids form on a copper grain boundary (where diffusion might be faster and hydrogen uptake and trapping might be enhanced), strain localisation could occur and promote hydrogen-assisted cracking between ligaments and voids. The role of Anodic Dissolution (AD) would be to enhance vacancy generation, so enabling HE where the dissolution itself does not account for the crack advance in the case of hydrogen-induced cracking. There is limited concern over vacancy annihilation as long as active dissolution prevails and vacancies are only needed within a small fracture process zone as opposed to an entire tensile bar. Moreover, under these conditions there would be no requirement for a semi-permanent large depth of hydrogen penetration such as the entire plastic zone or entire tensile bar as often assumed. In this case, SKB seems to infer that hydrogen must penetrate deeply and that hydrogen concentrations must develop that are far above the initial as-received concentrations throughout the tensile bar. However, in HE of high-performance materials, it is typically the local hydrogen concentration which matters and this is hard to detect because local probes are required. However, hydrogen trapping makes low global concentrations higher on local sites by an amplification factor. Finally, the premise that face-centred cubic materials are not susceptible to HE contradicts many years of published research on this topic.

There is also a concern that hydrogen pickup over time could be worse than seen in short term tests on copper if the microstructure is damaged and thus hydrogen solubility gradually increases over long repository timescales. It should also be noted that the OCP uptake case is more complex than net cathodic charging where

copper is not dissolved because there can be vacancy formation stimulated by AD. Hence, severe cathodic polarisation would not necessarily be the worst case or give the most severe HE conditions. In this sophisticated scenario, local hydrogen production and uptake as well as AD might create a special condition for local HE attack, such as on grain boundaries containing vacancies and voids. This vacancy injection-hydrogen embrittlement scenario under long term anoxic  $\text{HS}^-$  containing conditions is a remaining concern because sharp cracks must be considered instead of smooth tensile bars in order to properly dismiss this issue. Studies could be undertaken by groups capable of measuring extremely slow crack growth in pre-cracked specimens to examine whether it represents a viable scenario for anoxic SCC with low fluxes of sulphides.

In summary, classical HE involving deep penetration of hydrogen is not considered to be of concern, but the hydrogen-enhanced vacancy injection-embrittlement SCC scenario should be investigated further.

### **The effects of radiation on corrosion**

The effects of radiation can be reassessed in light of these discussions regarding SCC and HE. It has largely been discounted that radiation creates chemical species that trigger new modes of SCC or HE. The incremental additional corrosion from radiation oxidisers contributes a small amount to the uniform corrosion allowance. Radiation is not expected to change the microstructure which could be a factor towards increasing hydrogen solubility or the deformation mode if operative. With that said, the remaining effects of radiation on the SCC and HE processes mentioned above are of interest. The main remaining concern for radiation in the case of pitting, SCC or HE relates to whether the potential is shifted by oxidisers such that the prevailing reactions occur at a higher rate, and SCC or HE by the few remaining mechanisms espoused are somehow enhanced. However, strong potential dependencies are not found (subject to test limitations discussed above). Based on such considerations, it seems that incremental increases in dissolution depth are the only effects. Experiments to date do not suggest strong potential effects. Residual oxidisers marginally change corrosion rates, which marginally would contribute to the vacancy generation issue discussed above. In summary, the dose rate appears to be too low to affect pitting, SCC or HE, nor could it trigger new mechanisms.

# Content

<b>1. Introduction</b> .....	<b>1</b>
1.1. Background .....	1
1.2. Objective and Approach.....	2
1.3. Report Structure.....	2
<b>2. Main Review Findings</b> .....	<b>3</b>
2.1. Corrosion due to Reaction in Oxygen-free Water .....	3
2.2. The Sauna Effect .....	4
2.3. Pitting due to Reaction with Sulphide .....	7
2.4. Stress Corrosion Cracking due to Reaction with Sulphide .....	10
2.4.1. SCC under anoxic conditions with HS <sup>-</sup> .....	11
2.4.2. SCC under anoxic conditions by the vacancy injection - embrittlement mechanism .....	14
2.4.3. SCC under oxidizing conditions created by radiolysis .....	15
2.5. Hydrogen Embrittlement .....	16
2.6. The Effects of Radiation on Corrosion .....	20
<b>3. Conclusions</b> .....	<b>21</b>
<b>4. References</b> .....	<b>24</b>

# 1. Introduction

## 1.1. Background

In March 2011, the Swedish Nuclear Fuel and Waste Management Company, SKB, submitted an application for a licence to construct a repository for the disposal of spent nuclear fuel at Forsmark in Sweden. The safety concept for the repository, known as KBS-3, involves containment of the spent fuel in copper canisters that are surrounded by a clay buffer in deposition holes about 500 m deep in granitic rock. The repository licence application included a post-closure safety assessment that presented arguments and evidence in support of claims about the long-term safety of the repository. The post-closure safety assessment was reviewed by the Swedish Radiation Safety Authority (SSM) and examined by a Swedish Land and Environmental Court.

In 2018, SSM recommended that the Swedish Government approves the licence application, although a number of canister-related issues were identified that require resolution in the next phase of the licensing process. At the same time, the Swedish Land and Environmental Court sought presentation and evaluation of supplementary information on five issues relating to the long-term behaviour of copper canisters:

- a) Corrosion due to reaction in oxygen-free water.
- b) Pitting due to reaction with sulphide, including the influence of the ‘sauna effect’ on pitting.
- c) Stress corrosion cracking due to reaction with sulphide, including the influence of the sauna effect on stress corrosion cracking.
- d) Hydrogen embrittlement.
- e) The effect of radioactive radiation on pitting, stress corrosion cracking and hydrogen embrittlement.

SSM raised issues related primarily to items b), c) and d) where additional information is required for review in the next licensing phase.

In response, SKB has provided supplementary information in report TR-19-15 that summarises work and presents conclusions on the above-mentioned copper canister integrity issues, and discusses their significance to repository post-closure safety (SKB 2019). SSM is undertaking a review of the supplementary information provided by SKB, with the aim of providing a statement to the Government in September 2019.

To support this review process, SSM has requested that external experts who were involved in the review of SKB’s licence application assess how well the new information addresses the concerns raised by the Swedish Land and Environmental Court. SSM previously contracted Prof. John Scully of the University of Virginia, USA, and Dr Tim Hicks of Galson Sciences Ltd (GSL), UK, to provide a review of the treatment of copper corrosion in SKB’s post-closure safety assessment for the licence application (Scully and Hicks 2012). Prof Scully and Dr Hicks have thus been contracted by SSM to review how SKB has addressed the copper canister integrity issues raised by the Swedish Land and Environment Court. This Technical Note documents the results of the review. The review has focused on the main report of supplementary information produced by SKB, but external references and

reports on additional research and analysis undertaken by SKB to support arguments about copper canister integrity after disposal have also been considered. SSM plans to use the review results provided by external experts as a basis for its own review statement to the Swedish Government.

## **1.2. Objective and Approach**

The objective of the review task is to consider whether copper canister corrosion processes and mechanisms that could occur under evolving repository environments have been described properly and accounted for in SKB's analysis of copper canister performance.

The review assignment has focused on SKB's supplementary information report on copper canister integrity issues (SKB 2019) and numerous supporting reports and papers.

## **1.3. Report Structure**

The main review findings are presented in Section 2, which covers the issues relating to the long-term behaviour of copper canisters about which the Swedish Land and Environmental Court requested further information. The issue of corrosion in oxygen-free water is discussed in Section 2.1. A review of SKB's analysis of the potential for occurrence of the sauna effect is provided in Section 2.2, prior to discussion of pitting due to reaction with sulphide in Section 2.3 and stress corrosion cracking due to reaction with sulphide in Section 2.4. Section 2.5 discusses hydrogen embrittlement and Section 2.6 discusses the effects of radiation on copper corrosion. Conclusions arising from the review are presented in Section 3.

## 2. Main Review Findings

### 2.1. Corrosion due to Reaction in Oxygen-free Water

There has been much debate about the claim originally made by Hultquist (1986), and subsequently by others such as Bojinov and Makela (2003), Szakalos *et al.* (2007), Becker and Hermansson (2011) and Macdonald and Samin (2011), that spontaneous corrosion of copper in O<sub>2</sub>-free pure water could occur at a much greater rate than predicted by thermodynamic theory. It has been proposed that corrosion under anoxic conditions in pure waters could occur spontaneously by a Cu(I) compound formation mechanism:



Hedin *et al.* (2018) reviewed the results of recent experiments aimed at investigating this potential corrosion issue further, as summarised in Section 4 of SKB (2019). Hedin *et al.* (2018) noted that the existence of Cu(OH) has been reported (Korzhevyy *et al.* 2012), but it is thermodynamically unstable. Furthermore, established thermodynamic data cannot explain the extent of H<sub>2</sub> generation from copper in oxygen-free water reported by, for example, Szakalos *et al.* (2007). Key experiments considered by Hedin *et al.* (2018) are:

- The Uppsala experiment to reproduce the original two-chamber hydrogen evolution experiment that showed unexpectedly high hydrogen steady-state pressures, which were claimed to derive from copper corrosion by water. The setups were baked at high temperatures to oxidise the surfaces of the stainless steel chambers, reducing their hydrogen content, and copper samples were prepared by polishing, baking and, in some cases, surface scratching. High levels of hydrogen evolution were not detected in the Uppsala experiment. Further experiments were undertaken to examine copper oxidation in a setup in which the hydrogen was allowed to escape, but no CuO<sub>2</sub> was detected (Ottosson *et al.* 2016; Ottosson *et al.* 2017).
- The Micans experiment, in which copper pieces were placed in glass test tubes and immersed in O<sub>2</sub>-free water. Different qualities of copper sample were used and prepared with various combinations of polishing and baking. Samples with scratched surfaces initially generated large amounts of H<sub>2</sub>, and it was argued that this was due to the larger surface area for reactions with water. The H<sub>2</sub> generation ceased soon after the start of the experiments. Cu-OFP (oxygen-free, phosphorus-doped copper) samples did yield significant amounts of hydrogen, but this was not unexpected and was explained reasonably by the out-gassing of hydrogen in the copper metal.

Hedin *et al.* (2018) (and SKB 2019) argued that previously observed high hydrogen evolution rates can be accounted for as deriving from stainless steel in some experiment set-ups and, in others, observations of high corrosion rates can be attributed to in-leakage of air. There is no clear evidence to contradict SKB's explanations of the results of these experiments.

In summary, experiments conducted recently have investigated anoxic corrosion of copper facilitated by water reduction. Copper corrosion cells coupled to hydrogen permeation membranes and vacuum systems with detectors that sense hydrogen gas could not detect hydrogen above background levels. Flaws (access to the atmosphere

and O<sub>2</sub> leakage into anoxic test cells) corrupted some experiments. However, experimentally obtained pressures above background reported by Hultquist (1986) and others have never been duplicated. Also, theoretical calculations do not support the formation of the CuOH species necessary to obtain high equilibrium pressures. Existing thermodynamic theory and alternative expected compounds arrived at low H<sub>2</sub> pressures. Moreover, the copper alloys utilised contained ‘as received’ hydrogen levels of 0.5 ppm from processing that could be removed by outgassing. A thorough analysis of hydrogen at all stages was not obtained in the works discussed. Thus, it is found that the body of experiments does not provide evidence for spontaneous copper corrosion in oxygen-free water that is supported by corroborating diagnostics, nor consensus from multiple investigators. Statistical variations and measurements often are at, or near to, detection limits and this plagues inquiries.

The corrosion depth estimated from copper corrosion in oxygen-free water, if it did occur, is 1 mm in 10<sup>6</sup> years (SKB 2019); the copper container will have a thickness of 5 cm. Alterations and additions or improvements to the experimental methods used could be suggested, but the experiments conducted do serve to provide an upper pessimistic bound for the possible effects of corrosion by this pathway. It means that container corrosion will more likely be rate limited by sulphide mass transport to the container, which is a much more viable pathway for copper corrosion than corrosion in oxygen-free water from both thermodynamic driving force and kinetic perspectives. Any copper corrosion by sulphide attack would far exceed the corrosion depths of penetration that have been suggested could occur by anoxic corrosion in pure water in saturated bentonite backfill. Thus, corrosion by sulphide attack is of greater concern in safety assessments than any postulated corrosion in oxygen-free water. In conclusion, it is the opinion of these reviewers that consideration of corrosion in oxygen-free water by plausible scenarios has been exhausted and research should focus on the more relevant potential mechanism of copper attack by sulphide.

## 2.2. The Sauna Effect

Sulphide-induced pitting or Stress Corrosion Cracking (SCC) of copper exacerbated by a ‘sauna effect’ that is speculated to increase the salt concentration in the vicinity of the canister raises a concern over possible overlooked enhanced forms of corrosion attack. Prior to discussion of pitting and SCC (in Sections 2.3 and 2.4 respectively), SKB’s analysis of the sauna effect, as summarised in Section 3 of the supplementary information report (SKB 2019), is reviewed.

In the context of the KBS-3 repository, the sauna effect is the evaporation of water in a deposition hole, where the temperature is high because of the heat from the disposal canister, resulting in the concentration of salt in the remaining water and, potentially, precipitation. If groundwater continues to enter the deposition hole and leave as vapour, then salt will accumulate. In aggressive atmospheric corrosion conditions brought about by concentration of species such as sulphides or Cl<sup>-</sup>, the rate of corrosion attack can increase where there is wetting and drying with water vaporisation to enable salt concentration.

SKB (2019) argued that condensation of the vapour largely would occur in the bentonite buffer in the deposition hole as the vapour moves away from the canister, with little water leaving the deposition hole as vapour. On this basis, the amount of groundwater that can enter the deposition hole, and therefore the amount of salt that can be concentrated or precipitated in the deposition hole, is limited by the amount of water that is needed to fully saturate the bentonite in the deposition hole. The

diffusivity of water vapour in bentonite decreases as the saturation of the bentonite increases and is zero at full saturation so that vapour transport cannot occur. The argument that vapour condensation will occur close to the canister, thereby limiting the amount of salt that can accumulate while the bentonite saturates, is key to the claim that the sauna effect will have an insignificant impact on the rate of copper corrosion by pitting and SCC.

SKB (2019, Section 3.2.1) reported a number of laboratory experiments that show that water vapour is transported readily through dry bentonite pellets (such as would be placed in the slot between the bentonite blocks and the deposition hole wall), and that condensation is required in order for the bentonite to absorb water. Where conditions are amenable to condensation occurring a condensation nucleus will form that promotes further uptake. Bentonite blocks appear to provide such condensation conditions and therefore the presence of such blocks in the deposition holes is an important control on vapour transport distances.

Tests to investigate the sauna effect reported by Birgersson and Goudarzi (2017) are of particular significance. In these tests, conditions in a deposition hole are reproduced by surrounding a heater with bentonite blocks, introducing water in the bentonite below the heater and running the test for a number of days. The measurement of water-to-solid ratios in samples taken from Test 9 after 50 days do indicate increased water-to-solids ratios in samples taken from the upper parts of the experiment (samples #3 to #10), which is reasonably interpreted as resulting from condensation of water vapour. The sample measurements do indicate that there is a small amount of drying of the bentonite nearest to the heater, which presumably could lead to minor concentration of salt in the remaining water in the bentonite (e.g. samples #13, #14, #18, #19). However, there is no obvious mechanism for cycles of wetting and drying leading to salt accumulation in these regions; Birgersson and Goudarzi (2017) do not comment on this. Birgersson and Goudarzi (2017) do consider that water lost from the experiment occurs as a result of drying of the outer parts of the bentonite, with reference to water-to-solid ratios in samples taken from the top block (samples #1 and #2), although the water-to-solid ratios of these samples appear to be consistent with the initial values (16%). Birgersson and Goudarzi (2017) argue that the inner slot functions as an isolated system (i.e., water vapour is not transported from the inner slot to the outer environment), but there is no absolute confirmatory evidence for this. This is an important conclusion because the maximum water vapour transport distance affects the amount of salt that could concentrate as a result of evaporation of groundwater at the canister surface. The circulating water used in Test 9 was 0.6 M CaCl<sub>2</sub>, but there is no discussion of any measurements of salt concentration where vaporisation has been assumed to occur in the test or where condensation was observed to have occurred.

Tests undertaken by Åkesson *et al.* (2019) showed that bentonite (blocks or pellets) will not limit vapour transport unless condensation occurs. However, Åkesson *et al.* (2019) also estimated that the distributions of temperature and relative humidity in the deposition holes are likely to favour the occurrence of condensation, which would reduce the permeability for vapour transport and moisture redistribution.

Field tests appear to show no evidence of any significant sauna effect under disposal conditions (SKB, 2019, Section 3.3). Bentonite samples from the Prototype Repository experiment at the Äspö Hard Rock Laboratory (HRL) show no concentration of Cl above what would be expected in a saturated system as a result of mixing of Cl in groundwater with that initially present in partially saturated bentonite. However, samples of saturated bentonite from the canister mid-height were examined, where any evaporation and associated salt concentration would have

ceased if it had occurred at all, with subsequent diffusive redistribution of any elevated concentrations of Cl<sup>-</sup> in the saturated system. It would have been helpful if it had been confirmed that there was no increased concentration of Cl<sup>-</sup> in partially saturated or unsaturated regions of bentonite where evaporation might have been ongoing, perhaps with a continuing water supply to replace the evaporated water.

Analysis of samples from the Äspö HRL LOT test (heated Cu tubes surrounded by bentonite blocks) also found Cl<sup>-</sup> concentrations to be fairly uniform, with no evidence of increased concentrations resulting from the sauna effect. The samples were presumably fully saturated, which again suggests that conditions were not amenable to evaporation and Cl<sup>-</sup> concentration.

The explanation of results from the FEBEX experiment (heaters surrounded by bentonite blocks in a tunnel in granite) at Grimsel in Switzerland is not particularly clear. Chloride concentrations in the bentonite were measured when the experiment was dismantled after 18 years of heating and natural hydration. The chloride concentration was found to have decreased in bentonite near the tunnel walls and increased near the heater. This suggests that chloride was leached from the bentonite as the bentonite became saturated by groundwater (although the chloride concentration in the Grimsel groundwater was not reported), but evaporation and resultant chloride concentration occurred near the canister surface where the bentonite was not fully saturated. It is not clear how the water vapour would have been transported or where condensation occurred. SKB concluded that the data show no overall accumulation of chloride in the buffer surrounding the heater. However, there does appear to be a higher chloride concentration in the immediate vicinity of the heater.

SKB (2019, Section 3.3.4) concluded that the field experiments show no evidence for the existence of the sauna effect, which is generally a reasonable conclusion, although the increased chloride concentrations observed near the heater in the FEBEX experiments are not explained other than by an evaporation process. A clearer explanation of the process of chloride redistribution in the FEBEX experiment is needed, with a view on whether such a process could occur in deposition holes.

SKB (2019, Section 3.4.2; Birgersson and Goudarzi 2017) presented an estimate of the mass of groundwater that would need to flow into a deposition hole and leave as vapour in the 1,000-year thermal period in order to deposit sufficient chloride to result in supersaturated conditions when the bentonite eventually fully saturates. Reasonably, it was judged highly unlikely that such a process could continue for such a long period based on the expectation that condensation would occur near to the canister and that the bentonite would become saturated in tens of years at the assumed high groundwater flow rates.

In conclusion, SKB's analysis supports the argument that:

- Limited evaporation and concentration of chloride could occur near a canister.
- The evaporation process would be limited by the short transport distance of the water vapour before it condenses in the cooler bentonite, with the process ending when the bentonite becomes fully saturated. There is no viable mechanism for wetting and drying with vapour escape as might occur in an open system.

- The concentration of chloride near the canister would decrease as a result of diffusion (preceding by dissolution of any precipitates) in the saturated bentonite.
- Insufficient chloride could accumulate for supersaturated solutions to develop in the deposition hole bentonite in the 1,000 year thermal period.
- The concentration of chloride is unlikely to increase to as much as one mol/l, which is the minimum chloride concentration that SKB reports would be needed to effect corrosion processes (SKB 2019, Section 3.4.2).

Thus, it is reasonable for SKB to conclude that the sauna effect will be insignificant in the KBS-3 repository, although a clearer explanation of the observations from the FEBEX experiment would build further confidence in this conclusion.

The arguments above pertain to the behaviour of chloride, but the impacts on sulphides should also be considered. When the bentonite is saturated, sulphide arrival at the canister surface cannot exceed the mass-transport-limited rate. In the unsaturated state, the groundwater is vaporised in the bentonite near the disposal canister as discussed above, with the potential for sulphide concentration in the remaining water. Based on consideration of the arguments relating to chloride behaviour, it is anticipated that no significant sulphide concentrations would occur as a result of the sauna effect, but confirmatory arguments are required to support this expectation.

The gas phase concentration of sulphide can promote sulphide adsorption, but is limited by the low partial pressure of H<sub>2</sub>S in equilibrium with the low aqueous phase concentration as defined by Henry's law. It should also be mentioned that local corrosion sites (such as pits) require a sufficient cathodic area defined by the need for liquid groundwater or groundwater condensate adjacent to the pit to support the high anodic reaction rate in the pit. Atmospheric corrosion conditions that allow sauna effects may concentrate salts, but they also limit the cathode area containing aqueous groundwater necessary to sustain pits of sizes and depths that alter the safety case for canisters from the corrosion perspective.

### 2.3. Pitting due to Reaction with Sulphide

Concerns relating to HS<sup>-</sup> pitting have been considered previously by SKB (King *et al.* 2010, pp. 101 and 105; SKB 2002, pp. 55-66), focusing on the possibility of HS<sup>-</sup> induced localised corrosion during the long anoxic period. A limited amount of data exists regarding both E<sub>b</sub> (the breakdown potential at which pitting occurs) and E<sub>corr</sub> (the open circuit corrosion potential) that would be applicable to this period and ground water chemistry. The declining E<sub>corr</sub> with pH and improved passive film with pH are cited as reasons why this pitting should be dismissed (King *et al.* 2010, p.101). The strength of the passive film argument is not obvious since many materials pit and develop large pitting factors, particularly when well-passivated. Vasquez Moll *et al.* (1985) found E<sub>b</sub> = -0.74 V SCE in 0.01 mol-dm<sup>-3</sup> HS<sup>-</sup>. E<sub>corr</sub> was found to be -0.95 V SCE (King *et al.* 2010, p.82). On this basis, the 200 mV potential difference between E<sub>corr</sub> and E<sub>b</sub> was argued to minimise the chance of pitting by an HS<sup>-</sup> mechanism (King *et al.* 2010, p.102).

The question of pitting in Cl<sup>-</sup> plus sulphide environments remains a concern. Regarding the most recent pitting corrosion investigations reported by SKB (SKB, 2019, Section 5), the focus has been on:

- (a) corrosion electrochemistry such as Cyclic Potentiodynamic Polarisation (CPP) and electrochemical diagnostics searching for key indicators of local corrosion, such as passivity followed by breakdown potentials and lower passive current densities on the downward reverse portion of

upward/downward scans indicative of protective film formation upon an anodic scan;

(b) exposure studies of corrosion morphology including considerations of hot and humid conditions;

(c) consideration of corrosion under Sulphate-Reducing Bacteria (SRB) biofilms; and

(d) a search for environmental conditions (i.e.,  $\text{Cl}^-$  and sulphide combinations in bulk solution combined with applied sulphide fluxes) that produce a physically observed compact corrosion product layer instead of a porous one.

A compact layer was assumed to be able to function as a passive film, as suggested by parabolic film growth laws, unlike a porous layer often observed in the case of  $\text{Cu}_2\text{S}$  (Sharma 1980; Speight 2014, Section 8.2.5). The premise is that a compact layer would limit dissolution by field driven cation ejection or ionic transport of copper cations while a porous film would limit dissolution only sparingly by transport in pores such that corrosion rates would not decrease with time. Near-parabolic film growth was taken as evidence of a compact, passive film based on measured film thickness against time, whereas linear growth corresponded to a porous film (Chen *et al.* 2017; SKB, 2019, Section 5.3). The effects of a compact film are in contrast to mass transport in pores, which is subject to limited means to regulate the corrosion rate or produce non-uniform attack, such as could occur at breaks in passive layers. Testing was conducted over a range of sulphide and chloride concentrations, naturally occurring (Chen *et al.* 2017; King *et al.* 2017) and at applied potentials, and through utilisation of the Rotating Disk Electrode (RDE) method to regulate mass transport controlled sulphide transport fluxes in search of physical evidence of passive film formation (Martino *et al.* 2014, Martino *et al.* 2017, Martino *et al.* 2019a). A marker method suggested the film grew at the  $\text{Cu}_2\text{S}$  electrolyte interface (Martino *et al.* 2017). The RDE rotation rate boundary layer control was used to enhance sulphide fluxes. Film formation was taken to occur when the sulphide flux exceeded the film formation rate. Three regimes of film types were observed by Scanning Electron Microscopy (SEM) and Focused Ion Beam (FIB) cross-sectioning. These were Type I, Type II and Type III copper sulphide films, where Types I and II were porous and Type III was compact (Martino 2018; SKB, 2019, Section 5.3.2). The formation of a compact film (i.e., a passive film) requires a high sulphide concentration and a high sulphide flux (Martino *et al.* 2014, Martino *et al.* 2017). The presence of  $\text{Cl}^-$  suppresses  $\text{Cu}_2\text{S}$  film growth at low sulphide concentrations but the effect reduces as the sulphide to chloride ratio increases, suggesting competition for adsorption sites (SKB, 2019, Section 5.3.3).  $\text{Cl}^-$  likely has other effects such as on  $\text{Cu}_2\text{S}$  island or crystal morphology as well as shape. This should be better understood possibly through elucidating the effect of  $\text{Cl}^-$  on both  $\text{Cu}_2\text{S}$  and Cu surface energies as a function of factors such as crystal orientation and subsequent island morphologies in addition to consideration of emerging thinking regarding competitive adsorption of  $\text{Cl}^-$  and  $\text{S}^{2-}$ .

SKB (2019, Section 5.3.4) also reviewed several closely related publications arguing in favour of passivity of copper sulphide films (Mao *et al.* 2014; Dong *et al.* 2016; Kong *et al.* 2018). It should be noted that some of these papers also showed shallow pits on copper but with a tail on pit depth distributions (Huttunen-Saarivirta *et al.* 2019). This is significant because passivation implies that pitting is possible and the next step is to examine whether depths that could affect the repository safety assessment may be possible. Huttunen-Saarivirta *et al.* (2018) were in favour of passivity of films grown in SRB media in spite of poor electrochemical evidence and possible improbable Point Defect Model (PDM) oxide parameter calculations, such as

non-physical cation vacancy concentrations argued by Martino *et al.* (2019b). It turns out that some of this misunderstanding may be based on a typographical error in the original paper (Huttunen-Saarivirta, *et al.* 2018). Martino *et al.* (2019b) pointed out some weaknesses in the arguments presented by Huttunen-Saarivirta *et al.* (2018). It was found that:

- physical conditions for compact passive film formation were lacking at Open Circuit Potential (OCP);
- other electrochemical attributes indicative of passivity were very limited (no breakdown potential, and no theory to explain discrete sites of attack in contrast with activation of relatively uniform corrosion of entire surfaces with a low pitting factor);
- there was a lack of substantial lower currents upon downward scans following upward scans typical of other passive metal-electrolyte systems where the film grows upon anodic polarisation;
- there was a lack of the next level of electrochemical evidence, such as scratch or potential step repassivation experiments, confirming current density decay under conditions where a compact film is formed (i.e., a possible passive region).

It is interesting to note that RDE studies showed enhanced dissolution rates at current density independent of electrode potential which increased monotonically with RDE rotation rate. This is indicative of mass transport control not passive behaviour as posited by Huttunen-Saarivirta *et al.* (2019) because, in the opinion of these reviewers, it is unlikely that the inner compact film responsible for passivity was stripped by shear stress because the RDE operates in the laminar regime at most rotation rates. Another point was that the opposing groups used P-Cu versus OFP-Cu but no explanation was given by Huttunen-Saarivirta *et al.* (2019) for why the difference in copper material could account for differences in pitting susceptibility.

The compact  $\text{Cu}_2\text{S}$  film is a semiconductor and the impedance method was used to extract high field point PDM parameters, such as ionic defect densities. It should be noted that rather opaque Electrochemical Impedance Spectroscopy (EIS) fits to extract PDM model parameters are insufficient taken alone to support the case for pitting (Huttunen-Saarivirta *et al.* 2018). However, physical evidence of shallow pits was also demonstrated by Huttunen-Saarivirta *et al.* (2019). These investigations need to consider physically reasonable quantitative analysis of the electronic and physical properties of sulphide films as the starting condition for further consideration of pitting, as well as further electrochemical diagnostics besides an E-log(i) and cyclic potentiodynamic polarisation (CPP) plot. If such analysis does support the case for passivity, it is only a starting point for discussion not proof in and of itself of pitting to depths to be of consideration regarding the KBS-3 safety case.

The reviewers find much evidence for and some evidence against SKB's finding of lack of evidence for compact films under disposal conditions that would justify passivity. However, it is also suggested that a variety of electrochemical analysis options could have been employed to investigate the most compact and least compact films, providing a number of additional 'easy to obtain' diagnostics. Passive film limited copper corrosion is just one of many necessary, but not sufficient, conditions to justify pitting. A number of other conditions are required, such as a specific pit site brought about by formation of a triggering defect that specifically enables break down, and a theory for why there is formation of a non-protective chemistry in the anodic pit, such as a salt film and/or bare metal that persists at the 'pit-like' anode dissolving at high rate whilst a protective layer prevails on the remainder of the copper surface. Moreover, fast Anodic Dissolution (AD) is enabled by the exposure of the bare metal

or a salt covered surface of the pit at rates up to the anodic mass transport limit, while cathodic reactions occur on the remainder of the intact  $\text{Cu}_2\text{S}$  film. Distinct pit factors are found as a result of such anode-cathode separation. There was no valid scientific explanation put forth to explain why there could be a persistent anode with a uniquely aggressive pit chemistry that causes fast localised attack relative to an 'intact' cathode consisting of the remainder of the film. It is not plausible that a  $\text{CuCl}_x^n$  film could form that is more thermodynamically stable than the prevailing  $\text{Cu}_2\text{S}$  layer, and  $\text{Cu}^{n+}$  species are not very hydrolysable to enable local acidification. Fast cathodic kinetics on the supporting cathode are also required to support fast growth at limited anode sites developed on copper sulphide films. However, the evidence suggests that sulphides are so stable that there should be thermodynamically favoured (re)formation of a sulphide film which itself is very similar to the original film present all over the surface before bare copper was exposed by film breakdown. Thus, a rationale for why the breakdown site develops drastically different corrosion electrochemistry behaviour supported by distinctly different local chemistries is lacking.

In other work, corrosion morphologies were studied (Chen *et al.* 2017; Chen *et al.* 2019; King and Lilja 2014), but pitting factors deserve further explanation. The possibility of local attack was attributed to micro-galvanic corrosion which was relatively unexplained (Chen *et al.* 2019). This should be further understood as well as possible duplication of pitting conditions. In other related work, the effect of SRB and the possibility of a pit-like corrosion morphology under an SRB biofilm was investigated and not found to explain pitting (Gordon 2018).

Despite much evidence against pitting, which was for the most part very well supported by the experiments that were undertaken, the SKB work does not really explain what is different about observations of pitting in copper and overlooks the fact that pitting is sometimes seen in oil and gas applications where FeS films are formed on steels while other high  $\text{H}_2\text{S}$  conditions lead to more uniform attack. There is the opportunity to learn from this FeS observation and the opportunity to understand the technical basis and conditions for localised corrosion in sulphide systems where sulphide films dominate surfaces. This was not explored in the present set of studies.

## **2.4. Stress Corrosion Cracking due to Reaction with Sulphide**

It should be recognised that Stress Corrosion Cracking (SCC) has an initiation stage and a propagation stage. The initiation stage includes the formation of the initial defect or flawed defective region, and possibly a transition from this initial defect to a short crack and then long crack regime. The initiation stage generally requires some time period for formation of the 'flawed region' containing the metallurgical, chemical and mechanical condition for a crack to initiate and then transition into a propagating crack. This is termed the incubation time. In the later regime, long cracks are present and grow. The Slow Strain Rate Test (SSRT) general involves a smooth, tapered or notched tensile specimen which undergoes initiation and propagation. A pre-cracked specimen circumvents the first stage and moves directly to characterisation of the latter stage.

For SR-Site, the overall approach to the treatment of SCC phenomena under both oxic and anoxic conditions was based on comparing the required conditions for various SCC mechanisms with those expected in the repository environment (King and Newman 2010, p.3; King *et al.* 2010, p.114). Recent analysis has identified the need for further focus on the potential for SCC of copper in the presence of sulphides, as reflected in recommendations by the Land and Environmental Court

for further examination of SCC induced by reaction of copper with sulphides, taking account of the sauna effect. Unresolved issues concerning SCC are:

1. SCC in environments with combinations of sulphide and chloride.
2. SCC under anoxic conditions by a combination of  $\text{HS}^-$  induced effects and vacancy injection-embrittlement mechanism, in light of the strain localisation arguments associated with the Aaltonen mechanism. The effects of vacancy injection and hydrogen-induced vacancy formation (corrosion-induced vacancy formation) on thermally activated creep, strain localisation and possible formation of microvoids should also be reviewed.
3. The possible influence of the sauna effect on SCC.
4. Whether SCC requires anodic dissolution and could be rendered more favourable under the oxidising conditions created by gamma radiolysis.

These issues are discussed below.

### 2.4.1. SCC under anoxic conditions with $\text{HS}^-$

The Land and Environmental Courts recommended further consideration of anaerobic SCC mechanisms that do not require oxidised corrosion products (Taniguchi and Kawasaki 2008) and this was discussed in the previous review (Scully and Hicks 2012).  $\text{HS}^-$  induced stress corrosion of copper under anoxic conditions does not require a passive film, can occur under anoxic conditions, and could have relevant secondary effects such as vacancy and hydrogen injection (Taniguchi and Kawasaki 2008). King and Newman (2010) noted that the Aaltonen mechanism (Aaltonen *et al.* 1998; Aaltonen *et al.* 2004) should also be considered in connection with SCC in the presence of a sulphide film (King and Newman 2010, p.28; King *et al.* 2010, pp.130-132). SKB (2019, Section 6) has covered (a) experimental studies showing effects on copper interpreted as SCC in an attempt to duplicate or expand upon the work of Taniguchi and Kawasaki (2008), (b) assessment of the SCC phenomenon, (c) implications of literature studies compared to repository conditions and (d) conclusions. Recent work combined with older work was summarised by SKB (2019) to conclude that anodic dissolution-based SCC would be unlikely even after considering the sauna effect.

To reiterate:

- (a) in the saturated ground water case, the sulphide arrival rate cannot exceed the mass transport limited arrival flux at the canister surface and is technically at zero concentration at the canister surface under mass-transport-controlled dissolution; and/or
- (b) in the unsaturated case, the ground water is in equilibrium with the gas phase present, and while this gas phase concentration of sulphide can promote sulphide adsorption on a dry canister, it is limited by the low partial pressure of  $\text{H}_2\text{S}$  defined by Henry's law.

Since water vaporisation is not without limit due to bentonite saturation near the canister and zero subsequent transport, as discussed in Section 2.2,  $\text{H}_2\text{S}$  cannot concentrate beyond a certain limit in the aqueous state. Therefore, the equilibrium between the  $\text{pH}_2\text{S}$  in the gas phase and the concentrated groundwater, as well as between  $\text{H}_2\text{S}$  vapour and  $\text{H}_2\text{S}$  adsorption, reaches a limiting concentration and coverage (assuming a Langmuir isotherm) and concentration of  $\text{H}_2\text{S}$  stops.

The first question then is whether various levels of Cl<sup>-</sup> and sulphide can produce cracking with or without a passive film. Many of the arguments against a local SCC site for attack even at grain boundaries are the same as those expressed above in the case of pitting. Nevertheless, several SCC studies were reviewed by SKB (2019) that mostly utilised the Slow Strain Rate Testing (SSRT) method on tensile specimens (involving application of a slow dynamic strain in a potentially corrosive environment) and sometimes utilised U-bend specimens (Bhaskaran *et al.* 2013; Arilahti *et al.* 2011; Sipilä *et al.* 2014; Becker and Öijerholm 2017; Forsström *et al.* 2017, Taxén *et al.* 2018, Taxén *et al.* 2019). In these studies, various Cl<sup>-</sup> and sulphide levels, types of commercial and pure copper (and related inherent SCC susceptibility), tensile loads, and strain rates were considered. The sulphide concentrations, strain rates and in most case the tensile stresses applied in SSRT were all conservative (i.e., much worse) than would be experienced by a canister during and after deployment. Also, according to SKB's analysis, the canister is only expected to be under tensile stress near the lid and base when an isostatic load is imposed on the canister (SKB, 2019, Section 6.4.1). The analysis indicates that the tensile stresses will only penetrate the wall thickness at the base of the copper shell, so limiting the potential for SCC of the entire copper canister; the details of the analysis has not been reviewed here.

In addition, two studies refer to use of pre-cracked or defect-containing specimens at constant load and estimated an applied stress intensity factor of 9 MPa (m)<sup>1/2</sup>, which is relatively low (Arilahti *et al.* 2011; Sipilä *et al.* 2014; King 2004). Some tests were conducted over 6-14 weeks. Crack growth was unclear as was crack length resolution compared to the incremental length possible for the slow rates expected over repository lifetimes. These tests are valuable but the detection limit deserves further review, which was not conducted here.

Only two of five studies reviewed and discussed showed indication of SCC (or alternatively interpreted as sulphide-induced intergranular corrosion) and these studies often only showed evidence of crack length less than a single copper grain length (i.e., ~50 µm). Many arguments exist against an Anodic Dissolution (AD) based SCC mechanism. Primarily, an argument is made based on mass transport control, where the interfacial sulphide concentration drops to zero and, therefore, sulphides cannot accumulate (sulphide accumulation is a pre-requisite for crack growth as in the case of pits). Lack of detection of sulphur on copper surfaces was cited as verification of this line of reasoning. Other lines of reasoning include (a) the lack of passivity required for a slip dissolution mechanism<sup>1</sup> (as discussed in the context of pitting corrosion above), (b) the lack of enhanced susceptibility at anodic potentials typical of AD mechanisms of SCC, (c) the low tensile stresses and lack of dynamic plastic strain once stress relaxation lowers creep rates in deployed canisters, and (d) a lack of fractographic evidence of SCC on primary fracture surfaces compared to ductile overload failures. Evidence of SCC mainly consisted of secondary cracking on the tensile surface of the tensile bar. Furthermore, sulphide concentrations and transport rates required to develop the presence of sulphides at surfaces and subsequently obtain SCC in SSRT are four orders of magnitude greater in the laboratory SSRT than rationalised to actually be present on canisters, except for in the eroded buffer conditions. Furthermore, transport impedances in the crack

---

<sup>1</sup> In the slip dissolution mechanism of anodically-induced SCC, a passive film lowers the prevailing corrosion rate. If it is ruptured by deformation, fast dissolution rates result at least until re-passivation. In the slip dissolution model this constitutes the crack growth. This process may repeat as the moving crack tip and global stress-strain allow.

limit the transport process to these sites. Moreover, vacancies required by one AD mechanism (i.e., Aaltonen mechanism) are rationalised to be annihilated quickly if and when anodic dissolution is removed during testing (Aaltonen *et al.* 1998; Aaltonen *et al.* 2004). In other words, vacancies must be created continually by copper dissolution or vacancy annihilation and/or consumption at sinks (such as likely exist in the copper microstructure) occurs.

Considering this information, the following comments can be made:

- SCC requires a tensile stress, a susceptible material and microstructure and a causative environment. All three of these conditions may exist in a repository and none of these factors has been discounted so far.
- Both the reviewers and SKB (2019) agree that an extremely slow crack growth rate would likely be seen, if any, in the copper surface, especially if limited by sulphide transport.
- The issue of SCC incubation time, if any, before crack propagation has not been clarified; an incubation period associated with initiation is often seen in SCC. There are two concerns: whether incubation time challenges and possibly compromises the ability of short-term laboratory SSRT or even 14-week pre-cracked tests to detect SCC; and whether initiation or incubation time matters compared to the propagation time. It may well be that the incubation time is too long for SSRT and too short to be a factor in SCC lifetimes. Those are different but related issues. Considering that a few days is too long in the former and a few decades or even centuries is relatively short in the later this deserves more thought before arriving at dismissal of the phenomenon.

These factors in combination indicate that the SSRT is a poor method to assess copper susceptibility to SCC in this system under the circumstances that are prevalent. For instance, if the incubation time is equal or greater than the short test period, no SCC will be observed. Moreover, slow crack growth rates that could affect canisters over hundreds or thousands of years are too slow to be reasonably detected by the SSRT. This is because the tensile specimen will plastically achieve ductile overload failure prior to sufficient crack growth when the latter is slow relative to the time duration of the SSRT, which is typically 48-150 hrs. This is in fact a commonplace concern in the case of all FCC (face-centred cubic) materials with slow crack growth rates evaluated for SCC by the SSRT method (Paneda *et al.* 2019). This is true regardless of whether the mechanism of attack is by an anodic dissolution or hydrogen embrittlement mechanism. There was mention of a few pre-cracked studies but results were not clearly expressed in SKB (2019) and their importance not realised. A crack resolution of about 1  $\mu\text{m}$  without drift or noise over a several week period would be necessary. Moreover, lack of SCC over a broad range of conditions was not exhaustively proven.

Consider the case where surface cracks extend less than one grain diameter i.e.  $\sim 100 \mu\text{m}$  in 72 hours during a SSRT as often reported. In this case, the crack growth rate would be about  $3.9 \times 10^{-10} \text{ m/s}$ , neglecting initiation incubation time which was not addressed in SKB (2019). Now consider the hypothetical crack growth rate possible in 1000 years over 5 cm of copper, again ignoring incubation time. The crack growth rate is about  $10^{-12} \text{ m/s}$ . This crack growth rate cannot be detected by observation of surface crack in an SEM as it translates into a crack depth less than a micrometre. Thus, it is reasonable to assert that slow cracking cannot be accessed by SSRT if SCC is extremely slow (an additional test limitation is that it includes a mix of initiation and propagation which means that the test time must be greater than the time to initiation as well as being exacerbated by slow crack growth). Some authors

claimed decreases in ultimate tensile strength and in elongation to failure during SSRT (Taniguchi and Kawasaki 2008), but there is concurrent general dissolution and no serious mechanics analysis accompanies these claims.

The bottom line is that SKB (2019) reports cracking that was only seen under laboratory test conditions where the sulphide flux was four orders of magnitude greater than would be present in the repository. This is true but only because SCC at a lower flux could not be readily detected even if occurring. SCC could eventually be dismissed on the basis of the need for a critical sulphide flux but this remains unproven because possible growth rates at a lower flux could not be explored. In other words, it must be recognised that the SSRT would not detect very slow environmental cracking which might be supported by slower sulphide fluxes. Fracture mechanics cracking experiments at fixed applied stress intensity factor by experts capable of monitoring extremely slow crack growth rates (such as with low background voltage noise if crack extension is monitored by electrical potential drop) would provide more convincing evidence that SCC can be ruled out entirely. This issue is discussed further in the context of hydrogen embrittlement in Section 2.5.

#### 2.4.2. SCC under anoxic conditions by the vacancy injection - embrittlement mechanism

The previous review (Scully and Hicks 2012) and the Land and Environmental Court considered the issue of vacancy injection as a part of the question regarding sulphide-induced SCC and hydrogen embrittlement (HE). SKB (2019) further considers this issue to determine whether the required conditions overlap with the expected conditions in the repository (Aaltonen *et al.* 1998; Aaltonen *et al.* 2004; King and Newman 2010; King *et al.* 2010; Yagodzinsky *et al.* 2010). SKB (2019, Section 6.2.6) considered further the vacancy injection-embrittlement scenario for the case of copper under long term anoxic HS<sup>-</sup> containing conditions to determine whether it represents a viable scenario for anoxic HS<sup>-</sup> induced SCC (Aaltonen *et al.* 1998; Aaltonen *et al.* 2004; Arioka *et al.* 2010; King and Newman 2010; King *et al.* 2010; Yagodzinsky *et al.* 2010; Arioka *et al.* 2011). The implications of hydrogen enhanced vacancy formation in connection with the vacancy/embrittlement mechanism is relevant to both SCC and HE in sulphides where the primary cathodic reactions lead to hydrogen production (Suzuki and Itoh 1984; Zurek 1987; Davanas and Solomon 1990; Unigovski *et al.* 2005; Wolski and Laporte 2008; Arioka *et al.* 2010; Yagodzinsky *et al.* 2010; Arioka *et al.* 2011).

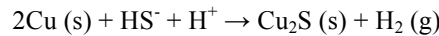
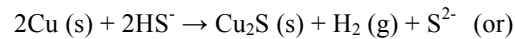
The background is as follows:

- The conceptual framework for this process is that both dissolution and hydrogen ingress promote vacancy formation.
- Cavity formation by vacancy condensation occurs prior to brittle crack advance.
- Cavities form a brittle crack path, and ductile rupture of constrained ligaments between cavities might create a scenario for embrittlement.

Studies at the Institute of Nuclear Safety, Japan, have reported extensively on the role of cavities in crack advance in creep and SCC in steels and Ni-base alloys 600 and 690, albeit over the temperature range from 280 to 360°C (Arioka, *et al.* 2010; Arioka, *et al.* 2011).

Hydrogen has been reported to promote super-abundant vacancy formation in many FCC materials (Fukai *et al.* 2001a; Fukai *et al.* 2001b; Fukai 2003; Fukai *et al.* 2003). Others have shown that the vacancy formation energy is lowered by hydrogen-vacancy trapping by energy equal to the trap binding energy (McLellan and Angel 1995; Counts *et al.* 2010; Counts *et al.* 2011).

Regarding the application of this phenomenon to copper, Aaltonen *et al.* (1998), Aaltonen *et al.* (2004), King and Newman (2010), King *et al.* (2010), Yagodzinskyy *et al.* (2010) and Jagodzinski *et al.* (2000) reported vacancy injection during dissolution in Cu accompanying SCC in nitrate solutions. Taniguchi and Kawasaki (2008) reported SCC of Cu in Na<sub>2</sub>S under anaerobic conditions but did not investigate specifically for vacancies. Putting these two independent observations together, the question is whether vacancy injection can occur in copper under anaerobic sulphide conditions and promote SCC. Both dissolution and hydrogen production mechanisms are verified under O<sub>2</sub> free anaerobic conditions in the presence of HS<sup>-</sup>:



Vacancy injection has been reported during dissolution in copper (Aaltonen *et al.* 1998; Aaltonen *et al.* 2004). H-vacancy interactions are also reported in copper (Fukai *et al.* 2001a; Fukai *et al.* 2001b; Fukai 2003; Fukai *et al.* 2003; Counts *et al.* 2010; Counts *et al.* 2011). This issue was considered in current treatments reviewed in SKB (2019) (Fukai *et al.* 2001a; Fukai *et al.* 2001b; Fukai 2003; Fukai *et al.* 2003; Counts *et al.* 2010; King and Newman 2010, pp.28-30; King *et al.* 2010, pp.130-131; Counts *et al.* 2011) and dismissed as not impactful towards SCC because anodically induced vacancies were quickly annihilated or found sinks when anodic dissolution was ‘turned off’. Vacancy injection was demonstrated at 1 mA/cm<sup>2</sup> applied anodic current density while anodic rates of 10<sup>-8</sup> mA/cm<sup>2</sup> are argued to prevail for the safety assessment (SKB 2019, Section 6.2.6). Even for eroded buffer, the anodic current density is estimated to be 10<sup>-5</sup> mA/cm<sup>2</sup>. For these reasons SKB (2019) makes the argument that SCC is unlikely. The potential influence of the sauna effect has already been dismissed, as discussed in Section 2.2.

However, note that vacancy injection at 10<sup>-5</sup> or 10<sup>-8</sup> mA/cm<sup>2</sup> may be difficult to detect in a tensile bar if it relies on detection by tensile bar creep where the entire tensile bar must experience vacancies in order to produce global creep (Huutilainen *et al.* 2018). Therefore, creep at the lower current densities would be difficult to detect for large diameter tensile bars since inward vacancy diffusion occurs at the self-diffusion rate of copper which is quite slow. This means that only the outer layer of the bar would contain new vacancies and detection might be difficult at low current densities. Therefore, the line of reasoning presented in SKB (2019) does not prove lack of existence of hydrogen stabilised vacancies at sharp crack tips over short distances. Instead of using tensile bars, more could be done to disprove the presence of vacancies and voids at crack tips over short distances.

### 2.4.3. SCC under oxidizing conditions created by radiolysis

Another unresolved issue is the need to consider the effects of special oxidising radicals and molecules like O<sub>2</sub>, H<sub>2</sub>O<sub>2</sub>, O<sub>2</sub><sup>-</sup> and HNO<sub>3</sub> produced from gamma radiolysis of pure water on SCC. In Cl<sup>-</sup> waters, additional oxidisers like Cl<sub>2</sub>, and ClO<sup>-</sup> may be produced. The analysis of corrosion induced by radiation effects

considers specifically the effect on uniform corrosion and results appear to be restricted to waters of low salinity (King *et al.* 2010, pp.135-137). Radiation is covered in Section 8 of SKB (2019), where it is mentioned that there is also little basis for evidence of microstructure alterations. Radiation did not affect mechanical properties. The gamma dose rate decreases to low levels and the amount of damage by corrosion is low during the period where the dose rate is high. Radiation does not produce corrosive agents or species that render copper prone to SCC and the dose rates appear to be several orders of magnitude below what is required to observe electrochemical effects. For instance, little effect on  $E_{\text{corr}}$  was reported which tends to argue against a special effect of these species on SCC from the threshold perspective (King *et al.* 2010).

## 2.5. Hydrogen Embrittlement

Classical Hydrogen Embrittlement (HE) such as by the HEDE (hydrogen enhanced decohesion embrittlement) and HELP (hydrogen enhanced local plasticity) mechanisms or the older blister pressurisation mechanism are not considered to be of concern with copper under disposal conditions. The high ductility of commercial pure copper alloys eliminated HEDE from possibility as large applied stresses cannot be developed at plastically blunted crack tips and hydrogen solubility is low in copper. A few other concerns were not considered further in this report, such as ‘hydrogen sickness’ which is regarded as a mature topic handled largely by commercial best practices and control of welding conditions and oxidation.

What remain to consider are modes of hydrogen embrittlement best described as hydrogen-induced SCC. For instance, hydrogen-induced vacancy formation, void or cavity formation in concentrated areas may localise deformation and produce damage<sup>2</sup>. Anodic dissolution plays a role because the anodic rate and cathodic rates are coupled. More dissolution is supported by more hydrogen production. In the case of hydrogen-induced SCC produced in this manner, the key contributor may be production of damaged regions by hydrogen.

SKB (2019) considered the implications of hydrogen enhanced vacancy and void formation. The SKB report considered that HE is precluded because:

- (a) the main source of hydrogen is O<sub>2</sub>-free cathodic reduction of water, H<sup>+</sup> or HS<sup>-</sup> during sulphide-induced copper corrosion;

---

<sup>2</sup> There are overlaps between ‘anodic’ SCC and hydrogen-induced SCC. First, it should be recognised that hydrogen production is coupled to anodic dissolution under freely corroding conditions and so these processes are unavoidably coupled under natural conditions. In both, vacancy formation may play a large role. They are overlapping processes and cannot be completely separated. For instance, during anodic SCC, anodic dissolution is a strong contributor to crack advance while hydrogen may act indirectly, such as by only facilitating vacancy formation through lowering of vacancy formation energies which in turn may enhance deformation. Enhanced deformation brings about more dissolution. In contrast, during hydrogen-induced SCC, crack advance is produced by concentration of voids and highly localised deformation largely enabled by hydrogen if there is enough hydrogen absorption which constitutes the path for crack advance. Here the crack advance is along the damaged region itself. Anodic dissolution here only acts indirectly to produce more vacancies and is not directly responsible for crack growth. So, in this study, anodic SCC and hydrogen-induced SCC are not completely different but differ in emphasis.

(b) the permeation rate is low; and

(c) there is an extremely low uptake efficiency associated with this form of hydrogen uptake leading to hydrogen concentrations too low to produce hydrogen embrittlement

It was argued that the rate of the OCP hydrogen generation from  $\text{HS}^-$  was extremely low because it generated a coupled cathodic reaction that is restricted by the rate of Cu oxidation to form  $\text{Cu}_2\text{S}$  during OCP corrosion (as discussed in Section 2.4.2). Therefore, hydrogen production would be limited by the slow rate of mass transport controlled, sulphide-induced corrosion of copper. It was also argued that low global hydrogen contents were measured during SCC testing (SKB 2019). It was generally difficult to load copper with hydrogen, although in a few cases 10 wppm hydrogen was achieved (Martinsson and Sandström 2012; Leijon *et al.* 2018).

Nine papers were reviewed in SKB (2019) that discussed various pertinent research studies in this area. In these papers, SSRT was mostly undertaken to address HE (Lousada and Korzhavyi 2019; Yagodzinskyy 2018; Forsström *et al.* 2017; Leijon *et al.* 2018). Some of the testing used driven cathodic charging which is arguably more severe from the standpoint of hydrogen production rate than the slower rate of hydrogen production and uptake seen at OCP (Martinsson and Sandström, 2012). However, it should be noted that hydrogen production is no longer coupled with dissolution in such driven cathodic testing. Furthermore, it was found that hydrogen pickup in such driven systems, even with assorted recombination poisons, was only a factor of  $\sim 10^{-4}$  of the production rate. However, low pickup rates are common in many materials in many hydrogen charging environments and are not normally alone considered to be a strong basis for dismissal of HE (Ha *et al.* 2013; Troconis *et al.* 2017; McMahon *et al.* 2019). Another key observation was that hydrogen bubbles or voids in the copper were seen within about the first 100  $\mu\text{m}$  depth beneath copper surfaces and that significant hydrogen did not penetrate deeper into the copper. This is well known dating to Wampler *et al.* (1976). A cornerstone of the SKB argument against HE is that:

(d) deeper hydrogen penetration was not observed and that the voids trapped and essentially sequestered most of the hydrogen in a surface layer without further penetration; and

(e) as-received hydrogen levels are often almost as large as those seen in testing suggesting minimal uptake in conditions related to the repository

The suggestion is that hydrogen uptake over various locations in copper is limited. SKB also argues that Lynch (2012) confirms that FCC nickel-based materials and austenitic stainless steels are not susceptible to HE. This view is wholly unsupported by decades of literature on HE. In fact, many of the Jackson Hole Wyoming Hydrogen in Metals Conferences dating to 1976 often contained sections on hydrogen embrittlement of nickel base, austenitic stainless steel, aluminium base materials. Finally, there are plenty of theoretical and experimental studies on FCC materials (Gangloff *et al.* 2012; Gangloff *et al.* 2014, Ai *et al.* 2013, Young and Scully 2002). In summary, HE was ruled out by SKB mainly on arguments (a)-(e) listed above.

Several of these assumptions are addressed below. SKB (2019) relies on an assumption that embrittlement requires deep penetration of hydrogen in order for there to be a risk of HE, although this is not certain. Hydrogen penetration beyond near surface voids is mainly a concern in non-pre-cracked SSRT tests where a

tensile bar is utilised with a substantial diameter and damage is mainly relied upon to be detected by a change in mechanical properties over a large portion of the tensile bar diameter. In order for this to be observed in a typical SSRT, HE or SCC must penetrate into the tensile bar over tens or hundreds of micrometres, ideally some substantial fraction of the tensile diameter, or there must be many SCC surface cracks that change the compliance of the bar (Paneda *et al.* 2019). This requires relatively fast cracking and little incubation time to initiation (i.e., negligible nucleation barrier) such that many cracks form within the short time frame of the test method. Stated another way, the SSRT is not a suitable method for assessing HE susceptibility for forms of environmental cracking that require decades or hundreds of years to occur (Andresen 2019). Similar to the case of SCC, pre-cracked specimens are recommended but long-term tests with sensitive detection are required in order for these tests to be useful (Andresen 2019).

Finally, an argument is put forth in SKB (2019) that the hydrogen concentration will be  $10^{-3}$  wppm. This calculation is reasonable in that the parameters used in the determination are fair choices. However, this neglects the evidence of 1000-100,000-fold enhancements of hydrogen at trap sites such as grain boundaries, which in other metals often provide strong hydrogen trap binding energies. Not enough work has been done to rule out this possibility for copper but data are limited. This local level behaviour cannot be seen by global measurements, especially if bulk levels are averaged over areas that do not contain hydrogen. If these possibilities were realised, HE would not be ruled out.

Alternatively, inspection for surface cracking and formation of shallow cracks may be one of the only viable ways to detect SCC or HE susceptibility by this method when the crack growth rate is slow (assuming the environment and mechanical driving forces are appropriate). Some of the studies consider this approach. Consideration of a slowly moving crack tip under conditions where crack uptake is local to the crack tip is warranted. As discussed above in the case of SCC, a slow 'hydrogen assisted' crack growth rate process only requires sub-micrometre penetration of a small fraction of the hydrogen (and the vacancies) produced into the fracture process zone ahead of the crack tip in order to hypothetically support environmental cracking. Since hydrogen is localised to voids on a grain boundary, bulk global compositions of hydrogen averaged over regions that do not contain hydrogen are possibly misleading and would underestimate local trapped values. The local concentration of hydrogen is not portrayed well by the global concentration in these cases. In the case of copper, hydrogen likely does not produce decohesion but may instead help generate vacancies which can, in turn, localise strain as well as function as strong hydrogen traps which could concentrate hydrogen along boundaries in some FCC materials<sup>3</sup> (Young and Scully 2002).

An argument can be made that shallow hydrogen penetration can support slow crack rates and that this typically is not detected in SSRT tests of less than one hundred hours duration. Moreover, uncertain incubation times further exacerbate the ability of a short-term test to detect HE. For instance, consider a moving line source of hydrogen where absorption and uptake only occur locally from a moving crack tip represented by a line describing the crack front across the width of a single edge notch specimen. Consider a slow crack growth rate  $v$  of  $10^{-12}$  m/s with a  $D_{\text{eff,H}}$  of  $10^{-13}$  m<sup>2</sup>/sec, where  $D_{\text{eff,H}}$  is the effective hydrogen transport rate and  $v$  is the HE crack velocity. In this case, hydrogen penetration ahead of the crack occurs over a

---

<sup>3</sup> A high vacancy hydrogen binding energy is seen in FCC Al alloys but has not been extensively studied.

distance compatible with a micrometre scale fracture process zone occupied by the vacancies, hydrogen and voids.

This type of analysis has been effective in rationalising HE in AA 7050 subjected to cracking in humid air (Young and Scully 2002). The main point is that slow hydrogen diffusion, low global concentrations and low solubility does not preclude HE. This type of analysis shows that Lynch (2012) incorrectly assumed that FCC alloys were immune to some modes of hydrogen embrittlement based on arguments of limited absorption and uptake of hydrogen due to slow hydrogen diffusion. However, Lynch (2012) neglected the moving line source approach and local hydrogen uptake in small fracture process zones. The ramifications of such local tip hydrogen uptake must be discussed.

One scenario, for instance, is that vacancies or clusters of voids form on a copper grain boundary (where diffusion might be faster and hydrogen uptake and trapping might be enhanced) and enhanced strain localisation occurs. This in turn could promote hydrogen-assisted cracking between ligaments and voids. The role of Anodic Dissolution (AD) would be to enhance vacancy generation, so enabling HE, where dissolution itself does not account for the majority of the crack advance. There is little concern over vacancy annihilation as expressed in SKB (2019) as continual active dissolution creates a small fracture process zone that might crack in a semi-continuous manner. Moreover, under these conditions there would be no requirement for semi-permanent large depth of hydrogen penetration such as the entire plastic zone or entire tensile bar. (In fact, only if a smooth tensile bar is used is a great depth of hydrogen penetration necessary as discussed above). In this case, SKB (2019) seems to infer that hydrogen must penetrate deeply and that hydrogen concentrations must develop that are far above the initial as-received concentrations. However, in the case of HE of high-performance materials, it is typically the local hydrogen concentration which matters and this is hard to detect because local probes are required. The same argument might be made over hydrogen cracking of FCC Al which irrefutably occurs at low total hydrogen levels near as received global concentrations (Young and Scully 2002).

There is also a concern that hydrogen pickup over time could be worse than seen in short term tests on copper if the microstructure is changed and thus hydrogen solubility gradually increases over long repository timescales. It should also be noted that the OCP uptake case is more complex than net cathodic charging where copper is not dissolved because there can be vacancy formation stimulated by both AD and hydrogen. Hence, severe cathodic polarisation would not necessarily be the worst case or the most severe HE condition, as often assumed. In this sophisticated scenario, local hydrogen production and uptake as well as AD might create a special condition for local HE attack, such as on grain boundaries containing vacancies and voids. For all these reasons, the vacancy injection-hydrogen embrittlement scenario under long term anoxic  $\text{HS}^-$  containing conditions was not entirely dismissed. Slow crack growth can be an issue in the safety assessment. Studies could be undertaken by groups capable of measuring extremely slow crack growth in pre-cracked specimens should they exist to examine whether it represents a viable scenario for anoxic SCC with low fluxes of sulphides. The methods such as developed by Andresen (2019), Arioka *et al.* (2008) and Arioka *et al.* (2015) with pre-cracked or notched specimens must be deployed and tested at constant applied stress intensity factors over the long term in preference to smooth tensile bars in short term SSRT which might not be able to detect HE subjected to this mechanism.

## **2.6. The Effects of Radiation on Corrosion**

The effects of radiation should be reassessed in light of these discussions regarding SCC and HE. It has largely been discounted that radiation creates chemical species that trigger new modes of SCC or HE that have not been discussed above. Radiation dose rates also decline with time. The incremental additional corrosion from radiation oxidisers contributes a small amount to the uniform corrosion allowance. Radiation is not expected to change the microstructure which could be a factor towards increasing hydrogen solubility or deformation mode, if operative. With that said, the remaining effects of radiation on the SCC and HE processes mentioned above are of interest. The main remaining concern for radiation in the case of pitting, SCC or HE relates to whether the potential is shifted by oxidisers such that the prevailing reactions that drive SCC or HE occur at a higher rate and SCC or HE by the few remaining mechanisms espoused are somehow enhanced. Based on such considerations, it seems that incremental increases in dissolution depth are the only effects, but radiation impacts on slow crack growth is unknown. Experiments to date do not suggest strong potential effects (SKB 2019, Section 8). Residual oxidisers marginally change corrosion rates, which might marginally contribute to the vacancy generation issue discussed above.

### 3. Conclusions

1. Current experimental evidence for spontaneous copper corrosion in O<sub>2</sub> free waters lacks corroborating diagnostics and broad consensus from multiple investigators. Further diagnostic experiments to resolve the issue of spontaneous copper corrosion were vigorously pursued. No novel assessments of hydrogen production and hydrogen gas generation during O<sub>2</sub> free copper corrosion resulted in hydrogen levels above background. Thus, no experiments replicated the result of experiments that claimed to show O<sub>2</sub> free corrosion of copper. Theoretical calculations of energies associated with CuOH compound formation did not theoretically substantiate or provide evidence to support the formation of this compound and more commonly accepted thermodynamically stable compounds are implicated. Assuming that O<sub>2</sub> free uniform corrosion is spontaneous, kinetic models have been developed for formation of CuOH in pure water. These kinetic models for spontaneous uniform corrosion rates are non-conservative as composed in the past and relied on key tenets that ensure low rates. Evidence supporting these key tenets and assumptions was strengthened in this report and upper bound rates were established which demonstrated that negligible additional corrosion occurred. It is the opinion of these reviewers that consideration of the matter by plausible scenarios has been exhausted.
2. The potential for the sauna effect (evaporation of water resulting in concentration of salts) to enhance sulphide-induced localised corrosion of copper has been considered. Evidence from laboratory experiments, field tests and modelling analysis supports the view that limited evaporation and concentration of salts could occur near a canister. Some evaporation will occur where temperatures are high near the disposal canister, but the process would be limited by the short transport distance of the water vapour before it condenses. Also, the concentration of salts near the canister would decrease as a result of dissolution and diffusion once the bentonite saturates. The arguments about the sauna effect pertain to the behaviour of chloride and similar arguments could be presented for the behaviour of sulphide, but these have not been provided.
3. The land and environmental report recommended a need to explore possible long-term anaerobic pitting mechanisms such as by HS<sup>-</sup> pitting that cannot be dismissed based on the lack of oxidants since water reduction could support such local corrosion processes. SKB's recent investigations have focused on searching for environmental conditions (i.e., Cl<sup>-</sup> and sulphide combinations in bulk solution combined with applied sulphide fluxes) that produce a physically observed compact corrosion product layer instead of a porous one. A compact layer was assumed to be able to function as a passive film restricting dissolution as indicated by parabolic growth, unlike a porous layer. The reviewers understand SKB's finding that there is a lack of evidence for compact films under disposal conditions that would justify passivity, but also suggest that a variety of electrochemical analysis acquired in the case of the most compact and least compact films would have been useful. There is also an alternative view that has recently been bolstered by a recent rebuttal paper. Lack of evidence of passivity is just one step in the process to prove or disprove pitting. The conditions for

pitting versus uniform corrosion in rare circumstances on copper and iron sulphide systems should be explored through the literature and better understood.

4. An important recommendation of the Land and Environmental Court was to explore the viability of long-term anaerobic Stress Corrosion Cracking (SCC) by  $\text{HS}^-$  induced stress corrosion of copper under anoxic conditions requiring a passive film. The main concern is that of a long-term cracking mechanism that supports slow crack growth. Strong experimental and theoretical evidence was presented against the likelihood of an Anodic Dissolution based (AD) SCC mechanism. Primarily, a mass transport controlled argument is made that the interfacial sulphide concentration drops to zero and, therefore, sulphides cannot accumulate (sulphide accumulation is a pre-requisite for crack growth). Lack of detection of sulphur on copper surfaces was cited as verification of this line of reasoning. Other lines of reasoning include (a) the lack of passivity required for a slip dissolution mechanism (as discussed in the context of pitting corrosion), (b) the lack of enhanced susceptibility at anodic potentials typical of AD mechanisms of SCC, (c) the low tensile stresses and lack of dynamic plastic strain once stress relaxation lowers creep rates in deployed canisters, and (d) a lack of fractographic evidence of SCC on primary fracture surfaces compared to ductile overload failures. Furthermore, sulphide transport rates required to obtain SCC in SSRT are four orders of magnitude greater than actually rationalised to be present on canisters in most cases. Moreover, vacancies required by one AD mechanism were rationalised to be annihilated when anodic dissolution is removed and anodic dissolution under repository conditions are slow relative to laboratory studies. However, the reviewers and SKB agree that an extremely slow crack growth rate would likely be present under repository conditions, which in turn, means that the SSRT is a poor method of test to utilise to assess such susceptibility. The bottom line is that SKB reports cracking that was only seen under laboratory test conditions where the sulphide flux was four orders of magnitude greater than would be present in the repository. However, SSRT would not be able to detect slower environmental cracking which could be supported by a lower flux of sulphides such as seen under repository conditions. Fracture mechanics crack studies involving monitoring of extremely slow crack growth rates are useful and broader utilisation would provide more convincing evidence that SCC can be ruled out entirely.
5. Classical hydrogen embrittlement is not considered to be of concern. However, the implications of hydrogen enhanced vacancy formation and cracking by the Aaltonen mechanism should be considered. The vacancy injection-embrittlement SCC scenario under long-term anoxic  $\text{HS}^-$  containing conditions should be investigated further to determine whether it represents a viable scenario for anoxic SCC for the reasons stated herein. Furthermore, the role of vacancy injection enhanced by either anodic dissolution or hydrogen absorption and its indirect role in supporting creep deformation at enhanced rates over expected 'dry' thermally activated conditions should also be considered with focus on the fracture process zone at crack tips instead of smooth tensile bars. However, it must be recognised that creep measurements on bulk tensile bars do not represent local fracture process zones. Local hydrogen production and uptake as well as anodic dissolution might create a special condition for local HE attack,

such as on grain boundaries containing vacancies and voids. This vacancy injection-hydrogen embrittlement scenario under long term anoxic  $\text{HS}^-$  containing conditions is a remaining concern. Vacancies should be studied at crack tips. Studies could be undertaken by groups capable of measuring extremely slow crack growth in pre-cracked specimens to examine whether it represents a viable scenario for anoxic SCC with low fluxes of sulphides.

6. Regarding radiation, many different effects were discussed but discounted. For instance, it was posited that radiation does not adversely affect microstructures. Radiation is only estimated to cause incremental increases in dissolution depth. Experiments to date do not suggest strong potential effects. Residual oxidisers marginally change corrosion rates, which marginally would contribute to the vacancy generation issue discussed above. In general, the dose rate appears to be too low to affect prevailing mechanisms of pitting, SCC or HE, nor could it trigger new mechanisms.

## 4. References

- Aaltonen, P., Jagodzinski, Y., Tarasenko, A., Smouk, S. and Hanninen, H. (1998). Low-frequency internal friction of pure copper after anodic polarisation in sodium nitrite solution. *Corrosion Science* 40(6): 903-908.
- Aaltonen, P., Nevdacha, V., Tarasenko, O., Yagodzinskyy, Y. and Hanninen, H. (2004). Interactions of hydrogen in copper studied by internal friction technique. *Materials Science and Engineering a-Structural Materials Properties Microstructure and Processing* 370(1-2): 218-221.
- Ai, J.H., Ha, H.M., Gangloff, R.P. and Scully, J.R. (2013). Hydrogen diffusion and trapping in a precipitation-hardened nickel–copper–aluminum alloy Monel K-500 (UNS N05500), *Acta Materialia* 61 (9), 3186-3199 35.
- Åkesson, M., Börgesson, L., Sandén, T. and Goudarzi, R. (2019). Vapor Transport in Bentonite: Laboratory Investigations and Theoretical Study, SKBdoc 1712120 ver 1.0.
- Andresen, P.L. (2019). A Brief History of Environmental Cracking in Hot Water, *CORROSION*. 2019;75(3):240-253.
- Ariolahti, E., Lehtikuusi, T., Olin, M., Saario, T. and Varis, P. (2011). Evidence for internal diffusion of sulphide from groundwater into grain boundaries ahead of crack tip in Cu OFP copper. *Corrosion Engineering, Science and Technology* 46, 134 – 137.
- Arioka, K., Yamada, T., Terachi, T. and Miyamoto, T. (2008). Dependence of Stress Corrosion Cracking for Cold-Worked Stainless Steel on Temperature and Potential, and Role of Diffusion of Vacancies at Crack Tips, *CORROSION*.; 64(9):691-70
- Arioka, K. (2015). W.R. Whitney Award Lecture: Change in Bonding Strength at Grain Boundaries Before Long-Term SCC Initiation, *CORROSION*.;71(4):403-419.
- Arioka, K., Miyamoto, T., Yamada, T. and Terachi, T. (2010). Formation of Cavities Prior to Crack Initiation and Growth on Cold-Worked Carbon Steel in High-Temperature Water. *Corrosion* 66(1).
- Arioka, K., Yamada, T., Miyamoto, T. and Terachi, T. (2011). Dependence of Stress Corrosion Cracking of Alloy 690 on Temperature, Cold Work, and Carbide Precipitation-Role of Diffusion of Vacancies at Crack Tips. *Corrosion* 67(3).
- Becker, R. and Hermansson, H.-P. (2011). Evolution of hydrogen by copper in ultrapure water without dissolved oxygen. *SSM* 2011:34, Strålsäkerhetsmyndigheten.
- Becker, R. and Öijerholm, J. (2017). Slow strain rate testing of copper in sulfide rich chloride containing deoxygenated water at 90 °C. Stockholm: Swedish Radiation Safety Authority. (SSM 2017:02).
- Bhaskaran, G., Carcea, A., Ulaganathan, J., Wang, S., Huang, Y. and Newman, R.C. (2013). Fundamental aspects of stress corrosion cracking of copper relevant to the Swedish deep geologic repository concept. SKB TR-12-06, Svensk Kärnbränslehantering AB.

- Birgersson, M. and Goudarzi, R. (2017). Summary report on “Sauna” effects. SKB Report TR-17-07.
- Bojinov, M. and Makela, K. (2003). Corrosion of Copper in Anoxic 1M NaCl Solution. Posivia, Working Report 2003-45: 45-55.
- Chen, J., Qin, Z., Martino, T. and Shoesmith, D.W. (2017). Non-uniform film growth and micro/macrogalvanic, corrosion of copper in aqueous sulphide solutions containing chloride. *Corrosion Science*, 114, 72 – 78.
- Chen, J., Guo, M., Martino, T., Ramamurthy, S., Noël, J.J., Shoesmith, D., Lilja, C. and Johansson, A.J. (2019). The distribution of corrosion damage to copper surfaces exposed to aqueous sulphide solutions. SKBdoc 1706406, ver 1.0, Svensk Kärnbränslehantering AB.
- Counts, W.A., Wolverton, C. and Gibala, R. (2010). First-principles energetics of hydrogen traps in alpha-Fe: Point defects. *Acta Materialia* 58(14): 4730-4741.
- Counts, W., Wolverton, C. and Gibala, R. (2011). Binding of multiple H atoms to solute atoms in bcc Fe using first principles. *Acta Materialia* 59(14): 5812-5820.
- Davanas, K. and Solomon A.A. (1990). Theory of Intergranular Creep Cavity Nucleation, Growth and Interaction. *Acta Metallurgica Et Materialia* 38(10): 1905-1916.
- Dong, C., Mao, F., Gao, S., Sharifi-Asl, S., Lu, P. and Macdonald D.D. (2016). Passivity breakdown on copper: influence of temperature. *Journal of The Electrochemical Society* 163, C707–C717.
- Forsström, A., Becker, R., Öijerholm, J., Yagodzinskyy, Y., Hänninen, H. and Linder, J., (2017). Hydrogen absorption in copper as a result of corrosion reactions in sulphide and chloride containing deoxygenated water at 90 °C in simulated spent nuclear fuel repository conditions. In *Proceedings of EUROCORR 2017 – The Annual Congress of the European Federation of Corrosion, 20th International Corrosion, Congress and Process Safety Congress, Prague, Czechia, 3 – 7 September 2017*.
- Fukai, Y. (2003). Formation of superabundant vacancies in M-H alloys and some of its consequences: a review. *Journal of Alloys and Compounds* 356: 263-269.
- Fukai, Y., Haraguchi, T., Hayashi, E., Ishii, Y., Kurokawa, Y. and Yanagawa, J. (2001a). Hydrogen-induced superabundant vacancies and diffusion enhancement in some FCC metals. *Diffusions in Materials: Dimat2000, Pts 1 & 2* 194-1: 1063-1068.
- Fukai, Y., Shizuku, Y. and Kurokawa Y. (2001b). Superabundant vacancy formation in Ni-H alloys. *Journal of Alloys and Compounds* 329(1-2): 195-201.
- Fukai, Y., Mizutani, M., Yokota, S., Kanazawa, M., Miura, Y. and Watanabe, T. (2003). Superabundant vacancy-hydrogen clusters in electrodeposited Ni and Cu. *Journal of Alloys and Compounds* 356: 270-273.
- Gangloff, R.P. and Somerday, B.R. (2012). *Gaseous Hydrogen Embrittlement of Materials in Energy Technologies, Volume 1-2, Woodhead Publishing. Vol 1: The problem it characterization and effects on particular alloy classes, Ch16 Stainless Steels, San Marchi; Ch 17, Nickel Cobalt and Iran based Superalloys, J.A. Lee, Ch 19; J.R. Scully, Hydrogen Embrittlement of Al and Al-based Alloys.*

- Gangloff, R.P., Ha, H.M., Burns, J.T. and Scully, J.R. (2014). Measurement and Modeling of Hydrogen Environment-Assisted Cracking in Monel K-500, *Metallurgical and Materials Transactions A* 45 (10), 3814-3834 40.
- Gordon, A., Johansson, J., Pahverk, H., Börjesson, E. and Sjögren, L. (2018). Corrosion morphology of copper in anoxic sulphide environments. SKB TR-18-14, Svensk Kärnbränslehantering AB.
- Ha, H.M., Ai, J.-H. and Scully, J.R. 2013. Effects of prior cold work on hydrogen trapping and diffusion in API X-70 line pipe steel during electrochemical charging, *Corrosion* 70 (2), 166-184.
- Hedin, A., Johansson, A., Lilja, C., Boman, M., Berastegui, P., Berger, R. and Ottosson, M. (2018). Corrosion of copper in pure O<sub>2</sub>-free water? *Corros. Sci.* 137 (2018) 1–12.
- Hultquist, G. (1986). Hydrogen Evolution in Corrosion of Copper in Pure Water. *Corrosion Science* 26(2): 173-177.
- Huutilainen, C., Saario, T. and Toivonen, A. (2018). Review of the Aaltonen-mechanism. SKB R-18-03, Svensk Kärnbränslehantering AB.
- Huttunen-Saarivirta, E., Ghanbari, E., Mao, F., Rajala, P., Carpén, L. and Macdonald, D. (2018). Kinetic Properties of the Passive Film on Copper in the Presence of Sulfate-Reducing Bacteria. *J. Electrochem. Soc.*, 165(9) C450-C460.
- Huttunen-Saarivirta, E., Rajala, P., Carpén, L., Wang, J., Liu, F., Ghanbari, E., Mao, F., Dong, C., Yang, J., Sarfi-Asi, S. and Macdonald, D. (2019). Response to Comments on E. Huttunen-Saarivirta *et al.*, “Kinetic Properties of the Passive Film on Copper in the Presence of Sulfate-Reducing Bacteria”, [*J. Electrochem. Soc.*, 165(9) C450 (2018)], *J. Electrochem. Soc.*, 166(10) Y17-Y26.
- Jagodzinski, Y., Aaltonen, P., Smuk, S., Tarasenko, O. and Hanninen, H. (2000). Internal friction study of environmental effects on metals and alloys. *Journal of Alloys and Compounds* 310: 256-260.
- King, F. (2014). The effect of discontinuities on the corrosion behaviour of copper canisters. SKB TR-04-05, Svensk Kärnbränslehantering AB.
- King, F. and Lilja, C. (2014). Localised corrosion of copper canisters. *Corrosion Engineering, Science and Technology* 49, 420 – 424.
- King, F. and Newman, R. (2010). Stress corrosion cracking of copper canisters. SKB Report TR-10-04, Svensk Kärnbränslehantering AB.
- King, F., Lilja, C., Pedersen, K., Pitkänen, P. and Vähänen, M. (2010). An update of the state-of-the-art report on the corrosion of copper under expected conditions in a deep geologic repository. SKB, TR-10-67, Svensk Kärnbränslehantering AB.
- King, F., Chen, J., Qin, Z., Shoesmith, D. and Lilja, C. (2017). Sulphide mass-transport control of the Corrosion of copper canisters. *Corrosion Engineering, Science and Technology* 52, 210 – 216.
- Kong, D., Dong, C., Zhao, M., Ni, X., Man, C. and Li, X. (2018). Effect of chloride concentration on passive film properties on copper. *Corrosion Engineering, Science and Technology* 53, 122 – 130.

- Korzhavyi, P. A., Soroka, I.L., Isaev, E.I., Lilja, C. and Johansson, B. (2012). Exploring monovalent copper compounds with oxygen and hydrogen. *Proceedings of the National Academy of Sciences of the United States of America* 109(3): 686-689.
- Leijon, G., Ahlström, J. and Andersson-Östling, H.C.M. (2018). In situ hydrogen charging of OFP copper during creep. SKB R-17-17, Svensk Kärnbränslehantering AB.
- Lousada, C.M and Korzhavyi, P.A. (2019). Hydrogen sorption capacity of crystal lattice defects and low Miller index surfaces of copper. SKBdoc 1708457 ver 1.0, Svensk Kärnbränslehantering AB.
- Lynch, S.P. (2012). Hydrogen embrittlement phenomena and mechanisms. *Corrosion Reviews* 30, 105 – 123.
- Macdonald, D. D. and Samin, S.-A. (2011). Is Copper Immune to Corrosion When in Contact with Water and Aqueous Solutions? SSM 2011:09, Strålsäkerhetsmyndigheten.
- Mao, F., Dong, C., Sharifi-Asl, S., Lu, P. and Macdonald, D.D. (2014). Passivity breakdown on copper: influence of chloride ion. *Electrochimica Acta* 144, 391 – 399.
- Martino, T. (2018). Electrochemical and corrosion examination of copper under deep geologic conditions for the application of nuclear waste containers. PhD thesis. Western University, London, Canada.
- Martino, T., Partovi-Nia, R., Chen, J., Qin, Z. and Shoesmith, D.W. (2014). Mechanisms of film growth on copper in aqueous solutions containing sulphide and chloride under voltammetric conditions. *Electrochimica Acta* 127, 439 – 447.
- Martino, T., Chen, J., Qin, Z. and Shoesmith, D.W. (2017). The kinetics of film growth and their influence on the susceptibility to pitting of copper in aqueous sulphide solutions. *Corrosion Engineering, Science and Technology* 52, 61 – 64.
- Martino, T., Smith, J., Chen, J., Quin, Z., Noël, J.J. and Shoesmith, D.W. (2019a). The properties of electrochemically-grown copper sulphide films. *Journal of The Electrochemical Society* 166, C9–C18.
- Martino, T., Chen, J., Guo, M., Ramamurthy, S., Shoesmith, D.W. and Noël, J.J. (2019b). Comments on E. Huttunen-Saarivirta *et al.*, “Kinetic Properties of the Passive Film on Copper in the Presence of Sulfate-Reducing Bacteria”, *J. Electrochem. Soc.*, 166(10) Y13-Y16.
- Martinsson, A. and Sandström, R. (2012). Hydrogen depth profile in phosphorus-doped, oxygen-free copper after cathodic charging. *Journal of Materials Science* 47, 6768 – 6776.
- McLellan, R.B. and Angel Y.C. (1995). The Thermodynamics of Vacancy Formation in Fcc Metals. *Acta Metallurgica Et Materialia* 43(10): 3721-3725.
- McMahon, M.E., Harris, Z.D., Scully, J.R. and Burns J.T. (2019). The effect of electrode potential on stress corrosion cracking in highly sensitized Al–Mg alloys. *Materials Science and Engineering: A*, 767, 138399.

- Ottosson, M., Boman, M., Berastegui, P., Andersson, Y., Hahlin, M., Korvela, M., and Berger, R. (2017). Copper in ultrapure water, a scientific issue under debate. *Corros. Sci.* 122 (2017) 53–60.
- Ottosson, M., Boman, M., Berastegui, P., Andersson, Y., Hahlin, M., Korvela, M., and Berger, R. (2016). Copper in ultrapure water. SKB Report TR-16-01.
- Paneda, E., Harris, Z., Fuentes-Alonso, S., Scully, J.R. and Burns, J.T. (2019). On the suitability of Slow Strain Rate Tensile Testing for assessing hydrogen embrittlement susceptibility, *Corrosion Science*, submitted 2019.
- Szkalos, P., Hultquist, G. and Wikmark G. (2007). Corrosion of copper by water. *Electrochemical and Solid State Letters* 10(11): C63-C67.
- Scully, J.R. and Hicks, T.W. (2012). Initial Review Phase for SKB's Safety Assessment SR-Site: Corrosion of Copper. SSM Technical Note 6, Report 2012:21.
- Sharma, S.P. (1980). Reaction of copper and copper oxide with H<sub>2</sub>S. *Journal of The Electrochemical Society*, 127, 21 – 26.
- Sipilä, K., Arilahti, E., Lehtikuusi, T. and Saario, T. (2014). Effect of sulphide exposure on mechanical properties of CuOFP. *Corrosion Engineering, Science and Technology* 49, 410 – 414.
- SKB (2002). Corrosion of Copper in Alkaline Chloride Solutions. SKB Report TR-02-25, Svensk Kärnbränslehantering AB.
- SKB (2019). Supplementary Information on Canister Integrity Issues. SKB Report TR-19-15, Svensk Kärnbränslehantering AB.
- Speight, J.G. (2014). *Handbook of offshore oil and gas operations*. Elsevier Science.
- Suzuki, H. and Itoh, G. (1984). A Study of Intermediate Temperature Embrittlement in Pure Copper. *Journal of the Japan Institute of Metals* 48(10): 1016-1021.
- Taniguchi, N. and Kawasaki, M. (2008). Influence of sulfide concentration on the corrosion behavior of pure copper in synthetic seawater. *Journal of Nuclear Materials* 379(1-3): 154-161.
- Taxén, C., Flyg, J. and Bergqvist, H. (2018). Stress corrosion testing of copper in sulfide solutions. SKB TR-17-16, Svensk Kärnbränslehantering AB.
- Taxén, C., Flyg, J. and Bergqvist, H. (2019). Stress corrosion testing of copper in near neutral sulphide solutions. SKB TR-19-13, Svensk Kärnbränslehantering AB.
- Troconis, B.C.R., Harris, Z.D., Ha, H., Burns, J.T. and Scully, J.R. (2017). The effect of heat-to-heat variations in metallurgy and hydrogen-metal interactions on the hydrogen embrittlement of Monel K-500. *Materials Science and Engineering: A*, 703, 533-550.
- Unigovski, Y., Keren, Z., Eliezer, A. and Gutman, E.M. (2005). Creep behavior of pure magnesium and Mg-Al alloys in active environments. *Materials Science and Engineering a-Structural Materials Properties Microstructure and Processing* 398(1-2): 188-197.

Vasquez Moll, D., De Chialvo, M.R.G., Salvarezza, R.C. and Arvia, A.J. (1985). Corrosion and passivity of copper in solutions containing sodium sulphide. Analysis of potentiostatic current transients. *Electrochimica Acta* 30(8): 1011-1016.

Wampler, W.R., Schober, T. and Lengeler, B. (1976). Precipitation and trapping of hydrogen in copper. *Philosophical Magazine* 34, 129 – 141.

Wolski, K. and Laporte, V. (2008). Grain boundary diffusion and wetting in the analysis of intergranular penetration. *Materials Science and Engineering a-Structural Materials Properties Microstructure and Processing* 495(1-2): 138-146.

Yagodzinskyy, Y., Saukkonen, T., Kilpelainen, S., Tuomisto, F. and Hanninen, H. (2010). Effect of hydrogen on plastic strain localization in single crystals of austenitic stainless steel. *Scripta Materialia* 62(3): 155-158.

Yagodzinskyy, Y., Malitckii, E., Tuomisto, F. and Hanninen, H. (2018). Hydrogen-induced strain localisation in oxygen-free copper in the initial stage of plastic deformation. *Philosophical Magazine* 98, 727-740.

Young, G.A. and Scully, J.R. (2002). The effects of test temperature, temper, and alloyed copper on the hydrogen-controlled crack growth rate of an Al-Zn-Mg-(Cu) alloy, *Metallurgical and Materials Transactions A* 33 (4), 1167-1181 90.

Zurek, A. K. (1987). Brittle Cracks in Intrinsically Ductile Copper. *Scripta Metallurgica* 21(12): 1619-1622.





Authors

Peter Szakálos<sup>1</sup>  
Christofer Leygraf<sup>2</sup>

<sup>1</sup>Szakálos Materials Science AB

<sup>2</sup>Kungl. Tekniska Högskolan.

# Review Assignment for the Swedish Radiation Safety Authority: Corrosion of Copper Canister



# Abstract

According to The Land and Environmental Court in Nacka, Sweden, SKB should produce evidence, i.e. supplementary information, showing that the repository in the long-term will meet the requirements of the Environmental Code, concerning the following corrosion-related issues:

- a.** Corrosion due to reaction in oxygen-free water
- b.** Pitting corrosion due to reaction with sulphides, including the so-called Sauna effect on pitting corrosion
- c.** Stress corrosion cracking (SCC) due to reaction with sulphides, including the so-called Sauna effect on stress corrosion cracking
- d.** Hydrogen embrittlement (HE)
- e.** Influence of radioactive radiation on pitting corrosion, stress corrosion cracking and hydrogen embrittlement.

SKB has submitted supplementary information and a few new studies on canister integrity issues, especially regarding copper corrosion, as required by the Land and Environmental Court. This technical report concerns the review of that material. It can be concluded that none of the five issues (a-e) raised by The Land and Environmental Court has been met in a satisfactory way by the supplementary information provided by SKB. Main questions which are still far from being resolved concern:

- Salt enrichment in the deposition holes, the Sauna effect (issues b and c)
- Stress corrosion cracking & hydrogen embrittlement in unalloyed copper (c and d)
- General corrosion and pitting corrosion of unalloyed copper under current exposure conditions (a and b)
- The effect of simultaneous radioactive radiation and water exposure on copper integrity (e)

The overall conclusion is that the safety analysis SR-site (SKB-report TR-11-01) by no means can be regarded as trustworthy. Consequently it cannot be used as a basis for decision-makers in the Swedish government concerning the final storage of high-level waste.

# Contents

<b>Introduction</b> .....	<b>3</b>
<b>1. Discussion and conclusions concerning the five corrosions issues pointed out by The Land and Environmental Court</b> .....	<b>5</b>
<b>2. Salt enrichment in the deposition holes, the Sauna effect</b> .....	<b>7</b>
2.1. Short summary.....	7
2.2. The Sauna effect- introduction.....	7
2.3. Background data and information taken from different SKB-reports.....	8
2.4. SKB reports concerning the Sauna effect.....	11
2.4.1. Detailed comments on TR-15-09 and TR-17-07, concerning tests 1-9 of the Sauna effect.....	12
2.5. Detailed analysis and consequences of salt enrichment in a Forsmark repository (Sauna effect).....	15
<b>3. Stress corrosion cracking and hydrogen embrittlement in unalloyed copper (CuOFP)</b> .....	<b>17</b>
3.1. Short summary.....	17
3.2. Introduction SCC and HE.....	18
3.3. Slow strain rate testing of copper performed at Japan Atomic Energy Agency (JAEA).....	18
3.4. Slow strain rate testing of copper at Studsvik AB.....	19
3.4.1. Hydrogen measurement on SSRT-exposed samples.....	23
3.5. Hydrogen charging of bulk metal and welds due to copper corrosion.....	24
3.6. Hydrogen and hydroxide uptake of canister copper exposed 7 years in SKB prototype repository in the Äspö Hard rock laboratory.....	26
3.7. Precracked CT-specimens under constant load exposed in sulphide containing groundwater at room temperature.....	28
3.8. Retrieval and post-test examination of packages 4 and 5 of the MiniCan field experiment.....	29
3.9. A study of hydrogen effects on creep ductility.....	30
3.10. Microbial influence on corrosion of copper in the repository environment, Aalto University.....	31
3.11. Discussion and conclusions regarding SCC and hydrogen embrittlement (HE) and hydrogen sickness (HS) of unalloyed copper (CuOFP) in a deep repository environment.....	31
<b>4. General corrosion and pitting corrosion</b> .....	<b>34</b>
4.1. Short summary.....	34
4.2. General- and pitting corrosion- introduction.....	34
4.3. General copper corrosion in pure oxygen gas free water.....	35
4.4. Increased general copper corrosion in contact with bentonite.....	37
4.5. Microbial induced “corrosion” degradation of the bentonite buffer.....	38
4.6. Pitting corrosion in the repository environment.....	40
4.6.1. FEBEX, 18-year long term study in a repository environment.....	40
4.6.2. A 15-year exposure in pure anoxic water and observed pitting corrosion in the SKB-project Alternative Buffer Material (ABM).....	42
4.6.3. Pitting corrosion of copper in anoxic groundwater environment in the presence and absence of sulphate reducing bacteria (SRB).....	43

4.7. Discussion regarding pitting corrosion in a repository environment .....	44
<b>5. The effect of radioactive radiation. ....</b>	<b>44</b>
5.1. Summary.....	44
5.2. More detailed report.....	45
5.2.1. The difference between separate and combined effects of radiation and water exposure.....	45
5.2.2. High-energy synchrotron x-ray diffraction (HEXRD) .....	46
5.2.3. Discussion.....	48
<b>6. Summary .....</b>	<b>49</b>
<b>7. References .....</b>	<b>51</b>
<b>APPENDIX 1 .....</b>	<b>56</b>

# Introduction

The Land and Environmental Court in Nacka, Sweden, announced January 23, 2018, that:

The Swedish method for long-term storage of the Swedish nuclear waste (KBS-3) is permissible if:

**1.** Svensk Kärnbränslehantering AB (SKB) produces evidence that the repository in the long-term will meet the requirements of the Environmental Code, despite remaining uncertainties regarding how the protective capability of the canister may be affected by:

- a.** Corrosion due to reaction in oxygen-free water
- b.** Pitting corrosion due to reaction with sulphides, including the so-called sauna effect on pitting corrosion
- c.** Stress corrosion cracking due to reaction with sulphides, including the so-called sauna effect on stress corrosion cracking
- d.** Hydrogen embrittlement
- e.** Influence of radioactive radiation on pitting corrosion, stress corrosion cracking and hydrogen embrittlement.

**2.** The long-term responsibility for the final repository according to the Environmental Code has been clearly assigned.

SKB has submitted supplementary information and some few new studies on canister integrity issues, especially regarding copper corrosion as required by the Land and Environmental Court.

This technical report concerns the review of that material. With reference to the remaining uncertainties (a-e above) raised by the Environmental Code and addressed by SKB in the Supplementary Information this Technical Reports is divided into the following four Chapters.

2. Salt enrichment in the deposition holes, the Sauna effect (issues b and c)
3. Stress corrosion cracking & hydrogen embrittlement in unalloyed copper (c and d)
4. General corrosion and pitting corrosion (a and b)
5. The effect of radioactive radiation (e)

Additionally, condensed discussions and conclusions concerning the five corrosion issues pointed out by The Land and Environmental Court have been summarized in Chapter 1. More detailed information on these issues is presented in Chapters 2 o 5.

# 1. Discussion and conclusions concerning the five corrosion issues pointed out by The Land and Environmental Court

According to The Land and Environmental Court in Nacka, Sweden, SKB should produce evidence, i.e. supplementary information, showing that the repository in the long-term will meet the requirements of the Environmental Code, concerning the following issues:

- a. Corrosion due to reaction in oxygen-free water
- b. Pitting corrosion due to reaction with sulphides, including the so-called Sauna effect on pitting corrosion
- c. Stress corrosion cracking (SCC) due to reaction with sulphides, including the so-called Sauna effect on stress corrosion cracking
- d. Hydrogen embrittlement (HE)
- e. Influence of radioactive radiation on pitting corrosion, stress corrosion cracking and hydrogen embrittlement.

**Issue (a).** Corrosion in pure oxygen-free water is discussed in detail in section 4.3. It is concluded that copper corrosion by pure water has a much higher equilibrium hydrogen pressure than that of pure and dry  $\text{Cu}_2\text{O}$  since at least two more strictly anoxic corrosion products exist,  $\text{CuOH}$  and a hydrogen containing and somewhat distorted  $\text{Cu}_2\text{O}$ -crystal, see Figure 4.2. It is confirmed by Ab-initio calculations that the hydrogen equilibrium pressure is around 1 mbar for  $\text{CuOH}$  /Belonoshko A.B. and Rosengren A. 2012/. Since issue (a) also includes oxygen-free water corrosion in general it should be added that internal corrosion is found to take place as hydroxide formation ( $\text{CuOH}$ ) inside the copper metal when exposed to anoxic ground water, as shown in section 3.6. This internal corrosion process with  $\text{CuOH}$  is also confirmed by Ab-initio calculations /Korzavyi P. and Sandström R. 2014/. SKB has not incorporated these anoxic corrosion processes in the safety analysis. In the Supplementary information it is discarded as negligible which is obviously not true, since the internal corrosion by hydroxide formation can penetrate the copper canister within some few hundred years, as shown in Figure 3.13.

**Issue (b).** Pitting corrosion due to reaction with sulphides are described in sections 4.6.1 (FEBEX-project, Switzerland), 4.6.2 (ABM-project, Sweden) and 4.6.3(VTT SRB-project, Finland). All three projects detected pitting corrosion on unalloyed copper in different anoxic environments containing various sulphide-concentrations. The natural groundwater sulphide content was used in both the Swiss FEBEX-project and the Swedish ABM-project, i.e. possibly up to  $10^{-4}\text{M}$ . The Finnish VTT-project used synthetic ground water with sulphate which during anoxic conditions will be in equilibrium with sulphide, possibly up to  $10^{-3}\text{M}$ . The important conclusion is that unalloyed SKB-copper is susceptible to pitting corrosion when exposed to repository conditions and that the sulphur/sulphide content and natural SRB content has a clear impact on the pitting corrosion rate. A pitting corrosion rate of  $175\mu\text{m}$  was measured with the somewhat higher sulphur content and the presence of natural SRB, at only  $12^\circ\text{C}$ , in the Finnish project. Knowing that the Sauna effect with sulphur (and chloride) salt enrichment will be operating for more than 1000 years, see Chapter 2, it is obvious that several localised corrosion processes such as sulphide/SRB induced pitting corrosion will occur. SKB has made the conclusion in the Supplementary information that pitting corrosion “seems unlikely”, see section 4.7. This conclusion is obviously incorrect.

**Issue (c) and (d).** Stress corrosion cracking and hydrogen embrittlement. In reality, it is virtually impossible to distinguish between SCC and HE cracks in unalloyed copper when exposed to an anoxic environment containing hydrogen sulphide ions (HS<sup>-</sup>), such as in a deep repository environment. It is stated in the handbook entitled “Stress Corrosion Cracking Theory and Practice” /Raja V.S. and Shoji T. 2012/ that “SCC in some materials can involve generation and ingress of hydrogen at crack tips, and characteristics and mechanisms of SCC and HE have a lot in common.”

With this scientific background it is logical to incorporate issue (c) and (d) together since these are entangled and not possibly to fully separate in the case of copper in a repository environment. SCC and HE in a repository environment are described in sections 3.1 to 3.11, in which section 3.5, 3.6 and 3.9 are more focused on HE, including hydrogen sickness (HS). SKB seems not to believe in the new compelling results from the latest years which are compiled in the mentioned sections concerning SCC and HE/HS. SKB tries to explain the extensive crack formation in these studies by “manufacturing defects” and that “SCC has questionable scientific support”, the latter speculation could have been correct with the limited scientific knowledge before 2008, but not anymore. In case of a Forsmark repository with the prevailing Sauna effect (salt enrichment), it can be concluded that these issues (c) and (d) will be responsible for all early canister failures, i.e. up to 40% already within 100-200 years as discussed in section 3.11. More specifically, failures due to HE a HS will dominate since these degradation processes operate without any applied load, in contrast to SCC.

**Issue (e).** Influence of radioactive radiation on pitting corrosion, stress corrosion cracking and hydrogen embrittlement. The effect of radiation is discussed in detail in Chapter 5. It can be concluded that SKB has not performed any study on;

-radiation and pitting corrosion

-radiation and stress corrosion cracking

-radiation and hydrogen embrittlement

in a relevant repository environment (groundwater) or any multi-combination of these issues.

This implies that the uncertainties remain regarding the influence of radioactive radiation on pitting corrosion, stress corrosion cracking and hydrogen embrittlement.

SKB:s supplementary information as a response to the Swedish Ministry of Environment is consequently not complete. The Swedish Land and Environment Court statement published in early 2018, in which SKB’s plans were judged to be acceptable only if this additional information is provided, is therefore not fulfilled. To conclude, the basis for compliance to the environmental code is missing.

## 2. Salt enrichment in the deposition holes, the Sauna effect

### 2.1. Short summary

There are several SKB-reports concerning the Sauna -effect and the results are disappointing in several ways. Firstly, it is clear that it is impossible to inject water in the deposition holes without destroying the bentonite rings with cracking and piping. Secondly, water, as steam and moisture, will escape through the cracks and slots from the heated deposition holes and condensate in the colder tunnel above, thus accumulating sulphur and chloride salts in the holes. Thirdly, the salt enrichment which induces several severe corrosion processes on the unalloyed copper canister will continue until saturation/swelling is reached in the whole repository tunnel (fully flooded and pressurized). This insight is indicated in TR-17-15 /Sellin P. et al. 2017/, page 117, quote: *“The displacements (with cracks and channels) that take place are to a large part expected to be reversed by the late swelling of the other parts of the buffer”*. Finally, in a Forsmark repository, this saturation/swelling process of the tunnels that will create a proper counter pressure to neutralize the Sauna effect will unfortunately take several thousand years which is devastating for the life time of the copper canisters. In fact, the bentonite rings in the deposition holes will be destroyed as well by mineralization and cementation in a Forsmark repository. It can be concluded that SKB has not submitted any new information or studies concerning the sauna effect on pitting corrosion and stress corrosion cracking which was requested by the environmental court.

### 2.2. The Sauna effect- introduction

The major problem with a deep repository in the Forsmark site is the unusual slow ground water ingress which will jeopardise the barrier function of both the bentonite buffer and the copper canister. Each canister evolves 1700 W as heat which will generate temperatures on the outer surface close to 100°C and the bedrock surface in the deposition hole will reach 60°C. The temperature in the tunnel above the deposition holes will be stable around 12°C. Thus the groundwater that flows directly into a deposition hole will evaporate and condense in the colder tunnels. Different salts, i.e. chlorides, sulphates and sulphides will then be enriched in those deposition holes.

An argument against the seriousness of this Sauna effect or salt enrichment process has been that a counter pressure from the tunnel should stop the process. This could only happen if the tunnels would be water saturated sufficiently fast, which actually was the original idea with the KBS-3 model. However, it is expected to take a few to several thousand years to saturate and pressurize the repository in Forsmark /Sellin P. et al. 2017/, i.e. the bentonite buffer will not work properly for a long time, if ever. Thus, the “sauna” effect will result in severe salt enrichment and copper corrosion and a significant amount of premature canister failures in a Forsmark repository, these problems will be discussed in detail here.

## 2.3. Background data and information taken from different SKB-reports

Background data concerning the deposition holes, canisters and tunnels and general physical and chemical data connected to the Forsmark repository will be listed up below in bullet point's denoted a-j without any mutual ranking.

a) The drilled deposition holes in the bed rock have a diameter of around 1.8 meter and thus an area of 2.54 m<sup>2</sup>, see Figure 2.1.

b) The groundwater is highly pressurized at 500 meter depth, i.e. 50 bar which is around 15 times higher pressure than in normal tap water. An example of seeping groundwater in a drilled hole in Äspö hard rock laboratory at normal repository depth is shown in Figure 2.2.

c) The saturation pressure of 50 bar corresponds to 5 million Pa (N/m<sup>2</sup>) or 500 ton per square meter. The force on the bentonite top blocks in a deposition hole with seeping groundwater would thus reach more than 1200 tons if they would be hermetically tight. The only possibility to stop the water/moisture transport and bentonite ring cracking and push out from a heated deposition hole would be to create an equally high counter pressure from above, i.e. a fully water and pressure saturation of all bentonite in the whole deposition tunnel.

d) A fully flooded and saturated deposition hole with bentonite rings and a copper canister will contain 6.45 m<sup>3</sup> groundwater (SKB-TR 17-07).

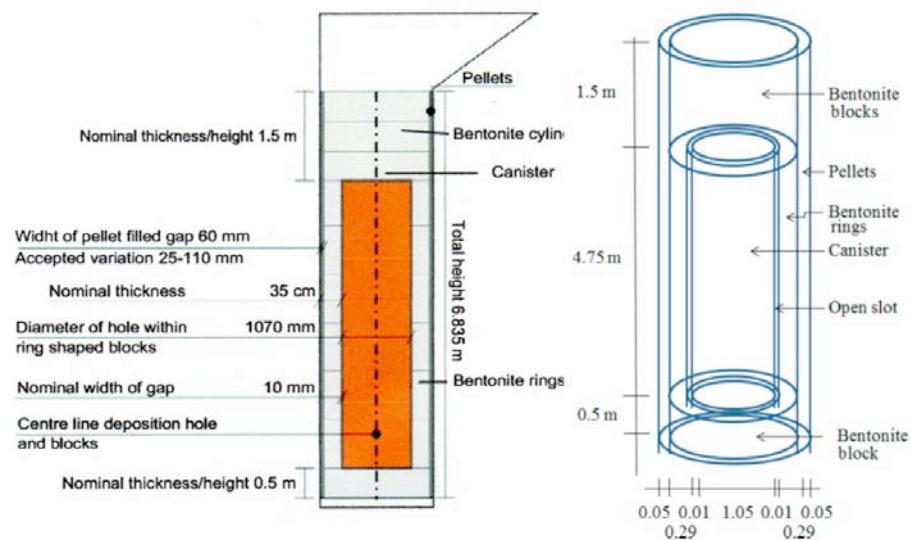


**Figure 2.1.** Configuration and geometry of the deposition hole with copper canister and bentonite buffer. From SKB-report TR-14-12 (to the left) and from SKB-report TR-17-15, Figure 9-1 (to the right). The drilled hole in the bed rock has a diameter of around 1.8 meter.



**Figure 2.2.** From Figure 3 in SKB-report R-05-44. Typical inflow pattern in Äspö hard rock laboratory showing high pressurized groundwater seeping out of a drilled rock surface. This photo is taken from a depth of only 220 m, i.e. the water pressure is around 22 bar, only half of that prevailing in a real repository. The cracks in the deposition holes in Forsmark are believed to be smaller but the pressure of the ground water is still 50 bar.

e) The groundwater at the Forsmark site contains around 0.95 wt-% mixed salts containing chlorides, carbonates, sulphates and sulphides, see Table 1.1. Unalloyed copper reacts with all of these species also under strictly anoxic (oxygen free) repository conditions since water molecules (moisture or liquid water) are present, see further Chapter 4.

Predicted groundwater composition for a repository at Forsmark (contents in mg/dm<sup>3</sup>)

	At emplacement	After saturation (<100 years after emplacement)	10000 years into the future
pH	6-8	7.0-7.9	7-9
$E_{\text{redox}}^*$	0 to -400	-200/-250	-200 to -300
Na <sup>+</sup>	300-2000	1700	100-1000
K <sup>+</sup>	2-13	13	2-10
Ca <sup>2+</sup>	150-1650	1650	20-1000
Mg <sup>2+</sup>	17-110	110	4-100
HCO <sub>3</sub> <sup>-</sup>	50-300	47	20-40
Cl <sup>-</sup>	500-5000	5500	200-5000
SO <sub>4</sub> <sup>2-</sup>	40-400	370	1-400
HS <sup>-</sup>	0-10	<0.01	0-1

\* mV SHE.

**Table 1.1.** Groundwater composition in the Forsmark repository. The higher range of sulphate and sulphide concentrations are around  $4 \times 10^{-3}$ M and  $3 \times 10^{-4}$  respectively /Rosborg B. and Werme L. 2008/.

f) The copper canister bentonite interface temperature peaks around 95°C after 20 years and is still around 40°C after 1000 years.

g) Approximately 20% of the deposition holes in Forsmark have at least one water seeping crack of significance (SKB TR-17-15), i.e. around 1384 copper canisters

will more or less directly experience the Sauna effect, see Figure 2.3. 854 deposition holes have an inflow of more than  $10^{-5}$  L/min ( $\geq 53$  litre/year) and 395 deposition holes has an inflow of more than  $10^{-4}$  L/min ( $\geq 530$  litre/year).

h) At least 10%, i.e. around 700 additional deposition holes (without seeping cracks), are situated close (some few meters) from a major water seeping crack in a deposition tunnel (SKB TR-17-15).

i) According to the authors in the original report SKB P-07-162 it can be concluded that the representative hydraulic conductivity ( $K_m$ ) of in situ conditions (pressurized bed rock) in Forsmark at 500 meter depth varies between  $10^{-13}$  to  $10^{-14}$  m/s (experimental measurements:  $1.6 \times 10^{-13}$  to  $6.4 \times 10^{-15}$  m/s). Matrix ground water flow in the bed rock means transport through microscopic porosity and cracks. These measurements show that the ground water transport through the bed rock matrix in Forsmark at 500 meter depth is particularly slow.

j) Given the low hydraulic conductivity in Forsmark, see point (i) above, there will be a distribution between 1500 to 15.000 years to flood and saturate all bentonite in the deposition holes and tunnels with water, see Figure 2.4. No deposition hole can be fully saturated before the whole tunnel is fully water saturated and pressurized. Around 50% of the deposition holes will be saturated after 3000 years and it will take up to 15.000 years to fully saturate the Forsmark repository and it will do so by water transport through the bed rock matrix (microscopic cracks) as well as by bed rock macroscopic cracks.

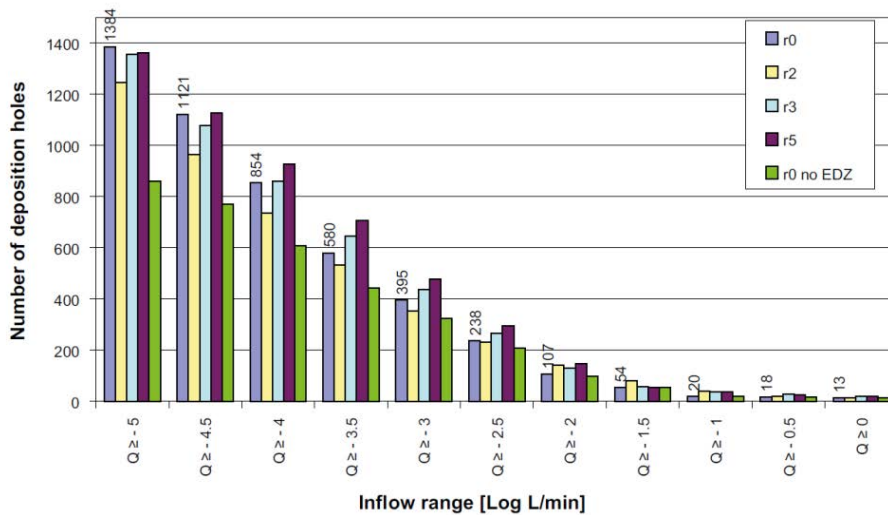


**Figure 2.3.** From SKB-report R-13-21, Fig. 3.4. Complementary cumulative distributions of the total inflow to each deposition hole for each case. According to case r0 (the five simulations r0-r5, give roughly the same outcome) there are 1384 deposition holes out of 6916 that have at least one crack that gives an inflow of ground water more than  $10^{-5}$  L/min ( $\geq 5.3$  litre/year). 854 deposition holes have an inflow of more than  $10^{-4}$  L/min ( $\geq 53$  litre/year) and 395 deposition holes has an inflow of more than  $10^{-3}$  L/min ( $\geq 530$  litre/year).

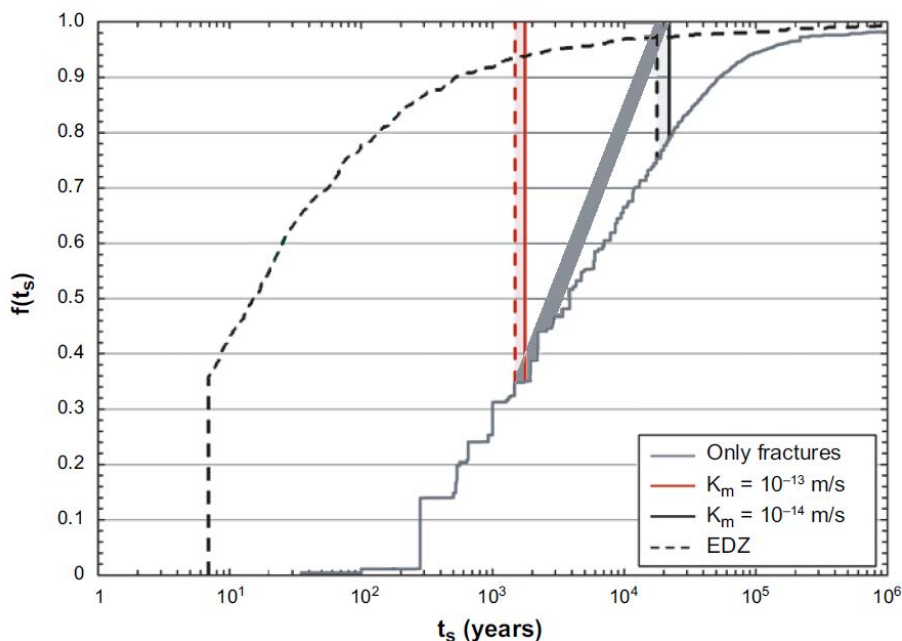


**Figure 2.4.** Modified graph based on Fig. 7-15 in /Sellin P. et al. 2017/. The solid grey line identifies the cumulative distribution of saturation times,  $f(t_s)$ , in the Forsmark repository calculated assuming no matrix flow, i.e. only flow via macro cracks. The vertical lines (red and black) identify the time interval within which all deposition holes will reach full saturation if the matrix hydraulic conductivity has the value  $K_m = 10^{-13}$  m/s and  $K_m = 10^{-14}$  m/s respectively, see point (i) above. The fat grey line represents a linear distribution (realistic simplification), taking into account the variations in measured  $K_m$  values in Forsmark. It is thus indicated that the last tunnel and deposition holes with the lowest hydraulic conductivity will be water saturated only after  $\geq 15.000$  years by matrix inflow and that it takes around 3000 years to saturate 50% of the deposition holes, mainly by cracks in the deposition holes and tunnels. The dashed black line identifies the distribution of saturation times if no flow resistance was present in the tunnels (only of theoretical interest).

## 2.4. SKB reports concerning the Sauna effect

Basically all SKB-reports concerning the Sauna effect /Birgersson M, Goudarzi R, 2013, 2016, 2017 and 2018/ have actually confirmed that unpressurized bentonite will experience displacements, cracking and piping in contact with liquid ground water, as shown in Figures 2.5 and 2.6. However, these cracking and piping processes should not be so dangerous according to SKB; “*The displacements (with cracks and channels) that take place are to a large part expected to be reversed by the late swelling of the other parts of the buffer*”, see page 117 in TR-17-15 /Sellin P. et al. 2017/. Obviously these displacements and cracks will occur in the bentonite blocks in the tunnels as well as in the deposition holes when in contact with ground water. The “late swelling” is most troublesome, since it might take several thousand, up to around 15.000 years (see point j) in a Forsmark repository, if at all, to “reverse” the cracks and water channels in the bentonite buffer. The important bentonite buffer barrier will thus not work during the most critical hot period and the unalloyed copper corrosion rate will not be reduced by any diffusion barrier.



**Figure 2.5.** From SKB-report TR-17-15, Fig 2.9. SKB has shown in several reports that it is impossible to add water to bentonite blocks without severe cracking under normal pressure.



**Figure 2.6.** From Figure 2-8 in SKB TR-15-09. Left: Test 3 at termination. Right: Bottom side of the bentonite ring showing a condensation “nucleus” and cracks. Severe cracking of the bentonite rings occurred already within 7 days, which was the experiment duration time.

SKB claims in the supplementary information, TR-19-15, section 3.2.1, page 34 /Hedin A. et al. 2019/ that virtually no water will escape to the tunnel through the top bentonite blocks. When reading the reports that SKB used as a basis for that conclusion, it is obvious that it has no scientific support, as will be discussed in detail in next section, 2.4.1.

#### 2.4.1. Detailed comments on TR-15-09 and TR-17-07, concerning tests 1-9 of the Sauna effect

These reports constitute the main studies financed by SKB regarding the Sauna effect, i.e. the water evaporation and salt enrichment process in the deposition holes.

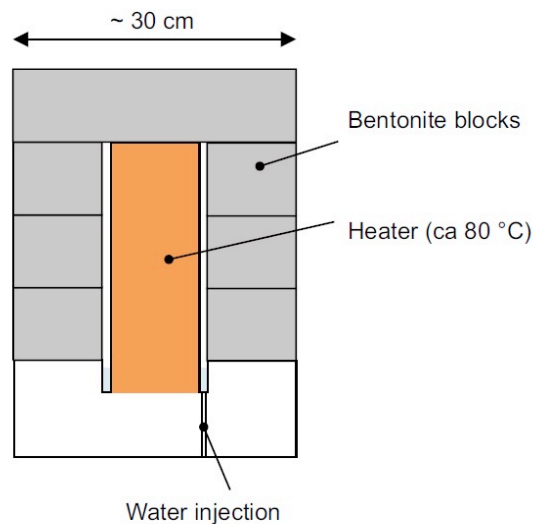


**Figure 2.7.** From Figure 2-1 in TR 15-09. The test set-up, which to a certain extent is a model of a KBS-3 deposition hole. Mounted on a plastic plate is a copper tube which is heated by circulating water to approximately 80 °C. “Water injection” seen to the left is actually a hole for low pressure water vapour to enter the slot between the Cu-heater and the bentonite rings. The outside of the set-up was covered by a plexiglass tube (not visible here).

Fundamentally, the set-up for Sauna tests 1-9, TR-15-09 and TR-17-07, has a known major flaw concerning the water supply system compared to the real repository situation. In reality the major supply of water will be by liquid water seeping out from bed rock cracks as shown in Figure 2.2 and not as moist air as in the set-up, see Figure 2.7. The authors Birgersson and Goudarzi, as well as SKB, are fully aware of that it has been proven impossible to inject liquid water without destroying the bentonite buffer totally with cracks and piping, as shown in Figure 2.5 and 2.6. The only way to solve this fundamental problem for the whole concept of KBS-3 is to apply a proper water counter pressure of 50 bar, i.e. reach saturation in the tunnels, so the cracks and piping would eventually heal, but unfortunately that will occur far too late in a Forsmark repository. The proper counter pressure in the tunnels will only be reached after around 2000-15.000 years, see Figure 2.4, thus the “sauna”-effect will be impossible to stop for several thousands of years in Forsmark. The main four arguments, already listed up in the Abstract in TR-17-07 that are claimed to indicate that “severe amount of salt in a KBS-3 deposition hole during the saturation process is highly unlikely and can be disregarded” are based on experiments that are not relevant due to several reasons:

1) Flawed water supply system in the used set-up, unpressurized moist air instead of seeping pressurized liquid water as it would be in a real repository, see description above. This point is fundamental and makes it impossible from this set-up to make any conclusions regarding the Sauna effect in a Forsmark repository.

2) Too short exposure times and thus too little water was added in the used set-up. The experiments which SKB refer to as relevant for calculating the seriousness of the Sauna effect are test 5 and 6. The volume of the bentonite rings used in the set-up can be estimated to be around 40 dm<sup>3</sup> and the water added was far too little to give any true indications of the Sauna effect:

-Test 5: In total 1.4 litre tap water without salt was added as ambient moist air during 21 days exposure.

-Test 6: In total 0.7 litre tap water without salt was added as ambient moist air during 90 days.

At least the same volume of water as the simulated deposition hole, i.e. 40 litre of water should have been injected during a sufficient long period to avoid flooding of the equipment. Furthermore, liquid water should have been injected directly to the bentonite and the water should be saline, not tap water, in order to have any implication on the seriousness of the Sauna effect.

3) The temperature gradient is not relevant in the test set-up. All bentonite in a given cross-section will be heated up significantly including the surrounding bed rock in a real deposition hole which means that a major part of the formed water vapour will condensate in the cold tunnel of around 12°C above the deposition hole, thus a vertical water transport out from the deposition hole is promoted. The outer part of the bentonite rings in the described set-up is effectively cooled by air convection in the room and the top part is not colder than the ambient temperature thus a vertical water transport is not promoted in a realistic way.

4) The only test that used salt water was Test 7 and that exposure did experience real Sauna effect with massive copper corrosion during only seven days of salt exposure, see Figure 2.8. However SKB omitted to discuss this at least more relevant test in their supplementary report TR-19-15.

Interestingly it is noted in the conclusions in TR-15-09 that “Vapour was shown to be able to be transported rather far in this types of slots without substantially being absorbed by the bentonite; a substantial amount of water was lost to the environment in tests where the slot was directly opened to the environment (test 2 and 3)”. This is relevant since the “open slots” can be compared with the cracks and piping in a real deposition hole in connection with the surrounding environment, i.e. the cold tunnel above. Thus test 2 and 3 imply a devastating Sauna effect with fast water transport and thus severe salt accumulation that will last for thousands of years until saturation of the tunnels is reached in Forsmark.



**Figure 2.8.** Detail from Figure 2-27 in TR 15-09. Severe corrosion of the copper heating tube after only seven days of laboratory exposure that at least reminds of the true Sauna effect, i.e. with only indirect contact with 0.6M chloride solution.

## 2.5. Detailed analysis and consequences of salt enrichment in a Forsmark repository (Sauna effect)

The deposition holes will basically be flooded/saturated in three different ways:

- i) by internal ground water bearing cracks in the deposition hole, around 1400 out of around 6916 deposition holes, see Figure 2.3.
- ii) by larger water bearing cracks in the tunnel. The seeping groundwater creates displacements and cracks in the bentonite blocks and eventually water paths and channels, preferably at the bentonite/bedrock interface at the tunnel floor due to gravity. The water channels will eventually reach the deposition holes and continue to create displacements and cracks in the bentonite rings around the heated copper canister thus starting the evaporation and salt enrichment process in those deposition holes. Around 40% of the deposition holes are expected to be flooded via larger cracks in the deposition holes or in the tunnels, i.e. around 2800 deposition holes, see Figure 2.4. Apparently, half of those, 1400 deposition holes (2400-1400), will be flooded via larger cracks in the tunnel.
- iii) the remaining 60%, around 4100 deposition holes, will be flooded by micro crack and porosity in the bed rock, i.e. matrix ground water flow and it will take around 3.000-15.000 years to reach saturation, see Figure 2.4.

The Sauna effect will have a severe impact on the copper corrosion during the first 1000 years since the temperature difference is large between the deposition hole (95°C to 40°C) and the cold tunnel above the deposition hole (around 12°C). However, salt enrichment in the deposition holes with increased copper corrosion will continue until the accumulated salt is dissolved which will take around 3000 years for half of the deposition holes when saturation is reached. For tunnels with restricted inflow from macroscopic cracks and with a bed rock hydraulic conductivity in the lower region, around  $10^{-14}$  m/s, it will take at least 15.000 years to dissolve the salt and stop the Sauna effect, see point (j), at page 6.

The most disturbing fact with the Forsmark repository is that the copper corrosion will be accelerated by salt accumulation and basically without any corrosion reduction by the bentonite buffer during the first thousands of years since no saturation is obtained. The first thousand years is critical to unalloyed copper since the corrosion rate roughly doubles with every 10 degrees of temperature increase /E. Mattsson 1997/. When unalloyed copper is heated to 80-90°C in moist environment with high concentration of mixed salts (chlorides, sulphates, sulphides and carbonates etc.) a corrosion rate of 300 micrometers per year (0.3 mm/year) should be expected. Most importantly, there are additional rapid degradation processes such as stress corrosion cracking (SCC), hydrogen embrittlement (HE), hydrogen sickness and radiolysis operating on the copper canisters, see further Chapter 3 and 5. When only considering the salt accumulation induced copper corrosion, i.e. a mix between atmospheric corrosion, general corrosion and pitting corrosion, following conclusions can be drawn (based on case r0, see Figure 2.3):

- 395 deposition holes/canisters will have an inflow larger than 530 liter per year corresponding to more than 5.3 kg mixed salts per year, see point (g) at page 6. Since unsaturated bentonite cannot hinder any transport (k) severe corrosion will occur. With this massive inflow of salt and freely evaporating water already when the canisters reaches its peak temperature around 90°C it can be concluded that all of them will collapse within 300 years already by general corrosion and pitting corrosion.
- 459 deposition holes/canisters (854-395) will have an inflow larger than 53 litre per year corresponding to more than 0.53 kg mixed salts per year (g). These canisters will experience almost the same corrosion rate as the previous 395 canisters since the local salt concentration will still be high enough within some

tenth of years albeit the canister maximum temperature might appear before the local corrosion environment has reached its peak in terms of corrosiveness. All canisters in this category are expected to collapse within 500 years and perhaps half of them within 300 years due to salt accelerated copper corrosion.

- 530 deposition holes/canisters (1384-854) will have an inflow larger than 5.3 litre per year corresponding to more than 0.5 kg mixed salts per year (g). Which still corresponds to more than 500 kg salt during the first one thousand “hot” years, i.e. with both heat and radiolysis. The fact that the all salt is inhomogeneously distributed or even accumulated locally in the respective deposition hole makes it most likely that all 530 canisters will collapse within 1000 years.
- The remaining 5532 canisters (80%), will slowly be saturated via cracks in the tunnels in combination with ground water matrix transport or solely by matrix transport which will take 3000 to 15000 years depending on the hydraulic conductivity in each tunnel. A slow salt accumulation will thus take place in all these deposition holes under a very long time period until saturation and salt dissolution initiates. Unalloyed copper will be seriously weakened due to salt induced corrosion and when the full pressure of 50 bar is applied on the canisters is most likely that the canisters will collapse. Thus one possible assessment would be that the failure distribution follows the saturation distribution according to the thick grey line in Figure 2.4. Important notice, this failure distribution is certainly not conservative since, as mentioned, SCC, HE, hydrogen sickness and radiolysis will shorten the canister life time in the whole population further, as will be discussed further in Chapter 3.

The Sauna effect will also destroy the bentonite buffer, as shown in Figure 2.9. When the salt crystals precipitate in the bentonite it will convert the clay to a brittle and cracked mineral “cake” for several thousand years and most likely it will never regain its original swelling and diffusion barrier properties.

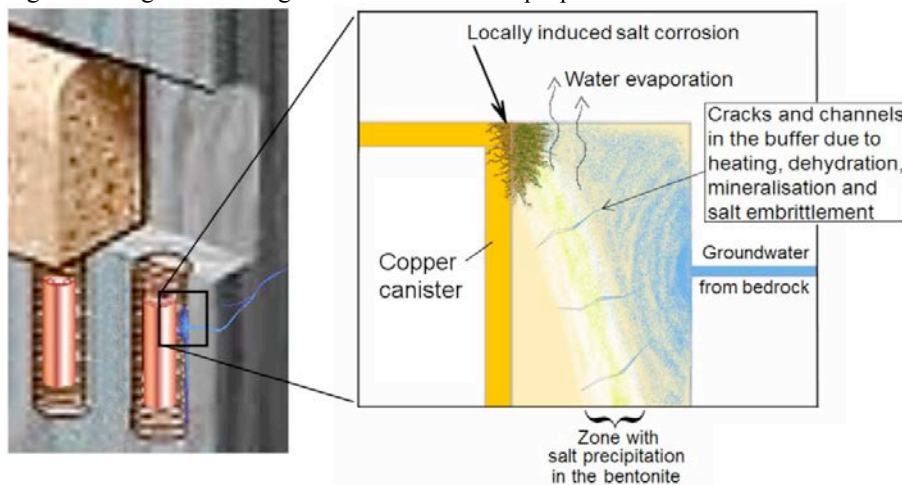


**Figure 2.9.** The Sauna effect in a repository with water evaporation, salt enrichment and copper corrosion. Furthermore, the precipitated salt will destroy the properties of the bentonite buffer /Szakálos P. and Seetharaman S. 2012/.

Professor Roland Pusch /Pusch R. 2019/ explains that "locally induced salt corrosion" occurs along the canister's entire mantle surface because the temperature is substantially higher at the canister's half height than at the ends, leading to dehydration and an open gap along the entire mantle surface. "Water evaporation" from the buffer clay up through the backfill in the tunnel therefore occurs in the gap along the entire mantle surface and the mechanical ("effective") swelling pressure there will be low for a very long time in a Forsmark repository. Up to a distance of 10-20 cm from the canister surface of the canister, mineral conversion from

“expandable smectite” to “non-expandable illite” (hydrous mica) will occur, thereby releasing silicon which precipitates as a cementing substance. Since horizontal and vertical drying cracks are formed before the silicon has been released and diffused into the buffer, these cracks will be filled with silicon aggregates and create precipitates that have much higher water permeability than the buffer clay in uncemented condition. When the temperature in the buffer clay begins to drop after 50 years and groundwater eventually penetrates, the silicon fillings will not provide self-healing but will remain as permeable layers in the clay. In other words, a devastating short-cut concerning the diffusional transport barrier properties of the bentonite. The scientific references supporting these conclusions are /Pusch, R. et al 2019/, /Pusch, R. 2015/, /Pusch R. et al. 2015/ and /Kasbohm, J. N. et al. 2019/

## 3. Stress corrosion cracking and hydrogen embrittlement in unalloyed copper (CuOFP)

### 3.1. Short summary

There is compelling scientific evidence that stress corrosion cracking (SCC), hydrogen embrittlement (HE) and hydrogen sickness (HS) will affect the copper canisters in a repository environment. SKB seems to believe that the surface cracks and hydrogen blisters observed in the copper grain boundaries in several studies are only “manufacturing defects”. In SKB R-18-03, /Huutilainen C. et al. 2018/, page 25, it is concluded: *“The findings of Taniguchi and Kawasaki (2008), and Becker and Öijerholm (2017) of claimed small (of the maximum depth of a few tens of microns) SCC cracks on the surface of copper after SSRT experiments in sulphide containing environments can be alternatively explained as follows. The pre-existing manufacturing defects (which Becker and Öijerholm showed to exist also in the unexposed material, that had never been in contact with the sulphide containing environment) extending to the specimen surface, open up due to the effect of surface active sulphide species on the cohesive forces of the opposing surfaces of a defect.”*. This explanation has no scientific support, on the contrary, it is scientifically erroneous to claim that the cracks shown in for instance Figure 3.1 should be initiated by pre-existing manufacturing defects in as-delivered copper. Virtually all grain boundaries in Figures 3.1 and 3.4-3.7 have initiated a crack close to the main fracture and for obvious reasons this cannot be due to pre-existing manufacturing defects, instead it is a scientific proof of sulphur induced SCC in copper. It was shown in a study connected to SKB’s prototype repository /Szakálos P. and Hultquist G. 2013/ that the whole canister thickness was hydrogen charged during only 7 years exposure at elevated temperature and that the canister was subjected to internal corrosion by hydroxide. A conservative safety analysis would estimate that 40% of the canisters collapse already within 100 years after repository closure and the remaining 60% within 1000 years after closure due to SCC, HE and HS (in the welds). SKB has chosen to not include these fast degradation processes in the safety analysis, despite the even more compelling evidence of today compared with the situation during the court process in 2017.

### 3.2. Introduction SCC and HE

Stress corrosion cracking (SCC) and hydrogen embrittlement (HE) are two degradation mechanisms that are related to each other and operate closely together in many cases, such as in a deep repository environment in combination with unalloyed copper. This will be discussed in detail in this chapter in relation to the KBS-3 model and whether SKB has considered and included these most important degradation mechanisms in their complementary information and safety analysis in an adequate way or not.

The most relevant scientific publications that have a direct impact on the KBS-3 model will be summarized and discussed here.

### 3.3. Slow strain rate testing of copper performed at Japan Atomic Energy Agency (JAEA)

/Taniguchi and Kawasaki 2008/ showed that unalloyed copper (CuOFP copper) is indeed sensitive to stress corrosion cracking (SCC) in sulphide containing sea water. Multiple cracks due to SCC, preferably in the copper grain boundaries are seen in Figure 3.1.

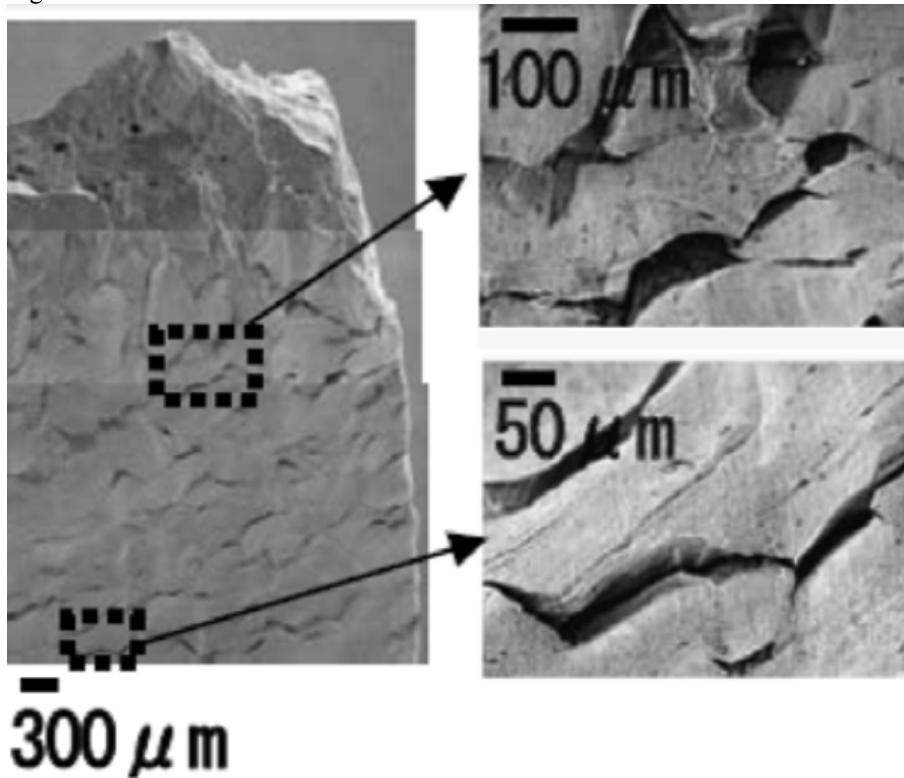


**Figure 3.1.** Fractured copper sample due to Stress Corrosion Cracking (SCC) in 0.01M sulphide containing seawater at 80°C after 7 days exposure. Initiation of minor cracks was detected at 0.001M sulphide concentration (not shown here). Slow strain rate testing (SSRT) results from Figure 10 in /Taniguchi and Kawasaki 2008/.

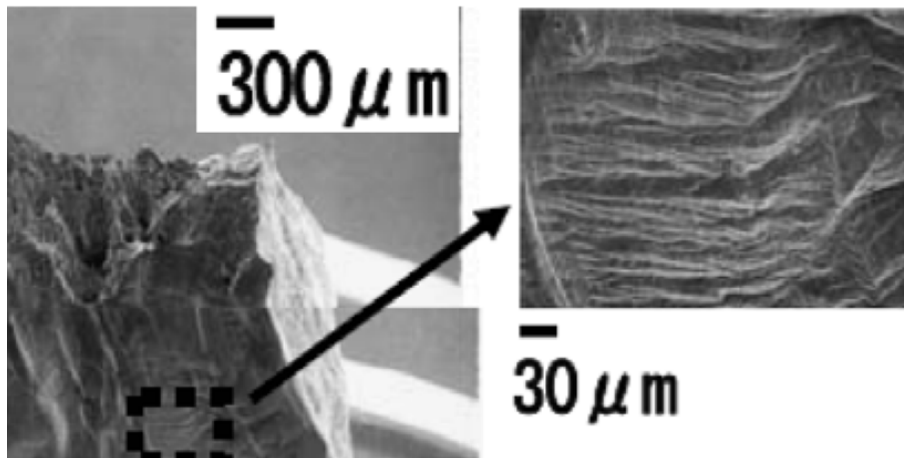


**Figure 3.2.** Crack-free copper surface when tested during the same conditions as in Figure 3.1 but with a sulphur free (inert) environment. No indication of any crack initiation visible in high magnification, see detailed micrograph to the right. Slow strain rate testing (SSRT) results from Figure 10 in /Taniguchi and Kawasaki 2008/.

Coupons were strained to fracture at a constant and ordinary extension rate of  $8.3 \times 10^{-7}$ /s. The test solutions in the cell were renewed every second or third day during the SSRTs in order to avoid decreased sulphide concentration.

The authors conclude regarding the use of copper canister in a repository: “rather early penetration due to SCC could be possible under high sulfide concentrations.” and “High sulfide concentrations could be achieved by a special process such as sulfate reduction due to microbial action. Although sulfate reduction by microbial action in buffer material is not likely to occur because sulfate reducing bacteria (SRB) can hardly proliferate in compacted bentonite”

However, there are two reasons why sulphide will be accumulated to dangerous concentrations in the Forsmark repository;

- 1) Sulphide and sulphate accumulation in the deposition holes due to water evaporation, i.e. the Sauna effect as described in previous chapter.
- 2) Sulphate reducing bacteria (SRB) convert sulphate to corrosive sulphide as will be discussed in sections 3.10, 4.5 and 4.6.3. SRB can survive and thrive in a Forsmark repository for several thousands of years since full pressure/compacted bentonite will only be achieved after such long time scales as described in previous chapter.

### 3.4. Slow strain rate testing of copper at Studsvik AB

Another important SSRT-study was performed by Studsvik AB and published in two scientific reports, /R. Becker, J. Öijerholm 2017/ and /Forsström A. et al. 2017/. Slow Strain Rate Testing (SSRT) has been frequently used within the nuclear industry for screening tests concerning SCC. However, the design life of a reactor is around 50–60 years, which is two orders of magnitudes shorter compared to the duration under which the copper material is suspected to be exposed for conditions which might initiate SCC in the final repository /R. Becker, J. Öijerholm 2017/. SSRT can be seen as a very slow tensile test with a duration of typically one to four weeks.

The specimens in this case were elongated to a certain strain, i.e. 9% at the thinnest part of the tapered samples after which any crack initiation is accounted for. With the experience from the nuclear industry it can be concluded that if cracking readily appears in SSRT under otherwise relevant exposure conditions, it is likely only a

matter of time before cracking appears in the real application /R. Becker, J. Öijerholm 2017/. The other extreme is if no cracks appear at all even if the specimen is exposed to stress equivalent to the tensile stress during prolonged SSRT. An example in this case is the nickel base material Alloy 690 TT in the non-cold worked state, which does not develop SCC under SSRT in simulated reactor environments. Indeed, the material has performed excellent in reactor applications for around 30 years, where to the best knowledge no case of SCC has been reported /R. Becker, J. Öijerholm 2017/. Thus if a material does not develop cracking during prolonged SSRT, it means that the material is very resilient towards initiation of SCC, however one can't draw the conclusion that the material is completely immune.

Testing parameters used at Studsvik AB in their experiments on SSRT: Temperature 90°C, NaCl 0.1 M, strain rate:  $7 \cdot 10^{-8} \text{ s}^{-1}$ , maximum strain: 9%. Testing time: 2 weeks.

Exposures 1 and 2 (specimen #3 and #4):  $10^{-3} \text{ M Na}_2\text{S}$

Exposures 3 and 4 (specimen #5 and #6):  $10^{-4} \text{ M Na}_2\text{S}$ ,

Exposure 5 (specimen #7):  $10^{-5} \text{ M Na}_2\text{S}$



**Figure 3.3.** Example of SSRT exposed sample, 9 % strain at the thinnest part of the tapered sample (not exposed to final fracture).

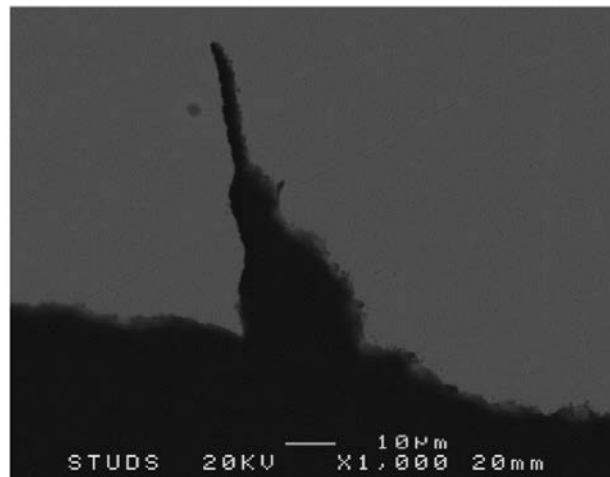


**Figure 3.4.** From Figure 16 in /R. Becker, J. Öijerholm 2017/: Specimen #3 ( $10^{-3} \text{ M}$  sulphide), SEM image of a crack observed at the narrowest part of tapered gage section.

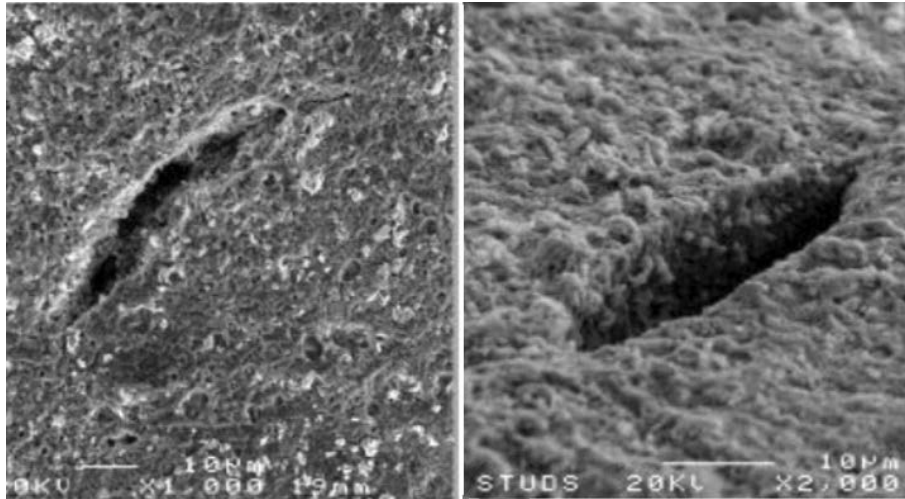


**Figure 3.5.** From Figure 2 in /Forsström A. et al. 2017/. Surface cracks near the narrowest part of Specimen #3 ( $10^{-3}$  M sulphide) after SSRT testing.

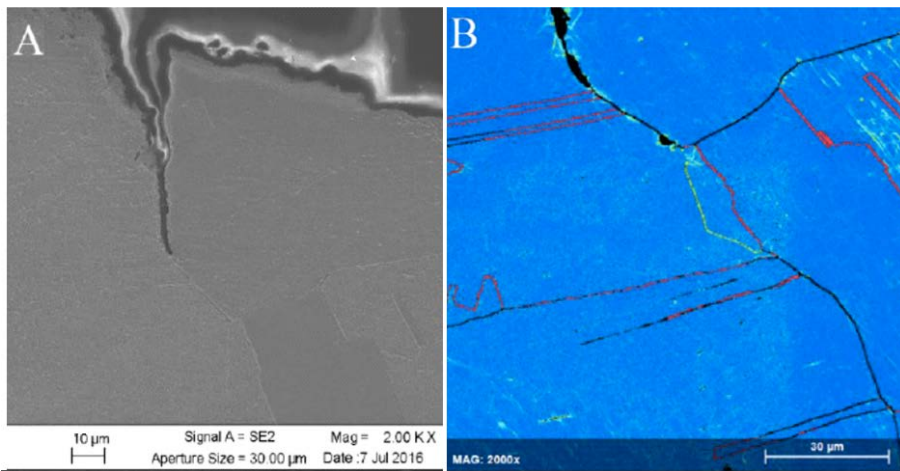


**Figure 3.6.** From Figure 3 in /Forsström A. et al. 2017/. Cross-section images of a SCC crack in the narrow section of Specimen #3. EBSD image showing crack propagation along a random grain boundary. Twin boundaries are marked in red and local misorientation in shades of green.

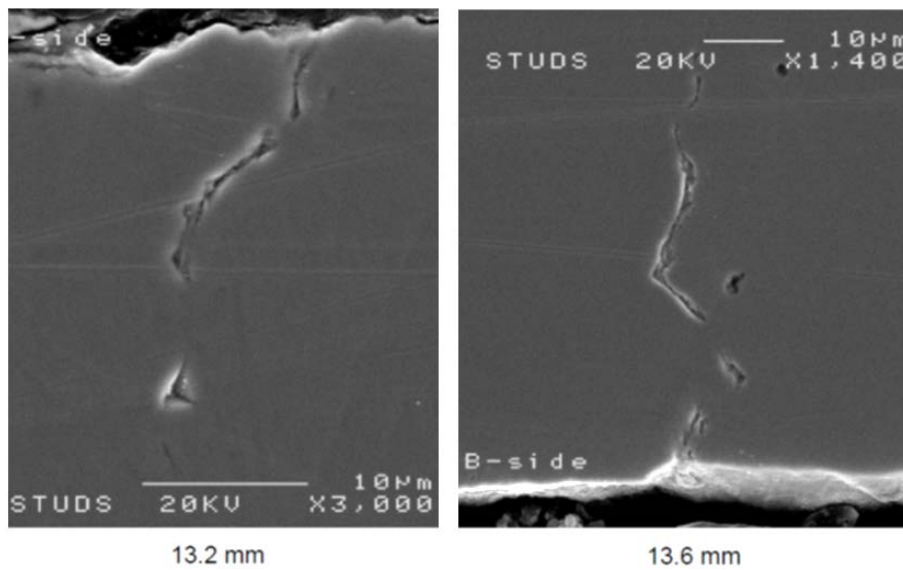


**Figure 3.7.** Part from Figure 21 in /R. Becker, J. Öjjerholm 2017/. Initiation of blisters and cracks could be detected also at lower sulphide concentrations quite far away from the narrowest part (with the highest stress) of the sample, i.e. at a distance of 13.2-13.6 mm. Exposures 3 (specimen #5) exposed to  $10^{-4}$  M sulphide.

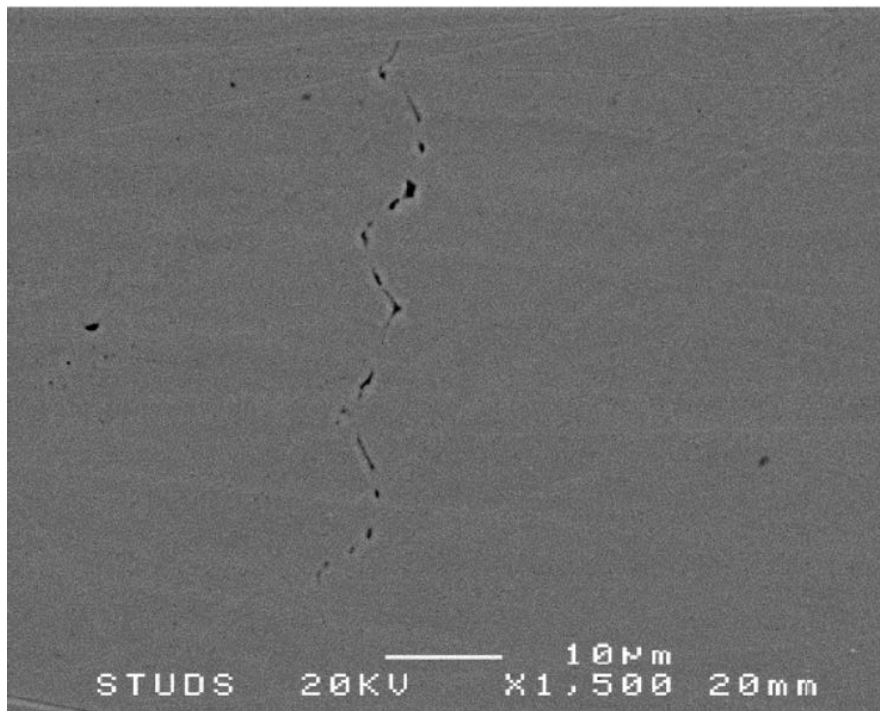


**Figure 3.8.** From Figure 22 in /R. Becker, J. Öjjerholm 2017/, specimen #5, ( $10^{-5}$  M sulphide). Defects in shape of blisters in the copper grain boundaries was detected deep inside the SSRT samples. In fact, similar defects were also found in the unloaded head section of the samples, irrespective of the sulphide content during the various exposures. These grain boundary blisters cannot be initiated by sulphur since they are formed deep inside the metal, they are instead initiated by fast moving hydrogen.

The defects  $10^{-4}$  M sulphide with only 9 % strain at the thinnest part of the tapered sample clearly shows the effect of sulphur and/or hydrogen on the initiation of SCC.

All these defects have indeed been initiated by the corrosive environment, compare with a copper sample SSRT-exposed in an inert environment, without any cracks and blisters, as shown in Figure 3.2.

### 3.4.1. Hydrogen measurement on SSRT-exposed samples

It is known that hydrogen can be transported fast in copper grain boundaries especially if they are decorated with hydrogen blisters /Forsström et al 2017/. The hydrogen content in the SSRT-exposed copper was measured by thermal desorption (TDS) and the most important conclusion, quote: “*The main finding of the TDS (hydrogen) measurements is remarkable; about two times increase of hydrogen content in the copper specimens subjected to SSRT in deoxygenated sulphide environment, when compared to hydrogen content in the as-supplied state of copper.*”

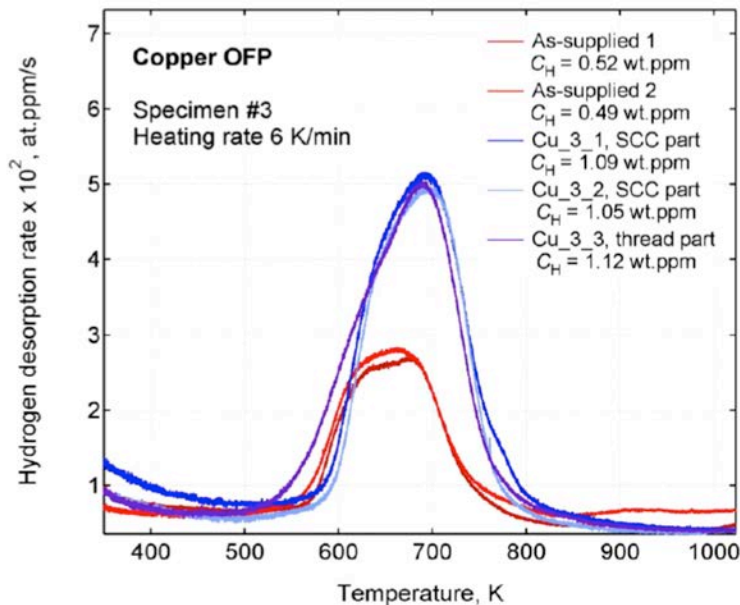


**Figure 3.9.** Hydrogen desorption curves (TDS) from /Forsström A. et al. 2017/ shows a systematically higher hydrogen content in the SSRT-exposed copper samples (blue and purple curves) compared with the as supplied SKB-copper metal (red curves). The TDS curves look similar for all tested samples, i.e. #3, #5 and #7. The systematic increase in hydrogen content in combination with the detected blisters in the inner sections of the copper samples (crack like defects, see Fig. 3.8) shows that copper exposed in an anoxic corrosive environment will suffer not only from SCC (surface cracking) but also from hydrogen induced grain boundary blisters and eventually cracking inside the bulk metal. This represents, in other words, the evidence for hydrogen embrittlement in oxygen free copper.

SKB argue that it is impossible for hydrogen to diffuse deep into the bulk metal in the thicker part of the SSRT-samples within the short time of two weeks, see page 93 in TR-19-15 /Hedin A. et al. 2019/: *At 90 °C, the diffusivity of H in Cu is around  $10^{-12} \text{ m}^2/\text{s}$ . With an approximate diffusion distance of 1 cm between the exposed part of the specimen and the unexposed sample, the diffusion time is of the order of  $0.012/(4 \times 10^{-12}) \text{ s}$  or almost 300 days, whereas the duration of the exposure was only about 14 days.*

This simple estimation based on bulk diffusion is wrong since the hydrogen has only to diffuse some few hundred micrometres, preferably in the grain boundaries, before

hydrogen blisters (and cracks) appear in the copper grain boundaries, as seen in several studies, see Figures 3.7, 3.8, 3.16 and 3.17. The effective grain boundary diffusion of hydrogen in copper with such blisters will be several decades faster than the estimation done by SKB, since hydrogen diffusion in a gas blister is instantaneous.

### 3.5. Hydrogen charging of bulk metal and welds due to copper corrosion

The only prerequisite for hydrogen embrittlement (“hydrogen sickness”) in oxygen containing copper is the presence of an anoxic environment with hydrogen on at least one side of the exposed copper metal. No load or stress in the copper metal is needed since the moving hydrogen atoms will simply react with the small oxide particles inside the copper metal under formation of water/steam blisters and eventually crack formation. In fact, this is exactly what will happen in the copper canister welds. The friction stir welds (FSW) will inevitably contain some oxygen particles. In TR-11-01 p. 173 it is stated that some oxide particles will always form in a FSW, also when using a shielding gas, especially at the inner lid/tube interface, i.e. at the root of the weld zone. /Savolainen K. et al 2008/ has studied the problem with hydrogen sickness in FSW in copper and shown that it is a real problem, see Figure 3.10.

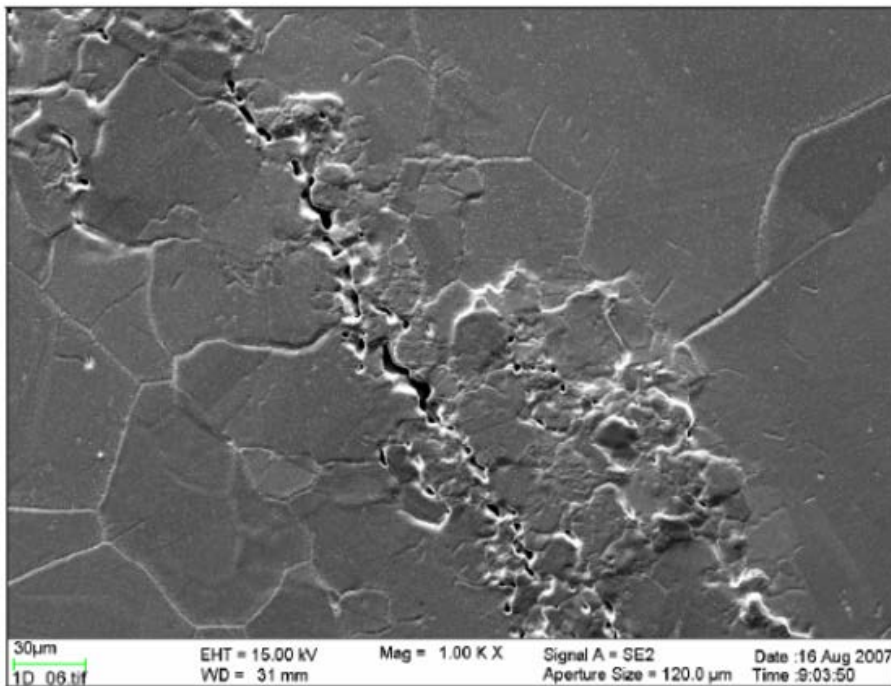


**Figure 15. Sample 1DV. Voids and heavy deformation are clearly visible at the region of entrapped oxide particles.**

**Figure 3.10.** Hydrogen sickness. SEM cross-section of a FSW in copper exposed to hydrogen at high temperature for 30 minutes, a stretch of voids, formerly as an oxide particle stretch, in the center of the FSW is visible /Savolainen K. et al 2008/.

SKB still claims in their complementary information /Hedin A. et al. 2019/, quote: *In conclusion, oxides can be detected with standard metallographic tests, and welds essentially oxide free can be produced using a properly designed gas shield.*

“Essentially oxide free welds” is not good enough since any tiny oxide particle will accelerate the hydrogen embrittlement/hydrogen sickness especially in unalloyed copper. The hydrogen charging process is driven by copper corrosion and it takes only 7-9 years in a repository environment to reach dangerous levels of hydrogen, see sections 3.6 and 3.8.

Most importantly, it is impossible to detect small oxygen particles and thin streaks of oxygen by any non-destructive testing /Björck M. et al. 2019/ and thus FSW is certainly not a safe weld method to use, at least not when welding unalloyed copper.

### *The weakest point of the copper canister, the friction stir weld*

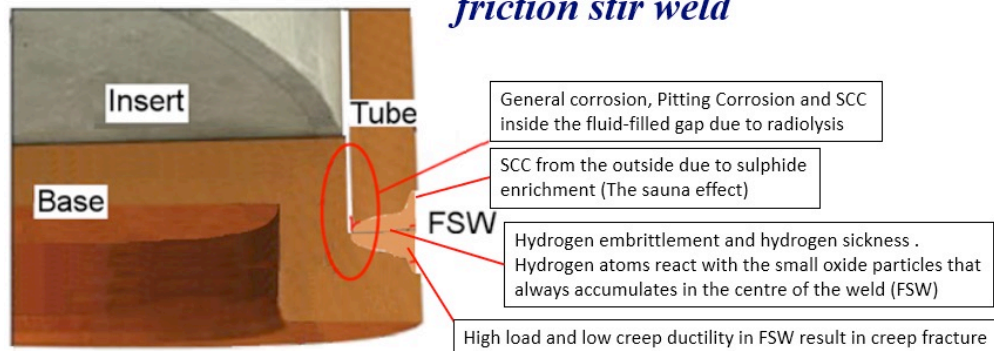


**Figure 3.11.** Detail from /Szakálos P. et al. 2017/. The weakest point of the canister is the Friction Stir Weld (FSW) and the fastest degradation mechanism is “hydrogen sickness” in the welds.

The copper canister is welded together by FSW as shown in Figure 3.11. A more detailed discussion concerning the “hydrogen sickness” in the canister welds can be found in SSM report 2012-17 /Szakálos P. and Seetharaman S./

When oxygen free copper (OFP-Cu) is considered, it seems that the copper metal must be surrounded by an anoxic environment which will induce a hydrogen charging process of the copper metal by corrosion. The copper will eventually suffer from internal hydrogen blisters in the grain boundaries and cracks, i.e. hydrogen embrittlement. It is known that a slow hydrogen charging takes place in copper metal already when exposed to pure water under strictly anoxic conditions, i.e. a slow charging process takes place by a copper corrosion reaction with water /G. Hultquist et al. 2008/ and /G. Hultquist et al. 2011/. The hydrogen content, measured by thermal desorption, increased from around 1 wt-ppm to 6-40 wt-ppm when exposed to pure anoxic water for several years. In fact, it was demonstrated that the exposed Cu-foils were embrittled by hydrogen since they failed a simple bending test after the long-term exposure in pure anoxic water /G. Hultquist et al. 2008/. Obviously, the hydrogen charging process is much faster (only 2 weeks) in corrosive groundwater containing sulphide /Forsström A. et al. 2017/ compared to slow corrosion and charging in pure water.

Normally, if an oxygen free copper tube is exposed to hydrogen on the inside but to oxygen/air on the outside it will not suffer from hydrogen embrittlement since the hydrogen gradient goes to zero at the oxidizing side, i.e. the hydrogen atoms moves only through the copper tube wall and react with oxygen molecules on the air side without causing any harm. The problematic fact of “hydrogen sickness” in oxygen containing copper and hydrogen embrittlement in oxygen free copper is that no load or stress is needed in the metal, grain boundary blisters and cracks form spontaneously by the influx of hydrogen. This is also confirmed in the SSRT-samples, see Fig. 3.8 where hydrogen blisters have been detected in the un-loaded parts of the samples.

From Discussions in /Forsström A. et al. 2017/, quotes: “The specimens were studied for hydrogen uptake during testing and the hydrogen content of copper increased from 0.5 wt.ppm to 1.2 wt.ppm during the short time SSRT testing of two weeks. This can be compared to the maximum allowed hydrogen content of copper in the KBS-3 concept, which is 0.6 wt.ppm. The current study suggests that the SCC cracking mechanism of copper in reducing anoxic sulphide environment is possibly related to hydrogen uptake in copper and hydrogen-enhanced opening of grain boundaries.” and from Conclusions in /Forsström A. et al. 2017/, quotes: “The increased hydrogen content indicates that corrosion reactions in sulphide and chloride containing anoxic conditions result in hydrogen absorption in copper even with a sulphide concentration of 0.00001 M. Similar hydrogen content in all the specimens, regardless of the environment, suggests rapid diffusion and saturation of copper with hydrogen.”

Obviously, the hydrogen charging process in these tests had reached its maximum rate already at the lowest sulphide content.

Considering the situation with the KBS-3 model when the whole copper sample, i.e. copper canister, is surrounded by an anoxic corrosive environment, it is obviously just a question of time until the whole canister is hydrogen charged and thus subjected to hydrogen blisters and cracks. This conclusion is supported by real exposures in the prototype repository, as will be discussed in next section.

### 3.6. Hydrogen and hydroxide uptake of canister copper exposed 7 years in SKB prototype repository in the Äspö Hard rock laboratory.

Measurements were performed by Gunnar Hultquist (KTH) and Mike Graham and his colleagues (NRC, Ottawa) the results were presented at a conference /Szakálos P. and Hultquist G. 2013/ and at the Land and Environmental Court in Nacka, Sweden, case no. M 1333-11, closing argument, KTH (Addendum 821).

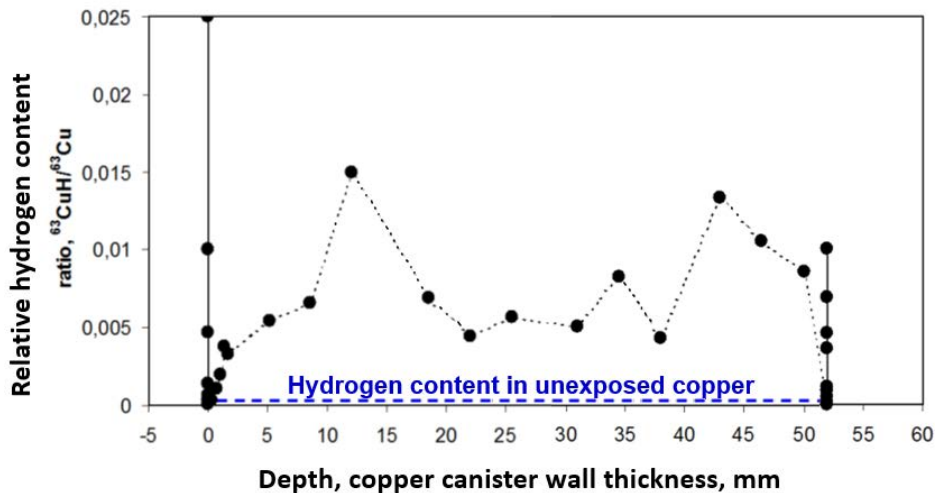


**Figure 3.12.** Full thickness canister copper exposed to the Swedish groundwater for seven years in the heated prototype repository, 80-90°C, at Äspö hard rock laboratory. The remarkable result shows that the copper canister is hydrogen charged throughout the whole thickness. The outermost surfaces have a very high H-content due to formation of corrosion products containing hydrogen and hydroxide. The hydrogen content in the first 10 mm of the inner/outer thickness has been subjected to spontaneous de-gassing when exposed to air since

the hydrogen activity in the copper metal in contact with air is close to zero. The accepted hydrogen content in canister copper is 0.6 weight-ppm which coincide with the blue dotted line (unexposed copper). The hydrogen is detected by SIMS measurements and based on the H/Cu-ratio it can be estimated that the average hydrogen content in the copper is significantly higher than 1 wt-ppm.

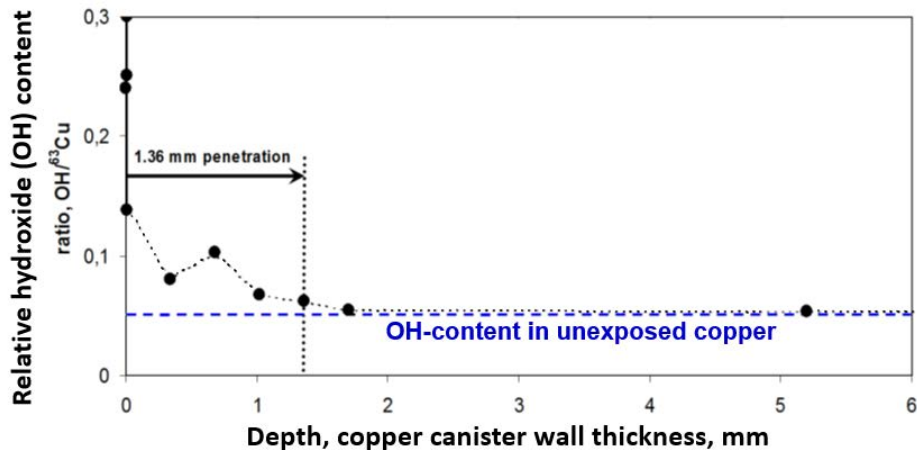


**Figure 3.13.** The hydroxide content of the first few mm of the full thickness canister copper exposed to the Swedish groundwater for seven years in the prototype repository at Äspö hard rock laboratory. The graph shows that hydroxide penetrates the copper metal, most probably in defects including grain boundaries. Once OH has entered the metal it is accumulated there, i.e. it is thermodynamically stable, i.e. evidence for internal anoxic corrosion. The hydroxide is detected by SIMS measurements.

Hydrogen atoms penetrate the whole canister thickness in shorter time than 7 years, at least when heated, as shown in Figure 3.12. The hydrogen originates mostly from the water molecules that have been actively involved in the various corrosion reactions on the copper surface that can take place in the complex chemistry of anoxic groundwater. If the concentration of hydrogen sulphide is high it is expected that most of the hydrogen in the H-charged copper metal originates from corrosion reaction with sulphide, which has surprisingly fast kinetics, as shown in /Forsström A. et al. 2017/. With an average value of only some few weight ppm of hydrogen in the copper metal it is obviously enough to initiate hydrogen blisters in the grain boundaries, as seen in Figure 3.8 /Forsström A. et al. 2017/. The penetration of hydroxide in the copper metal is much slower, i.e. 1.36 mm during the seven-year exposure, see Figure 3.13. However, it still indicates that the whole canister (50 mm) will be penetrated by hydroxides in the grain boundaries within some few hundred years. Both H and OH will increase in the copper metal when it is totally surrounded by a corrosive and anoxic environment. In fact, this is supported by Ab-initio calculations that show that both hydrogen and OH are thermodynamically stable already in a single point defect in the copper metal /Korzhavyi P. and Sandström R. 2014/. One single point defect can harbour up to 6 hydrogen atoms or, even more thermodynamically favourable, one OH species.

This means that anoxic copper corrosion takes place not only at the water/copper metal interface but also inside the copper metal, i.e. internal corrosion in the grain boundaries and other defects.

With the summarized knowledge of today it can be concluded that when the copper canister is exposed to an anoxic environment in a deep repository, it will be subjected to internal corrosion, SCC and most alarming, hydrogen blister formation in the grain boundaries, i.e. hydrogen embrittlement (HE). Based on the work by G. Hultquist regarding the SKB prototype repository it can be anticipated that 5 cm of

unalloyed copper will be penetrated by corrosion products (hydroxides) within some few hundred years and hydrogen blisters/hydrogen embrittlement may occur within some decades after the appearance of a strictly anoxic and corrosive environment. The copper canisters that will be exposed to accumulated sulphur containing salts (the Sauna effect) will be destroyed faster by SCC and HE.

### 3.7. Precracked CT-specimens under constant load exposed in sulphide containing groundwater at room temperature

/Ariilahti E. et al. 2011/ found convincing evidence for internal diffusion of sulphide from groundwater into grain boundaries ahead of crack tip in Cu OFP copper.

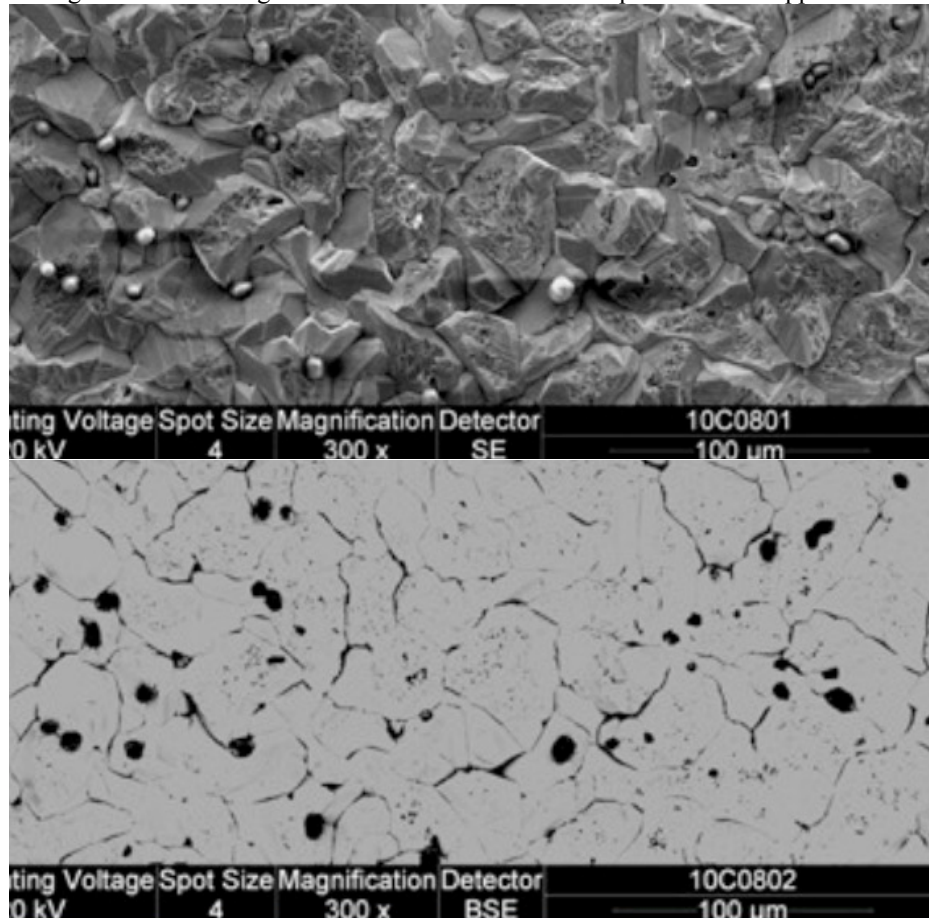


**Figure 3.14.** Detail from Figure 4 in /Ariilahti E. et al 2011/. The SEM-image at the top shows a post exposure fractured area ahead of the true crack tip for which EDS analysis showed average of 22.5 at-% sulphur. The backscatter electron image of the same area (bottom picture) shows darker sulphur-rich precipitates mostly at the grain boundaries.

It was concluded regarding the SEM-images in the paper (Fig. 3.14), quote: “*Figure 4 shows a comparison of normal and backscattered SEM images of a representative area ahead of the crack tip, revealing that there are some particles which seem like precipitates, and that also most grain boundaries that are perpendicular to the fracture surface contain a lighter phase, presumably a Cu-S precipitate.*” And from conclusions: “*These results suggest that the main driving force for the sulphur ingress into Cu OFP is the stress-strain field ahead of the crack tip.*”

It is obvious that the sulphur rich particles seen in the SEM-micrographs in Figure 3.14 are real precipitates that are incorporated in the metallographic structure, not any artefacts (dirt) produced by possibly erroneous sample preparation, as suggested in a later publication /Sipilä K, et al. 2014/ and /Huutilainen C. et al. 2018/

### 3.8. Retrieval and post-test examination of packages 4 and 5 of the MiniCan field experiment.

MiniCan is an *in situ* or field test of certain aspects of corrosion in the KBS-3 concept for deep geological disposal of spent nuclear fuel in bentonite embedded copper-cast iron canisters. The experiment is being performed by the Swedish Nuclear Fuel and Waste Management Company (SKB) at a depth of about 450 m in the Äspö HRL. The exposure time of the studied samples were 9 years. In package 4 (MiniCan 4) the canister was embedded in high density clay made from prefabricated blocks in direct contact with the copper surface, thus restricting water flow to the surface of the canister and associated samples. In package 5, there was no clay present in the experiment, meaning that the canister and samples were directly exposed to the ground water in the bore hole.

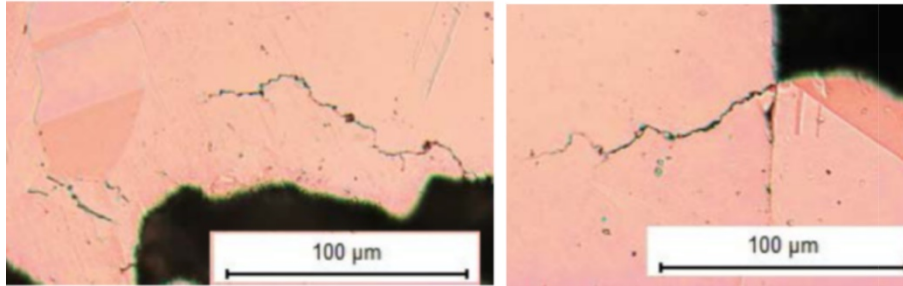


**Figure 3.15.** Details from Figure 4-7 in /Gordon A. et al. 2017/. Middle part of pre-crack of WOL sample M4 4:1 (MiniCan 4), showing smaller cracks emanating perpendicular to the direction of the main crack.

Both types of SCC samples, U-bend samples and pre-cracked samples (WOL), experienced unexpected damages and cracks as shown in Figures 3.15 and 3.16. From the report, quote:

*“These smaller cracks were notable as some of them were seen to be travelling perpendicular to the direction of the pre-crack (i.e. parallel to the load applied when fatiguing the specimens) and had more branches. These features are consistent with SCC but it is not possible to say if these smaller cracks are due to SCC in this instance or if they occurred during the original fatiguing of the samples.”*

Furthermore, post exposure hydrogen measurements showed that the copper metal was subjected to hydrogen charging and the highest value measured were around 1.8 wt-ppm (page 45) which actually is a higher hydrogen content than was measured in /Forsström A. et al. 2017/. With the knowledge of the recent publication by /Forsström A et al. 2017/ and the work by G. Hultquist, see section 3.6, it is obvious that the copper canisters are subjected to hydrogen charging and SCC in a repository environment and that it is only a question of time before hydrogen blisters and cracks occurs. The damages seen in Figure 3.16 are most likely hydrogen blisters, compare with Figure 3.8 and the feature of the thin cracks seen in Figure 3.15 are typical for SCC.

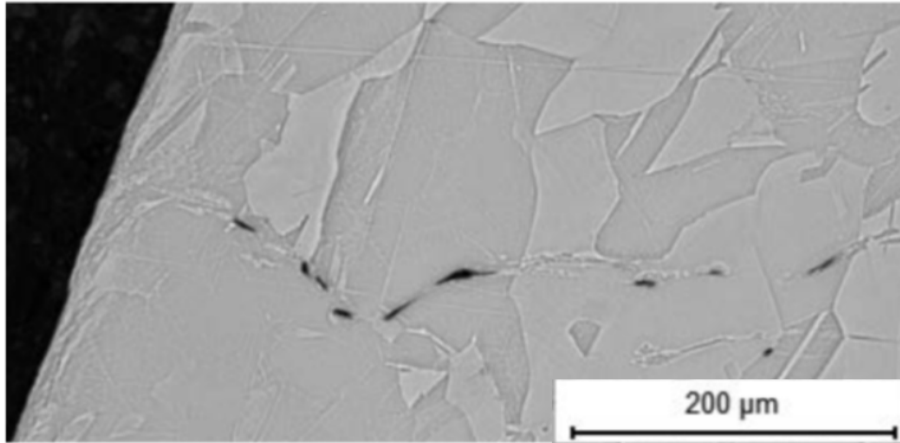


**Figure 3.16.** Details from Figure 4-5in /Gordon A. et al. 2017/. U-bend sample M4 1.1 had an area of cold deformation near the surface, but also present were pores which appeared to be aligned along the grain boundaries.

### 3.9. A study of hydrogen effects on creep ductility

Another problematic issue connected to hydrogen charging is the low creep ductility, here exemplified by Figure 3.17.

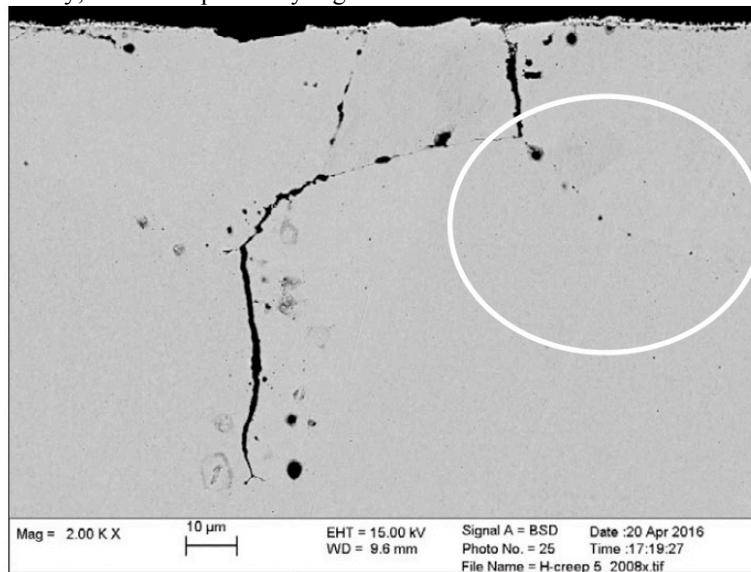


**Figure 3-8.** Specimen H-creep-05 tested at RT for 1 005.7 hours hydrogen charging time and creep stress of 170 MPa. Larger cracks were discovered. The specimen was tested in soft annealed condition without any pre-strain.

**Figure 3.17.** From /Leijon G. et al. 2017/. Hydrogen charging resulted in severe cracking, more than 100 μm deep cracks was formed already at room temperature. Hydrogen blisters was also detected in not yet cracked grain boundaries, see the encircled area.

However, SKB have made an overhasty assessment of the seriousness of hydrogen assisted creep, quote from /Hedin A. et al. 2019/ regarding the results in /Leijon G. et al. 2017/: “In their tests in which the creep rate was measured, the rate was either above or below results from standard creep tests in air indicating that the influence of hydrogen was limited and presumably smaller than the variation between samples.” More studies of hydrogen assisted creep are obviously needed before such conclusions could be made.

### 3.10. Microbial influence on corrosion of copper in the repository environment, Aalto University.

Microorganisms can accelerate canister corrosion in the nearfield in two ways, by hydrogen scavenging and by sulphide and/or acetate production. Microbial induced corrosion (MIC) by sulphate reduced bacteria (SRB) will indeed increase the SCC-failure distribution since the main effects of SRB are sulphur accumulation and conversion of sulphate to sulphide which results in SCC in unalloyed copper, as shown in Figure 3.18 /Carpén L. et al. 2016/.

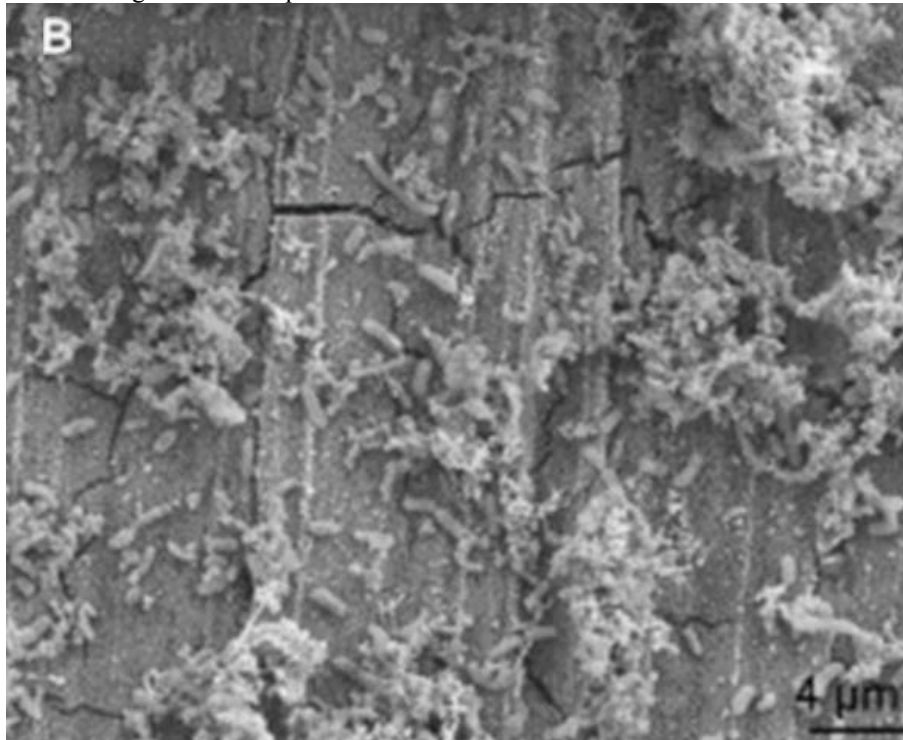


**Figure 3.18.** Microbial corrosion on the surface of unalloyed copper creates micro cracks due to sulphur enrichment. SRB colonies convert sulphate to sulphide which results in SCC/ Carpén L. et al. 2016/.

### 3.11. Discussion and conclusions regarding SCC and hydrogen embrittlement (HE) and hydrogen sickness (HS) of unalloyed copper (CuOFP) in a deep repository environment

All prerequisites for SCC and hydrogen embrittlement are fulfilled in a KBS-3 deep geological repository in Forsmark as described in the previous sections. These circumstances, i.e. the obvious risk for SCC, HE and HS are unfortunately not adequately discussed in SKB supplementary information on canister integrity issues and disregarded in the safety analysis. In SKB R-18-03 /Huotilainen C. et al. 2018/ it is concluded: *“The findings of Taniguchi and Kawasaki (2008), and Becker and Öijerholm (2017) of claimed small (of the maximum depth of a few tens of microns) SCC cracks on the surface of copper after SSRT experiments in sulphide containing environments can be alternatively explained as follows. The pre-existing manufacturing defects (which Becker and Öijerholm showed to exist also in the unexposed material, that had never been in contact with the sulphide containing*

*environment) extending to the specimen surface, open up due to the effect of surface active sulphide species on the cohesive forces of the opposing surfaces of a defect.” and in TR-19-15 at page 84 it is commented: “The involvement of absorbed H in the reported SCC of Taniguchi and Kawasaki (2008) and Becker and Öijerholm (2017) has not been proven and it is important to note that Bhaskaran et al. (2013) did not observe cracking when they cathodically polarised specimens.*

These comments are not supported by any scientific publication, on the contrary, it is scientifically erroneous to claim that the cracks shown in for instance Figure 3.1 should be initiated by *pre-existing manufacturing defects* in as-delivered copper. Virtually all grain boundaries in Figure 3.1 have initiated a crack close to the main fracture and for obvious reasons this cannot be due to *pre-existing manufacturing defects*, instead it is a scientific proof of sulphur induced SCC in copper. In fact, all surface cracks shown in Figure 3.1 and Figures 3.4-3.7 have clear evidence of being environmentally induced grain boundary cracks and have nothing to do with manufacturing defects since those would not be connected to the copper grain boundaries.

Furthermore, SKB seems to believe that the hydrogen induced blisters and cracks deeper inside the copper metal, as seen in Figure 3.8 are manufacturing defects as well, which is obviously wrong when understanding the mechanism of hydrogen charging of copper exposed to an anoxic environment. The maximum allowed hydrogen content of copper in the KBS-3 concept is 0.6 wt-ppm in order to avoid hydrogen embrittlement. The hydrogen content rises quickly in copper exposed to an anoxic and corrosive environment containing different concentrations of sulphide. The corrosion induced hydrogen charging of copper for only 2 weeks results in dangerous levels (1.2 wt-ppm) of hydrogen as shown in Figure 3.9 with formation of hydrogen blisters in the grain boundaries as shown in Figure 3.8. Furthermore, in a real repository exposure in the MiniCan-project, see section 3.8, even higher hydrogen content was detected in the copper metal (1.8 wt-ppm) and subsequent HE-blisters and SCC.

The comment that /Bhaskaran et al. 2013/ did not observe cracking when they cathodically polarised specimens is irrelevant since all slow strain rate tests at elevated temperature were performed too fast for SCC or HE to occur, i.e. with a strain rate of  $10^{-6}$  in combination with a preload of 70 MPa or 98MPa. The most relevant publications concerning SCC of copper, /Taniguchi and Kawasaki 2008/ and /Becker and Öijerholm 2017/ have used slower strain rates and no preload which explains why /Bhaskaran et al. 2013/ did not observe any cracking. Concerning hydrogen charging effects, /Bhaskaran et al. 2013/ did not perform any hydrogen measurements either before or after their slow strain rate tests.

From conclusions in the hydrogen embrittlement chapter in TR-19-15: “*The longest charging times that have been used are 6 weeks. Modelling results suggest that the surface layer with bubbles and cracks will not grow much even if very long times are considered. The reason is that bubbles and cracks create easy paths for the outflow of hydrogen and a steady state is eventually reached between inflow and outflow. For the copper canisters, only a very thin layer would be affected even if hydrogen charging comparable to the rate in the experiments were to occur. However, under repository conditions, the generation rate of hydrogen on the canister surface would be many orders of magnitude lower than in the experiments.*”

SKB seems not to understand that anoxic copper corrosion always includes an electrochemical hydrogen charging process and there is no thermodynamic reason why the hydrogen should just penetrate the surface layer, on the contrary it is already shown by Gunnar Hultquist at the Royal Institute of Technology, that the copper canister exposed in the prototype repository in fact was subjected to hydrogen charging throughout the whole thickness of 50 mm already after 7 years

exposure, as shown in Figure 3.12. The copper metal will unfortunately be decorated with hydrogen blisters and cracks, see Figures 3.8 and 3.16, long before a possibly steady state is eventually reached between inflow and outflow of hydrogen.

Regarding the reports of /Taxén et al. 2018, 2019/ they indeed detected surface cracks when following the procedure of /Taniguchi and Kawasaki (2008)/, however, they denoted the cracks as “intergranular attack”.

In TR-19-15 at pages 85-86 it is commented: *“The environmental conditions for which cracks have been reported are generally harsh compared with those to which the canisters will be exposed. // Not only is the minimum sulphide concentration at which cracking has been observed ( $10^{-3}$  mol/L, Becker and Öijerholm 2017) a factor of 10 to 100 times higher than that measured in the groundwater at Forsmark, but more importantly the flux of sulphide to the copper surface is orders of magnitude lower than the experimental fluxes, as long as the buffer is in place.”* and on page 86: *“It is thus concluded that the possibility of SCC in copper, even at high sulphide fluxes has questionable scientific support. Even if copper is susceptible to SCC in the presence of sulphide, the sulphide fluxes in the repository environment are far too low to induce the phenomena observed and sometimes interpreted as SCC.”*

In fact, cracks were already initiated at 10 times lower sulphide content, see Figure 3.7, i.e.  $10^{-4}$  mol/L, /Becker and Öijerholm 2017/. This is a highly relevant and probable sulphide concentration in a deep repository, especially at Forsmark with the sauna effect (sulphur salt enrichment) and non-saturated and non-functional bentonite buffer for several thousands of years as discussed in chapter 2. Furthermore, sulphate reducing bacteria (SRB) will thrive in a Forsmark repository with severe sulphide enrichment, as discussed in sections 3.10, 4.5 and 4.6.3. Based on the latest years new insights in H, OH and S penetration and internal corrosion of unalloyed copper under anoxic conditions it is just a question of time before SCC occurs in the canisters. Since hydrogen blisters in the copper grain boundaries could form already after two weeks of laboratory exposure in an anoxic and corrosive repository environment /Forsström A. et al. 2017/ and that the whole canister thickness is found to be hydrogen charged within 7-9 years of real exposure in the prototype repository /Szakálos P. and Hultquist G. 2013/ and in the MiniCan exposure, it should be obvious that HE and HS in the welds (see Figures 3.10 and 3.11) must be included in the safety analysis, especially since no external load or internal stresses are needed to initiate HE and HS in copper.

To conclude, SKB has not added any significantly new information or knowledge regarding SCC, HE and HS in their complementary information and reports, TR-19-15, TR-19-13 and TR-17-16, since the Land and Environmental Court in Nacka made their assessment 23 January 2018. With today's knowledge and collected findings, these fast degradation processes should all be included in the safety analysis SR-site as already described above. At least 40%, i.e. 2800 canisters, will be dependent on local inflow in the deposition holes and thus be subjected to the Sauna effect (salt enrichment) until being flooded after around 2000 years, see Figure 2.4 in previous chapter. Knowing that both SCC, HE and HS in the welds, operate with almost instant kinetics with respect to repository time scales it is important to make a conservative safety analysis. It is realistic to assume that 2800 canisters (40 %) collapse within 100 to 200 years after repository closure and that all remaining canisters collapse within 1000 years. A conservative safety analysis should therefore calculate with that 40% of the canisters collapse already within 100 years after repository closure and the remaining 60% within 1000 years after closure. More specifically, failures due to HE and HS will dominate in a Forsmark repository since these degradation processes operate without any applied load, in contrast to SCC.

This shows that the SR-site /Hedin A. et al. 2011/ (SKB safety analysis from 2011) is not valid anymore and that it cannot be used as basis for a decision concerning the final storage of high-level waste by the Swedish government.

## 4. General corrosion and pitting corrosion

### 4.1. Short summary

General corrosion in pure anoxic (free from dissolved oxygen) water is found to be more corrosive and detrimental to unalloyed copper than SKB has anticipated. There are several possible corrosion reactions in pure anoxic water, including internal corrosion and hydrogen charging of the bulk metal which are supported by theoretical calculations. A important long term study, FEBEX /Wersin P. and Kober F, 2017/ performed by SKB's Swiss equivalent NAGRA, has shown that unalloyed copper is susceptible to pitting corrosion in an oxygen free repository environment. In another study by /Marja-aho, M. et al.2018/, it was found that severe pitting corrosion was induced by sulphate reducing bacteria (SRB) in simulated geological nuclear waste repository at temperatures 10-12°C. It was concluded in the report that the copper sample in the biotic environment with SRB for 4 months had experienced the most severe corrosion, with the maximum corrosion rate reaching 175 µm/year. According to /Hedin A. et al. 2019/, SKB believes that a compact copper sulphide layer is needed on the copper surface in order to get pitting corrosion and that “neither biofilm formation nor localised corrosion in the presence of SRB have been observed under repository conditions”. Both statements are incorrect, no compact copper sulphide film is needed on the copper surface in order to get pitting corrosion during anoxic conditions, as shown in Figures 4.5, 4.6 and 4.8. Localised corrosion on copper has definitely been connected to SRB under repository conditions, see Figure 3.18 and Figure 4.10.

### 4.2. General- and pitting corrosion- introduction

General corrosion will most likely not be a cause of canister failure since there are much faster degradation mechanisms that will destroy the copper canisters in a Forsmark repository as discussed in detail in Chapter 3. However, general corrosion of copper is still detrimental since the corrosion rate will be accelerated by temperature, MIC and radiolysis. Unalloyed copper is very sensitive to a temperature increase and the corrosion rate is expected to double for every 10 degrees increased temperature /Mattsson E. 1997/. Anoxic (oxygen free) copper corrosion produces hydrogen, which gives energy to the microbes in the repository, see section 4.5. This means that the microbes act as a hydrogen sink and will thus accelerate the copper canister corrosion, furthermore copper ions and copper corrosion products as such are known to destroy the bentonite buffer, see section 4.4.

### 4.3. General copper corrosion in pure oxygen gas free water

An updated potential–pH diagram (Pourbaix) for copper metal in water is seen in Figure 4.1.

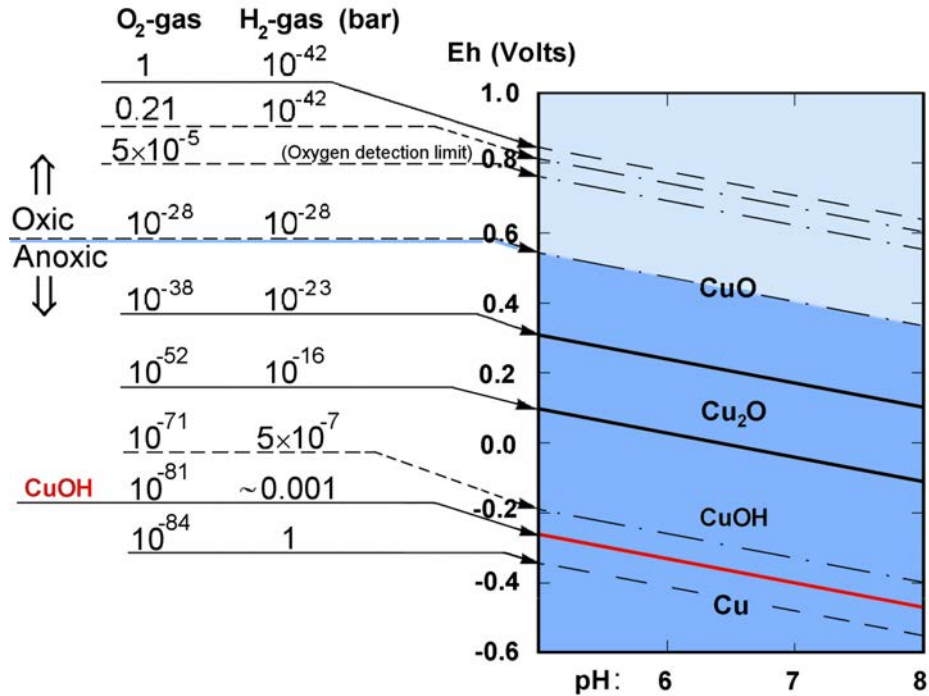


**Figure 4.1.** Pourbaix diagram based on /Szakálos P et al. 2007/. The light blue area at the top shows the oxic region with predominantly dissolved oxygen gas. The somewhat darker blue area shows the anoxic region with predominately dissolved hydrogen gas. The anoxic corrosion product Cu<sub>2</sub>O (cuprite) is only formed at very low oxygen and hydrogen partial pressures represented by the black solid lines. The solid red line marks the lower stability region for the monovalent hydroxide CuOH, which is stable up to around 1 mbar hydrogen gas pressure.

Cupric oxide (CuO) is formed predominantly in oxic environment and the absence of CuO when copper is exposed to water is a clear evidence for that an anoxic environment has prevailed. Copper exposed to strictly anoxic and pure water is visible in Figure 4.2. Only crystals of cuprite (Cu<sub>2</sub>O) is visible on the copper surface, but these Cu<sub>2</sub>O-crystals contain high amount of hydrogen which may explain why they are stable at a quite high hydrogen pressure of around 0.5 mbar at 50°C.

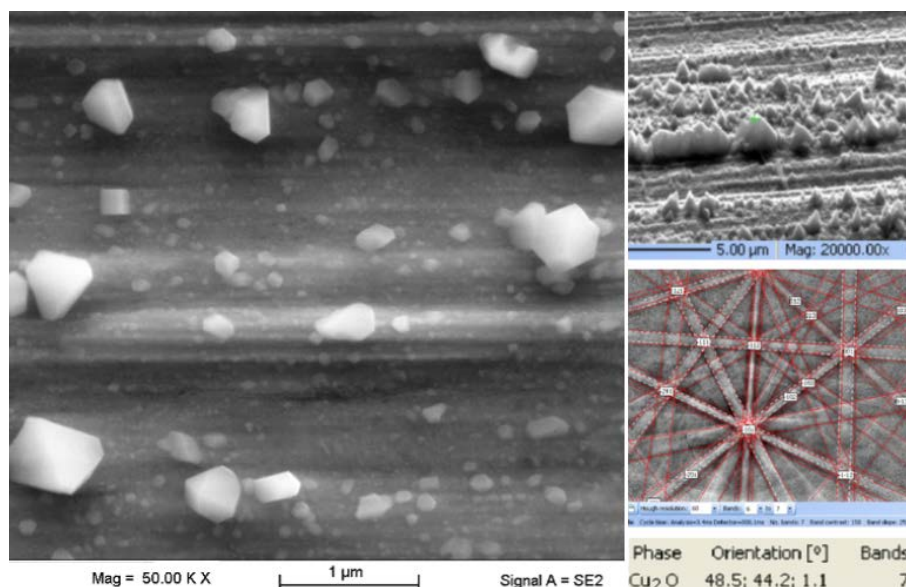


**Figure 4.2.** Unalloyed copper exposed to pure oxygen free water at 50°C for 12 months. The sample was moved directly from the anoxic water to the SEM/EBSD equipment to avoid any oxyc corrosion. The light crystals on the exposed surface have a somewhat distorted Cu<sub>2</sub>O-crystal structure, i.e. cuprite (detected by EBSD), but contain high amount of hydrogen (SIMS) /Szakálos P. and Hultquist G. 2013/ and Land and Environmental Court in Nacka, Sweden, case no. M 1333-11, Addendum 690.

These results with formation of a solid corrosion product consisting of hydrogenated Cu<sub>2</sub>O and hydroxide with an equilibrium hydrogen pressure roughly around 1 mbar in a strictly anoxic and pure water have been confirmed in several exposures in a project financed by the Swedish Radiation Safety Authority, see /Hultquist et al. 2013/, SSM-report 2013-07.

The non-crystalline corrosion product CuOH has experimentally been found to be stable up to a hydrogen pressure of around 1 mbar /Szakálos et al. 2007/, /Hultquist G. et al. 2009/, /Hultquist G. et al.2011/. Ab-initio calculations /Belonoshko A.B. and Rosengren A. 2010/, /Belonoshko A.B. and Rosengren A. 2012/ and /Johansson, A. J. et al. 2011/ have confirmed the stability of a CuOH-layer on copper. In fact, it is confirmed by Ab-initio calculations /Belonoshko A.B. and Rosengren A. 2012/ that the theoretical equilibrium hydrogen pressure for CuOH is around 1 mbar, as indicated in the Pourbaix diagram in Figure 4.1. Furthermore, it has been shown again both experimentally, see Figure 3.13 and theoretically that the monovalent hydroxide is stable, not only on the copper surface but also inside the copper metal in defects /Korzhavyi P. and Sandström R. 2014/. These combined findings explain why copper do corrode continuously in pure anoxic water.

According to old thermodynamic databases there exists only one anoxic copper corrosion product in pure water and that is a “dry” hydrogen free cuprite (Cu<sub>2</sub>O) that has a hydrogen equilibrium pressure of 10<sup>-16</sup> bar, as can be seen in Figure 4.1. However, there exists at least two more anoxic copper corrosion products, CuOH as shown in Figure 4.1 (red line) and a hydrogen “saturated” cuprite (Cu<sub>2</sub>O) as shown in Figure 4.2. Both these corrosion products have an equilibrium hydrogen pressure in the region of 0.1-1 mbar which means that copper corrodes much more in pure anoxic water than predicted by SKB and by old thermodynamic databases. In fact, several research groups around the world have confirmed Gunnar Hultquists original copper corrosion results /Hultquist G. 1986/ during the latest years /Becker R and Hermansson, H.-P. 2011/, /Bengtsson, A. et al. 2013/, /Cleveland C. et al. 2014/, /Kaufhold S. et al. 2017/, /He, X. et al. 2018/. However there is one research group

at Uppsala University led by Mats Boman and financed by SKB, that has not been able to detect any significant anoxic copper corrosion, but the research group has had problems concerning copper surface pre-treatment, hydrogen control, gas leakage and poor steel quality in the equipment during the years, problems which have been thoroughly described in /Szakálos P. et al. 2018/. In their rebuttal /Ottoosson M. et al 2018/ it is confirmed that they still have no control over the hydrogen release from the equipment. Despite all warnings from Assoc. prof. G. Hultquist (KTH) during the years, they still use Mo-free stainless steel, AISI 304L, which does corrode in heated pure anoxic water/steam, albeit with slow hydrogen release, but still enough to hinder the weak copper corrosion reaction. Furthermore, we understand that Ottoosson et al. still believe that their special copper sample pre-treatment with electrochemical polishing in phosphoric acid and high temperature furnace heat treatments will not affect the initiation of copper corrosion in pure anoxic water. We still strongly disagree with that assumption.

SKB refers also to a recent anoxic copper corrosion study by /Senior N A. et al. 2019/, which in fact detects substantial amount of hydrogen which was evacuated from the equipment 1-2 times per month. The experimental set-up with a large copper surface area (2600 thin copper wires in a small jar with water) is suitable for studying sensitive equilibrium reaction but not corrosion rates and certainly not a “conservative upper bound on copper corrosion rates” as SKB claims in /Hedin A. et al. 2019/, at page 51.

According to SKB /Hedin A. et al. 2019/, page 47 in the supplementary information, quote: *“No stable Cu-O-H compound that could act as the thermodynamic driving force of a continuing corrosion reaction in pure, O<sub>2</sub>-free water was found. Furthermore, surface reactions between water and the copper or copper oxide surface may lead to the oxidation of about one half of a monolayer of copper at most, potentially releasing a corresponding amount of hydrogen. This is far too little to explain the results observed by Hultquist et al. (2011, 2015)”*

Obviously, SKB has not made any thorough literature survey in the field of copper corrosion and did not take in any new information in the Land and Environmental Court in Nacka, Sweden, case no. M 1333-11, since there is convincing scientific evidence that at least two more anoxic corrosion products exist in the Cu-O-H system. With both experimental (Figure 3.13 and Figure 4.2) and Ab-initio calculations showing that the monovalent hydroxide does not only form on the copper surface but also in defects in the bulk metal (internal corrosion), the measured hydrogen pressures and increased copper corrosion observed in /Hultquist et al. 2011, 2015/ are certainly expected with the scientific knowledge of today.

The latest year’s research has shown that the seriousness of anoxic copper corrosion, by water molecules alone, is detrimental since both OH and H penetrates and accumulates in the copper metal by time. This inevitably results in internal corrosion and severe degradation of the mechanical properties, as discussed in Chapter 3.

#### **4.4. Increased general copper corrosion in contact with bentonite**

The copper canister will be in close contact with bentonite clay in a deep repository which is not only positive. It has been shown that copper corrosion may increase since the clay acts as a sink for copper ions and that in turn destroys the bentonite. Results from SKB’s LOT-project are shown in Figure 4.3.

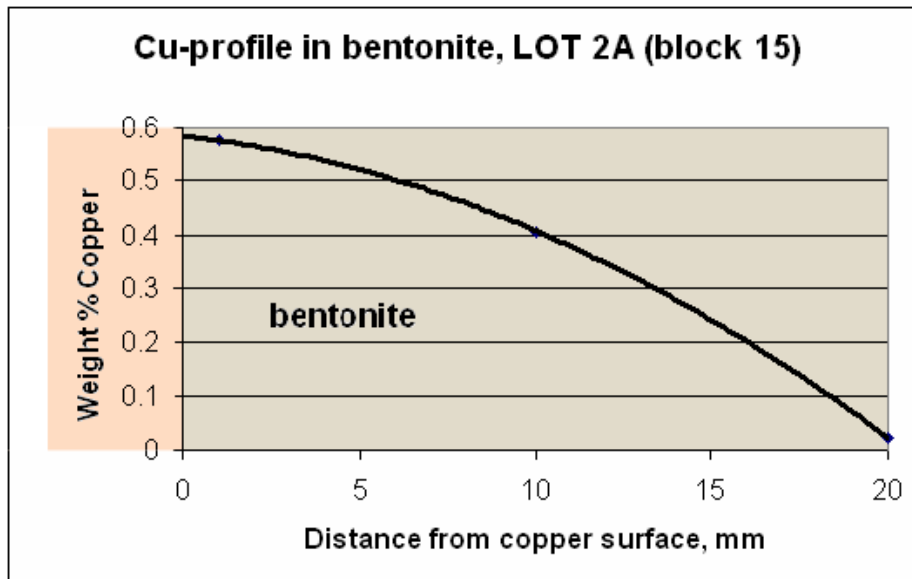


**Figure 4.3.** The bentonite acts as a Cu-ion sink and both copper and bentonite mutually destroy each other in an accelerated manner. Raw data from /Karnland O. et al. 2009/. LOT A2, Appendix 6; Characterization of the A2 parcel, Bundesanstalt für Geowissenschaften und Rohstoffe.

Heated copper surrounded by bentonite and groundwater was exposed for 5 years in the Äspö hard rock laboratory. A significant part of the copper in bentonite is precipitated as Cu- and Cu(Fe)-sulphides, representing ca 4  $\mu\text{m}/\text{y}$  in corrosion rate. Considering the total amount of copper corrosion products, especially the thick layer on the copper surface, which is not included in Figure 4.3, it is most likely that the copper corrosion rate is around 10  $\mu\text{m}/\text{y}$  (pitting corrosion not taken into account).

#### 4.5. Microbial induced “corrosion” degradation of the bentonite buffer

New research has shown that not only the copper canister will be attacked by the prevailing microbes in a deep repository but also the bentonite buffer, see Figure 4.4. Microorganisms such as SRB can accelerate degradation of bentonite-based buffers and influence the long-term behaviour of plug systems and seals /Taborowski T. et al, 2019/ and /Pedersen K. et al. 2017/. The sulphide producing bacteria can, as shown in Figure 4.4, destroy the bentonite buffer by consuming iron from the clay mineral and precipitate quite large numbers of iron sulphide mineralizations. It was concluded in /Taborowski T. et al, 2019/, that the important swelling properties are jeopardised, quote:

“In MX-80 the lowest sulphide concentration produced the highest swelling pressure and the highest sulphide concentration the lowest swelling pressure. This indicates that the oxidation of sulphide to sulphur and concomitant with the reduction of a range of different ferric iron minerals to ferrous iron negatively affected the swelling pressure in MX-80.”

Anoxic (oxygen free) copper corrosion produces hydrogen, which gives energy to the microbes in the repository /Taborowski T. et al, 2019/. This means that the microbes act as a hydrogen sink and will thus accelerate the copper canister corrosion, furthermore copper ions and copper corrosion products as such are known to destroy the bentonite buffer see section 4.4. Furthermore, the fast degradation of

the bentonite by microbes, within months, with significant reduction of the bentonite swelling pressure will, in combination with cementation, cracking, piping and erosion of the buffer, as discussed in section 2.5, deprive the barrier properties of the bentonite clay in a Forsmark repository.



Black colonies of iron sulphide produced by sulphide producing bacteria in Asha bentonite at 1750 kg/m<sup>3</sup> wet density and with addition of lactate and sulphide producing bacteria



Black colonies of iron sulphide produced by sulphide producing bacteria observed during sampling of test cell with GMZ bentonite.

**Figure 4.4.** Details from page 79 in /Taborowski T. et al, 2019/. Sulphate reducing bacteria (SRB) are found to be capable of destroying fully pressurized bentonite by precipitation of iron sulphide mineralizations.

## 4.6. Pitting corrosion in the repository environment

### 4.6.1. FEBEX, 18-year long term study in a repository environment.

An 18-year long term study, FEBEX (Full-scale Engineered Barrier EXperiment in Crystalline Host Rock), performed by SKB's Swiss equivalent NAGRA (National Cooperative for the Disposal of Radioactive Waste), has shown that unalloyed copper is susceptible to pitting corrosion in an oxygen free repository environment, see Figures 4.5 and 4.6.

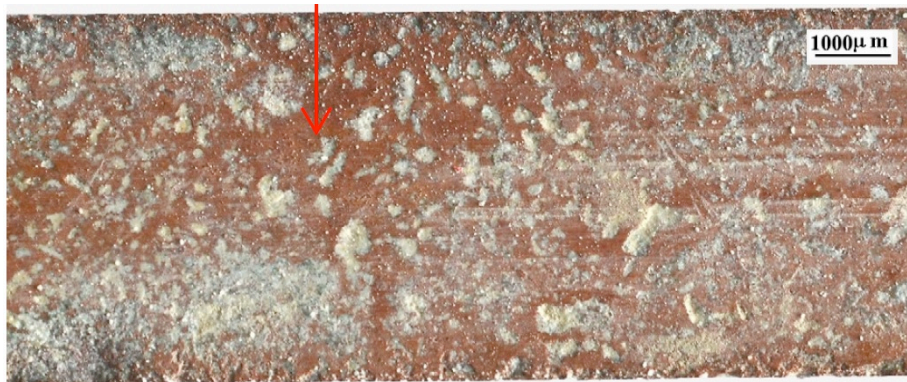


**Figure 4.5.** A macrograph showing an exposed copper sample severely attacked by pitting corrosion, from Appendix B in the FEBEX-report /Wersin P. and Kober F 2017/.

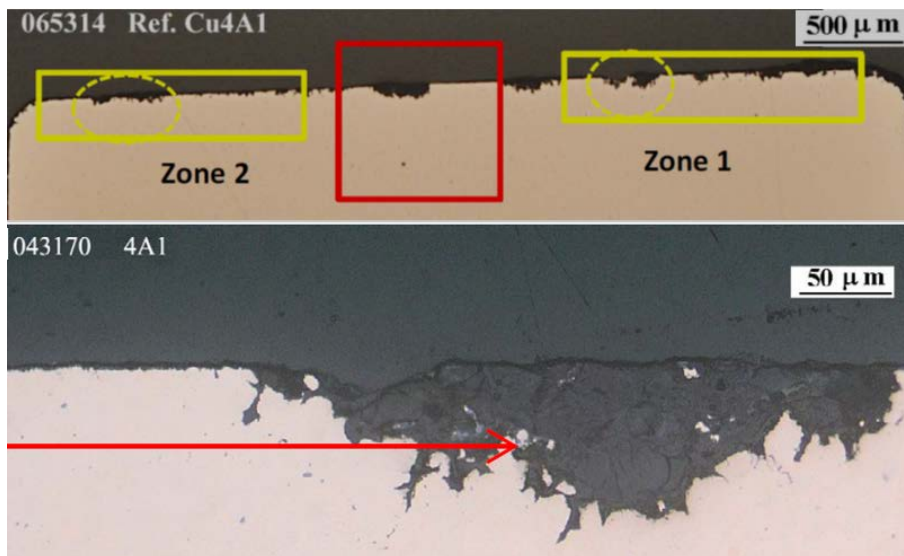


**Figure 4.6.** Metallographic cross-sections showing the exposed copper sample with pitting corrosion, up to 100 μm in depth. From Appendix B in the FEBEX-report /Wersin P. and Kober F 2017/.

It is commented in the report, concerning the corroded copper samples, that “No effects of anaerobic corrosion could be observed on these surfaces.” This is a strange comment since the corrosion products and the corrosion features are consistent with anoxic copper corrosion. The only copper oxide detected is  $\text{Cu}_2\text{O}$  (no  $\text{CuO}$ ) and as seen in Figure 4.1 that indicates that the exposure was indeed anoxic. Furthermore, quote from page 28 concerning copper corrosion: “These pits

were filled with clay material and little or no Cu-corrosion products.” This feature, with no corrosion product in the pits is a clear evidence of anoxic dissolution corrosion. The pits would have been covered with copper oxides if dissolved oxygen would have been present. Minerals and water with  $\text{Fe}^{2+}$ -ions is further evidence for that normal anoxic groundwater has prevailed in the long-term exposure.

It has recently been proven in a parallel study by the same organisation, NAGRA, that all oxygen that remains after the closure of a deep repository tunnel is consumed fast by the prevailing bio-/chemistry in the bentonite pore water, as shown in Figure 4.7. It is stated in the report /Müller H. 2017/: “The surrounding minerals confirm that the environment was indeed oxygen free and it is expected that any remaining oxygen was consumed during the first month after closure of the test repository.”

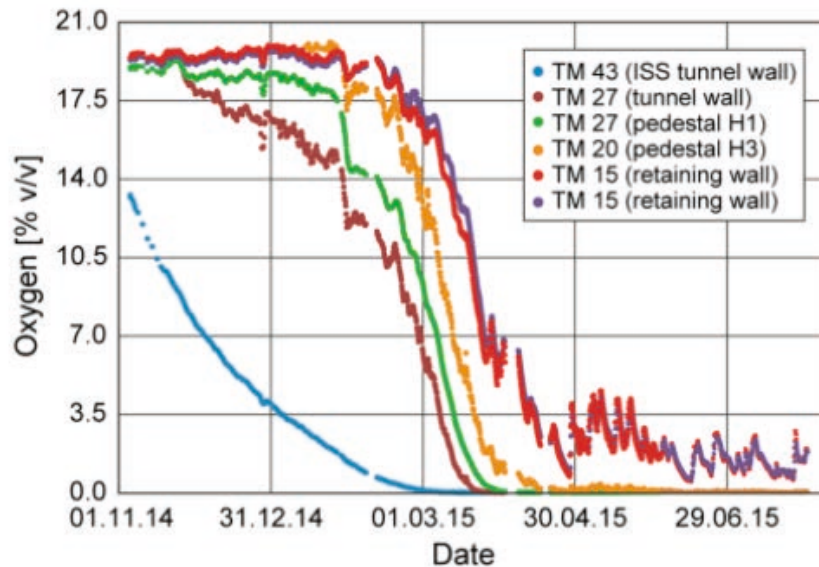


**Fig. 11** Oxygen concentrations at different measurement locations along the FE tunnel from November 2014 (shortly after backfilling started) until July 2015

**Figure 4.7.** Monitoring of the oxygen content in a deep repository. All oxygen was consumed already during the first months after closure of the test repository /Müller H. et al. 2017/.

The FEBEX-report /Wersin P. and Kober F 2017/ confirms that an alloyed copper (Cu-Ni), is much more corrosion resistant than unalloyed copper in a deep geological repository:

*“Analysis of copper and Cu-Ni alloy coupons placed close to the heater revealed moderate corrosion effects with general corrosion as the main corrosion mode. The total corrosion depth estimated from one sample was  $\sim 9 \mu\text{m}$ . For the Cu coupons, in some spots localised corrosion with maximum penetration lengths of 20-100  $\mu\text{m}$  was observed. Cu-Ni alloys showed less corrosion than the unalloyed Cu samples.”* Additionally, it was shown that stainless steels were attacked by different localised corrosion processes, but titanium metal (with and without welds) was virtually unaffected during the 18-year exposure.

#### 4.6.2. A 15-year exposure in pure anoxic water and observed pitting corrosion in the SKB-project Alternative Buffer Material (ABM)

Another evidence for that unalloyed copper is sensitive to pitting corrosion also in pure anoxic water is seen in Figure 4.8.

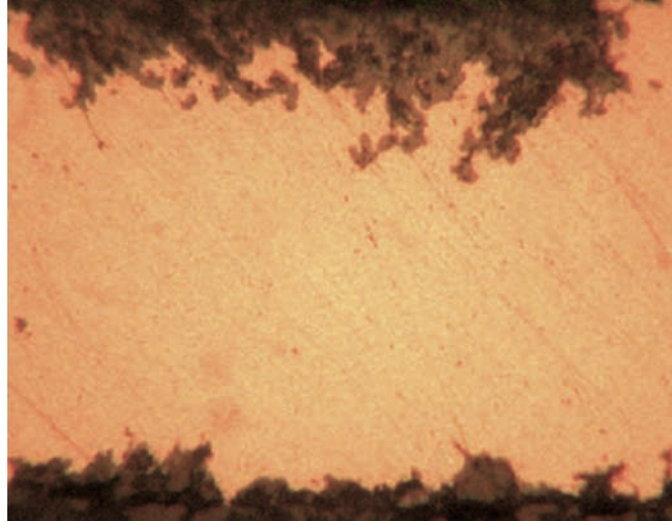


**Figure 4.8.** Light optical cross-section of the initially 100µm thick copper foil after 15 years exposure in distilled anoxic water at room temperature. Localised corrosion attack is clearly visible. Scale: the height of the micrograph is 90 µm. /Hultquist G. et al. 2008/.

The long-term exposure was performed in a set-up with an air-tight palladium membrane in the lid that allowed hydrogen to escape from the equipment, thus allowing the anoxic copper corrosion process to continue.

In the SKB-project Alternative Buffer Material (ABM) /Gordon A. et al. 2018b/ it is clear that pitting corrosion has occurred, see Figure 4.9. The copper samples were exposed to heated (80°C) groundwater and bentonite during 5 years in Äspö Hard Rock Laboratory.

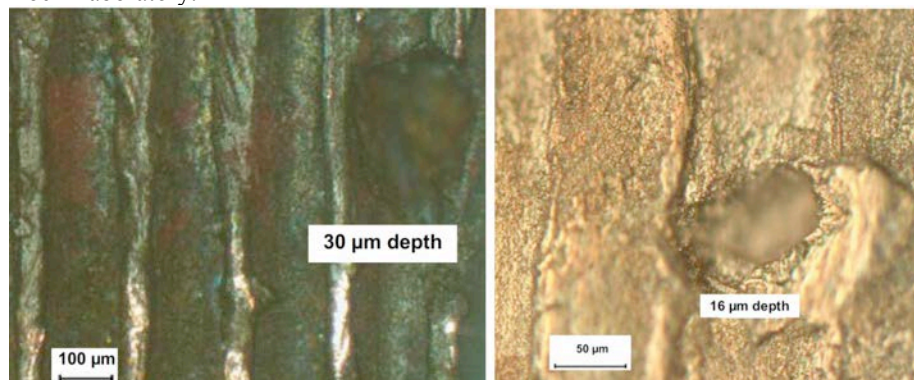


**Figure 4.9.** Example of pitting corrosion on one acid cleaned sample (to the right) and an un-cleaned sample to the left /Gordon A. et al. 2018b/. Maximum pitting corrosion rate: 6 µm/year.

#### 4.6.3. Pitting corrosion of copper in anoxic groundwater environment in the presence and absence of sulphate reducing bacteria (SRB)

SRB have been proven to induce severe pitting corrosion on unalloyed copper in an anoxic repository environment, see Figure 4.10.

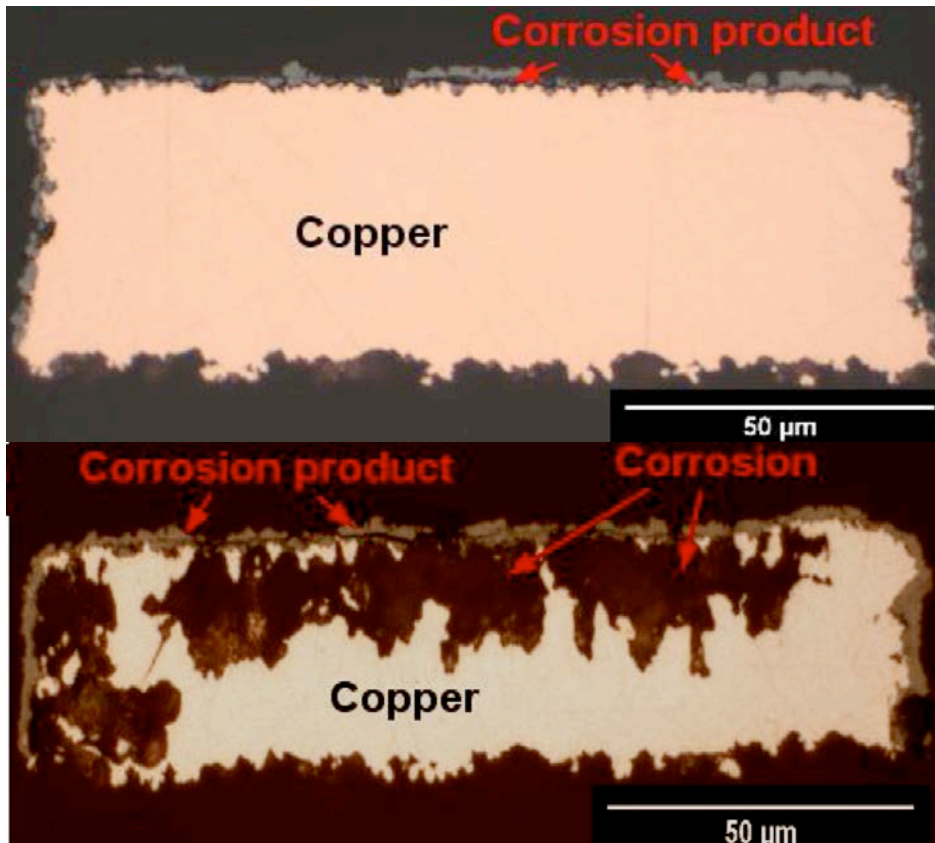


**Figure 4.10.** Results from Figure 5 in /Marja-aho M. et al. 2018/. Corrosion tests performed in simulated geological nuclear waste repository, at temperatures 10–12°C and oxygen level below 1 ppm. Simulated groundwater, with chemical composition of groundwater stabilized with bentonite. The micrograph at the top shows a cross-section, originally 200×35µm<sup>2</sup>, of a sample exposed for 4 months without SRB (abiotic environment) and micrograph at the bottom shows a sample exposed 4 months with naturally occurring SRB in groundwater (biotic environment).

It was concluded in the report that the copper sample in the biotic environment with SRB for 4 months had experienced the most severe corrosion, with the maximum instantaneous corrosion rate reaching 175 µm/year.

SKB have financed much shorter studies, 10-32 days, with copper exposed to SRB, see report TR-18-14 /Gordon A et al. 2018/, where pitting corrosion was detected despite short exposure times. The deepest pitting corrosion detected was 10-20 µm/month which indeed indicate severe SRB-induced pitting corrosion in the long term, as shown in /Marja-aho M. et al. 2018/, however that was not discussed at all in the conclusions in /Gordon A et al. 2018/.

## 4.7. Discussion regarding pitting corrosion in a repository environment

According to SKB /Hedin A. et al. 2019/, page 74 in the supplementary information, SKB believes that a compact copper sulphide layer is needed on the copper surface in order to get pitting corrosion, quote:

*“...The sulphide fluxes are below the threshold fluxes for formation of a compact film (a prerequisite for a passive film to give pitting). • Localised corrosion of copper due to the presence of a metabolically active biofilm of SRB on the canister surface exposed directly to the ground water seems unlikely, since neither biofilm formation nor localised corrosion in the presence of SRB have been observed under repository conditions.”*

Both statements are obviously incorrect, no compact copper sulphide film is needed on the copper surface in order to get pitting corrosion during anoxic conditions, as shown in Figures 4.5,4.6 and 4.8. Localised corrosion on copper has definitely been connected to SRB under repository conditions, see Figure 3.18 and Figure 4.10.

If we consider the most unlikely situation where SCC, HE and HS do not occur in a Forsmark repository then the canisters would fail by pitting corrosion and general corrosion accelerated by temperature, radiation, MIC and salt enrichment/the Sauna effect. The corrosion rate can vary considerably and in a case with no influence from MIC and radiation an average corrosion rate of 5-10  $\mu\text{m}$  per year is realistic, see sections 4.4 and 4.6 (LOT, FEBEX, ABM projects). More severe pitting corrosion can occur with MIC as seen in Figure 4.10, with measured corrosion rates up to 175 $\mu\text{m}$  at 10-12°C in a repository environment. Assuming the canisters may collapse when 50% of the wall thickness has been consumed by corrosion, i.e. 25 mm, and that the persistent corrosion rate during the first thousand years could be up to 10  $\mu\text{m}$  per year, it would indicate, that the canisters would collapse within 2500 years. This shows again that the SR-site /Hedin A. et al. 2011/ (SKB safety analysis from 2011) is not valid anymore and that it cannot be used as basis for a decision concerning the final storage of high-level waste by the Swedish government.

## 5. The effect of radioactive radiation.

### 5.1. Summary.

In the SKB-report /Hedin A. et al. 2019/ regarding this issue is concluded “...that irradiation will cause insignificant levels of radiation damage in the canister materials. This is concluded on the basis of revised calculations of radiation damage and to some degree also demonstrated by new experiments”.

This overall conclusion is based on experimental /Padovani C. et al. 2019/ and theoretical /Yang Q. et al 2019/ investigations in which copper is exposed to gamma radiation alone, without any simultaneous exposure to any aqueous environment. However, the situation turns out to be completely different if copper is exposed not only to radiation but simultaneously also to an aqueous environment. In our Concluding Speech at Nacka Land and Environmental Court on Oct 26, 2017, it was exactly this condition, the combined effect of gamma radiation and water exposure, that was stressed by us to possibly impose an obvious threat on copper’s mechanical integrity.

To our surprise this combined effect has not at all been dealt with in /Hedin A. et al. 2019/. All conclusions in the experimental study /Padovani C. et al. 2019/ have been based on the exposure of copper to gamma radiation under an inert atmosphere, not

to gamma radiation in water and some aqueous environment. Our conclusion is therefore that SKB in the main report /Hedin A. et al. 2019/ and the supporting reports /Padovani C. et al. 2019/ and /Yang Q. et al 2019/ by no means have met the arguments presented by us in the Court and formulated by the Court as an unresolved issue.

To fill some gaps in our lack of fundamental understanding of the combined effect of gamma radiation and oxygen-free water in SKB-copper we will use a unique technique based on high-resolution X-ray diffraction performed at the synchrotron radiation facility DESY in Hamburg, Germany. Below follow more details concerning the arguments put forward by SKB, and also more details on the new measurements to be performed at DESY. The intent is that these measurements will shed more light on the possible changes in microstructure of SKB-copper during simultaneous exposure to gamma radiation and oxygen-free water.

To conclude: The combined effect on the microstructure of SKB-Cu of radiation and water exposure is still an unresolved issue and has not been met by SKB in their Supplementary Study /Hedin A. et al. 2019/. This fact and also the circumstance that there is a new high-precision tool available for these investigations forms strong argument that one needs to wait before a final decision can be made regarding copper as canister material for long-term storage of nuclear waste.

## **5.2. More detailed report.**

### **5.2.1. The difference between separate and combined effects of radiation and water exposure**

In their Concluding Speech at Nacka Land and Environmental Court against SKBs application for final disposal of nuclear waste on Oct 26, 2017, the authors argued that the combined effect of gamma radiation and water exposure could result in additional phenomena which were not yet explored and understood. These include the formation of defects in the bulk of copper when the metal undergoes gamma-radiation annealing and structural alterations of the surface and sub-surface layers of copper, also the enhanced diffusion of hydrogen atoms into the bulk. Important spin-off effects of gamma radiation are the additional hydrogen sources produced during exposure in aqueous environments, and their further implications. Radiation effects outside the copper canister can result in further increase in hydrogen production at the copper/water interface. In addition, radiation inside the copper canister can result in increased hydrogen transport in the metal, also in hydrogen induced vacancy formation during early plastic deformation with increased risk of creep deformation, hydrogen embrittlement and stress corrosion cracking.

These arguments were taken by the Court and formulated as one of the five unresolved corrosion-related issues in their statement to the Government, Jan 23, 2018.

An obvious consequence of the KBS-3 concept is that copper will be simultaneously exposed to ionizing radiation and aqueous environments representative for long-term repository conditions. In view of this, the Swedish Nuclear Fuel and Waste Management Co. (SKB) has initiated several investigations in order to explore the effect of gamma radiation on the microstructure and integrity of copper. Guinan analysed gamma-spectra supplied by SKB for the spent fuel canisters and concluded that no practical effect of radiation could be discerned of any physical property changes of copper, such as yield stress, creep rate, segregation, dimensional change or brittleness /Guinan M. 2001/. As a result of the Court statement, the calculations by Guinan were recently repeated using more updated computational techniques for

exploring possible radiation damages in copper /Yang Q. et al 2019/. In agreement with Guinan, it was concluded that no significant radiation-induced damage of copper could be seen. A complementary experimental research programme was initiated in parallel to examine possible effects induced by gamma radiation on the microstructure of copper by using several highly sensitive characterization techniques /Padovani C. et al. 2019/. When comparing copper samples irradiated up to the full repository dose of 100 kGy with unirradiated control samples it was concluded that no radiation effect could be discerned with respect to copper microstructure and some material properties. Hence, the overall conclusion from these theoretical and experimental investigations is that gamma radiation alone, under conditions given by the KBS-3 concept, seems to impose no constraints on copper used as canister material for spent nuclear fuel.

The situation turns out to be different if copper is exposed not only to radiation but simultaneously also to an aqueous environment. When copper has been exposed to similar gamma radiation rates and doses in an aqueous environment, significant effects could be observed both with respect to localized corrosion of copper /Björkbacka Å. et al. 2012/ and /Björkbacka Å. et al. 2013/ and with respect to increased uptakes of hydrogen in the bulk of copper /Lousada C. M. et al 2016/. Both effects turned out to increase with the total dose of gamma radiation. The results were discussed in terms of production of H-atoms at the water-copper interface induced by gamma radiation, enhanced transport of H-atoms into copper and the formation of defects in the bulk of copper induced by the combined effect of hydrogen and radiation /Lousada C. M. et al 2016/.

Despite the Court statement and to our great surprise, SKB has not initiated any studies of SKB-copper exposed to simultaneous gamma radiation and an aqueous environment. In order to provide more information on the possible combined influence of gamma radiation and water on copper, studies will be undertaken within the next months based on a largely unexplored technique related to this issue, high-energy synchrotron x-ray diffraction (HEXRD, 8). The technique takes advantage of the high-flux of high-energy photons generated by a synchrotron source and has found many new opportunities for in situ probing of, e.g., structural phase transformations or small lattice parameter changes of individual grains in a polycrystalline metal matrix. In what follows, we explain the technique in some detail, also some reports from the scientific literature with relevance for the possible new insight generated.

### 5.2.2. High-energy synchrotron x-ray diffraction (HEXRD)

The study to be undertaken is a collaboration between scientists at KTH Royal Institute of Technology, Stockholm, Sweden, and Deutsches Elektronen-Synchrotron DESY, Hamburg, Germany. Copper specimens from SKB copper will be prepared in the same way as in previous work /Björkbacka Å. et al. 2012/, i.e. polished copper placed in 10 mL deaerated Millipore Milli-Q water in glass beakers and exposed to gamma radiation using a Cs-137 gamma source at KTH Royal Institute of Technology with a dose of radiation up to around 100 kGy, representing a total dose of a copper canister during 100,000 years of final disposal in the Swedish bedrock /Björkbacka Å. et al. 2012/.

HEXRD measurements in transmission mode (Debye-Scherrer method) will be performed at the German Synchrotron radiation facility (DESY) PETRA III beamline P21.2. Here, the samples will be mounted onto a high-precision motorized multiaxial positioning and rotary stage with their radiation-exposed surfaces being parallel to the incident x-rays, see Figure 5.1.

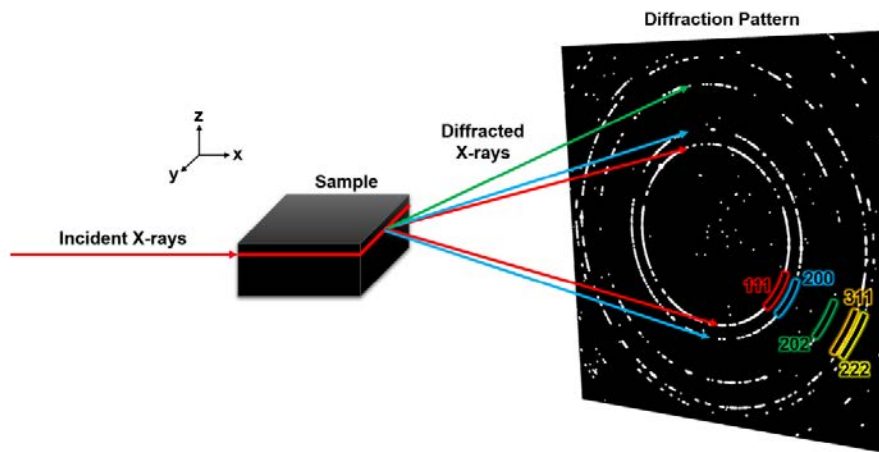


**Figure 5.1.** Experimental setup of high-energy x-ray diffraction measurements showing x-rays radiating the copper specimen and the diffracted x-rays with the 2D diffraction pattern collected by a detector.

The samples will be irradiated with the x-rays through the width of the specimen by angle of 45° and scanned from top to bottom in 20 μm steps (z-direction). The position of the scan direction through the specimen is shown in Figure 4.2.

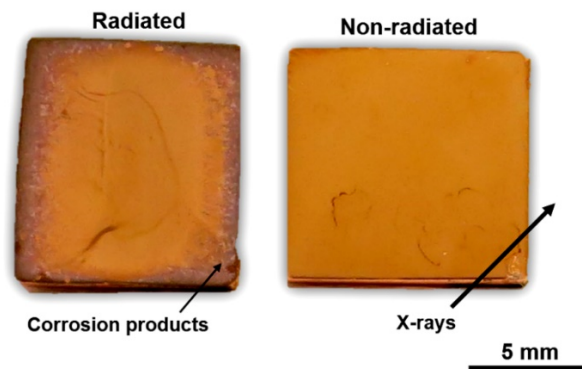


**Figure 5.2.** Photograph of some of the copper samples to be investigated. The radiated specimen in this case was exposed to oxygen-free water for 64 hours with a simultaneous exposure to 28.6 kGy of gamma radiation. The non-radiated specimen was exposed to oxygen-free water for 64 hours only. The bar shows the scan direction of x-rays through the specimen.

The x-rays have an energy of 72 keV with a beam size of 18 μm perpendicular to the sample surface and 55 μm to its horizontal. With a sample-to-detector distance of 1.6 m the first five full diffraction rings (Figure 5.1) with the highest intensities will be collected. During each scan, the sample is moved parallel to its surface (in the y-direction) by 2 mm to collect more diffraction signals from each z-position and thereby improving statistics. The samples will be scanned from 200 μm above the upper surface down to 200 μm below the lower surface, capturing the entire specimen thickness. The surface is defined as that position where the first analysable diffraction patterns with intensities strong enough can be seen. Using Match! XRD analysis software to read the d-spacing of each diffraction peak, the lattice constant,  $a$ , can be calculated using the classical relationship between d-spacing and each reflector:

$$a = d_{hkl} \cdot \sqrt{(h^2 + k^2 + l^2)}$$

The average of all five values will be considered as the lattice constant. The standard deviation obtained in introductory studies of SKB-copper at DESY shows that the

accuracy in determining the lattice constant is  $\pm 0.0005 \text{ \AA}$ . This is an accuracy by far higher than can be achieved with any conventional x-ray diffraction technique.

### 5.2.3. Discussion

Figure 5.2 is a photograph of the copper samples investigated from our introductory studies, showing the surface of the irradiated and non-irradiated specimens. The irradiated specimen in this case was exposed for 64 hours in oxygen-free water corresponding to a total gamma dose of 28.6 kGy. The surface appearance is similar to what has been previously observed /Guinan M. 2001/, /Björkbacka Å. et al. 2013/ and is caused by a thin layer of mainly cuprite ( $\text{Cu}_2\text{O}$ ), which is unevenly distributed along the copper surface. The radiation-induced corrosion of copper has been the subject of extensive investigations /Björkbacka Å. 2015/ measured both as the concentration of dissolved copper in the water solution and as the formation of cuprite. Earlier analysis has shown that the corrosion effects increase with radiation dose /Björkbacka Å. et al. 2013/. For comparison, on the sample exposed to oxygen-free water without radiation for 64 hours no visible layers of corrosion products were seen.

An earlier observed consequence of the simultaneous exposure of copper to gamma radiation and oxygen-free water is an accelerated ingress of hydrogen into copper, which increases with gamma radiation dose in the interval from around 35 to 70 kGy /Lousada C. M. et al 2016/. Hydrogen in steels has been the subject of extensive experimental and computational investigations because of the well-known risk of loss in metal ductility and hydrogen induced brittle failures at stresses below the yield stress of the susceptible steel /Barrera O. et al 2018/. The modes of failure mechanisms include hydrogen-induced decohesion of adjacent metal atoms, hydrogen-enhanced local plasticity, hydrogen-induced phase transformations and hydrogen-enhanced strain-induced vacancy formation /Barrera O. et al 2018/. For copper, much less information is available on hydrogen-related microstructural effects than for steel. It has been concluded through computational studies that H-atoms accumulate in vacancy-type defects and change their properties /Ganchenkova M. G. et al. 2014/. The results may be a marked change in dislocation slips and in early plastic straining of copper /Yagodzinskyy Y. et al. 2018/. Earlier studies have also shown that hydrogen in copper can cause changes in the physical properties of copper, such as tensile yield stress /Butt M. Z. 1983/ and hardness /Kim J. J. and Byrne J. G. 1983/. The mechanisms for these observations have been described in terms of hydrogen interaction with dislocations and hydrogen pinning effects of point defects. Cathodically charged hydrogen into copper has furthermore resulted in a decrease in ultimate tensile strength and in the failure strain of copper /Panagopoulos C. N. and Zacharopoulos N. 1994/

In order to shed more light onto the possible combined effect of gamma radiation and exposure in oxygen-free water the introductory studies based on HEXRD are planned to determine possible lattice-spacing changes with higher precision than ever. It is expected that the combined effect of radiation and water exposure results in local changes of microstructure, which is probably stronger near the surface region of the exposed SKB-Cu material closest to the water. Hence, the studies at DESY should focus on the precise positioning of the sample with radiation dosages up to 100 kGy.

## 6. Summary

There are several SKB-reports concerning the Sauna-effect and the results are disappointing in several ways. Firstly, it is clear that it is impossible to inject water in the deposition holes without destroying the bentonite rings with cracking and piping. Secondly, water, as steam and moisture, will escape through the cracks and slots from the heated deposition holes and condensate in the colder tunnel above, thus accumulating sulphur and chloride salts in the holes. Thirdly, the salt enrichment which induces several severe corrosion processes on the unalloyed copper canister will continue until saturation/swelling is reached in the whole repository tunnel (fully flooded and pressurized). Finally, in a Forsmark repository, the saturation/swelling process in the tunnels that will create a proper counter pressure to neutralize the Sauna effect will unfortunately take several thousand years which is devastating for the lifetime of the copper canisters. It can be concluded that SKB has not submitted any new information or studies concerning salt enrichment (the Sauna effect) on pitting corrosion and stress corrosion cracking, which was requested by the Environmental Court (E.C.), items (b) and (c).

There is compelling scientific evidence that fast degradation by stress corrosion cracking (SCC), hydrogen embrittlement (HE) and hydrogen sickness (HS) will penetrate the copper canisters in a repository environment. SKB seems to believe that the surface cracks and hydrogen blisters observed in the copper grain boundaries in several studies are only “manufacturing defects”. This explanation has no scientific support at all, and we can conclude that SKB has not seriously considered the uncertainties connected to (c), (d) and (e), as was requested by the E.C. The new evidence for these fast degradation mechanisms in copper shows that the safety analysis SR-site /Hedin A. et al. 2011/ is obsolete.

In their Supplementary Study /Hedin A. et al. 2019/ SKB has given more evidence that radiation effects alone cause no significant effects on the microstructure of copper. However, the situation turns out to be completely different if copper is exposed not only to radiation but simultaneously also to an aqueous environment. This was exactly the condition that was stressed by the authors to impose an obvious threat on copper’s mechanical integrity. To our surprise this condition has not at all been dealt with in the Supplementary Study /Hedin A. et al. 2019/ and in the supporting reports Padovani C. et al. 2019/ and /Yang Q. et al 2019/. To conclude, the combined effect of radiation and exposure in an aqueous environment on the microstructure of SKB-Cu is still an unresolved issue, i.e. request (e) by the E.C.

An issue not commented by the E.C. is the fast degradation of the bentonite buffer by microbes which has shown to significantly reduce the bentonite swelling pressure /Taborowski T. et al, 2019. Furthermore, the added degradation processes with copper ion infiltration in the clay minerals (due to copper corrosion), cementation, cracking, piping and erosion of the buffer, as discussed in sections 2.5, 4.4 and 4.5, deprive the barrier properties of the bentonite clay in a Forsmark repository. The combined effect of failures of both the engineered barriers at the same time, i.e. bentonite and copper, must be included in the safety analysis as a main scenario according to SSMFS 2008:21, especially considering the Forsmark specific problems.

In a study connected to SKB’s prototype repository /Szakálos P. and Hultquist G. 2013/ it was shown that the whole canister thickness was penetrated by hydrogen during only seven years exposure at elevated temperature and that the canister was subjected to internal corrosion by hydroxide. At least 40%, i.e. 2800 canisters, will be dependent on local inflow (Figure 2.3) in the deposition holes and thus be subjected to the Sauna effect (salt enrichment) until being flooded after around 2000 years (Figure 2.4). A conservative safety analysis would estimate that 40% of the canisters collapse already within 100 years after repository closure due to SCC, HE

and HS (in the welds) and the remaining 60% within 1000 years after closure due to SCC, HE and internal corrosion. More specifically, failures due to HE and HS will dominate in a Forsmark repository since these degradation processes operate without any applied load, in contrast to SCC, see section 3.11.

If we consider the most unlikely situation where SCC, HE and HS do not occur in a Forsmark repository then the canisters would fail by pitting corrosion and general corrosion accelerated by temperature, radiation, microbial induced corrosion (MIC) and salt enrichment (the Sauna effect). The corrosion can vary considerably and copper corrosion rates in the range from 5  $\mu\text{m}$  to 175  $\mu\text{m}$  per year are documented, see sections 4.4 and 4.6. Again, it can be concluded that SKB has not considered corrosion by pure anoxic water (a) and pitting corrosion (b) in a proper way. A realistic estimation based on only general- and pitting corrosion indicates that the canisters would collapse within 2500 years. In fact, in an 18-year long experiment in a real repository environment, FEBEX /Wersin P. and Kober F 2017/, it was shown that unalloyed copper was the least corrosion resistant metallic material tested.

The overall conclusion is that the SR-site safety analysis /Hedin A. et al. 2011/ is not valid anymore and that it cannot be used as basis for a decision concerning the final storage of high-level waste by the Swedish government.

## 7. References

- Arilahti E, Lehtikuusi T, Olin M, Saario T, Varis P, 2011. Evidence for internal diffusion of sulphide from groundwater into grain boundaries ahead of crack tip in Cu OFP copper. *Corrosion Engineering, Science and Technology* 46, 134 – 137.
- Barrera O. et al 2018. Understanding and mitigating hydrogen embrittlement of steels: a review of experimental, modelling and design progress from atomistic to continuum, *Journal of Material Science*, 53 (2018) 6251-6290.
- Becker R and Hermansson, H.-P. 2011. Evolution of Hydrogen by Copper in Ultrapure Water Without Dissolved Oxygen, Swedish Radiation Safety Authority SSM Report 2011:34 (2011), ISSN: 2000-0456.
- Becker R. and Öjjerholm J. 2017. Slow strain rate testing of copper in sulfide rich chloride containing deoxygenated water at 90 °C., SSM Report number 2017:02.
- Belonoshko A.B. and Rosengren A. 2010. Ab Initio Study of Water Interaction with a Cu Surface. *Langmuir* 26, 16267–16270. (2010)
- Belonoshko A.B. and Rosengren A. 2012. A possible mechanism of copper corrosion in anoxic water. *Phil. Mag.* 92, 4618-4627 (2012)
- Bengtsson A., Chukharkina A., Eriksson L., Hallbeck B., Hallbeck L., Johansson J., Johansson L., Pedersen K. 2013. Development of a method for the study of H<sub>2</sub> gas emission in sealed compartments containing canister copper immersed in O<sub>2</sub> free water, (2013) SKB Rapport TR-13-13.
- Bhaskaran G, Carcea A, Ulaganathan J, Wang S, Huang Y, Newman R C, 2013. Fundamental aspects of stress corrosion cracking of copper relevant to the Swedish deep geologic repository concept. SKB TR-12-06, Svensk Kärnbränslehantering AB.
- Birgersson M, Goudarzi R, 2013. Studies of vapor transport from buffer to tunnel backfill (“sauna” effects). SKB R-13-42, Svensk Kärnbränslehantering AB.
- Birgersson M, Goudarzi R, 2016. Vapor transport and sealing capacity of buffer slots (“sauna” effects). SKB TR-15-09, Svensk Kärnbränslehantering AB.
- Birgersson M, Goudarzi R, 2017. Summary report on “sauna” effects. SKB TR-17-07, Svensk Kärnbränslehantering AB.
- Birgersson M, Goudarzi R, 2018. Investigations of gas evolution in an unsaturated KBS-3 repository. SKB TR-18-11, Svensk Kärnbränslehantering AB.
- Björck M, Taxén C, Vuoristo T, Elger R, Zavalis T, Wikström L, Sparr M, 2019. Embedded oxide particles in FSW. Posiva SKB Report 10, Posiva Oy, Svensk Kärnbränslehantering AB
- Björkbacka Å, Hosseinpour S, Leygraf C, Jonsson M, 2012. Radiation induced corrosion of copper in anoxic aqueous solution, *Electrochemical and Solid-State letters*, 15 C5-C7.

- Björkbacka Å, Hosseinpour S, Johnson M, Leygraf M, Jonsson M, 2013. Radiation induced corrosion of copper for spent nuclear fuel storage, *Radiation Physics and Chemistry*, 92, 80-86.
- Björkbacka Å. 2015. Radiation induced corrosion of copper, Doctoral Thesis, KTH Royal Institute of Technology, Stockholm, Sweden, ISBN 978-91-7595-710-4
- Butt M. Z. 1983. Effect of hydrogen attack on the strength of high purity copper, *J. Material Sci. Lett.*, 2 (1983) 1-2
- Carpén L., Rajala P., and Bomberg M. 2016. Microbial influence on corrosion of copper in the repository environment. Copper corrosion seminar, 15.12.2016 Aalto University, Otaniemi.
- Chen J, Qin Z, Martino T, Shoesmith D W, 2017. Non-uniform film growth and micro/macrogalvanic corrosion of copper in aqueous sulphide solutions containing chloride. *Corrosion Science*, 114, 72 – 78.
- Chen J, Qin Z, Martino T, Guo M, Shoesmith D W, 2018. Copper transport and sulphide sequestration during copper corrosion in anaerobic aqueous sulphide solutions. *Corrosion Science*, 131, 245 – 251.
- Cleveland C., Moghaddam, S., Orazem, M.E. 2014. Nanometer-scale corrosion of copper in de-aerated deionized water, *J. Electrochem. Soc.* 161 (2014) C107–C114.
- Forsström A, Becker R, Öijerholm J, Yagodzinskyy Y, Hänninen H, Linder J, 2017. Hydrogen absorption in copper as a result of corrosion reactions in sulphide and chloride containing deoxygenated water at 90 °C in simulated spent nuclear fuel repository conditions. In *Proceedings of EUROCORR 2017 – The Annual Congress of the European Federation of Corrosion, 20th International Corrosion Congress and Process Safety Congress, Prague, Czechia, 3 – 7 September 2017.*
- Ganchenkova M G, Yagodzinskyy Y N, Borodin V A, Hänninen H, 2014. Effects of hydrogen and impurities on void nucleation in copper: Simulation point of view. *Philosophical Magazine* 94, 3522 – 3548.
- Gordon A., Sjögren L., Taxén C., Johansson A. J. 2017. Retrieval and post-test examination of packages 4 and 5 of the MiniCan field experiment, (2017) SKB rapport TR-16-12.
- Gordon A, Johansson J, Pahverk H, Börjesson E, Sjögren L, 2018. Corrosion morphology of copper in anoxic sulphide environments. SKB TR-18-14, Svensk Kärnbränslehantering AB.
- Gordon A., Pahverk H., Börjesson E., Johansson A. J. 2018b. Examination of copper corrosion specimens from ABM 45, package 5. SKB technical report TR-18-17.
- Guinan M W, 2001. Radiation effects in spent nuclear fuel canisters, SKB Technical Report TR-01-32.
- He, X., Ahn T. and Gwo J.-P. 2018. Corrosion of Copper as a Nuclear Waste Container Material in Simulated Anoxic Granitic Groundwater. *Corrosion*, Feb 2018, Vol.74(2), pp.158-168.
- Hedin A. et al. 2011. Long-term safety for the final repository for spent nuclear fuel at Forsmark. Main report of the SR-Site project SR-Site main report, SKB TR-11-01

- Hedin A. et al. 2019. Supplementary information on canister integrity issues. SKB TR-19-15, Svensk Kärnbränslehantering AB.
- Hultquist G. 1986. Hydrogen evolution in corrosion of copper. *Corros. Sci.*, 26, 173-176 (1986)
- Hultquist G. Szakálos P., Graham M.J., Sproule G.I., Wikmark G. 2008. "Detection of hydrogen in corrosion of copper in pure water", Proceedings of the 2008 International Corrosion Congress (2008) 1–9, Paper 3884.
- Hultquist G. Szakálos P., Graham M.J., Belonoshko A.B., Sproule G.I., Gråsjö, Dorogokupets P., Danilow B., Aastrup T., Wikmark G., Chuah G.K., Eriksson J.C., Rosengren A., 2009. "Water corrodes copper", *Catal. Lett.* 132 311–316.
- Hultquist G. Graham M.J., Szakálos P., Sproule G.I., Rosengren A., Gråsjö L., 2011. Hydrogen gas production during corrosion of copper by water. *Corros. Sci.* 53 310–319.
- Hultquist G., Graham M.J., Kodra O., Moisa S., Liu R., Bexell U., Smialek J.L. 2013. Corrosion of copper in distilled water without molecular oxygen and the detection of produced hydrogen, SSM-report 2013-07.
- Hultquist G., Graham M.J., Kodra O., Moisa S., Liu R., Bexell U., Smialek J., 2015. Corrosion of copper in distilled water without oxygen and the detection of hydrogen. *Corros. Sci.* 95 162–167. (2015)
- Huutilainen C., Saario T., Toivonen A. 2018. Review of the Aaltonen-mechanism. SKB-report R-18-03.
- Johansson, A. J. Lilja, C. Brinck, T. 2011. On the formation of hydrogen gas on copper in anoxic water. *The Journal of Chemical Physics*, 28, Vol.135(8)
- Karland O. et al. 2009. Long term test of buffer material at the Äspö Hard Rock Laboratory, LOT project. Final report on the A2 test parcel. SKB-report TR-09-29.
- Kasbohm, J., Nguyen-Thanh, L., Hoang-Minh, T., Pusch, R., Knutsson, S. Pham, T. N. 2019. Mechanisms of Mineralogical Alteration of Dioctahedral Smectites in Contact with Water – A Review. In: *Earth Sciences and Geotechnical Engineering*.
- Kaufhold S., Dohrmann R., Gröger-Trampe J. 2017. Reaction of native copper in contact with pyrite and bentonite in anaerobic water at elevated temperatures, *Corr. Eng., Sci. and Tech.*, 52 (2017) 349-358.
- King F. and Newman R. 2010. SKB Report number TR-10-04.
- Korzhavyi P. and Sandström R. 2014. Monovacancy in copper: Trapping efficiency for hydrogen and oxygen. *Computational Materials Science* 84 (2014) 122–128
- Leijon G. et al. 2017. In situ hydrogen charging of OFP copper during creep. SKB report R-17-17.
- Lousada C M, Soroka I L, Yagodzinsky Y, Tarakina N V, Todoshchenko O, Hänninen H, Korzhavyi P A, Jonsson M, 2016. Gamma radiation induces hydrogen absorption by copper in water. *Nature Scientific Reports* 6, 24234. doi:10.1038/srep24234

Marja-aho, M., Rajala, P., Huttunen-Saarivirta, E., Legat, A., Kranjc, A., Kosec, T., Carpén, L. 2018. "Copper corrosion monitoring by electrical resistance probes in anoxic groundwater environment in the presence and absence of sulfate reducing bacteria" *Sensors and Actuators A* 274 (2018) 252–261.

Mattsson E. 1997. Projekt Inkapsling, PM 97-3420-22.

Müller H. et al. 2017. Implementation of the full-scale emplacement (FE) experiment at the Mont Terri rock laboratory. *Swiss J. Geosci.* (2017) 110:287–306.

Ottosson, M., Boman, M., Berastegui, P., Andersson, Y., Hahlin, M., Korvela, M., Berger, R. 2018. Response to the comments by P. Szakálos, T. Åkermark and C. Leygraf on the paper "Copper in ultrapure water, a scientific issue under debate". *Corrosion Science*, Sep 2018, Vol.142, p.308

Padovani C., Pletser D., Jurkschat K., Armstrong D., Dugdale S., Brunt D., Faulkner R., Was G., Johansson. A. J. 2019. Assessment of microstructural changes in copper due to gamma radiation damage, SKB Technical Report TR-19-12.

Panagopoulos C. N. and Zacharopoulos N. 1994. Cathodic hydrogen charging and mechanical properties of copper, *J. Materials Sci.*, 29 (1994) 3843-3846

Pedersen K., Bengtsson, A., Blom, A., Johansson, L., Taborowski, T. 2017. Mobility and reactivity of sulphide in bentonite clays – Implications for engineered bentonite barriers in geological repositories for radioactive wastes. *Applied Clay Science* Volume 146, 15 September 2017, Pages 495-502.

Pusch R. 2019. Personal Communication 2019 09-12.

Pusch, R., Yong, R.N., Nakano, M., 2019. *Geologic Disposal of High-Level Radioactive Waste*. CRC Press, New York (Taylor & Francis Group).

Pusch, R., 2015. *Bentonite Clay, Environmental Properties and Applications*. CRC Press, New York (Taylor & Francis Group).

Pusch R., Kasbohm J., Knutsson S., Yang T., Nguyen-Thanh L. 2015. The Role of Smectite Clay Barriers for Isolating High-Level Radioactive Waste (HLW) In Shallow and Deep Repositories. *Procedia Earth and Planetary Science* 15, p. 680 – 687.

Raja V.S. and Shoji T. 2011. *Stress Corrosion Cracking Theory and Practice*, Woodhead Publishing Book Series in Metals and Surface Engineering, ISBN 978-1-84569-673-3.

Rosborg B. and Werme L 2008. *J. Nuclear Materials* 379 (2008) pp. 142-153  
Savolainen K., Saukkonen T., Mononen J., and Hänninen H. 2008. Entrapped Oxide Particles in Friction Stir Welds of Copper. 7th Int. Symposium on Friction Stir Welding. Awaji Island, Japan 20-22 May, 2008.

Sellin P. et al. 2017. Long re-saturation phase of a final repository Additional supplementary information. SKB TR-17-15

Senior N A., Newman R C, Artymowicz D, Binns W J, Keech P G, Hall D S. 2019. Communication– A method to measure extremely low corrosion rates of copper metal in anoxic aqueous media. *Journal of The Electrochemical Society* 166, C3015–C3017.

Sipilä K., Arilahti, E., Lehtikuusi, T., Saario, T. 2014. Effect of sulphide exposure on mechanical properties of CuOFP. *Corrosion Engineering, Science and Technology* 49, 410 – 414.

Szakálos P., Hultquist G., Wikmark G. 2007. Corrosion of Copper by Water. *Electrochem Solid State Lett.* 10:C63 (2007)

Szakálos P. and Hultquist G. 2013. Scientific symposium arranged by the Swedish National Council for Nuclear Waste: New insights into the repository's engineered barriers, Stockholm, 20 –21 November 2013

Szakálos P. and Seetharaman S. 2012. Corrosion of copper canister, SSM-report 2012-17.

<http://www.stralsakerhetsmyndigheten.se/Global/Publikationer/Rapport/Technical%20Note/2012/SSM-Rapport-2012-17.pdf>

Szakálos P., Rosengren A., Leygraf C., Seetharaman S. 2017. Land and Environmental Court in Nacka, Sweden, case no. M 1333-11, closing argument, KTH (Addendum 821).

Szakálos P., Åkermark, T., Leygraf, C. 2018. Comments on the paper “Copper in ultrapure water, a scientific issue under debate” by M. Ottosson, M. Boman, P. Berastegui, Y. Andersson, M. Hahlin, M. Korvela, and R. Berger. *Corrosion Science*, 09/2018, Vol.142, C, pp.305-307

Taborowski T. et al, 2019. Microbiology In Nuclear waste Disposal, MIND, Horizon 2020 project, grant agreement no. 661880. Deliverable D2.4, v2.

Taniguchi N and Kawasaki M, 2008. Influence of sulfide concentration on the corrosion behavior of pure copper in synthetic seawater. *J. of Nuclear Materials*, 379, pp 154–161.

Taxén C., Flyg J., Bergqvist H. 2018. Stress corrosion testing of copper in sulfide solutions. SKB-report TR-17-16.

Taxén C., Flyg J., Bergqvist H 2019. Stress corrosion testing of copper in near neutral sulfidesolutions. SKB -report TR-19-13.

Wersin P. and Kober F, 2017. FEBEX-DP, Metal Corrosion and Iron-Bentonite Interaction Studies. *Arbeitsbericht NAB* 16-16.

Yagodzinskyy Y., Malitckii, E., Tuomisto, F., Hänninen, H. 2018. Hydrogen-induced strain localisation in oxygen-free copper in the initial stage of plastic deformation, *Philosophical Magazine* 98 (2018) 727-740

Yang Q. Toijer E., Olsson P. 2019. Analysis of radiation damage in the KBS-3 canister materials, SKB Technical Report TR-19-14

# Coverage of SKB reports

Following reports have been covered in the review.

**Table 1:** SKB-Reports covered in the review.

Reviewed report	Reviewed sections	Comments
<i>[insert SKB report number and title]</i>	<i>[insert reviewed sections]</i>	<i>[insert comments, if any]</i>
SKB TR-19-15. Supplementary information on canister integrity issues	All	
SKB TR-18-11. Investigations of gas evolution in an unsaturated KBS-3 repository.	All	
TR-18-14. Corrosion morphology of copper in anoxic sulphide environments.	All	
TR-17-16. Stress corrosion testing of copper in sulfide solutions.	All	
TR-19-13. Stress corrosion testing of copper in near neutral sulfide solutions.	All	
R-18-03. Review of the Aaltonen-mechanism	All	
R-17-17. In situ hydrogen charging of OFP copper during creep	All	
Posiva SKB Report 10. Embedded oxide particles in FSW.	Chapters/Sections: 1., 3.1, 3.2.1, 4.1, 4.5 and 5	
TR-19-14. Analysis of radiation damage in the KBS-3 canister materials,	All	

---

TR-19-12. Assessment of microstructural changes in copper due to gamma radiation damage. All

---

TR-18-17. Examination of copper corrosion specimens from ABM 45, package 5. All

---

Following additional SKB-reports has been covered partially or fully:  
TR-13-13, R-13-42, TR-15-09, TR-17-07, TR-16-12, TR-01-32, TR-11-01, TR-09-29, TR-10-04, TR-17-15, SKB TR-12-06 and the preliminary SKB-report ID: 1602591.





**Authors**

Oswaldo Pensado  
Stuart Stothoff

Southwest Research Institute  
San Antonio, Texas.

Review Assignment for the Swedish  
Radiation Safety Authority:  
Independent Canister Integrity  
Modelling and Dose Assessment



# Abstract

This report documents an evaluation of SKB's supplementary information on canister integrity issues (SKB Technical Report TR-19-15 dated March 2019). The Swedish Radiation Authority (SSM) assigned independent parties to review information in SKB TR-19-15, focusing on different aspects of the SKB supplied information, such as (i) materials science considerations, (ii) performance assessment (PA) and radionuclide transport computations, and (iii) biosphere modelling. The focus of this report is on aspect (ii), with limited discussion of aspects (i) and (iii) where pertinent. Information in this report conveys the independent view of Southwest Research Institute® (SwRI®).

The document SKB TR-19-15 addressed five issues posed by the Land and Environmental Court, namely

- a) Corrosion due to reaction in oxygen-free water.
- b) Pitting due to reaction with sulphide, including the influence of the sauna effect on pitting.
- c) Stress corrosion cracking due to reaction with sulphide, including the influence of the sauna effect on stress corrosion cracking.
- d) Hydrogen embrittlement.
- e) The effect of radioactive radiation on pitting, stress corrosion cracking and hydrogen embrittlement.

Using a combination of laboratory experiments, field testing, and numerical analyses, SKB concluded that each process is either unlikely or of minor consequence to merit full consideration in a PA of the geologic repository system, with the exception of pitting corrosion of the copper canister promoted by hydrogen sulphide ion carried in the groundwater. SKB implemented a simplified assessment for pitting corrosion, and concluded this process would result in minor consequences that do not change the conclusions of the 2011 SR-Site analysis.

SwRI examined the SKB arguments and technical basis for excluding five Land and Environmental Court issues, and agreed with the SKB's conclusions, but recognizing that the emphasis of the SwRI review effort was on radionuclide transport computations; other independent groups were tasked by SSM to evaluate materials science and biosphere modelling aspects of the SKB analyses. Localized corrosion (interpreted by SKB to result from micro-galvanic corrosion, and of similar corrosion damage morphology than pitting corrosion) required further consideration, because high sulphide concentrations and fluxes—where micro-galvanic corrosion has been detected experimentally—cannot not be unequivocally ruled out to arise in deposition holes of the repository system. The number of canisters potentially affected by localized corrosion was estimated, a PA model was used to compute dose consequences of a localized corrosion scenario, and similar results to the SKB's dose estimates were derived. An alternative scenario was examined where micro-galvanic corrosion was postulated to occur sooner than considered by SKB; the average calculated dose consequences were of similar magnitude to the SKB dose consequences of a scenario of delayed micro-galvanic corrosion occurrence (with the delay related to erosion of the buffer barrier).

The unsaturated buffer and saturated buffer scenarios were examined in detail to consider effects of sulphate reducing bacteria (SRB). For the saturated scenario, it was concluded unlikely for sulphide to cause failure of canisters in 10<sup>6</sup> years, because of slow diffusion of dissolved sulphide in saturated bentonite. For the

unsaturated case, the production of sulphide by SRB, diffusion of sulphide gas in the gas phase through the buffer material and eventual reaction of sulphide with copper mediated by water were considered. It was concluded that the rate of sulphide gas supply would be constrained and, consequently, cause negligible damage to the copper canisters. A key assumption of the analysis is that the sulphide concentration in bentonite porewaters is small ( $\leq 10^{-6}$  mol/L) independently of the source (from groundwater or from SRB), which assumption is based on experimental studies by SKB. Such small concentrations heavily limit the presence of sulphide gas in air. Other factors limiting diffusion of sulphide gas through the bentonite include water saturation, bentonite porosity, and absolute air pressure. Because of those factors and the limited time for the buffer material to saturate with water (after saturation, transport becomes dominated by diffusion of dissolved sulphide), the amount of sulphide damage to copper canisters during the unsaturated period is expected to be negligible.

# Contents

<b>1</b>	<b>Introduction</b> .....	<b>1</b>
<b>2</b>	<b>SKB Analysis of Localized Corrosion of the Copper Canister</b> .....	<b>2</b>
2.1	Localized Corrosion Abstraction .....	2
2.2	Number of Canisters Affected by Localized Corrosion .....	4
2.3	Radionuclide Release Computations Accounting for Localized Corrosion .....	13
2.4	Robustness Calculation .....	15
<b>3</b>	<b>Saturated and Unsaturated Buffer Scenarios</b> .....	<b>18</b>
3.1	Saturated Buffer Conditions.....	18
3.2	Unsaturated Buffer Conditions.....	21
3.2.1	Experimental Support.....	21
3.2.2	Gas Transport Computations .....	22
<b>4</b>	<b>Conclusions</b> .....	<b>36</b>
<b>5</b>	<b>References</b> .....	<b>38</b>
	<b>APPENDIX 1 Coverage of SKB reports</b> .....	<b>41</b>

# 1 Introduction

This report documents an independent review of SKB's supplemental information on canister integrity issues in the Technical Report SKB TR-19-15 (SKB, 2019), which SKB prepared to address five issues posed by the Land and Environmental Court, namely

- a) Corrosion due to reaction in oxygen-free water.
- b) Pitting due to reaction with sulphide, including the influence of the sauna effect on pitting.
- c) Stress corrosion cracking due to reaction with sulphide, including the influence of the sauna effect on stress corrosion cracking.
- d) Hydrogen embrittlement.
- e) The effect of radioactive radiation on pitting, stress corrosion cracking and hydrogen embrittlement.

The focus of the review was on radionuclide transport and performance assessment (PA) calculations. SKB implemented a combination of laboratory experiments, field testing, and numerical analyses, to conclude that most issues highlighted by the Land and Environmental Court can be ruled out, with the exception of pitting corrosion. SKB found that a form of galvanic corrosion, giving rise to a corrosion morphology of features similar to pitting corrosion, cannot be dismissed for relatively high hydrogen sulphide flux conditions that may arise at a small number of deposition holes. SKB performed simplified computations of a localized corrosion scenario, and concluded that even if localized corrosion occurred, the consequences would be minor and that conclusions of the 2011 SR-Site analysis would remain valid. The SKB localized corrosion analyses are summarized and evaluated in Section 2. Section 3 presents an analysis of sulphide corrosion for saturated buffer and unsaturated buffer scenarios, including the effect of sulphate-reducing bacteria. Conclusions are presented in Section 4. Section 5 is the list of references. An appendix lists the SKB documents considered in this report.

## 2 SKB Analysis of Localized Corrosion of the Copper Canister

We examined the SKB analysis addressing the five issues posed by the Land and Environmental Court, and agreed with the SKB conclusions that most issues can be excluded with the exception of localized corrosion of the copper canister. Key aspects of the technical basis and simplifications for PA computations are evaluated in this chapter.

### 2.1 Localized Corrosion Abstraction

SKB evaluated localized corrosion mediated by a  $\text{Cu}_2\text{S}$  film (SKB, 2019, Section 5). For metals forming passive films, those films are passive only under a range of electrical potentials; pitting corrosion can occur when the electrical potential exceeds the *pitting potential*. Pitting corrosion may be initiated at local defects on the passive film; the passivated surface behaves as a cathode, and active metal dissolution occurs at the film defects eventually forming pits. SKB concluded that  $\text{Cu}_2\text{S}$  films are not passive, but porous films, except possibly under conditions when the supply of dissolved sulphide is not limited. Several studies sponsored by SKB (e.g., Chen et al., 2017, 2018, 2019) reported localized corrosion morphologies for copper in anaerobic aqueous sulphide solutions, which SKB interpreted as resulting from galvanic corrosion. Under galvanic corrosion, cathodic and anodic islands of comparable size develop on the metal surface, giving rise to metal roughening (but not deep, high-aspect-ratio pits). SKB concluded that the micro-galvanic corrosion morphologies appear in solutions of relatively high sulphide concentration ( $>10^{-4}$  mol/L); at lower sulphide concentrations, corrosion fronts are more uniform. SKB compared the maximum pit depth to the average depth of the corrosion front (Chen et al., 2019), and estimated a maximum ratio of 20, from experiments spanning up to approximately 1,700 days (SKB, 2019, Table 5-1). Based on these observations, SKB used the maximum factor of 20 as a “pitting factor” in simplified PA computations. In the simplified PA, SKB assumed that the corrosion rate would increase by a factor of 20 only for cases of relatively high hydrogen sulphide fluxes at the canister surface.

SKB derived a *transition criterion* to apply the factor of 20 based on a hydrogen sulphide flux, as follows. Measurements of film thickness versus time by Chen et al. (2017) indicate that the  $\text{Cu}_2\text{S}$  film grows following a power law of time [i.e., an equation of the form  $d(t) = A t^n$ ] in hydrogen sulphide solutions (Figure 2-1). For conditions with relatively high hydrogen sulphide ion concentration ( $[\text{HS}^-] > 10^{-4}$  mol/L), compact  $\text{Cu}_2\text{S}$  films develop that offer increasing resistance to the transport of copper ions through the film with increasing film thickness. The film growth rate is computed as the time-derivative of the power law:  $d'(t) = A n t^{n-1}$ . As time increases, the growth rate decreases and tends towards zero (for exponents  $0 < n < 1$ )—this decreasing rate indicates more difficult transport of copper ions through the  $\text{Cu}_2\text{S}$  film as the compact film thickens. For porous films, the film transport resistance is not the factor limiting the growth of the film; instead, the limiting factor is the rate of supply of the hydrogen sulphide ion,  $\text{HS}^-$ . For experiments with low  $[\text{HS}^-]$ , the rate of film growth is constant (i.e., the film thickness increases linearly with time, as in the case of  $[\text{HS}^-] = 5 \times 10^{-5}$  mol/L in

Figure 2-1). SKB concluded that to form a compact Cu<sub>2</sub>S film, the rate of supply of HS<sup>-</sup> must at least exceed the rate of supply for formation of porous films {i.e., greater than [HS<sup>-</sup>]=5×10<sup>-5</sup> mol/L in Figure 2-1}. SKB assumed that the film porosity was 50 percent, and considered the density and molecular mass of Cu<sub>2</sub>S to be 5.6 g/cm<sup>3</sup> and 159.14 g/mol, respectively, to transform a growth rate of 0.063 nm/hr (=1.75×10<sup>-14</sup> m/s; film growth rate for the case [HS<sup>-</sup>]=5×10<sup>-5</sup> mol/L in Figure 2-1) to an equivalent HS<sup>-</sup> flux of 3×10<sup>-10</sup> mol/(m<sup>2</sup>-s):

$$\begin{aligned} \text{flux}(\text{HS}^-) &= (1 - \text{porosity}) \times 1.75 \times 10^{-14} \text{ m/s} \times \frac{5.6 \times 10^6 \text{ g/m}^3}{159.14 \text{ g/mol}} \\ &= 3 \times 10^{-10} \text{ mol/(m}^2\text{-s)} \end{aligned} \quad (2-1)$$

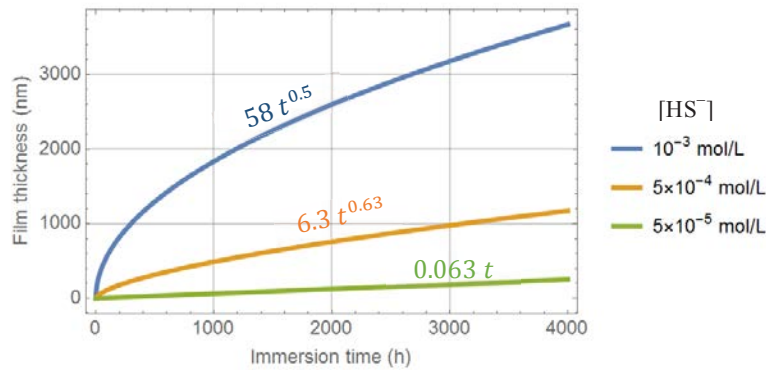


Figure 2-1. Cu<sub>2</sub>S film growth versus time, according to Chen et al. (2017).

SKB considered the flux of 3×10<sup>-10</sup> mol/(m<sup>2</sup>-s) to be a required minimum hydrogen sulphide ion flux for a compact film to form, and possibly micro-galvanic corrosion to affect copper. Note that exceeding the threshold flux is a necessary but not sufficient condition for the formation of a compact Cu<sub>2</sub>S film.

We examined the SKB localized corrosion analysis in the document SKB TR-19-15, and agree with the conclusion that formation of a passive Cu<sub>2</sub>S film is unlikely, and, consequently, agree that pitting corrosion is also unlikely. Hydrogen sulphide ion is more likely to attack copper in the form of general corrosion. However, there is experimental evidence of corrosion roughening of the copper surface through a micro-galvanic corrosion process. Such micro-galvanic corrosion has only been observed in anaerobic solutions at relatively high sulphide ion concentrations ([HS<sup>-</sup>] > 10<sup>-4</sup> mol/L). The approach SKB developed for the simplified PA computations, based on a threshold HS<sup>-</sup> flux is reasonable. At low [HS<sup>-</sup>] in solution, it is expected that the rate of supply or flux of HS<sup>-</sup> towards the copper canister will control the quality of the Cu<sub>2</sub>S film (i.e., compact versus porous), which in turn controls the onset of micro-galvanic corrosion. Setting a flux equal to 3×10<sup>-10</sup> mol/(m<sup>2</sup>-s) as a necessary condition for the formation of a compact Cu<sub>2</sub>S film is well supported by the experimental data available.

We highlight that the sulphide ion flux 3×10<sup>-10</sup> mol/(m<sup>2</sup>-s) is a low bound for necessary conditions to form a compact Cu<sub>2</sub>S film. Actual sulphide ion fluxes promoting the formation of a compact Cu<sub>2</sub>S film are very likely much higher. For example, Figure 2-2 shows equivalent sulphide ion fluxes to support film growth rates consistent with the curves in Figure 2-1. Assuming a film of 50 percent porosity, a Cu<sub>2</sub>S film growth rate of 1 nm/hr is equivalent to a dissolved sulphide ion flux of 4.89×10<sup>-9</sup> mol/(m<sup>2</sup>-s). Figure 2-2 incorporates this conversion factor [4.89×10<sup>-9</sup> mol/(m<sup>2</sup>-s) per nm/hr of film growth] to transform growth rates in units of nm/hr to fluxes in units of mol/(m<sup>2</sup>-s). At 1 hour, the equivalent sulphide ion

fluxes forming compact  $\text{Cu}_2\text{S}$  films (cases  $[\text{HS}^-]=10^{-3}$  mol/L and  $[\text{HS}^-]=5\times 10^{-4}$  mol/L) are at least two orders of magnitude higher than the SKB assumed  $3\times 10^{-10}$  mol/( $\text{m}^2\text{-s}$ ) threshold. A more refined threshold controlling the transition from porous to compact  $\text{Cu}_2\text{S}$  film may be much higher than the assumed  $3\times 10^{-10}$  mol/( $\text{m}^2\text{-s}$ ) threshold.

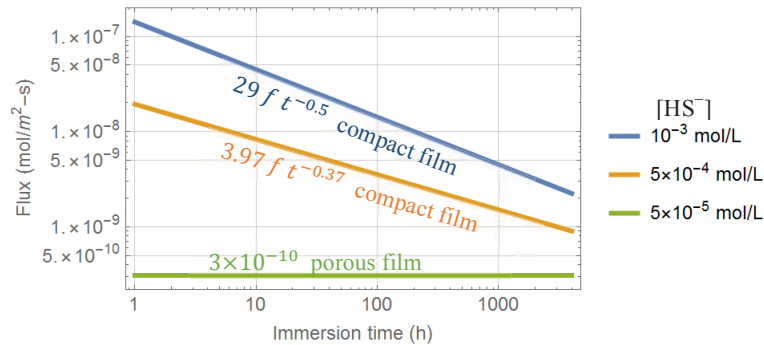


Figure 2-2. Equivalent dissolved-sulphide ion fluxes to support  $\text{Cu}_2\text{S}$  film growth rates of Figure 2-1. The factor  $f$  is a conversion factor ( $f = 4.89\times 10^{-9}$ ) to transform  $\text{Cu}_2\text{S}$  film growth rates in units of nm/hr to sulphide ion fluxes in units of mol/( $\text{m}^2\text{-s}$ ), assuming 50 percent film porosity.

We note that power laws of the form  $d(t) = A t^n$  arise commonly from experiments in multiple systems quantifying film growth and propagation of corrosion fronts, including pitting corrosion. When the exponent  $n$  is less than 1 (which is the most common case), the growth rate slows with time.

Finally, we agree on selecting a factor of 20 to evaluate the effect of micro-galvanic corrosion. In metals exhibiting pitting corrosion, pitting corrosion rates can be a few orders of magnitude greater than general corrosion; however, those rates may decrease with time, for example due to build-up of corrosion products, polarization of the surface, and evolution of the environment.<sup>1</sup> Considering a factor of 20 to assess the effect of micro-galvanic corrosion is reasonable, well within the range of other metals affected by localized corrosion (e.g., Cesen et al., 2014). SKB conservatively omitted likely decreases in corrosion rates with time in the simplified PA computations.<sup>1</sup>

## 2.2 Number of Canisters Affected by Localized Corrosion

SKB evaluated the time it would take for canisters to fail by hydrogen sulphide induced corrosion (SKB, 2010a). Under saturated conditions the buffer is a diffusive barrier. SKB concluded that it would take longer than one million years for canisters to fail, even omitting hydrogen sulphide solubility constraints in the buffer (constraints that would reduce diffusion rates). SKB concluded that the only scenarios under which canisters could fail within one million years were related to buffer erosion and consequential direct contact of groundwater (carrying hydrogen

<sup>1</sup> Pitting corrosion commonly follows a power growth law of the form  $d(t) = A t^n$ , with  $0 < n < 1$  and  $d$ =pit depth. The propagation rate,  $d'(t)$ , decreases with time when  $0 < n < 1$ .

sulphide) with the copper canister (SKB, 2010a). SKB evaluated a scenario where a water-carrying fracture intercepts the deposition hole and erodes a limited volume of buffer material until the groundwater directly contacts the canister. SKB assumed that sulphide carried in the groundwater would attack an area on the canister equal to a half-ring (radius equal to the canister outer radius, ~50 cm) of height equal to the buffer initial thickness along the radial direction (35 cm). The corrosion rate is inversely proportional to the attack area on the copper canister. SKB considered ten realizations of the hydrogeological model (i.e., 10 random distribution sets of fractures intercepting the repository), and three different models or empirical equations correlating the fracture transmissivity and fracture size or aperture (referred to as *correlated*, *uncorrelated*, and *semi-correlated*). SKB used the semi-correlated model as the reference case of the SR-Site analysis, because SKB regarded the semi-correlated description of the hydrogeological system to be the most realistic. The semi-correlated model predicted lower flow rates per canister than the uncorrelated and correlated models. The uncorrelated model, on the other hand, predicted the highest flow rates. Approximately 40 percent of the deposition holes were computed to be intercepted by fractures, based on the statistics of the realizations of the hydrogeological model. SKB proposed to implement a rejection criterion for deposition holes intercepted by relatively large fractures [Extended Full Perimeter Intersection Criterion—(EFPC)], and with the EFPC, the number of deposition holes intercepted by fractures would be reduced to approximately 30 percent.

SKB concluded that conditions leading to buffer erosion that cause failure of the canister within one million years were rare. In the SR-Site base case, SKB computed the expected number of failed canisters in  $10^6$  years to be 0.117, out of approximately 6,000 canisters in the system (SKB, 2010a, Figure 5-8, semi-correlated base case). SKB implemented a sensitivity analysis considering alternatives for buffer erosion volume, different time frames for active buffer erosion and the onset of advective flow conditions, effect of rock spalling in deposition tunnels on flow, and various empirical equations relating the transmissivity to the fracture size (i.e., the correlated, uncorrelated, and semi-correlated hydrogeological models). The number of canisters failed for the different cases are summarized in SKB TR-10-66 (SKB, 2010a, Figures 5-7 and 5-8). For most cases, the expected number of failed canisters is less than 1.

A total of 56 canister failure times (i.e., for failure times less than  $10^6$  years) for the semi-correlated base case are listed in SKB TR-10-50 (SKB, 2010b; Table 4-3, case referred to as Central Corrosion Case). We implemented the following back-of-the-envelope probability computation to check the expected number of failed canisters. SKB considered a total of 10 realizations of the hydrogeological model (semi-correlated base case), each with 6,916 fractures (SKB, 2010b). For each fracture, SKB accounted for 46 discrete concentrations of hydrogen sulphide ion in the groundwater (SKB, 2010a, Figure 4-4). Therefore, the total number of combinations SKB considered was  $10 \times 6,916 \times 46 = 3,181,360$ . Out of those possible combinations, only 56 combinations produced canister failure times less than  $10^6$  years (SKB, 2010b, Table 4-3). Thus, the probability per canister to fail within  $10^6$  years is  $56/3,181,360 = 1.76 \times 10^{-5}$ . According to the Data Report SKB TR-10-52 (SKB, 2010c), the number of canisters in the system is 6,103. Therefore, the expected number of failed canisters in  $10^6$  years is  $6,103 \times 10^3 \times (1.76 \times 10^{-5}) = 0.11$ ; this number compares well to the number 0.117 in SKB TR-10-66 (SKB, 2010a, Figure 5-8). If localized corrosion, in the form of micro-galvanic corrosion, were to occur, the number of failed canisters may change as well as the failure time distribution, compared to data in SKB TR-10-50 (SKB, 2010b; Table 4-3).

SKB adopted a simplified approach to estimate the number of canisters affected by micro-galvanic corrosion and the distribution of canister failure times. First, SKB set a sulphide ion flux equal to  $3 \times 10^{-10}$  mol/(m<sup>2</sup>-s) (see Section 2.1 in this report) as a necessary condition for the onset of micro-galvanic corrosion. Using this criterion, SKB concluded that localized corrosion of the copper canister would not occur for the unsaturated and saturated buffer conditions, because computed maximal sulphide ion fluxes were below  $3 \times 10^{-10}$  mol/(m<sup>2</sup>-s). SKB concluded that groundwater may supply a large enough sulphide ion flux to cause micro-galvanic corrosion on copper containers, but only for the eroded buffer conditions with extreme (and rare) combinations of sulphide ion concentration in the groundwater and water flow rates. SKB considered flow rates computed using the correlated hydrogeological model, which predicts higher flow rates per canister than the semi-correlated model, but less than the uncorrelated model. SKB computed the canister failure time considering hydrogen sulphide copper corrosion with an enhancement factor of 20 for cases when the sulphide ion flux exceeded  $3 \times 10^{-10}$  mol/(m<sup>2</sup>-s). SKB analysed two alternatives for buffer erosion. In the first alternative, SKB used the same buffer erosion model considered in the SR-Site analysis to establish the onset of advective conditions on the canister. In the second alternative, SKB assumed that advective conditions would be established after 20,000 years. SKB asserted that it takes longer than 20,000 years for advective conditions to be established (even in the absence of buffer erosion). The shortest buffer erosion time for the correlated hydrogeological model is approximately 75,000 years, which is much longer than the 20,000 years assumed by SKB. SKB computed mean annual dose consequences equal to 0.74 µSv for alternative one and 1.03 µSv for alternative two.

We could not precisely verify the SKB computations of the number of canisters affected by micro-galvanic corrosion, because only limited information is available in reports related to flow rates for the correlated hydrogeological model. However, information is available for the semi-correlated hydrogeological model that can be used to estimate the expected number of failed canisters. For example, SKB TR-10-66 (SKB, 2010a; Figure 5-6) presents copper corrosion rates assuming direct contact of the groundwater with the copper canister (i.e., ignoring any possible protection by the buffer) and assuming a sulphide ion concentration equals to  $10^{-5}$  mol/L for the semi-correlated hydrogeological model [that figure is reproduced in Figure 2-3(a) of this report]. The two curves in Figure 2-3(a) correspond to the case where fractures may intercept deposition holes without any repository design screening (legend “All deposition holes”), and to the case where the EFPC is implemented during construction to exclude interception of deposition holes by large fractures (legend “EFPC rejection”). The cumulative distribution function (CDF) can be transformed to a conditional CDF (conditional on a fracture intercepting a deposition hole) by shifting the curves vertically to start at 0, and normalizing by the fraction of fractures intercepting deposition holes (~40 percent for the “All deposition holes” case, and ~30 percent for the “EFPC rejection” case). The conditional CDF for the case “All deposition holes” is displayed in Figure 2-3(b) (black dots). The continuous curve in Figure 2-3(b) is a log-normal fit computed by matching the 0.95 and 0.98 quantiles. The log-normal curve was designed to match the upper tail of the corrosion rate distribution, because the interest is only on the high corrosion rates that have the potential to lead to canister failure within one-million years. It is noted that the corrosion rates are linearly proportional to the sulphide ion concentration in groundwater.

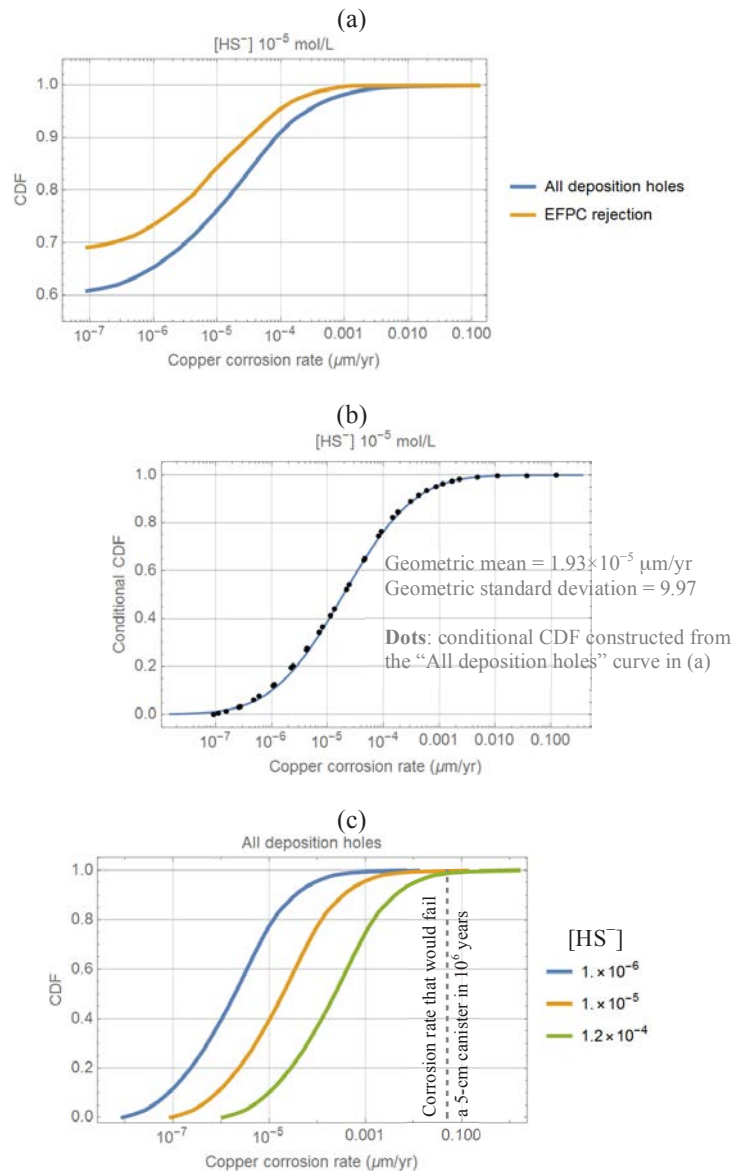


Figure 2-3. (a) Distribution of corrosion rates assuming direct contact of groundwater with the copper canister, for the semi-correlated hydrogeological base case. Data were digitized from SKB TR-10-66 (SKB, 2010a; Figure 5-6). (b) Conditional CDF considering the "All deposition holes" case from (a), and a log-normal distribution fitting the 0.95 and 0.98 quantiles (the continuous curve is the log-normal fit). (c) The conditional CDF for different sulphide ion concentrations is derived by proportionally scaling corrosion rates in (a).

The distribution of corrosion rates for other sulphide ion concentrations can be simply derived by proportionally scaling the corrosion rates. Figure 2-3(c) shows an examples of conditional CDFs for other sulphide ion concentrations than  $10^{-5}$  mol/L. In logarithmic scale, the proportional scaling is equivalent to a horizontal displacement of the distribution [Figure 2-3(c)]. The spread of corrosion rates in Figure 2-3 is exclusively a function of the variability in flow rates in fractures intercepting deposition holes.

We derived the distribution of corrosion rates accounting for the distribution of sulphide ion concentration as follows. The cumulative distribution of sulphide ion concentration, based on 46 samples of groundwater from the Forsmark area below 50 m depth, is provided in SKB TR-10-66 (SKB, 2010a; Figure 4-4). A digitized version is reproduced in Figure 2-4. The maximum measured concentration was  $1.2 \times 10^{-4}$  mol/L, and 45 of the 46 samples had a concentration less than or equal to  $1.2 \times 10^{-5}$  mol/L. We applied log-linear interpolation to compute the CDF as a continuous function of the sulphide ion concentration,  $s$ , assuming a maximum concentration of  $1.2 \times 10^{-4}$  mol/L. The continuous function is denoted as  $F(s)$ .

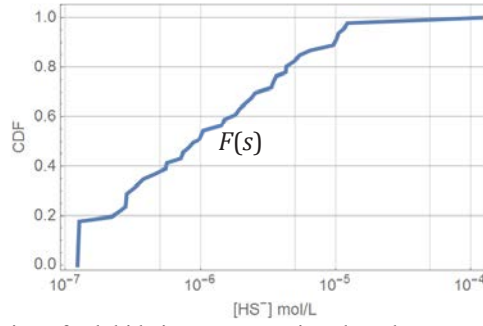


Figure 2-4. Distribution of sulphide ion concentrations based on groundwater samples of the Forsmark area below 50 m depth [data digitized from 46 points in SKB TR-10-66 (SKB, 2010a; Figure 4-4)].

The log-normal distribution, as a function of the geometric mean and geometric standard deviation is defined as

$$C(x; L\mu, L\sigma) = \frac{1}{2} \operatorname{erfc} \left( \frac{L\mu - \ln x}{\sqrt{2} L\sigma} \right) \quad (2-2)$$

Where  $x$  is the corrosion rate,  $\operatorname{erfc}$  is the complementary error function,  $\ln$  is the natural logarithm function, and

$$\begin{aligned} L\mu &= \ln GM = \ln(\text{geometric mean}) \\ L\sigma &= \ln(\text{geometric standard deviation}) \end{aligned} \quad (2-3)$$

We used the log-normal fit in Figure 2-3(b) as the reference distribution for the corrosion rate, making an adjustment to the geometric mean (the geometric mean is represented by the symbol  $GM$ ) to match an expected value of the number of failed canisters reported in SKB TR-10-66 (SKB, 2010a), which adjustment is later explained.

For any arbitrary sulphide ion concentration,  $[\text{HS}^-]=s$ , the corrosion rate distribution is estimated as

$$C\left(x; \ln \frac{GM s}{10^{-5} \text{ mol/L}}, L\sigma\right) = \frac{1}{2} \operatorname{erfc}\left(\frac{\ln \frac{GM s}{10^{-5} \text{ mol/L}} - \ln x}{\sqrt{2} L\sigma}\right) \quad (2-4)$$

The concentration  $10^{-5}$  mol/L is the reference concentration for the data in Figure 2-3. The term  $GM s/(10^{-5} \text{ mol/L})$  in Eq. (2-4) is the proportionally scaled corrosion rate geometric mean corresponding to the sulphide ion concentration  $s$ . The average corrosion rate distribution, integrating the variability in sulphide ion concentration, is estimated as

$$C_{av}(x) = \int_{1.2 \times 10^{-7}}^{1.2 \times 10^{-4}} C\left(x; \ln \frac{GM s}{10^{-5}}, L\sigma\right) \rho(s) ds \quad (2-5)$$

The unit, mol/L, is omitted in Eq. (2-5) for brevity. The integration limits  $1.2 \times 10^{-7}$  mol/L and  $1.2 \times 10^{-4}$  mol/L are the minimum and maximum sulphide ion concentrations in Figure 2-4, and  $\rho(s)$  is the probability density function for the groundwater sulphide ion concentration. Equation (2-5) can be numerically integrated, by applying a change of variables. The continuous cumulative distribution function for the sulphide ion concentration in Figure 2-4 is denoted as

$$p = F(s) \quad (2-6)$$

where  $p$  is the cumulative probability ( $0 \leq p \leq 1$ ), and  $F(s)$  is the cumulative distribution function in Figure 2-4. The probability density function  $\rho(s)$  is defined as the derivative of  $F(s)$

$$\rho(s) = F'(s) \quad (2-7)$$

The sulphide ion concentration can be computed as a function of the probability  $p$  with the inverse function  $F^{-1}$

$$s = F^{-1}(p) \quad (2-8)$$

Applying the change of variables  $p = F(s)$ , Eq. (2-5) becomes

$$C_{av}(x) = \int_0^1 C\left(x; \ln \frac{GM F^{-1}(p)}{10^{-5}}, L\sigma\right) dp \quad (2-9)$$

It is straightforward to numerically compute the integral in Eq. (2-9). Selecting an equidistant partition of the probability range, with  $N$  points (e.g.,  $N=1000$ ), such that

$$p_i = \frac{i}{N} \text{ with } i = 1, 2, 3, \dots, N \quad (2-10)$$

Then the integral is approximated as

$$C_{av}(x) \cong \frac{1}{N} \sum_{i=1}^N C\left(x; \ln \frac{GM F^{-1}(p_i)}{10^{-5}}, L\sigma\right) \quad (2-11)$$

We selected  $L\sigma$  consistent with the geometric standard deviation in Figure 2-3(b) ( $L\sigma = \ln(9.97) = 2.3$ ); however, the geometric mean, symbol  $GM$ , was treated as an adjustable parameter to match an average reported by SKB (SKB, 2010a). SKB computed an expected number of failed canisters equal to 0.175, for the case where groundwater was assumed to directly contact canisters (SKB, 2010a, Figure 5-8, Case F, semi-correlated and initial advection). We solved the equation

$$0.39 \times 6000 \times \frac{1}{N} \sum_{i=1}^N C \left( 0.05 \mu\text{m}/\text{yr}; \ln \frac{GM F^{-1}\left(\frac{i}{N}\right)}{10^{-5}}, L\sigma \right) = 0.175 \quad (2-12)$$

The factor  $0.39 \times 6000$  is the approximated number of canisters intercepted by fractures. The corrosion rate  $0.05 \mu\text{m}/\text{yr}$  is the minimum corrosion rate that would penetrate a 5-cm thick canister in  $10^6$  years. The value of  $GM$  obtained by solving Eq. (2-12) was  $GM = 1.33 \times 10^{-5} \mu\text{m}/\text{yr}$ . The adjusted reference log-normal distribution is compared to the conditional CDF of corrosion rates in Figure 2-5(a).

The log-normal distribution requires adjustment for the following reasons. The log-normal distribution is only an approximation, intended to extrapolate corrosion rate frequencies in the high tail of the distribution. SKB implemented a numerical approach, with 10 realizations of the semi-correlated hydrogeological model, 6,916 fractures per realization, and 46 possible sulphide ion concentrations per fracture, to compute approximately  $3.2 \times 10^6$  corrosion rates, from which bulk and tail statistics were derived. Although the bulk of the distribution of corrosion rates SKB computed can be approximated by a log-normal distribution, the upper tail should differ from log-normal (note, for example, that the SKB numerical distribution has a finite upper tail while the tail of the log-normal distribution is infinite). The log-normal approximation considered in this report is only intended to yield reasonable estimates of corrosion rates, from which canister failure times and the number of failed canisters can be computed (accounting for micro-galvanic corrosion). An adjusted  $GM$  was used to derive distribution tail statistics closer to those computed by SKB.

Figure 2-5(b) displays the average corrosion rate,  $C_{av}(x)$ , computed using Eq. (2-11) (blue curve). Figure 2-5(b) also includes a sample of log-normal CDFs, where each distribution (grey curve) is associated with a specific value of the sulphide ion concentration. Only 40 of such curves are presented in Figure 2-5(b); however, the average  $C_{av}(x)$  was computed with 1000 curves [i.e.,  $N=1000$ ] in Eq. (2-11)].

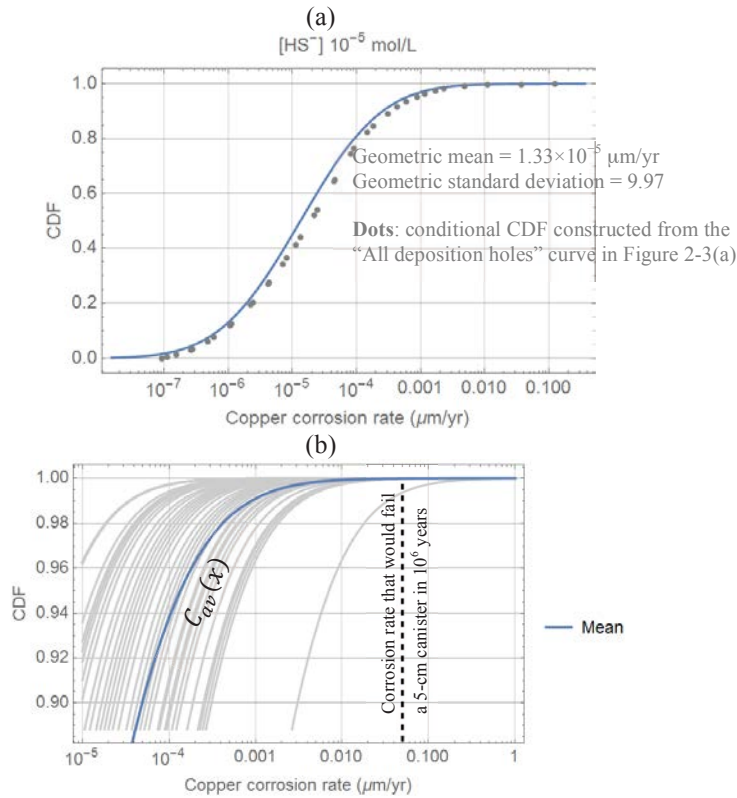


Figure 2-5. (a) Adjusted log-normal fit to match an expected number of failed canisters equal to 0.175 [value from SKB TR-10-66 (SKB, 2010a; Figure 5-8, Case F)]. The dots are the conditional CDF constructed from the “All deposition holes” data in Figure 2-3(a). (b) Average CDF [blue curve,  $C_{av}(x)$ ] numerically computed using Eq. (2-11) ( $N=1000$ ); the gray curves in (b) are log-normal distributions for different values of  $[HS^-]$ .

The cumulative distribution of the corrosion rate,  $C_{av}(x)$ , was used to compute the distribution of failure times and the number of canisters failed at  $10^6$  years, accounting for micro-galvanic corrosion, as follows. SKB assumed a factor of 20 increase in the corrosion rates, when the sulphide ion flux exceeded  $3 \times 10^{-10} \text{ mol}/(\text{m}^2\text{-s})$  (see Section 2.1 in this report). Such sulphide ion flux corresponds to a corrosion rate equal to  $0.14 \text{ } \mu\text{m}/\text{yr}$  (considering a copper density equal to  $8.96 \text{ g}/\text{cm}^3$ , a molar mass of  $63.55 \text{ g}/\text{mol}$ , and assuming that one mole of  $HS^-$  reacts with two moles of copper to form  $Cu_2S$ ). Such corrosion rate would penetrate a 5-cm thick canister in approximately 360,000 years. Accordingly, we applied a factor of 20 only to corrosion rates in excess of  $0.14 \text{ } \mu\text{m}/\text{yr}$ . The distribution of corrosion rates (upper tail) with and without the factor 20 are shown in Figure 2-6(a), in the form of complementary CDF. The complementary CDF function, with the factor 20 effect, is denoted as  $R(x)$ . The CDF of the canister failure time, assuming advective conditions at the canister (i.e., assuming direct contact of the groundwater carried in fractures with the canister) is simply  $R(d/t)$  ( $d$ =canister thickness= $5 \times 10^4 \text{ } \mu\text{m}$ ,  $t$ =elapsed time). If a delay time is considered for the onset of advective conditions (for example associated with buffer erosion), the CDF is computed as  $R(d/t - t_b)$  ( $t_b$  = buffer delay time; SKB assumed  $t_b=20,000$  years). If micro-galvanic corrosion and buffer delay times are ignored, the CDF of the canister failure time is defined as  $1 - C_{av}(d/t)$ . These alternative CDFs for the canister failure time are depicted in Figure 2-6(b).

The small probabilities on the vertical scale in Figure 2-6(b) indicate that conditions causing canister failure are rare (assuming that measured sulphide ion concentrations in groundwaters sampled in the Forsmark area represent or bound concentrations that may be occur in the future, and that the flow rate magnitudes are as low as computed with the SKB semi-correlated hydrogeological model). The micro-galvanic corrosion factor of 20 has a null effect on changing the number of canisters failed by corrosion within  $10^6$  years; it only changes the timing of failure of canisters contacted by fractures carrying relatively high flow rates and relatively high sulphide ion concentrations. For the analysed case of the semi-correlated hydrogeological model, the expected number of canisters failed at  $10^6$  years is 0.175 assuming initial advective conditions, and it is slightly less (0.170) if a delay of 20,000 years to establish advective conditions is assumed.

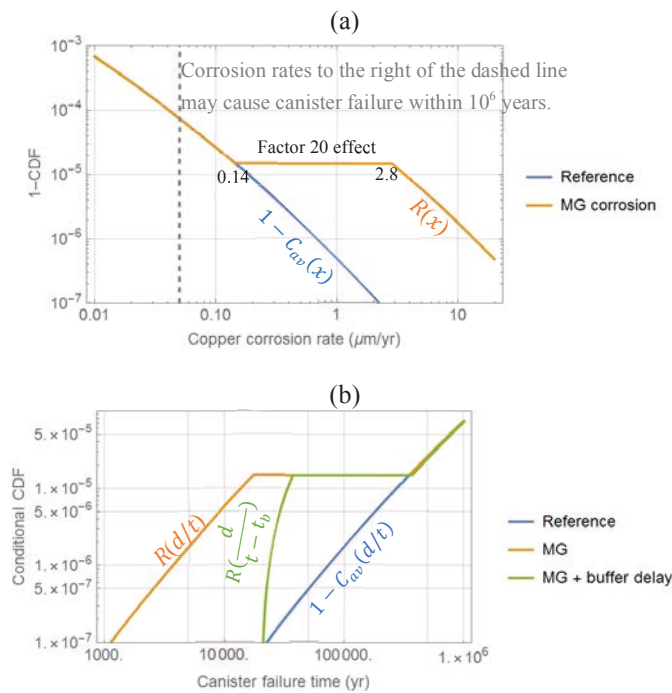


Figure 2-6. (a) Complementary CDF (i.e.,  $1 - \text{CDF}$ ) of the corrosion rates, ignoring (blue curve) and accounting (yellow curve) for micro-galvanic (MG) corrosion. Corrosion rates are assumed to increase by a factor of 20 when the corrosion rate exceeds  $0.14 \mu\text{m/yr}$  (assumed threshold for the onset of micro-galvanic corrosion). (b) CDF of the canister failure time disregarding micro-galvanic corrosion and assuming advective conditions at the canister at all times (blue curve); considering a factor of 20 to account for micro-galvanic corrosion (yellow curve); and considering in addition a delay time for the onset of advective conditions ( $t_b=20,000$  years).

The number of canisters failed is so small that for consequence analyses in a PA model, a conditional sampling strategy must be adopted. The standard approach is assuming one canister is failed per realization, and then scale consequences by the expected number of failed canisters (0.175 or 0.170). This approach was implemented for the PA computations discussed in Section 2.3. To sample the failure time of the canister failed per realization, the truncated CDF in Figure 2-7 was implemented in the PA model. In a realization, a random probability  $p$  is uniformly sampled ( $0 \leq p \leq 1$ ), then the curves in Figure 2-7 were used to compute the canister failure time corresponding to the sampled probability  $p$ . We assumed a lower bound of 500 years for the micro-galvanic corrosion case, and 20,000 years for the case including the delay to establish advective conditions. It is understood

that cases with short failure times and early releases may be unrealistic, because it can take many thousands of years for advective conditions to be established at the canister surface. The PA computations are only intended to provide simplified estimates of consequences.

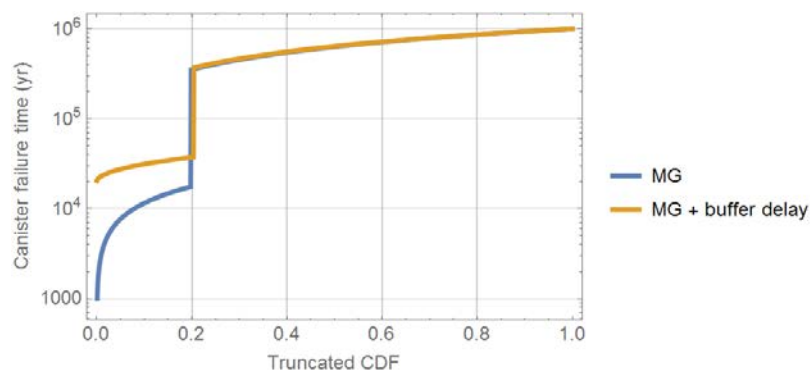


Figure 2-7. Canister failure time as a function of a sampled probability  $p$  ( $0 \leq p \leq 1$ ) implemented in a PA model to examine consequences of early canister failure due to micro-galvanic (MG) corrosion. For the blue curve it was assumed initial advective conditions at canisters; for the yellow curve, it was assumed a delay of 20,000 years to establish advective conditions.

## 2.3 Radionuclide Release Computations Accounting for Localized Corrosion

SKB examined consequences of micro-galvanic corrosion using a PA model and reported results in SKB TR-19-15 (SKB, 2019). SKB adopted a similar model to the SR-Site analysis referred to as the central corrosion case (SKB, 2010b, Section 4.4), but adjusted to account for relatively early canister failure due to micro-galvanic corrosion. We used a previously developed model, and modified it to include the failure time distribution functions in Figure 2-7. The model and data sources are explained in detail in SSM reports (Pensado, 2017; Pensado et al, 2014; Pensado and Mohanty, 2012). As with the conditional sampling approach for the central corrosion case, in each realization of the PA model, it was assumed failure of one canister at a random time sampled according to the distributions in Figure 2-7. Consequences were scaled by the expected number of failed canisters (0.175 for the case assuming initial advective conditions at canisters, and 0.170 for the case assuming a 20,000 year delay).

The results of the independent model are compared to SKB results in Figure 2-8(a). SKB results were digitized from SKB TR-19-15 (SKB, 2019; Figure 9-2), and labelled as Curves 1 and 2 in Figure 2-8. Curve 1 corresponds to the correlated hydrogeological model, assuming 20,000 years to establish advective conditions at canisters, and accounting for micro-galvanic corrosion. Curve 2 corresponds to the SKB buffer erosion model, instead of assuming a 20,000 year of delay for advective conditions. Curves 3 and 4 were computed with our independent PA model. We used 500 realizations to compute annual doses. In Curve 3, we assumed a 20,000 year delay for the onset of advective conditions. We used the curve labelled

“MG + buffer delay” in Figure 2-7 to sample the canister failure time, and used a factor of 0.175 to scale dose estimates. In Curve 4, we assumed initial advective conditions at the canisters, employed the curve labelled “MG” in Figure 2-7 to sample the canister failure time per realization, and used a factor of 0.170 to scale dose estimates. In our computations (Curves 3 and 4) in Figure 2-8(a), we considered information from the semi-correlated hydrogeological model. The mean annual effective dose shows oscillations (more visible in Curve 4), because of the consideration of instant release radionuclide inventories and inventories embedded in carbon steel structures, which cause spikes in each realization at the time of canister failure. The oscillations are statistical artefacts arising from the consideration of a relatively small number of realizations (500 realizations in our computations), and individual realizations with dose spikes. In Figure 2-8(b) an alternative comparison is presented, intended to address the effect of the correlated hydrogeological model.

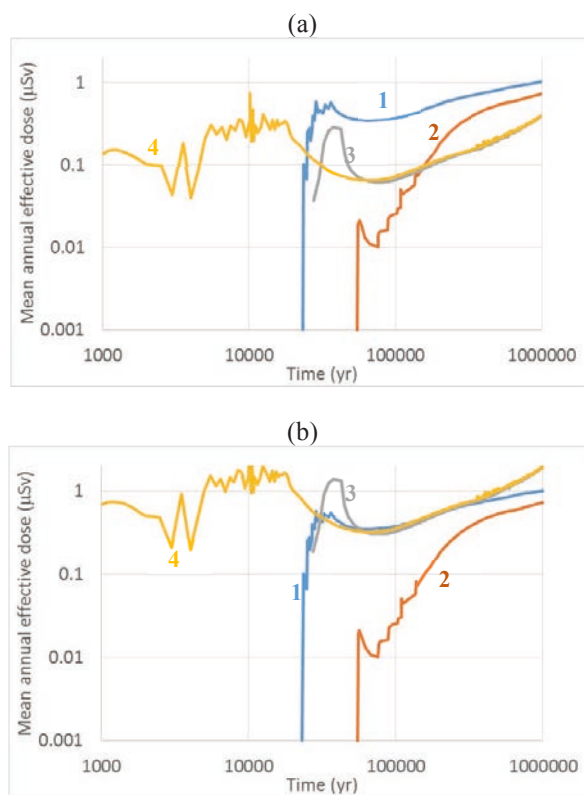


Figure 2-8. Mean annual dose estimates, accounting for micro-galvanic corrosion of copper canisters. Curves labelled 1 and 2 are SKB results, digitized from Figure 9-2 in SKB TR-19-15. See the main text for explanation of Curves 3 and 4. In (a), the expected number of failed canisters at  $10^6$  years was set to 0.175 (Curve 3) and to 0.170 (Curve 4). In (b), the expected number of failed canisters was set to 0.861 for both Curves 3 and 4.

Curves 3 and 4 in Figure 2-8 were computed as previously explained with one difference: the dose consequences were scaled by the expected number of failed canisters for the correlated hydrogeological model (0.861 according to information in Figure 5-8 in SKB TR-10-66). The dose consequences compare well to the SKB Curve 1. At  $10^6$  years, our independent estimates are a factor of 2 higher, which is a reasonable difference given overall model differences (discussed in detail in other SSM reports; e.g., Pensado, 2017). We conclude that the SKB PA model to evaluate

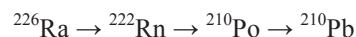
the effect of micro-galvanic corrosion is consistent with the simplifications and assumptions SKB stated.

## 2.4 Robustness Calculation

SKB evaluated an extreme scenario, assuming all canisters are emplaced with a penetrating defect 4 mm in diameter. The defect was assumed to transition to a large hole, 10 cm in diameter, after 10,000 years. SKB considered two variants of the system: in case A the rest of the system was assumed to remain intact, and in case B the buffer was assumed to degrade according to models used in the SR-Site assessment. Because buffer erosion would only affect few deposition holes, the difference between cases A and B is minimal. To simplify the analysis, only case A is examined in this section. SKB updated the biosphere model explicitly accounting for land uplift, and computed landscape dose conversion factors (LDFs) as a function of time. SKB stated that the case A beyond 50,000 years is similar to a “what if” case of the SR-Site assessment (SKB, 2011, Figure 13-62, and SKB, 2010b, Figure 6-64).

We updated the independent PA model to incorporate the robustness calculation case A. The case A is very similar to the growing pinhole scenario of the SR-Site analysis (SKB, 2010b, Section 6.3). A previous model to simulate the growing pinhole scenario (Pensado, 2017) was updated to account for a canister hole 10 cm diameter in size at 10,000 years. The independent PA approximated well results of the SR-Site growing pinhole (e.g., Pensado and Mohanty, 2012). SKB compared annual doses after 50,000 years to results in Figure 6-64 of SKB TR-10-50, corresponding to a case where all canisters are initially emplaced with a large penetrating hole, and radionuclide releases initiate after 100 years. The SKB annual dose for that “what if” case were well approximated with an independent PA model (Pensado, 2017). SKB assumed that approximately 1/6 of the deposition holes were intercepted by water-flowing fractures, and considered distributed LDFs from Table 3-7 of SKB TR-10-50. Therefore, for case A we also assumed that only 1/6 of the canisters would contribute to release, and the distributed LDFs from Table 3-7 in SKB TR-10-50 were used to transform activity releases in Bq/yr units to doses in Sv/yr units. The water flow rates per canister accounted for the effect of thermally induced rock spalling in the deposition holes. The solubility of radium-bearing phases was decreased by a factor 0.0015 to account for radium-barium co-precipitation, as was done in the previous study (Pensado, 2017).

SKB mean dose estimates for case A are presented in Figure 2-9 (continuous curves, digitized from Figure 9-3 of SKB TR-19-15) and compared to results of the independent PA model (dashed curves). Figure 2-9(a) includes mean annual dose for the decay chain



The independent PA did not include  $^{210}\text{Po}$ ; the corresponding annual dose in Figure 2-9(a) was estimated assuming secular equilibrium of  $^{210}\text{Po}$  and  $^{210}\text{Pb}$  (i.e., the activity of  $^{210}\text{Po}$  was assumed equal to the activity of  $^{210}\text{Pb}$ ). A LDF equal to  $4.47 \times 10^{-12}$  Sv/yr per Bq/yr was used for  $^{210}\text{Po}$  (SKB, 2010b, Table 3-7). The independent PA dose estimates in Figure 2-9(a) are lower than results in Figure 9-3 in SKB TR-19-15, in consistency with the SKB assertion that the biosphere model updates for  $^{226}\text{Ra}$  are slightly less favourable.

Figure 2-9(b) compares  $^{14}\text{C}$ ,  $^{129}\text{I}$ , and  $^{135}\text{Cs}$  doses computed with the independent PA and the updated SKB model. The independent PA outputs  $^{14}\text{C}$  annual doses that are up to a factor of 1,000 higher than the updated SKB model. SKB stated that oscillations in the  $^{14}\text{C}$  curve result from land uplift in the first few thousands of years. SKB stated that the decrease in the  $^{129}\text{I}$  dose is due to the incorporation of site-specific information. On the other hand, the  $^{135}\text{Cs}$  dose is higher than the SR-Site model. SKB asserted that the increasing  $^{135}\text{Cs}$  trend results from accumulation of  $^{135}\text{Cs}$  in the biosphere throughout the assessment time, which may not be realistic. Instead, SKB explained that the biosphere should be eradicated by glaciers every 100,000 years or so, removing the accumulated radioactive contamination (SKB, 2019). Figure 6-64 of SKB TR-10-50 indicates a variation of the  $^{135}\text{Cs}$  annual dose by less than a factor of 10, from 10,000 years to  $10^6$  years, which is consistent with the independent PA model (SKB, 2010b). The factor of 100 variation from 70,000 years to  $10^6$  years in the SKB annual doses is likely associated with updates to the biosphere model.

Figure 2-9(c) includes dose estimates for complementary radionuclides.  $^{36}\text{Cl}$  was not included in the independent PA, because such radionuclide contributed in minor extent to doses of the SR-Site analyses documented in SKB TR-10-50. The  $^{36}\text{Cl}$  annual dose in Figure 2-9(c) (continuous blue curve) is consistent with the  $^{36}\text{Cl}$  annual dose in Figure 6-64 of SKB TR-10-50. SKB stated that  $^{79}\text{Se}$  dose estimates decreased due to the incorporation of site-specific information in the updated model. The decrease was significant (more than a factor of 100); the updated peak dose estimate was less than  $0.01 \mu\text{Sv}$  and outside the range of the plot in Figure 9-3 in SKB TR-19-15. The peak annual dose contribution of  $^{59}\text{Ni}$  is greater than  $0.01 \mu\text{Sv}$  in the independent PA. Figure 6-64 of SKB TR-10-50 indicates a maximum  $^{59}\text{Ni}$  annual dose on the order of  $0.09 \mu\text{Sv}$ . SKB did not identify any relevant update in the biosphere model with respect to  $^{59}\text{Ni}$ . In the updated SKB computations, it was expected the peak mean annual  $^{59}\text{Ni}$  dose to exceed  $0.01 \mu\text{Sv}$  (based on information in Figure 6-64 of SKB TR-10-50). Therefore, updates to the SKB biosphere model appear to also have affected the  $^{59}\text{Ni}$  annual dose.

SKB concluded that even if all canisters were compromised at emplacement, the remaining barriers are sufficient to keep the system within the dose risk limit. This conclusion can only be supported by relying on the updated biosphere model, but not with the biosphere model used in the SR-Site assessment. A parallel review effort sponsored by SSM was aimed at enhanced evaluation of the biosphere model (Walke and Newson, 2019).

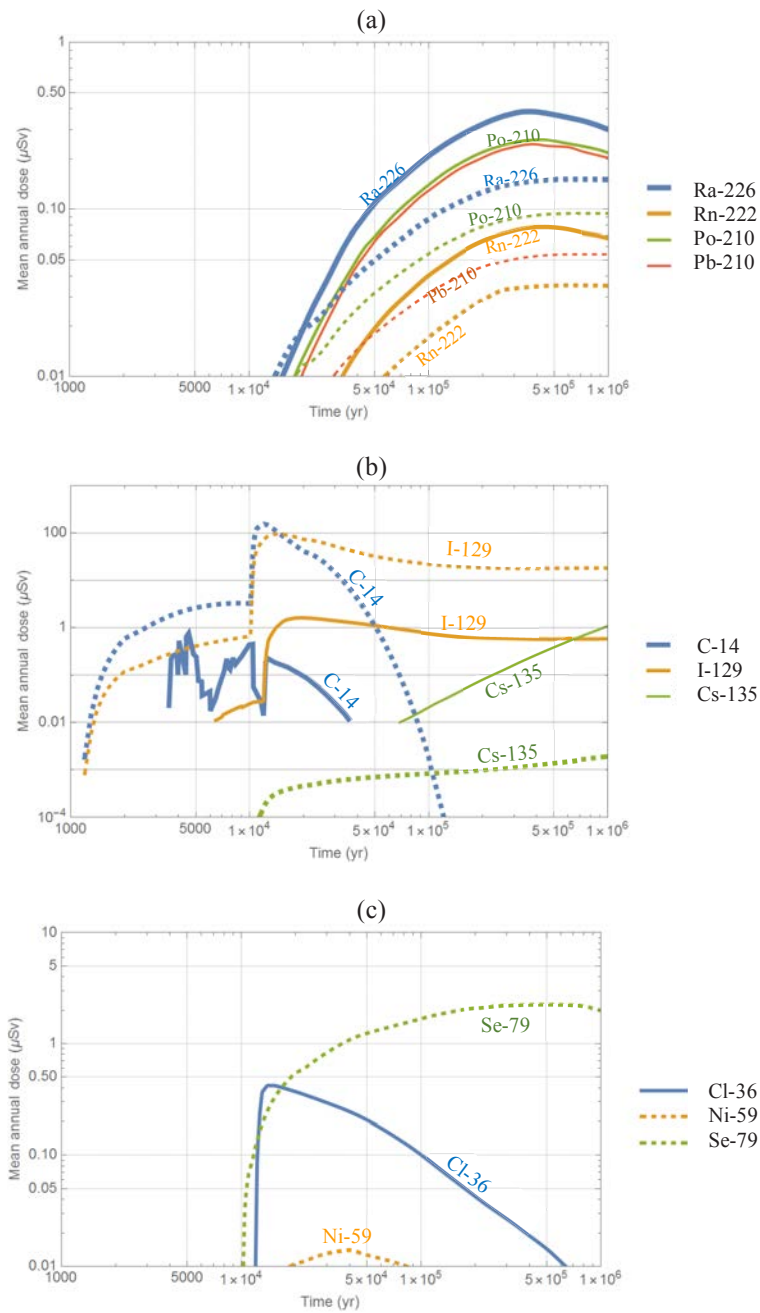


Figure 2-9. Mean annual dose estimates, robustness calculation case. Continuous curves in (a), (b), and (c) were digitized from Figure 9-3 in SKB TR-19-15. The dashed curves were computed with an independent PA model (see a detailed description of the modelled system in the text). Ni-59 and Se-79 [dashed curves in (c)] were included in the independent PA model, but not in Figure 9-3 in SKB TR-19-15; on the other hand, the independent PA did not include Cl-36 [continuous curve in (c)], but Figure 9-3 in SKB TR-19-15 reports relatively important contribution of Cl-36 to total dose estimates.

### 3 Saturated and Unsaturated Buffer Scenarios

In this section, hydrogen sulphide attack of copper canister materials is evaluated for two scenarios of saturated and unsaturated buffer conditions.

#### 3.1 Saturated Buffer Conditions

SKB evaluated the potential effect of sulphide produced by sulphate-reducing bacteria (SRB) (SKB, 2010a). SKB concluded that the amount of organic matter in the deposition hole is limited and any sulphide produced from bacterial activity would cause negligible damage to the copper of canisters. However, there will be a substantial amount of organic matter in the deposition tunnel and the backfill, and a mass-balance argument alone is not sufficient to exclude damage of canisters by sulphide that could be generated by SRB. For example, SKB estimated that organic matter in the backfill bentonite in the deposition tunnel would correspond to approximately 13,600 moles of sulphide per canister.

SKB stated that diffusive transport would constrain the supply of sulphide originating from the deposition tunnel. SKB developed a more definite exclusion argument based on the rate of  $Cu_xS$  production, from experiments with highly compacted bentonite and natural groundwater at Äspö (Masurat et al., 2010). Masurat et al. (2010) measurements are listed in Table 3-1. Table 3-1 also includes the equivalent corrosion rates (assuming formation of  $Cu_2S$ ), and the depth of the corrosion front at  $10^6$  years. SKB concluded that bacteria would not produce sulphide at a sufficient rate to cause failure of the canister in  $10^6$  years (SKB, 2010a). Furthermore, SKB noted that the Masurat et al. (2010) measurements included addition of lactate to bentonite as a source of energy and organic carbon to support SRB, and that the Masurat et al. (2010) measurements did not separate effects of sulphide in groundwater from sulphide produced by SRB. Therefore, SKB concluded that the rate of sulphide production by SRB measured by Masurat et al. (2010) is an upper bound to rates that might naturally occur.

Table 3-1. Rate of production of  $Cu_xS$  reported by Masurat et al. (2010) for two different compacted Wyoming bentonite MX-80 densities

Bentonite density (kg/m <sup>3</sup> )	Copper sulphide production (mol/mm <sup>2</sup> -day)	Equivalent copper corrosion rate (µm/yr)	Corrosion front depth at 10 <sup>6</sup> years (mm)
2,000	$3.4 \times 10^{-14}$	$1.76 \times 10^{-4}$	0.18
1,800	$4.2 \times 10^{-13}$	$2.18 \times 10^{-3}$	2.17

The report SKB TR-19-15 (SKB, 2019) focused on the question of localized corrosion. SKB ruled out localized corrosion caused by sulphide produced from SRB, or from sulphide in groundwater. Some indications of localized corrosion were observed in rich SRB media, with sulphide concentrations becoming as high as  $1.2 \times 10^{-2}$  mol/L at the end of 32-day exposure (Gordon et al., 2018), but SKB concluded that the required conditions to make SRB thrive and produce enough sulphide to be of concern would be far from attainable in a repository setting.

With respect to the sulphide carried in groundwater, SKB concluded that the possible sulphide fluxes at the canister surface (accounting for the presence of the buffer as a diffusive barrier) were far below  $3 \times 10^{-10}$  mol/(m<sup>2</sup>-s) (see Section 2.1 in this report) so that localized corrosion or micro-galvanic corrosion would not occur.

We examined the SKB analysis for buffer saturated conditions, as a limiting long-term state. We agree that under saturated conditions, the supply of sulphide in groundwater will be slow and will not exceed  $3 \times 10^{-10}$  mol/(m<sup>2</sup>-s), the assumed threshold for the onset of micro-galvanic corrosion. We refer to SSM sponsored work by Stothoff and Manepally (2013) for a detailed evaluation of diffusive transport through the buffer material. These authors examined diffusion processes controlling the supply of hydrogen sulphide ion carried in the groundwater were examined and concluded that, based on independent modelling, the rate of sulphide ion transport is too slow [below  $3 \times 10^{-10}$  mol/(m<sup>2</sup>-s)] to compromise the canisters in 10<sup>6</sup> years, even accounting for rock spalling effects and unsealed spaces between bentonite rings. The only scenarios that could cause canister failure in 10<sup>6</sup> years were related to situations where the buffer was compromised (for example due to erosion).

Stothoff and Manepally (2013) examined a hypothetical extreme scenario for localized delivery of hydrogen sulphide ion to the copper canister surface. A small pipe (1 mm diameter) of void space was postulated to exist within the buffer material, tangentially touching the canister [Figure 3-1(a), not drawn to scale]. The small pipe was assumed to capture all of the flow of the fracture intercepting the deposition hole. A zero sulphide ion concentration at the pipe-canister contact region and at the pipe terminus was assumed. The initial contact region was assumed to have a constant geometry in COMSOL<sup>®</sup> simulations (i.e., growth of the corrosion front was not simulated in COMSOL). Using the flux at the initial contact region, a rate of sulphide ion supply to the canister was computed. A hemispherical corrosion front was assumed to develop, with a radius growing with time. The time of canister failure was defined as the time it would take for the radius of the hemisphere to be the same as the copper canister thickness (5 cm). Figure 3-1(b) is the conditional cumulative distribution of the failure time, assuming a sulphide ion concentration in groundwater equal to 10<sup>-5</sup> mol/L and considering only deposition holes intercepted by fractures.<sup>2</sup> The data in Figure 3-1(b) used data from one realization of the semi-correlated hydrogeological model (with 6,916 fractures) SKB provided to SSM.

For the assumed corrosion process, the failure time is inversely proportional to the sulphide ion concentration. Implementing the average approach described in Section 2.2, and the distribution of sulphide ion concentration in groundwater in Figure 2-4, the average cumulative distribution for the failure time (average over the sulphide concentration distribution) was computed [Figure 3-1(c), red curve]. Figure 3-1(c) also includes three other curves at fixed sulphide ion concentrations, for comparison. The conditional probability for canisters to fail within 10<sup>6</sup> years is 0.003 for this extreme scenario [i.e., the value of the mean CDF in Figure 3-1(c) at 10<sup>6</sup> years is 0.003].

It is emphasized that the pipe sulphide delivery scenario is not realistic. Rather, this scenario was developed to gain insights from an extreme case with localized delivery of sulphide. Even if all of the flow intercepting a deposition hole was focused through a narrow pipe, and this pipe furthermore focused delivery of

---

<sup>2</sup> The failure time distribution function result was not directly reported in the work by Stothoff and Manepally (2013). The same data these authors employed to prepare Figure 21 of the SSM Technical Note 2013:36 was used to construct the failure time distribution function in Figure 3-1(b).

sulphide ion to the canister, canister failure would still be rare [i.e., the probability of failure within  $10^6$  years equal to 0.003 from Figure 3-1(c), for canisters in deposition holes intercepted by fractures; or probability  $\sim 0.4 \times 0.003 = 0.0012$  for all canisters—assuming that only  $\sim 40$  percent of the deposition holes are intercepted by fractures]. The value in considering this scenario is that it illustrates constraints in flow rates and sulphide concentrations in groundwater that make failure of the canister by corrosion to be of very low probability, giving confidence in the conclusions SKB reached that, under saturated conditions, sulphide-induced corrosion would take a long time to cause canister failure.

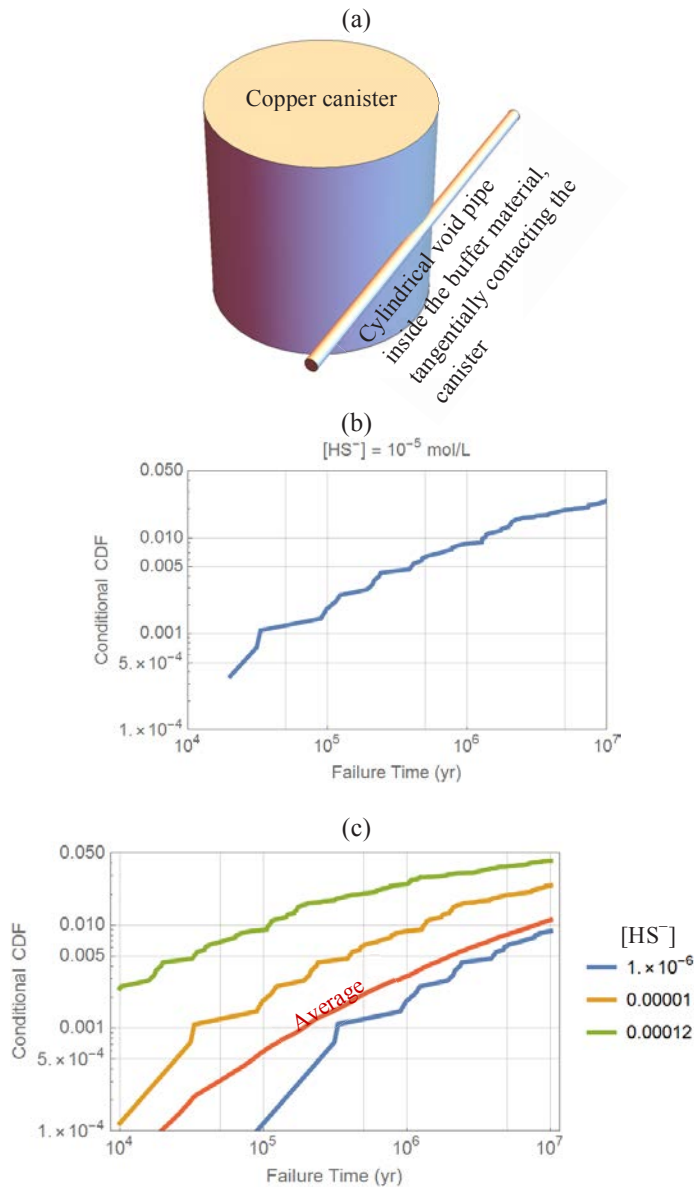


Figure 3-1. (a) Extreme sulphide delivery scenario considered in the SSM Technical Note 2013:36 (Stothoff and Manepally, 2013). (b) Conditional cumulative canister failure time distribution, derived considering one realization of the SKB semi-correlated hydrogeological model, and  $[HS^-]$  in groundwater equal to  $10^{-5}$  mol/L. (c) Conditional cumulative canister failure time distribution (red curve) computed considering the groundwater sulphide concentration distribution in Figure 2-4. Three other curves at unique values of  $[HS^-]$  are provided in (c) for comparison.

Based on previous review work by Stothoff and Manepally (2013) and independent computations by these authors, we agree with the SKB conclusion that in saturated-buffer conditions, copper canisters will not fail in  $10^6$  years, provided the sulphide groundwater concentrations are as low as in Figure 2-4 and that the water flow rates are as low as SKB computed using the semi-correlated hydrogeological model.

With respect to SRB effects, we agree with the SKB conclusion that damage of copper canisters from sulphide produced by SRB is very likely to be minor, based on the *in situ* experiments by Masurat et al. (2010) (see Table 3-1). In addition, experiments by Svensson et al. (2017) indicate that the effective solubility of sulphide in bentonite groundwaters is heavily constrained, falling below experimental detection limits. Svensson et al. (2017) concluded that bentonite can remove (by unknown mechanisms) significant amounts of sulphide from solution (up to 10 kg of sulphide per 1,000 kg of bentonite). The low sulphide concentrations in bentonite porewaters would strongly limit rates of sulphide diffusion in the buffer material. Production rates of sulphide by SRB and sulphide transport rates are expected to be too low to cause failure of canisters in  $10^6$  years and micro-galvanic corrosion. Other experiments where substantial sulphide concentrations and potential micro-galvanic corrosion were detected, were performed in laboratory settings (e.g., Gordon et al., 2018), under conditions favouring bacterial growth and with direct contact of SRB products with copper. Those conditions are not expected to occur in the proposed repository.

## 3.2 Unsaturated Buffer Conditions

### 3.2.1 Experimental Support

Under unsaturated buffer conditions, hydrogen sulphide may diffuse in the gas phase within the buffer in the form of  $H_2S$  gas, and then react with copper on the canister surfaces, mediated by water. SKB performed experiments exposing copper in the head space of a chamber with temperature and relative humidity control, to a flowing mixture of nitrogen and  $H_2S$  for up to 30 days [all experiments at 1 bar pressure (0.987 atm), and without oxygen] (Gordon et al., 2018). SKB used gas mixtures with 10 and  $10^4$  ppm  $H_2S$  (ppm by weight). SKB estimated those gas proportions would be equivalent to a dissolved  $HS^-$  concentration equal to  $2.13 \times 10^{-7}$  mol/L and  $2.13 \times 10^{-4}$  mol/L, respectively (Gordon et al., 2018). SKB examined the extent of sulphide attack to copper. Average mass loss and average corrosion depths (averages computed from 5 coupons) SKB measured are provided in Table 3-2.

Table 3-2. Average copper mass loss from H<sub>2</sub>S (gas) exposure (original data from Gordon et al., 2018, Tables 2-6 and 3-7); relative humidity 70–80 percent; temperature 80–90 °C; total pressure = 1 bar; no oxygen in the system)

ID	H <sub>2</sub> S (gas) (weight ppm)	HS <sup>-</sup> (aq) (mol/L)	Duration (days)	Average mass loss (g/m <sup>2</sup> )	Average depth (µm)	Corrosion rate µm/yr
A	10	2.13×10 <sup>-7</sup>	10	1.84	0.21	7.67
B	10	2.13×10 <sup>-7</sup>	30	10.26	1.15	13.99
C	10 <sup>4</sup>	2.14×10 <sup>-4</sup>	10	4.62	0.52	18.98
D	10 <sup>4</sup>	2.14×10 <sup>-4</sup>	30	21.29	2.39	29.08

The corrosion rates in Table 3-2 were simply computed as the ratio of the average depth and the exposure duration. The different corrosion rates for different exposure durations indicate that the depth does not grow linearly with time, at least for the limited exposure times examined (10 and 30 days).<sup>3</sup> SKB hypothesized that the preformed protective oxide film on copper initially changes the reaction rate (until all Cu<sub>2</sub>O is transformed to Cu<sub>2</sub>S), causing the apparent non-linear change in depth with exposure time.

Corrosion rates in Table 3-2 must be used with caution. Although the sulphide concentration increased by a factor of 1,000 from tests A and B to C and D, the corrosion rates only increased by a factor of 2 or 3. Thus, corrosion rates may be a function of kinetic rates and sulphide transport limitations through Cu<sub>2</sub>S scales, and be weakly dependent on gas flow rates and gas concentrations. Consequently, the corrosion rates in Table 3-2 may be maximal corrosion rates, under abundant supply of sulphide in gas phase. In contrast, in repository settings, it is expected that the availability of sulphide will be limited, and that the rate of sulphide transport through the buffer material will constrain copper corrosion rates. Transport-limited corrosion rates are expected to be much smaller than the corrosion rates reported in Table 3-2. SKB estimated transport-limited corrosion rates (e.g., SKB, 2019, Figure 2-14) that were much lower than rates in Table 3-2.

The objective of the SKB studies was to examine whether localized corrosion may be exhibited under conditions with relatively abundant supply of sulphide, and not to measure corrosion rates to be used for PAs. SKB did not detect signs of localized corrosion or micro-galvanic corrosion in any of the copper coupons (only limited cross sections were examined) for the limited testing times in these experiments. SKB recognized that more extended examination of copper surfaces may be required to confirm the non-occurrence of localized corrosion. It is noted that the corrosion rates in Table 3-2 are relatively large, representative of general corrosion. Those relatively large corrosion rates do not indicate formation of a protective Cu<sub>2</sub>S film, which is a requirement for corrosion to become localised at Cu<sub>2</sub>S film defects.

### 3.2.2 Gas Transport Computations

SKB implemented gas transport computations that were aimed at estimating corrosion rates in unsaturated buffer conditions (SKB, 2019). The concept implemented in the SKB transport model is presented in Figure 3-2. In the SKB

<sup>3</sup> If the penetration depth was linear with time, the 30-day depth would be approximately equal to 3 times the 10-day depth, and such is not true

concept, the deposition tunnels are more likely to saturate before the deposition holes, and the deposition holes are more likely to resaturate from water flowing from the deposition tunnels. SKB experiments indicate that SRB requires liquid water to become active (SKB, 2019, Section 2.4); therefore, SRB are more likely to first become active in the deposition tunnels and produce sulphide there.

SKB assumed the total sulphide concentration in solution in the tunnels to equal  $10^{-6}$  mol/L (i.e.,  $[\text{HS}^-] + [\text{H}_2\text{S}(\text{aqueous})] = 10^{-6}$  mol/L). This  $10^{-6}$  mol/L assumption is based on experimental results by SKB. The experiments indicated the presence of  $\text{H}_2\text{S}$  in the gas phase but did not detect sulphide in solution (in contact with bentonite or not) (SKB, 2019, Section 2.4). Eriksson and Hedin (2018) refer to work by Lundgren (2013) as additional support to the  $10^{-6}$  mol/L assumption. Svensson et al. (2017) investigated the solubility of sulphide in waters containing bentonite, and found that bentonite removed sulphide from the solution to levels below detection limits. Svensson et al. (2017) estimated 1,000 kg of bentonite could remove up to 10 kg of sulphide from the solution, although the removal mechanism is not well understood.

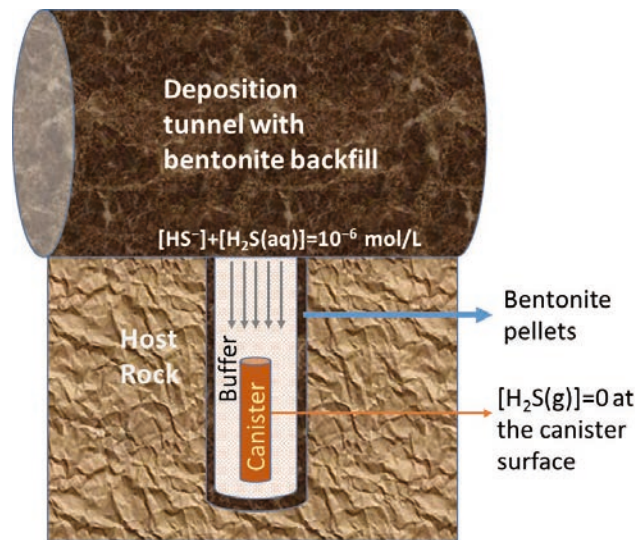


Figure 3-2. System represented in the SKB sulphide gas transport model (not drawn to scale). The “deposition tunnel” is the top tunnel. The “deposition hole” is the hole drilled into the tunnel floor to emplace the canister and the buffer material.

SKB implemented the  $10^{-6}$  mol/L assumption as a boundary condition (concentration in solution) at the deposition tunnel-deposition hole interface (see Figure 3-2). The concentration in the gas phase at the deposition tunnel-deposition hole interface was estimated using Henry’s law, assuming a neutral pH. SKB implemented a COMSOL model to simulate heat transfer and water diffusion and water redistribution, assuming no water inflow from the host rock.<sup>4</sup> SKB simulated diffusion of  $\text{H}_2\text{S}$  (gas) through the buffer material and through the bentonite pellets around the deposition hole (region pointed by the blue arrow in

<sup>4</sup> To simulate no-water-inflow conditions, SKB assumed a constant amount of water in the deposition hole at all times. Initially a fixed amount of water was assumed uniformly distributed throughout the deposition hole, and later redistributed due to the thermal gradient (water moves away the canister thermal source). The water distribution becomes uniform again at late times, when the system cools off and the thermal gradient disappears. No-water-inflow conditions are pessimistic with regards to sulphide transport towards the copper canister.

Figure 3-2). At the copper canister surface, SKB assumed the concentration of H<sub>2</sub>S (gas) to be zero (to simulate rapid reaction of copper with sulphide). The water redistribution model and the gas transport model were coupled through the sulphide gas diffusion coefficient, which is dependent on the local water saturation (diffusion slows with increasing water saturation). SKB computed peak sulphide fluxes equal to  $6.5 \times 10^{-11}$  mol/(m<sup>2</sup>-s) at the canister surface, which is less than the assumed threshold  $3 \times 10^{-10}$  mol/(m<sup>2</sup>-s) for micro-galvanic corrosion. The equivalent copper corrosion rate associated with that sulphide flux is 0.029 µm/yr. Assuming a buffer saturation time of 5,000 years, the accumulated damage over that time at this rate would be 0.15 mm. SKB also considered a model accounting for water inflow and increasing water saturation of the buffer with time, and computed even smaller gas fluxes because gas diffusion rates decrease as pores in the buffer material saturate with water.

We evaluated the transport computations SKB implemented, and found some shortcomings, although not sufficient to change the SKB conclusions. For example, SKB seems to have dismissed corrections to Henry's constant, the sulphide dissociation constant, and the H<sub>2</sub>S(gas) diffusion coefficient with temperature. However, our independent assessment found that those temperature corrections would have a limited effect on diffusive flux estimates. SKB applied corrections to the H<sub>2</sub>S(gas) diffusion coefficient to account for variable water saturation, but dismissed pressure corrections. Pressure corrections lower the effective diffusion coefficient estimates at depth. The dependence of the H<sub>2</sub>S(gas) diffusion on bentonite of variable saturation is uncertain, and we examined effects of alternative dependencies than considered by SKB. We also concluded that the rate of supply of H<sub>2</sub>S in the gas phase is slow and unlikely to cause major damage of the copper canister. Details of the independent analysis are provided as follows.

The SKB sulphide gas transport computations are detailed by Eriksson and Hedin, (2018). SKB considered a constant diffusion coefficient equal to  $1.5 \times 10^{-5}$  m<sup>2</sup>/s for diffusion of H<sub>2</sub>S in air. This diffusion coefficient is at least 4 orders of magnitude greater than typical diffusion of solutes in water. Given the contrast in diffusion coefficient magnitude, gas transport would be expected to be much faster than transport of species dissolved in water. However, diffusion of gases under elevated pressure, and through bentonite with variable saturation, is not necessarily much faster than diffusion of solutes in porewater. In fact, at high water saturation and in small pore spaces, diffusion of dissolved species may be faster than diffusion of gases.

Empirical formulas are available to estimate diffusion coefficients in air. For example the formula for the FSG method is defined as (Lyman et al. 1982; Clark, 1996, Eq. 6.23)

$$D_{AB} = \frac{10^{-3} T^{1.75} \sqrt{\frac{1}{m_A} + \frac{1}{m_B}}}{p (V_A^{1/3} + V_B^{1/3})^2} \quad (3-1)$$

where the subscript *A* represent air properties and *B* properties of the gas diffusing in air; *T* is the absolute temperature (K), *p* is the total pressure (atm), *m* is the molar mass (g/mol; *m<sub>A</sub>*=28.97 g/mol is the average molar mass of air), and *V* is the molar volume (cm<sup>3</sup>/mol; *V<sub>A</sub>*=20.1 cm<sup>3</sup>/mol is the average molar volume of air). A similar formula is available for general binary gas systems, indicating that the diffusion coefficient is proportional to  $\sqrt{1/m_A + 1/m_B}$  (where *A* may be any gas other than

air) and inversely proportional to the pressure,  $p$  (e.g., Bird et al., 1960, Eq. 16.4–13). Instead of using Eq. (3-1), we estimated the diffusion coefficient of  $H_2S$  in air based on the argon diffusion coefficient at 1 atmosphere, adjusted by a factor

$$D_{H_2S} \approx \frac{\sqrt{1/m_A + 1/m_{H_2S}}}{\sqrt{1/m_A + 1/m_{Ar}}} D_{Ar} = 1.04 D_{Ar} \quad (3-2)$$

The adjusting factor 1.04 is a first-order adjustment, computed using  $m_A = 28.96$  g/mol,  $m_{H_2S} = 34.04$  g/mol, and  $m_{Ar} = 39.95$  g/mol. Argon was employed as reference, because its molar mass is similar to hydrogen sulphide. Considering information on argon diffusion in excess air at 1 atm (Engineering ToolBox, 2018), the diffusion coefficient  $D_{H_2S}$  is approximated as

$$D_{H_2S} \approx \frac{1}{p} (-0.0394 + 4.15 \times 10^{-4} T + 1.32 \times 10^{-6} T^2) \quad (3-3)$$

$D_{H_2S}$  is in units of  $cm^2/s$ ,  $p$  is the total pressure in atmosphere units, and  $T$  is the absolute temperature (Kelvin units). Figure 3-3 shows the estimated diffusion coefficient as a function of temperature and hydrostatic pressure.<sup>5</sup>

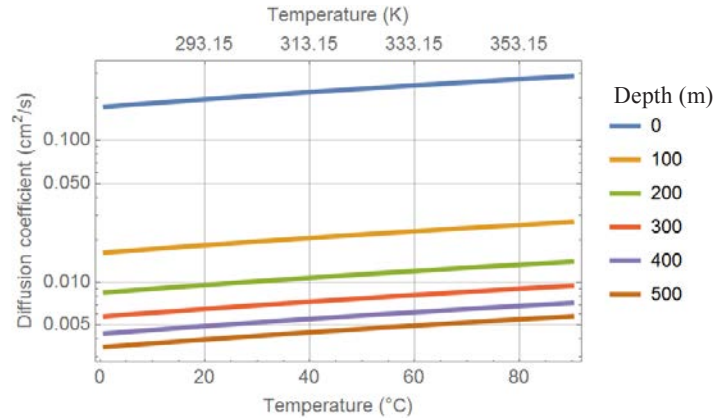


Figure 3-3. Estimated diffusion coefficient of  $H_2S$ (gas) in excess air, as a function of temperature and hydrostatic pressure.<sup>5</sup>

The diffusion coefficient changes by less than a factor of 2 when the temperature changes from 1 °C to 90 °C. On the other hand, the diffusion coefficient decreases by a factor of 50 from a depth of 0 m to 500 m. Thus, the diffusion coefficient is more sensitive to hydrostatic pressure changes than to temperature changes. SKB considered a gas diffusion coefficient equal to  $0.15$   $cm^2/s$ , which is close to estimates in Figure 3-3 at 0 m or 1 atm and at low temperatures. By dismissing pressure corrections to the diffusion coefficient, SKB overestimated the rate of  $H_2S$ (gas) transport towards the copper canister.

The diffusion coefficient requires a further adjustment to account for transport in a porous medium. The effective diffusion coefficient in a porous medium is defined as

$$D_{eff} = \theta S_g \tau(\theta, S_g) D_{H_2S} \quad (3-4)$$

<sup>5</sup> The hydrostatic pressure is computed as  $\rho g h + 101,325$  Pa, where  $\rho$  is the water density,  $g$  is the gravitational acceleration ( $9.81$   $m/s^2$ ), and  $h$  is the water depth.

where  $\theta$  is the medium porosity,  $S_g$  is the gas saturation,<sup>6</sup> and  $\tau(\theta, S_g)$  is referred to as tortuosity and is a function of  $\theta$  and  $S_g$ . The tortuosity is commonly found to be a power law of the porosity and the gas saturation

$$\tau(\theta, S_g) = \theta^m S_g^n \quad (3-5)$$

The exponents  $m$  and  $n$  are established through experiments or through theoretical considerations (e.g., Chau and Or, 2005; Thorbjørn et al., 2008; Fathi et al., 2017; Hu et al., 2018). The empirical function  $\tau(\theta, S_g)$  is a correction to the gas diffusion coefficient to account for collisions of gas molecules with the porous matrix.

For small-pore systems with low gas saturation, diffusion is regulated by particle collisions with the solid matrix and fluid embedded in the pores, instead of controlled by gas-gas particle collisions. SKB considered the function (Eriksson and Hedin, 2018)

$$\tau(\theta, S_g) = \theta^{1/3} S_g^{7/3} \quad (3-6)$$

based on a function previously used by Masum et al. (2012) in a study of multicomponent gas flow through a compacted clay buffer. The effective diffusion coefficient is much smaller than the gas diffusion coefficient. For example, in the initial conditions SKB considered,  $\theta=0.39$ ,  $S_g=0.265$ ,  $\tau=0.033$ , and  $D_{eff} = 0.0034 D_{H_2S}$ .

The power law in Eq. (3-5) is uncertain. As previously stated, multiple studies of gas diffusion in porous systems indicate power laws of the form of Eqs. (3-5) and (3-6), with different values of the exponents  $m$  and  $n$ . Scanlon et al. (2001; Table 8.2) compiled  $\tau(\theta, S_g)$  functions reported in the literature, including cases with  $m=n=4/3$ ,  $3/2$ , or  $7/3$ . Example alternative values of the relative effective diffusion coefficient,  $D_{eff}/D_{H_2S} = \theta S_g \tau$ , are presented in Figure 3-4. The blue curve corresponds to the tortuosity function SKB considered, Eq. (3-6). Other alternatives predict a higher effective gas diffusion coefficient at low gas saturation. If the empirical power laws are valid at low gas saturation, the low gas saturation gas diffusion becomes negligibly small, and mass transport is dominated by diffusion of dissolved species in porewater.

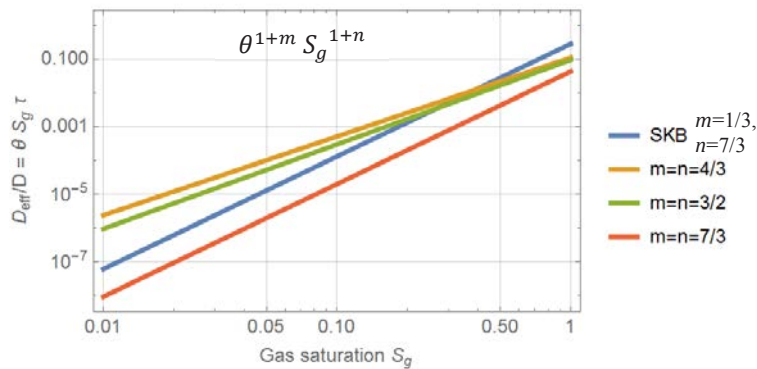


Figure 3-4. Example alternative values of the relative effective diffusion coefficient as a function of the gas saturation (assumed porosity= $\theta=0.39$ )

<sup>6</sup> The water saturation  $S_w$  is defined as the fraction of the pore volume filled with water, and  $S_g=1-S_w$ .

SKB appears to have defined the boundary condition at the deposition tunnel-deposition hole interface using a fixed temperature value of the sulphide dissociation constant and Henry's constant to compute the  $H_2S(gas)$  concentration as a function of the dissolved  $H_2S(aq)$  and of the pH (resulting in  $H_2S(gas) = 1.7 \times 10^{-7}$  mol/L at the deposition hole top boundary). We considered the following expression to define Henry's constant as a function of the temperature (NIST, 2019)

$$\frac{[H_2S(aq)]}{P_{H_2S}} = K_H(T) \quad (3-7)$$

$$K_H(T) = 0.1e^{2200\left(\frac{1}{T} - \frac{1}{298.15}\right)} (0.754 + 1.88 \times 10^{-3} T - 3.59 \times 10^{-6} T^2)$$

$K_H$  is mol/bar-L units.  $P_{H_2S}$  is the partial pressure of  $H_2S(gas)$ . The quadratic function  $0.754 + 1.88 \times 10^{-3} T - 3.59 \times 10^{-6} T^2$  is the density of water as a function of temperature, in units of kg/L. The Henry's constant for sulphide is a decreasing function of temperature.

The acid dissociation constant,  $K_a$ , as a function of temperature is computed as (Sun et al., 2008)

$$K_a = \frac{[H^+][HS^-]}{[H_2S(aq)]} \quad (3-8)$$

$$K_a(T) = 10^{-15.35 + 0.0457 T - 5.97 \times 10^{-5} T^2}$$

$K_a(T)$  is in mol/L units, and it is an increasing function of the temperature. Combining Eqs. (3-7) and (3-8) and assuming an ideal gas, the gas concentration  $[H_2S(gas)]$  (in units of mol/L) as a function of  $T$ , pH, and the total sulphide in solution ( $[HS^-] + [H_2S(aq)]$ ) is

$$[H_2S(gas)] = \frac{120.3e^{-2200\left(\frac{1}{T} - \frac{1}{298.15}\right)} ([HS^-(aq)] + [H_2S(aq)])}{[1 + K_a(T) 10^{pH}] T (0.754 + 1.88 \times 10^{-3} T - 3.59 \times 10^{-6} T^2)} \quad (3-9)$$

The concentration  $[H_2S(gas)]$  as a function of temperature and pH is displayed in Figure 3-5, for the case  $[HS^-(aq)] + [H_2S(aq)] = 10^{-6}$  mol/L.

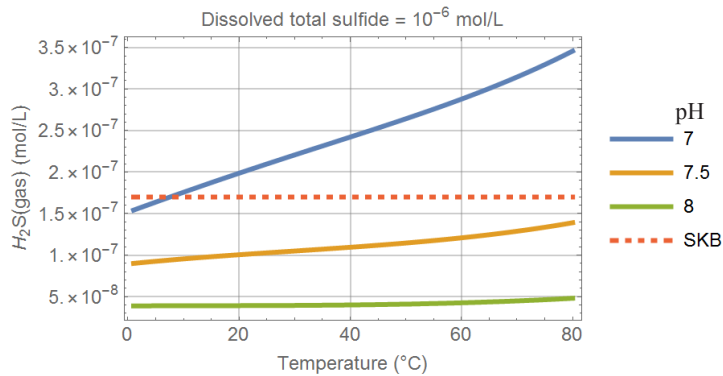


Figure 3-5.  $H_2S$  gas concentration as a function of temperature and pH, assuming  $[HS^-(aq)] + [H_2S(aq)] = 10^{-6}$  mol/L. The dashed line is the SKB boundary condition assumption ( $1.7 \times 10^{-7}$  mol/L) in the COMSOL no-water-inflow computations.

The  $H_2S$  gas concentration moderately increases with increasing temperature, and significantly increases with increasing pH. At pH 7, our estimates of the  $H_2S(gas)$

concentration generally moderately exceed the value SKB adopted in the COMSOL simulations,  $1.7 \times 10^{-7}$  mol/L (dashed line in Figure 3-5). We used Eq. (3-9) to perform a simplified computation of the sulphide flux,  $J_{H_2S}$ :

$$J_{H_2S} = \theta S_g \tau D_{H_2S} \frac{[H_2S(\text{gas})]}{L} \quad (3-10)$$

$L$  is the diffusive distance; other terms were previously defined. The following inputs were considered

$\theta$	— 0.39, bentonite porosity
$S_g$	— 0.265, gas saturation (water saturation = 0.735)
$m$	— 4/3, see Eq. (3-5)
$n$	— 4/3, see Eq. (3-5)
$L$	— 0.35 m, diffusive distance, buffer material radial thickness

Equation (3-10) corresponds to one-dimensional steady-state flux, with a fixed concentration  $[H_2S(g)]$  [Eq. (3-9)] at a distance  $L$ , and zero sulphide concentration at distance 0. The radial distance  $L=0.35$  m was considered, to account for the case where sulphide may quickly diffuse along bentonite pellets (region indicated by the blue arrow in Figure 3-2) and then radially inwards through the buffer until it reacts with the copper canister. The sulphide flux was computed as a function of time and temperature, considering the canister temperature in Figure 2-2 of SKB TR-19-15 [a digitized version is reproduced in Figure 3-6(a)]. The sulphide flux and the equivalent copper corrosion rate are displayed in Figure 3-6(b), as a function of time and hydrostatic pressure. A sulphide flux of  $1 \text{ mol}/(\text{m}^2\text{-s})$  corresponds to a copper corrosion rate equal to  $4.47 \times 10^8 \text{ mm/yr}$ ; this conversion factor was applied to compute the right axis scale of the plot in Figure 3-6(b). For comparison purposes, Figure 3-6(b) also includes the maximum flux SKB computed for the no-water-inflow case [dashed line,  $6.5 \times 10^{-11} \text{ mol}/(\text{m}^2\text{-s})$ ]. The corrosion rate was integrated in time to compute the cumulative penetration in Figure 3-6(c).

As the backfill and buffer saturate, the air pressure increases to equilibrate with the hydrostatic pressure, slowing down gas diffusion rates. The cumulative penetration of the corrosion front in Figure 3-6(c) is minor to negligible, even for the case of constant total pressure equal to 1 atm (depth = 0 m). Saturated conditions may be established in a few thousands of years, at which point gas transport by diffusion would become negligible. SKB states that SRB may require a limited pressure range to be active, well below pressures established at depths between 400 and 500 m below the water table.

The peak sulphide flux SKB computed,  $6.5 \times 10^{-11} \text{ mol}/(\text{m}^2\text{-s})$  [dashed line in Figure 3-6(b)], is comparable to the fluxes in Figure 3-6(b), case depth = 0 m (the analysis by SKB considered a reference diffusion coefficient at 1 atm). We estimated higher fluxes [maximum equal to  $1.7 \times 10^{-10} \text{ mol}/(\text{m}^2\text{-s})$ ] than the SKB maximum because of the assumed tortuosity function yielding an effective diffusion coefficient of higher magnitude, considered a shorter characteristic diffusive length (0.35 m radial distance versus 2.5 m vertical distance considered by SKB—vertical distance from the canister top to the deposition tunnel), and a higher  $H_2S(\text{gas})$  concentration at the deposition hole boundary [see Figure 3-5, dashed line]. In both the SKB and our simplified computations, the cumulative corrosion damage would be minor to negligible during the unsaturated period.

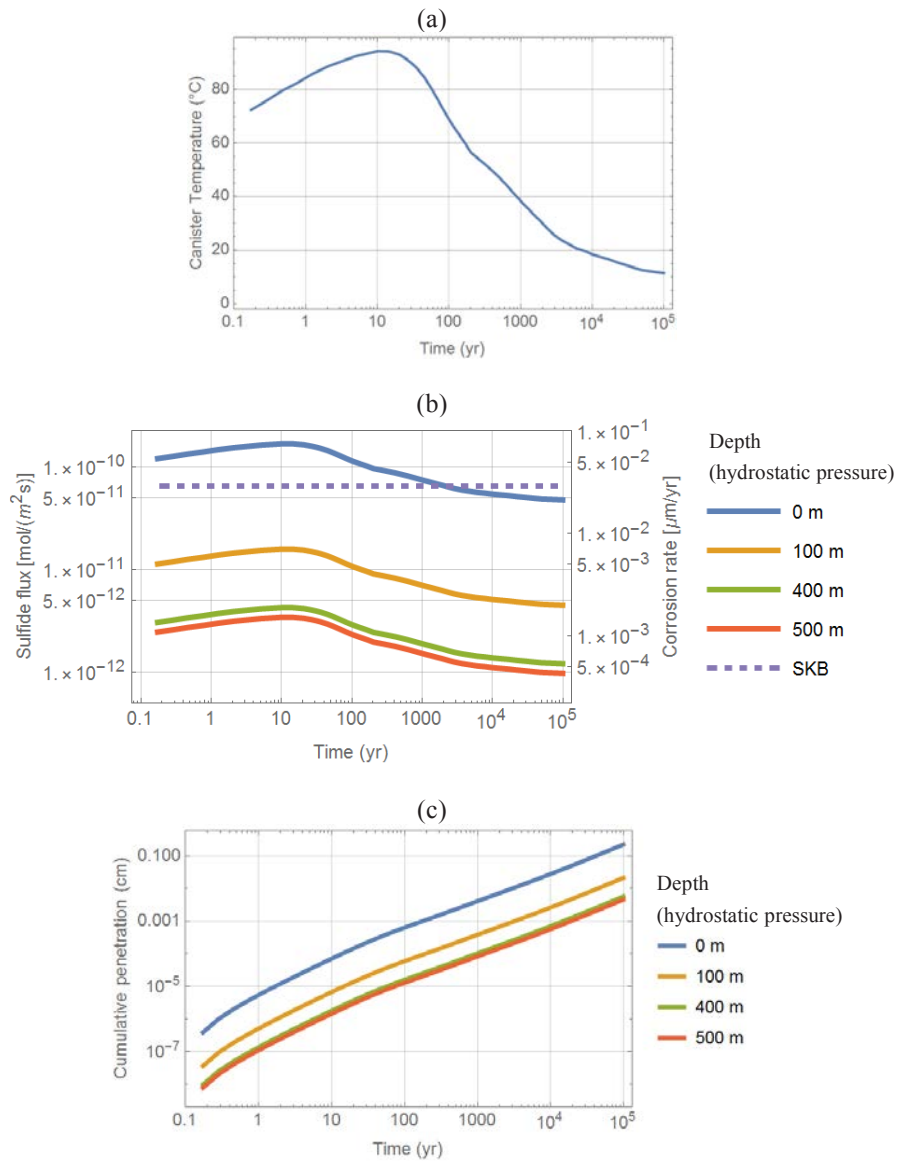


Figure 3-6. (a) Canister temperature versus time (data digitized from Figure 2-2 in SKB TR-19-15); (b) Sulphide flux (left axis) and corresponding corrosion rate (right axis) as a function of time [the dashed line is the maximum flux SKB computed for the no-water-inflow case,  $6.5 \times 10^{-11}$  mol/(m<sup>2</sup>-s)]; (c) Cumulative penetration of the corrosion front as a function of time

The sulphide flux  $6.5 \times 10^{-11}$  mol/(m<sup>2</sup>-s) corresponds to the maximal value SKB computed at the top lid canister edge. We implemented a COMSOL model to understand why the edges experience higher sulphide fluxes. The model considered a uniform temperature and air saturation (=0.265). A constant H<sub>2</sub>S(gas) concentration was assumed at the deposition hole-deposition tunnel interface consistent with Eq. (3-9), a zero sulphide concentration was imposed at the canister surface, and a zero-flux condition was imposed at all rock/buffer surfaces. The model accounted for a gap region filled with bentonite pellets (region pointed by the blue arrow in Figure 3-2), and small gaps between cylindrical buffer bentonite rings placed above the canister. The top canister lid included an additional rim, 10 cm in height, mimicking the SKB model. The model implemented an axis-symmetric cylindrical geometry.

Figure 3-7 shows sulphide flux streamlines and iso-flux curves (curves with equivalent-magnitude fluxes). The COMSOL model confirms that the highest sulphide fluxes would occur at the top lid right canister edge [Figure 3-7(b)]. The convex edges (convex from the outside canister perspective) focus the flux lines in a smaller area (and increase the magnitude of the flux), while the concave edges spread the flux lines (and decrease the magnitude of the flux). The top right edge is affected by sulphide coming directly from the deposition tunnel, and from the gap region with the bentonite pellets.

An infinitely sharp edge is singular, with fluxes of arbitrarily large magnitude. However, if high sulphide fluxes were established, initial corrosion would smooth sharp edges and cause fluxes to decrease in magnitude. The apparent flux spikes are self-arresting, and decay towards smaller values comparable to fluxes a short distance away from the edge, as the edges become smoother. We hypothesize that the maximal flux SKB reported is dependent on the grid size of the finite element model around the canister edge.

Figure 3-8(a) displays the magnitude of the flux normal to the canister surface, around the canister contour (0 m represents the canister center top and ~6 m is the center bottom), considering air pressure = 1 atm, temperature = 90 °C, and  $n=m=1/3$  [tortuosity function exponents, Eq. (3-5)]. The flux exhibits downward spikes at the concave edge and upward spikes at the convex edges. The plot in Figure 3-8(a) includes two curves for two different representations of edges. The blue curve corresponds to a sharp edge case, Figure 3-8(b), and the green curve to a round edge, Figure 3-8(c). The spike of the blue curve ( $\sim 3 \times 10^{-10}$  mol/m<sup>2</sup>-s) is higher than the spikes of the green curve ( $\sim 9 \times 10^{-11}$  mol/m<sup>2</sup>-s). The blue spike can be made arbitrarily taller by considering a sharper edge and very fine mesh. Two blue spikes (for two convex edges at the top) converge to a single maximum (green curve) as the top edges become smooth. Additional rounding of the edge in Figure 3-8(c) has minimal effect on the green curve maximum. Therefore, there is a degree of ambiguity of spikes computed with sharp edges. The model with rounded edges is more objective: the fluxes are similar independently of the geometry, provided rounded edges are used in the model.

Figure 3-9(a) displays the normal flux (normal to the canister surface) along the canister contour, at three air pressures (rounded edge model). The sulphide flux is very sensitive to changes in the air pressure. The SKB maximum flux for the no-water-inflow case,  $6.5 \times 10^{-11}$  mol/(m<sup>2</sup>-s), compares well to fluxes for the case depth=0 in Figure 3-9(a). Figure 3-9(b) is the translation of the normal fluxes to a corrosion depth on the copper canister, after 10<sup>5</sup> years, assuming constant temperature (90 °C), water saturation, and constant air pressure throughout. The

maximum corrosion front depth compares well with the simplified estimates in Figure 3-6(c). Changes in the saturation, air pressure, and temperature as time progresses will further constrain the transport of hydrogen sulphide in gas phase.

The maximum sulphide flux SKB computed,  $6.5 \times 10^{-11}$  mol/(m<sup>2</sup>-s), is concluded to be a conservative estimate of H<sub>2</sub>S(gas) fluxes. To facilitate keeping track of and comparing the alternative assumptions discussed in this section, Table 3-3 summarizes the main assumptions of the SKB computations [leading to the  $6.5 \times 10^{-11}$  mol/(m<sup>2</sup>-s) maximum H<sub>2</sub>S(gas) flux estimate], as well as assumptions of simplified computations in Figure 3-6 and Figure 3-9, and a qualitative summary of the effects of those assumptions on H<sub>2</sub>S(gas) flux computations. The majority of the assumptions in the SKB computations have a conservative bias. The most influential assumption in the SKB no-water-inflow case was ignoring effects of the hydrostatic pressure on the effective diffusion coefficient. Figure 3-6 and Figure 3-9 indicate that the maximum flux SKB computed for H<sub>2</sub>S(gas),  $6.5 \times 10^{-11}$  mol/(m<sup>2</sup>-s), is well above alternative estimates accounting for hydrostatic pressure corrections.

Therefore, we agree with the SKB conclusion that corrosion by sulphide gas during the unsaturated period is unlikely to cause major damage to the copper canisters, provided the sulphide solubility in solution is heavily constrained by the bentonite of the deposition tunnel backfill and buffer.

Table 3-3. Summary of key assumptions in the simplified computations by SKB and implemented in this report

Case	Assumption	Effect of Assumption
SKB no-water- inflow case	No water inflow	This assumption is conservative. The H <sub>2</sub> S gas flux is overestimated. Considering water inflow and gradual saturation of the buffer would decrease H <sub>2</sub> S fluxes.
	Hydrogen sulphide dissociation constant and Henry's constant computed at a fixed temperature, and pH = 7	This assumption is related to the H <sub>2</sub> S(gas) concentration at the deposition hole boundary defining a boundary condition. Assuming pH 7 is a conservative assumption. The H <sub>2</sub> S(gas) concentration significantly drops with increasing pH (Figure 3-5). Assuming a fixed temperature may underestimate the H <sub>2</sub> S(gas) concentration (e.g., Figure 3-5). However, the total sulphide concentration is unknown, below experimental detection limits. SKB assumed a total sulphide concentration equal to 10 <sup>-6</sup> mol/L, and from that assumption derived [H <sub>2</sub> S(gas)]=1.7×10 <sup>-7</sup> mol/L. Based on [H <sub>2</sub> S(gas)] as a function of temperature and pH (Figure 3-5), postulating [H <sub>2</sub> S(gas)]=1.7×10 <sup>-7</sup> mol/L for the deposition hole boundary condition is a reasonable alternative assumption.
	Maximum flux 6.5×10 <sup>-11</sup> mol/(m <sup>2</sup> -s)	The thermal gradient mobilizes water away the canister, which tends to expedite transport of H <sub>2</sub> S(gas) in dry regions. However, water accumulating away the canister slows down H <sub>2</sub> S(gas) transport on the wet regions. Slowing and expediting transport processes are at simultaneously at play throughout the buffer. It is difficult to judge <i>a priori</i> if a system with a non-uniform water saturation results in faster or slower H <sub>2</sub> S(gas) transport than a system with a uniform water saturation. However, because the competing and counteracting processes, different assumptions on the temperature distribution (e.g., uniform versus non-uniform) are expected to have only a minor to moderate effect on the rate of H <sub>2</sub> S(gas) transport.
Simplified computations in Figure 3-6	Constant air pressure = 1 atm	This assumption is highly conservative. The effective diffusion coefficient of H <sub>2</sub> S(gas) is inversely proportional to the air pressure [e.g., Eq. (3-3)]. SKB assumed pressure = 1 atm to estimate the effective H <sub>2</sub> S(gas) diffusion coefficient, and ignored the hydrostatic pressure
	Constant water and gas saturation	This assumption has a dominant conservative effect. Assuming water redistribution expedites gas transport in regions of low water saturation (dry regions); however, the buffer material and deposition holes gradually saturate until the H <sub>2</sub> S(gas) transport negligibly contributes to the sulphide flux (the sulphide flux eventually becomes dominated by the flux of dissolved sulphide ion).
	Variable temperature as a function of time, per Figure 3-6(a)	This assumption is realistic. Transport of sulphide gas is fast and slows down as the system temperature drops.
COMSOL simulations in Figure 3-9	Diffusive path length equal to 0.35 m (equal to buffer material thickness)	This assumption is conservative. The actual diffusive pathways is a combination of a vertical (2.5 m) and radial path (0.35 m) for sulphide to reach the canister.
	Constant water and gas saturation	This assumption has a dominant conservative effect. See a previous related entry for more commentary.
	Constant temperature, 90 °C	This assumption is conservative. The temperature will decrease with time. Assuming an elevated constant temperature overestimates the H <sub>2</sub> S(gas) concentration at the deposition hole boundary, and the rate of diffusion. Competing effects are at play with regards to uniform versus non-uniform temperature and water distribution, and the effect of temperature and water distribution is expected to be secondary to the effect of assuming an elevated temperature at all times.

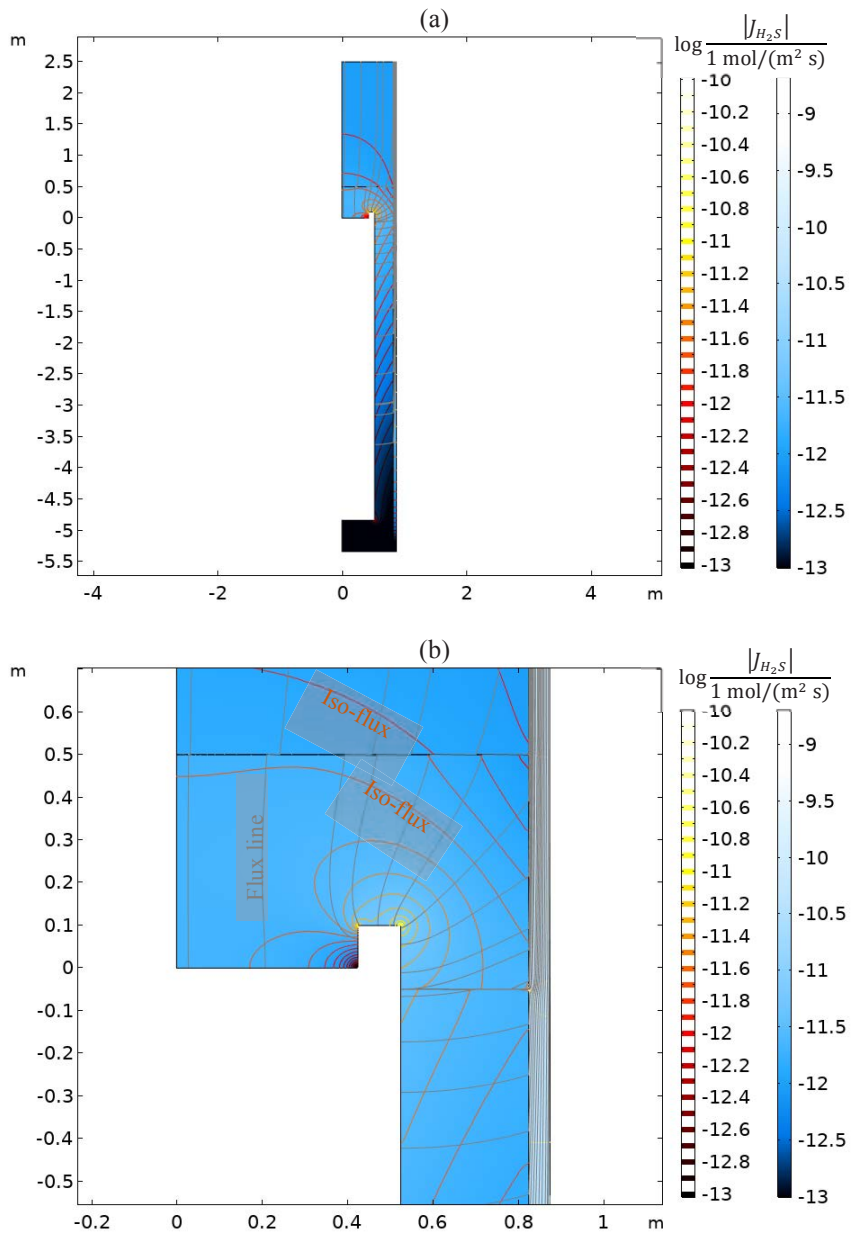


Figure 3-7. Flux lines and iso-flux curves computed with a COMSOL model; (a) modelled domain (cylindrical geometry), (b) zoom-in region.

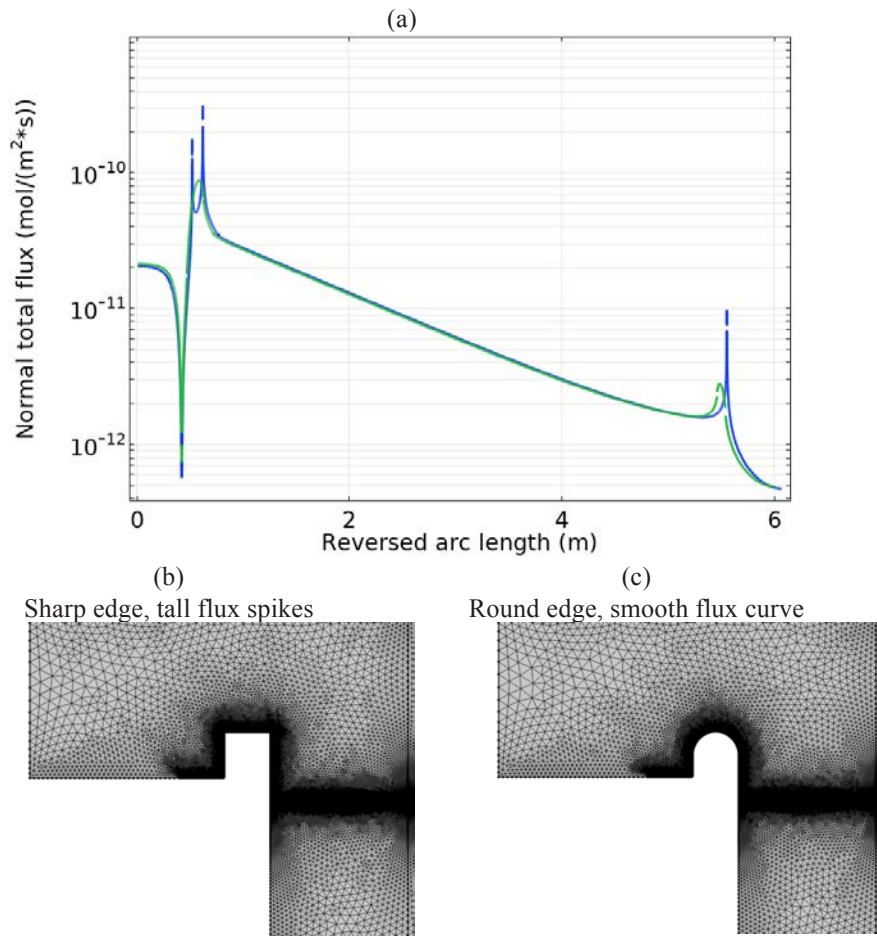


Figure 3-8. (a) Normal sulphide flux (normal to the canister surface) versus position around the canister (0 m represents the top canister at the center, and ~6 m is the bottom canister at the center). The top plot includes two curves, corresponding to a sharp edge (b), and to a rounded edge (c).

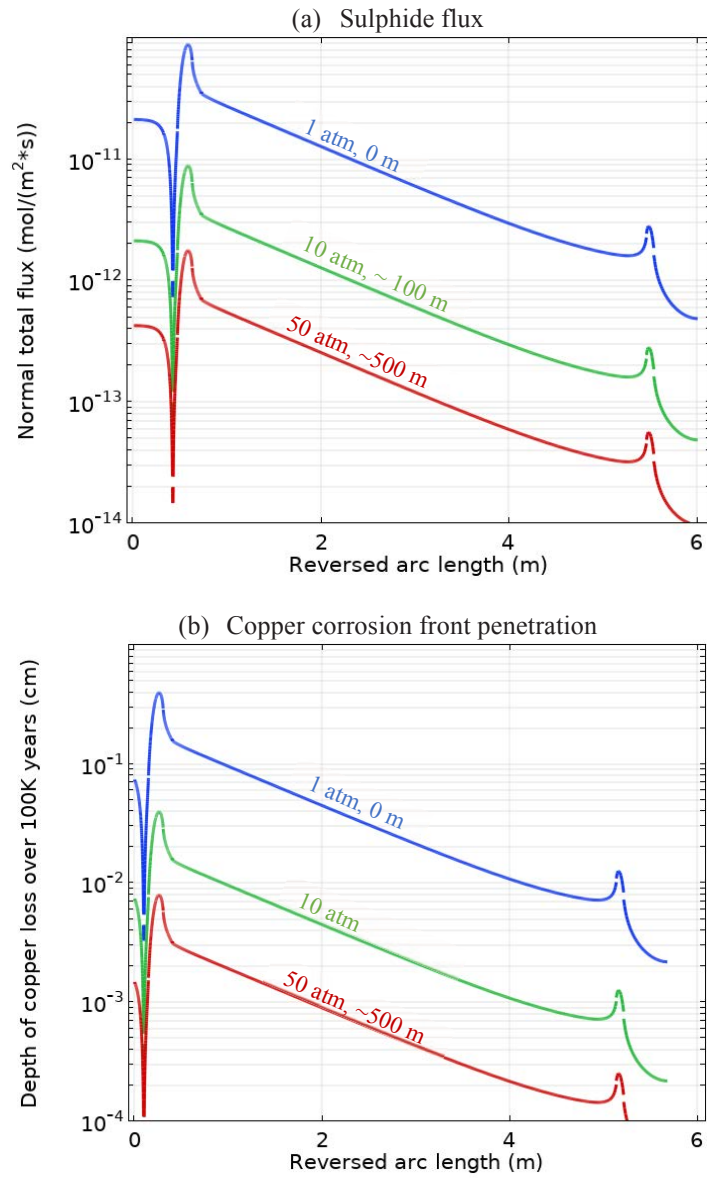


Figure 3-9. (a) Normal sulphide flux (normal to the canister surface) versus position around the canister (0 m represents the center top canister, and ~6 m is the center bottom canister) and versus air pressure. (b) Corresponding penetration of the corrosion front over  $10^5$  years, assuming constant conditions (e.g., constant temperature, 90 °C, constant air pressure, and constant water saturation)

## 4 Conclusions

The additional information SKB provided to address questions posed by the Land and Environmental Court was evaluated, focusing on radionuclide transport and PA computations. SKB concluded that localized corrosion, in the form of micro-galvanic corrosion, could not be unequivocally excluded to occur in the repository, and provided an evaluation of potential consequences. We examined the evaluation of micro-galvanic corrosion using independent computations. We concluded that the simplifications SKB considered to evaluate micro-galvanic corrosion are appropriate [e.g., considering a threshold sulphide flux for the onset of micro-galvanic corrosion equal to  $3 \times 10^{-10}$  mol/(m<sup>2</sup>-s), and a related enhancement factor to corrosion rates equal to 20]. The assumed threshold of  $3 \times 10^{-10}$  mol/(m<sup>2</sup>-s) is a necessary but not sufficient condition for micro-galvanic corrosion to occur. Micro-galvanic corrosion has not been observed in systems exposing copper to those low sulphide fluxes, and much higher fluxes may be required for the onset of micro-galvanic corrosion. It was concluded, considering flow rates from the semi-correlated hydrogeological model, that the probability for conditions exceeding the assumed threshold for micro-galvanic corrosion is low. The expected number of canisters affected by micro-galvanic corrosion is less than 1 in 10<sup>6</sup> years. SKB dose estimates were reasonably verified using an independent PA model.

Scenarios for sulphide corrosion during the unsaturated and saturated periods were examined, including effects by SRB. Indications of micro-galvanic corrosion due to sulphide produced by SRB have been observed in the laboratory; however, the associated experimental conditions are not expected to occur in repository settings. Experiments by Masurat et al. (2010) under more relevant repository settings indicate production of sulphide at limited rates, not sufficient to compromise the canister in 10<sup>6</sup> years even if transport limitations were ignored. Groundwater is the most important source of sulphide. Considering results of the SKB semi-correlated hydrogeological model and sulphide concentrations observed in the Forsmark area, it is concluded that groundwater sulphide will not cause failure of the canister provided the buffer is a diffusive barrier, protecting the canister from direct contact with the groundwater. Scenarios considering sulphide in groundwater were evaluated in detail by Stothoff and Manepally (2013).

For the unsaturated scenario, SKB reported experiments with freely flowing sulphide gas under controlled relative humidity and temperature and measured relatively high corrosion rates, but without indication of localized corrosion or micro-galvanic corrosion. Those high corrosion rates are not expected to be directly applicable to repository conditions, because SRB are expected to become initially active at locations distant from canisters, possibly in the deposition tunnels, so that corrosion rates become limited by rates of sulphide transport. SKB implemented simplified computations of diffusion of sulphide gas in air trapped in deposition holes, and reaction with the copper canister. Although some shortcomings were identified in the SKB computations, those shortcomings do not change the SKB conclusions. SKB concluded that canister damage by sulphide produced by SRB would be minor or negligible; this conclusion was verified with independent computations in this report. A key assumption in those computations is that the total sulphide concentration in bentonite porewaters is small (e.g., less than or equal to 10<sup>-6</sup> mol/L). This small concentration is supported by experiments reported by SKB (2019) and by Svensson et al. (2017). In both sets of experiments, sulphide was below detection limits in solution. Although the mechanism is not well known,

Svensson et al. (2017) estimated that 1,000 kg of bentonite could remove up to 10 kg of sulphide from the solution.

The independent assessment reported here agrees with the SKB conclusion that micro-galvanic corrosion would not affect dose estimates of the SR-Site analysis. The following are identified as key analyses supporting the SKB conclusions.

- The hydrogeological flow models, particularly the semi-correlated model that predict low flow rates per intercepted deposition hole.
- The measured sulphide concentrations in the Forsmark area, indicating that concentrations are unlikely to exceed  $1.2 \times 10^{-4}$  mol/L, and that concentrations in excess of  $1.2 \times 10^{-5}$  mol/L are rare.
- Measurements (or attempts to measure) sulphide concentrations in bentonite porewaters. The experimental evidence indicates that sulphide concentration in bentonite porewaters is small, independently of the source (groundwater or from SRB activity).

Overall conclusions may need to be re-analysed if future information changes the conclusions of the key analyses stated in the previous bullets.

SKB updated the biosphere model, significantly changing dose estimates of  $^{14}\text{C}$ ,  $^{129}\text{I}$ ,  $^{135}\text{Cs}$ , and  $^{79}\text{Se}$ . In the case of  $^{14}\text{C}$ , dose estimates decreased by up to a factor of 1,000 with respect to the model used in the SR-Site assessment. Using the updated model, SKB concluded that the total annual dose would remain below the risk limit, even if all canisters were initially penetrated by a small hole. Those revised dose estimates may be important to address remaining safety issues. A parallel review effort sponsored by SSM evaluated the updated SKB biosphere model (Walke and Newson, 2019).

## 5 References

- Bird, R.B., W.E. Stewart, and E.N. Lightfoot. 1960. "Transport Phenomena." John Wiley & Sons: New York.
- Cesen, A., T. Kosec, A. Legat, V. Bokan-Bosiljkov. 2014. "Corrosion Properties of Different Forms of Carbon Steel in Simulated Concrete Porewater." *Materiali in tehnologije / Materials and technology*, Vol. 48, No. 1, 2014, pp. 1–57.
- Chau, J.F., and D. Or. 2005. "Simulation of gaseous diffusion in partially saturated porous media under variable gravity with lattice Boltzmann methods." *Water Resources Research*, Vol. 41, W08410, doi:10.1029/2004WR003821.
- Chen, J., Z. Qin, T. Martino, and D.W. Shoesmith. 2017. "Non-uniform film growth and micro/macrogalvanic corrosion of copper in aqueous sulphide solutions containing chloride." *Corrosion Science*, 114, 72–78.
- Chen, J., Z. Qin, T. Martino, M. Guo, and D.W. Shoesmith. 2018. "Copper transport and sulphide sequestration during copper corrosion in anaerobic aqueous sulphide solutions." *Corrosion Science*, 131, 245–251.
- Chen, J., M. Guo, T. Martino, S. Ramamurthy, J.J. Noël, D.W. Shoesmith, C. Lilja, and A.J. Johansson. 2019. "The distribution of corrosion damage to copper surfaces exposed to aqueous sulphide solutions." SKBdoc 1706406, ver 1.0, Svensk Kärnbränslehantering AB.
- Clark, M.M. 1996. "Transport Modeling for Environmental Engineers and Scientists." New York: John Wiley & Sons.
- Engineering ToolBox, 2018. "Air - Diffusion Coefficients of Gases in Excess of Air." Available at: [https://www.engineeringtoolbox.com/air-diffusion-coefficient-gas-mixture-temperature-d\\_2010.html](https://www.engineeringtoolbox.com/air-diffusion-coefficient-gas-mixture-temperature-d_2010.html) [Accessed August 14, 2019].
- Eriksson, P., and A. Hedin. 2018. "Modelling of sulphide fluxes in unsaturated buffer and backfill for a KBS-3 repository." SKBdoc 1696975 ver 2.0, Svensk Kärnbränslehantering AB.
- Fathi, H., A. Raoof, S.H. Mansouri, and M.Th. van Genuchten. 2017. "Effects of Porosity and Water Saturation on the Effective Diffusivity of a Cathode Catalyst Layer." *Journal of the Electrochemical Society*, 164 (4) F298-F305.
- Gordon, A., H. Pahverk, E. Börjesson, L. Sjögren, O. Karlsson, H. Bergqvist, F. Lindberg, and A.J. Johansson. 2018. "Corrosion morphology of copper in anoxic sulphide environments." Technical Report TR-18-14, Svensk Kärnbränslehantering AB (SKB, Swedish Nuclear Fuel and Waste Management Co.): Stockholm, Sweden. December 2018.
- Hu, W., Y. Jiang, D. Chen, Y. Lin, Q. Han, and Y. Cui. 2018. "Impact of Pore Geometry and Water Saturation on Gas Effective Diffusion Coefficient in Soil." *Appl. Sci.* 2018, Vol. 8, 2097; doi:10.3390/app8112097.
- Lundgren, C. 2013. "Kemirapport 2013-01 Sulfidanalys av bentonitvattenblandning." SKBdoc 1385099 ver 1.0, Svensk Kärnbränslehantering AB. (In Swedish.)

Lyman, W.J., W.F. Reehl, and D.H. Rosenblatt. 1982. "Handbook of Chemical Property Estimation Methods." American Chemical Society: Washington, DC.

Masum, S.A., P.J. Vardon, H.R. Thomas, Q. Chen, and D. Nicholson. 2012. "Multicomponent gas flow through compacted clay buffer in a higher activity radioactive waste geological disposal facility." *Mineralogical Magazine* 76, 3337–3344

Masurat P., S. Eriksson, and K. Pedersen. 2010. "Microbial sulphide production in compacted Wyoming bentonite MX-80 under in situ conditions relevant to a repository for high-level radioactive waste." *Applied Clay Science*, 47, pp 58–64, 2010.

NIST. 2019. "NIST Chemistry WebBook, SRD 69." National Institute of Standards and Technology. <https://webbook.nist.gov/cgi/cbook.cgi?ID=C7783064&Mask=10>

Pensado, O. 2017. "2017:15 Radionuclide release rates associated with bounding cases featuring relatively early canister failures in a spent fuel repository." Stockholm, Sweden: Strålsäkerhetsmyndigheten (SSM–Swedish Radiation Safety Authority). <https://www.stralsakerhetsmyndigheten.se/en/publications/reports/waste-shipments-physical-protection/2017/201715/>

Pensado, O., S. Mohanty, and B. Sagar. 2014. "2014:29 Technical Note, Independent Modelling of Radionuclide Transport, Evaluation of Colloid Transport Modelling–Main Review Phase." Stockholm, Sweden: Strålsäkerhetsmyndigheten (SSM–Swedish Radiation Safety Authority). <https://www.stralsakerhetsmyndigheten.se/en/publications/reports/waste-shipments-physical-protection/2014/201429/>

Pensado, O., and S. Mohanty. 2012. "Technical Note 2012:58 Independent Radionuclide Transport Modelling – Reproducing Results for Main Scenarios." Stockholm, Sweden: Strålsäkerhetsmyndigheten (SSM–Swedish Radiation Safety Authority). <https://www.stralsakerhetsmyndigheten.se/en/publications/reports/waste-shipments-physical-protection/2012/201258/>

Scanlon, B.R., J.P. Nicot, and J.W. Massmann. 2001. "Soil Gas Movement in Unsaturated Systems." Book chapter in "Soil Physics Companion," edited by A.W. Warrick. CRC Press: Boca Raton, December 28, 2001. [http://www.beg.utexas.edu/staffinfo/Scanlon\\_pdf/ScanlonSoilPhysComp02.pdf](http://www.beg.utexas.edu/staffinfo/Scanlon_pdf/ScanlonSoilPhysComp02.pdf)

SKB. 2019. "Supplementary information on canister integrity issues." Technical Report TR-19-15. Svensk Kärnbränslehantering AB (SKB, Swedish Nuclear Fuel and Waste Management Co.): Stockholm, Sweden. March 2019.

SKB. 2011. "Long-term safety for the final repository for spent nuclear fuel at Forsmark, Main report for the SR-Site project, Volume III." Technical Report TR-11-01, Volume III. Svensk Kärnbränslehantering AB (SKB, Swedish Nuclear Fuel and Waste Management Co.): Stockholm, Sweden. March 2011.

SKB. 2010a. "Corrosion calculations report for the safety assessment SR-Site." Technical Report TR-10-66. Svensk Kärnbränslehantering AB (SKB, Swedish Nuclear Fuel and Waste Management Co.): Stockholm, Sweden.

SKB. 2010b. "Radionuclide transport report for the safety assessment SR-Site." Technical Report TR-10-50. Svensk Kärnbränslehantering AB (SKB, Swedish Nuclear Fuel and Waste Management Co.): Stockholm, Sweden. December 2010.

SKB. 2010c. "Data report for the safety assessment SR-Site." Technical Report TR-10-52. Svensk Kärnbränslehantering AB (SKB, Swedish Nuclear Fuel and Waste Management Co.): Stockholm, Sweden. December 2010.

Stothoff, S., and C. Manepally. 2013. "Technical Note 2013:36 Review and assessment of aspects of the Qeq concept." Stockholm, Sweden: Strål säkerhets myndigheten (SSM–Swedish Radiation Safety Authority).

Sun, W., S. Nestic, and D. Young. 2008. "Equilibrium Expressions Related to the Solubility of the Sour Corrosion Product Mackinawite." *Ind. Eng. Chem. Res.* 2008, 47, 1738-1742

Svensson D., C. Lundgren, and P. Wikberg. 2017. "Experiments with bentonite and sulphide—results from experiments 2013–2016." SKB P-16-31, Svensk Kärnbränslehantering AB.

Thorbjørn, A., P. Moldrup, H. Blendstrup, T. Komatsu, and D.E. Rolston. 2008. "A Gas Diffusivity Model Based on Air-, Solid-, and Water-Phase Resistance in Variably Saturated Soil." *Vadose Zone J.* Vol. 7, 1276–1286 (2018); doi:10.2136/vzj2008.0023.

Walke, R. and R. Newson. 2019. "Review of Assignment for the Swedish Radiation Safety Authority: Biosphere review and independent dose assessment of complementary information relating to spent nuclear fuel canister integrity" Part 4 of this review report.

# Coverage of SKB reports

Following reports have been considered in conducting this review.

**Table A-1: List of reports consulted and evaluated in completing the task**

Reviewed report	Reviewed sections	Comments
SKB TR-19-15	All	Main report
SKBdoc 1696975	All	Sulphide gas diffusion computations
SKB TR-18-14	All	Exposure of copper coupons to sulphide gas and biofilms
SKB TR-10-66	Section 5.3	Corrosion computations in support of the SR-Site analysis. Estimates on the number of canisters affected, under various scenarios, are provided
SKB TR-10-50	Section 4.3, 4.4, 6.3	Radionuclide transport for the SR-Site analysis
SKB TR-10-52	Section 3.1.3	Source for number of canisters in the repository: 6,103
P-16-31	All	Report indicating that the solubility of sulphide in bentonite porewaters is low



**Authors**

Russell Walke  
Rebecca Newson

Quintessa Limited Henley-on-Thames, UK

Review of Assignment for the Swedish  
Radiation Safety Authority:  
Biosphere review and independent  
dose assessment of complementary  
information relating to spent nuclear  
fuel canister integrity



# Abstract

In April 2019, the Swedish Nuclear Fuel and Waste Management Company (SKB) submitted complementary information relating to its licence application for construction, possession and operation of a KBS-3 spent nuclear fuel repository at the Forsmark site. The new material included (i) further consideration of canister-related corrosion processes in response to the deficiencies identified by the Court, as well as (ii) providing additional robustness calculations. This technical note describes review of biosphere modelling related aspects of the additional compliance and robustness calculations.

## Conclusions relating to the new corrosion calculations

SKB uses updated flux to dose conversion factors (LDFs) in assessing the potential dose consequences of new corrosion calculations. The updated LDFs correct for omissions in the original analysis identified in SSM's reviews. The inclusion of a contribution from Po-210 in groundwater released to the biosphere is well founded. However, the conceptual basis for the inclusion of a dose factor for Rn-222 is not well described.

## Conclusions relating to the new robustness calculations

In assessment of potential dose consequences of new hypothetical robustness calculations, SKB has chosen to modify the way in which the potential doses are evaluated. The modifications significantly reduce potential doses assessed for key radionuclides in the original analyses, notably C-14, Se-79 and I-129. Using the updated biosphere modelling, SKB presents results that remain below the dose that corresponds to the risk limit (within a factor of about five). The modifications to the biosphere modelling make the analyses inconsistent with all of the other analyses supporting the SR-Site assessment.

The modified representation of the biosphere draws on updated sorption ( $K_d$ ) and equilibrium concentration ratios (CRs) used in the more recent SR-PSU assessment for the SFR facility at Forsmark. Changes to  $K_d$  values are based on more extensive use of site-specific data and are well justified. Changes to CR values are presented by SKB as better-representing sorption and uptake at Forsmark, drawing on major sampling campaigns at Forsmark and its vicinity. It is notable that significant reductions in CR values for Se-79 and I-129 are primarily not based on new site-specific data. The changes to CR values for Se-79 and I-129 result in very significant (two or three orders of magnitude) reductions in associated dose consequences compared to the original SR-Site assessment.

In the new robustness calculations, SKB explicitly models radionuclide releases to the biosphere using time-dependent fluxes rather than using LDF values. This approach is described in SKB (2019a) as being "considerably more realistic". This statement is true for timescales up to future cold climate periods, but it is not true thereafter. It is unrealistic to model perpetual temperate conditions to a million years. This approach results in artefacts in the results, such as continued accumulation of very long-lived radionuclides including Cs-135, as noted by SKB in its explanation of the results.

The SR-Site assessment included modelling of radionuclide releases to a single biosphere object as well as modelling of distributed releases, informed by particle

tracking of releases from across the repository footprint. The approach adopted for the new robustness calculations is not clearly described by SKB.

Finally, it is notable that the sudden widening of canister defects at 10,000 years in the new robustness calculations occurs relatively shortly after complete terrestrialisation. This is favourable for C-14, for which the most significant exposures arise when lakes remain present in the landscape.

# Contents

<b>1. Introduction</b> .....	<b>1</b>
<b>2. Updated compliance calculations</b> .....	<b>1</b>
2.1. Conclusions from original review .....	2
2.2. Updated LDF model used by SKB .....	2
2.3. Review of the consequence analysis .....	4
<b>3. Additional robustness calculations</b> .....	<b>5</b>
3.1. Changes to biosphere $K_d$ and CRs .....	5
3.2. Implications of changes to biosphere $K_d$ and CRs .....	7
3.3. Use of time-dependent flux to the biosphere .....	8
<b>4. Overall conclusions</b> .....	<b>9</b>
<b>5. References</b> .....	<b>11</b>
<b>APPENDIX 1</b> .....	<b>13</b>

# 1. Introduction

In 2011, the Swedish Nuclear Fuel and Waste Management Company (SKB) submitted a licence application for construction, possession and operation of a KBS-3 spent nuclear fuel repository at the Forsmark site. This application has been reviewed by SSM, who submitted a statement to the Swedish Land and Environment Court in June 2016 and a statement to the Swedish Government in January 2018 recommending approval of the application. The Land and Environment Court published a statement in early 2018 in which SKB's plans were judged to be acceptable only if additional information is provided to show that the requirements of the Environmental Code are fulfilled despite uncertainties relating to a number of canister-related corrosion processes.

In April 2019, SKB submitted new material further reviewing and assessing potential canister-related corrosion processes in response to the deficiencies identified by the Court, as well as providing additional robustness calculations (SKB, 2019a). SSM is required to review the new material submitted by SKB, and to provide a statement to the Government late September 2019.

SSM has contracted external experts involved in reviewing the original 2011 licence application to support an assessment of how well the new material supplied by SKB addresses the concerns raised by the Court. This technical note documents review of the biosphere and dose assessment component of the new material.

The review focuses on SKB (2019a). The new material presented by SKB includes changes to the way in which the assessment is undertaken in comparison to the original licence application. Changes relating to the representation of the biosphere and assessment of potential doses are described in SKB (2015) and SKB (2019b), which are, therefore, also encompassed in this review.

The technical note is structured in the following way.

- Updated compliance calculations presented in Section 9.3 of SKB (2019a) are reviewed in Section 2.
- Additional robustness calculation presented in Section 9.4 of SKB (2019a) are reviewed in Section 3.
- Overall conclusions are presented in Section 4.

References are given in Section 5. Coverage of SKB reports and supporting material is described in Appendix 1.

## 2. Updated compliance calculations

Some notable conclusions from the original review of biosphere modelling undertaken by SKB in support of its SR-Site assessment are highlighted in Section 2.1. Changes to the LDF model employed by SKB relevant to the analysis presented in SKB (2019a) are reviewed in Section 2.2. The consequence analysis for the new corrosion cases are then reviewed in Section 2.3, drawing on accompanying independent radionuclide transport calculations.

## 2.1. Conclusions from original review

In interpreting the biosphere and dose consequences presented by SKB for the updated compliance calculations, the observations made in reviewing the original licence application need to be borne in mind. Some notable aspects and review findings are highlighted below.

- Uncertainty in potential landscape development is managed by SKB through use of the most pessimistic landscape dose factors (LDFs) calculated over a full interglacial cycle for a range of different sub-catchments (termed ‘biosphere objects’) that may potentially receive contaminated groundwater discharges (SKB, 2010).
- The level of averaging, normalisation and interpolation of hydrology and hydrogeology within sub-catchments (termed ‘biosphere objects’) receiving potentially contaminated groundwater discharges means that the biosphere modelling that supports the landscape dose factors (LDFs) used by SKB is based on a very abstract representation of water flows (Walke, 2013; Klos et al., 2014).
- The coarse vertical discretisation used in SKB’s biosphere object model means that the timescale of radionuclide migration, retention, decay and in-growth is poorly represented within a system for which the timescale of terrestrialisation due to post-glacial uplift is identified by SKB as being an important factor (Walke, 2013).
- The ‘global warming’ variant considered in SKB’s analyses is represented by extending the length of the interglacial period, but maintaining a present-day climate. Representation of a warmer climate, with increased potential for irrigation from a groundwater well, would result in higher LDFs (Walke and Limer, 2014).

## 2.2. Updated LDF model used by SKB

The LDF values used for compliance calculations presented in Section 9.3 of SKB (2019a) are made on the basis of modelling that corrects omissions identified in the assessments that supported the original licence application. The main changes reflect the representation of Po-210 and Rn-222 in the analyses and are described in SKB (2015).

### Accounting for Po-210 in the far-field release to the biosphere

Po-210 is a radionuclide in the U-238 decay chain that is relatively short-lived (half-life 138 days) and is typically explicitly represented in long-term safety assessments for radioactive waste disposal as in-growing from Pb-210, which in-turn in-grows from Ra-226. Shorter-lived progeny of Ra-226 and Pb-210 are typically represented as being in secular equilibrium with their parent radionuclide and accounted for in the associated dose coefficients.

In the SR-Site licence application, Po-210 was not explicitly modelled in the geosphere, but was explicitly modelled in the biosphere and has an associated LDF (Table 4-1, SKB, 2010). Its exclusion in geosphere modelling meant that no dose contribution was calculated for Po-210 in groundwater discharged to the biosphere or drilled well (identified in Pensado, 2012 and Walke and Limer, 2014). The only dose contribution from Po-210 in the original licence application arose through its in-growth within the U-238 decay chain within the biosphere itself. The analysis

described in SKB (2019a) corrects this omission by including a concentration for Po-210 in the groundwater discharge to the biosphere by assuming secular equilibrium with Pb-210, as described in SKB (2015).

### Accounting for Rn-222

SKB (2015) also describes how the LDF models used in SKB (2019a) have been updated to include a further contribution from Rn-222. Radon is a noble gas and Rn-222 is a short-lived (half-life 3.8 days) daughter of Ra-226 in the U-238 decay chain. A model for diffuse release of Rn-222 gas from a spent nuclear fuel repository to the biosphere was included in SKB's SR-Can assessment (Avila, 2006). Section 2c of SKB (2015) refers to the SR-Can model as a means of including a contribution from Rn-222 from a drilled well, quoting a resulting LDF value of  $5.1 \cdot 10^{-14} \text{ Sv Bq}^{-1}$ .

The model in Avila (2006) is described as being for a release of gas from the repository. The conceptual basis for using a model for Rn-222 gas release as a basis for calculating a dose conversion factor for Rn-222 reaching the biosphere in groundwater is not discussed in SKB (2015). The model converts a flux of Rn-222 to the biosphere into an associated effective dose. Application of this model to a groundwater release in SKB (2015) means that decay and dispersion during transport from the point of far-field release to the point of exposure is ignored. Given the short half-life of Rn-222 much would be expected to decay before reaching the upper regolith either in groundwater or as gas. Most Rn-222 giving rise to exposure in the biosphere from the groundwater pathway would likely arise through its ingrowth from Ra-226 decay in the upper regolith. This source of Rn-222 does not appear to be accounted for in the SKB analysis.

It is noted that the area over which Rn-222 is released in the model of Avila (2006) is only  $10,000 \text{ m}^2$ . This area is smaller than the minimum terrestrial size of biosphere objects modelled in the SR-Site assessment (even at the start of terrestrialisation). The assumptions within the Avila (2006) model are, therefore, compatible with potential exposures arising within a single biosphere object, consistent with the way in which LDF's are calculated for other radionuclides.

The parameterisation used in SKB (2015) is consistent with that described in Section 13.8 of SKB (2011), where potential radon doses for a gas pathway are also discussed. Both sets of SKB calculations, presumably, draw on Avila (2006). Benke and La Plante (2012) note that SKB (2011) use favourable values for the building volume and ventilation rate compared to international recommendations and studies:

- the reference building volume used by SKB of  $1000 \text{ m}^3$  is high relative to recommendations for a masonry building in UNSCEAR (2000) of  $250 \text{ m}^3$  and the mean volume from US EPA (2011) surveys of  $492 \text{ m}^3$ ; and
- the reference ventilation rate used by SKB of  $2 \text{ hr}^{-1}$  is high relative to recommendations for a masonry building in UNSCEAR (2000) of  $1 \text{ hr}^{-1}$  and a mean value from US EPA (2011) surveys of  $0.45 \text{ hr}^{-1}$ .

Use of either the UNSCEAR (2000) or US EPA (2011) values would increase the dose implications from Rn-222 by a factor of 8 or 9, respectively, compared to the reference parameterisation adopted by SKB.

Based on the description of SKB (2015) and Avila (2006), a combined (outdoor plus indoor) LDF for Rn-222 of about  $1 \cdot 10^{-14} \text{ Sv/Bq}$  was calculated independently. This

is considered to be close enough to verify the LDF value of  $5.1 \cdot 10^{-14}$  Sv/Bq reported in SKB (2015).

### 2.3. Review of the consequence analysis

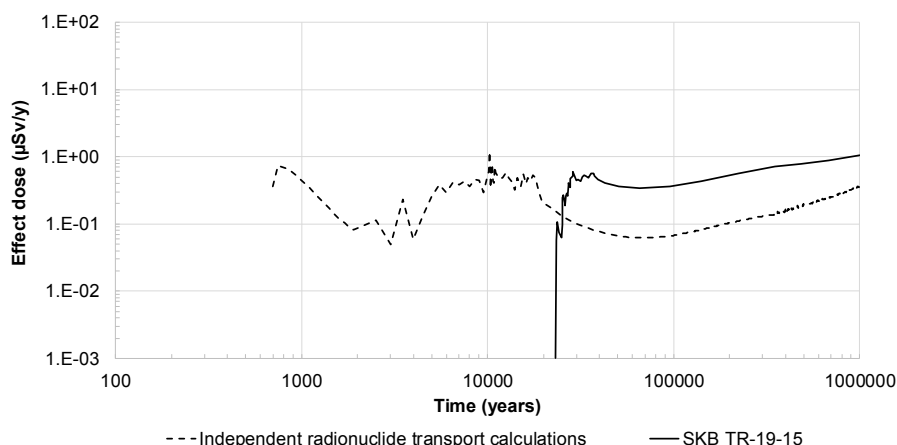
A separate independent review of the new corrosion analyses and radionuclide transport modelling presented in SKB (2019a) has been undertaken and is documented in Pensado and Stothoff (2019). Pensado and Stothoff (2019) include independent radionuclide release and transport calculations.

The far-field fluxes independently calculated by Pensado and Stothoff (2019) have been combined with the original SR-Site LDF values (SKB, 2010) for the new corrosion cases with and without early advection in Figure 1 and Figure 2. In the figures shown below, a contribution from Po-210 in groundwater is accounted for by assuming secular equilibrium with Pb-210 and contribution from Rn-222 is accounted for, consistent with SKB (2015).

The figures show reasonable agreement in the magnitude of the maximum calculated effective doses. Note that the figures show results based on the statistical average number of canister failures. The number of canister failures for the new corrosion cases is assessed by SKB (2019a) to be extremely small at less than one out 6000 canisters on a one million year timescale.

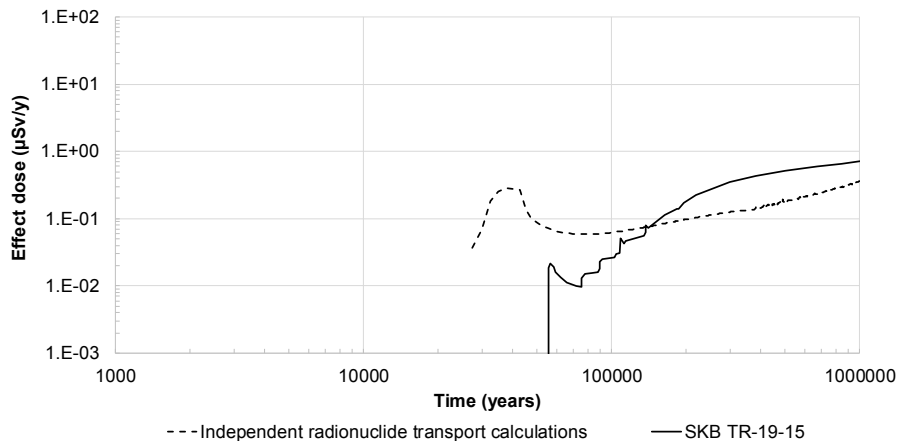
Discrepancies between the timescales of radionuclide releases to the biosphere highlighted by Figure 1 and Figure 2 are discussed in Pensado and Stothoff (2019). The independent results shown in Figure 1 and Figure 2 are consistent with those shown in Figure 2-8(a) in Pensado and Stothoff (2019) and, therefore, verify the use of SKB's LDF values to convert from a flux to the biosphere to potential exposure rates in that report.

**Figure 1:** Comparison of total effective dose consequence of independent radionuclide release and transport calculations for the new corrosion case *with* early advection



Note for Figure 1: Using far-field fluxes calculated by Pensado and Stothoff (2019) and LDF values from SKB (2010), taking account of SKB (2015) for Po-210 and Rn-222.

**Figure 2:** Comparison of total effective dose consequence of independent radionuclide release and transport calculations for the new corrosion case *without* early advection



Note for Figure 2: Using far-field fluxes calculated by Pensado and Stothoff (2019) and LDF values from SKB (2010), taking account of SKB (2015) for Po-210 and Rn-222.

### 3. Additional robustness calculations

In addition to new corrosion calculations, SKB (2019a) includes a new bounding case where all canisters fail at an early stage. This case is intended to illustrate the overall robustness of the KBS-3 concept. The calculation is based on the pessimistic assumption that all canisters have small millimetre-sized penetrating defects or fractures. The canisters saturate after 1,000 years, such that some radionuclides can be released; there is then a sudden widening of the defect after 10,000 years. A variant is also assessed in which the buffer is also gradually lost from the deposition holes with the highest groundwater flow rates.

In assessing the potential dose consequences of the additional robustness calculations, SKB has chosen to change the way in which the biosphere is represented.

1. Updated parameter values representing sorption ( $K_d$ ) and transfers to plants and animals (CR) have been employed.
2. The time-dependent biosphere model has been applied to the calculated radionuclide fluxes, rather than using the LDF values that represent the maximum potential doses over time.

This makes the assessment of doses presented in SKB (2019a) inconsistent with all of the other analyses supporting the SR-Site licence application.

#### 3.1.Changes to biosphere $K_d$ and CRs

Changes to the biosphere  $K_d$  and CR values supporting the new robustness calculations presented in SKB (2019a) are described in SKB (2019b). The updated parameter values draw on parameterisation adopted for SKBs SR-PSU assessment for extension of the SFR facility for low and intermediate level radioactive waste at Forsmark (SKB, 2014a). SKB used updated assumptions in parametrising  $K_d$  and transfers to plants and animals in the SR-PSU assessment, including use of more extensive information derived from characterisation of the Forsmark area.

In reviewing  $K_d$  and CR assumptions supporting the SR-PSU assessment, Walke et al. (2017) observed that there are considerable changes in some of the parameter values (up to four orders of magnitude variation for some geometric means). The differences are, to some extent, explained by a greater preference for site-specific data in the SR-PSU assessment. Where data is lacking for some distributions, site-specific element analogue data is used in preference to element-specific literature data. The review highlights the significant uncertainty attributed to this approach, as is acknowledged in the SKB data compilations. The review also highlights examples where the choice of element analogue is poorly justified (notably for Tc, Np and Pa).

### $K_d$ and CR changes for iodine and selenium

SKB (2019a) highlights the “more favourable” parameterisation for I-129 and Se-79, in particular, that results from the use of the SR-PSU data set. These are two radionuclides of particular importance to the SR-Site assessment; their LDF values are dominated by ingestion of food (Table 4-1, SKB, 2010). Given their importance in the context of SR-Site, the updated  $K_d$  and CR values for these radionuclides have been further reviewed.

For  $K_d$ , the changes for iodine and selenium reflect reliance on site-specific data developed after the SR-Site assessment was submitted. The changes are, therefore, consistent with previous guidance from SSM towards preference for site-specific information.

- Using the SR-PSU dataset, iodine is subject to greater retention (higher  $K_d$ ) in the lower regolith, but lower retention (lower  $K_d$ ) in the mid- and upper regolith layers. The changes are within about a factor of two of the original SR-Site parameter values.
- Using the SR-PSU dataset, selenium is subject to greater retention (higher  $K_d$ ) in all regolith layers. The increase in  $K_d$  is between about a factor of two to about a factor of eight.

For transfers to foodstuffs (focus here is on cereals, tubers and vegetables), the SR-PSU dataset (Tröjbom et al., 2013) has been reviewed.

- The SR-PSU CR for *iodine to cereal* is based on a small amount (n=10) of data from Forsmark, which is used to justify about a factor of ten reduction in the geometric mean.
- The SR-PSU CRs for *iodine to tubers* and *vegetables* are not based on site data. The values are drawn from an international compilation of parameter values (IAEA, 2010), which is used to justify reductions in the geometric means by factors of 10 and 36 for tubers and vegetables, respectively<sup>1</sup>.
- The SR-PSU CR for *selenium to cereals* is based on a small amount (n=6) of data from Forsmark, which is used to justify a reduction in the geometric mean by about a factor of 900.
- In the absence of any site-specific data for *selenium* transfer to *tubers* and *vegetables*, the SR-PSU assessment adopted the site-specific values measured for cereals, resulting in reductions in the geometric means by about a factor of 700 and 1200, respectively.

---

<sup>1</sup> IAEA (2010) is quoted as the source reference for the value of 0.2 kg<sub>dw</sub>/kg<sub>C</sub> for the CR for iodine to tubers in SR-Site and for the value of 0.022 kg<sub>dw</sub>/kg<sub>C</sub> in SR-PSU. The latter value has been verified as part of the present study.

The large reductions in the CR to tubers and vegetables for iodine are, therefore, not based on site-specific data. IAEA (2010) was available at the time of the SR-Site assessment and was used by SKB to support some of the other CR values. The significant reductions in CR to tubers and vegetables reflect a change in preference of SKB.

The very large reductions in CR to tubers and vegetables for selenium are also not based on site-specific data for these types of foodstuff. The reductions are based on data for transfer to the grain and stem of cereal plants. For reference, Posiva compare CR values for a range of crops for selenium in Table 17-170 of Posiva (2014). The comparison shows that the Forsmark data collected on behalf of SKB is significantly lower than literature data for other crops. Table 17-171 and the associated discussion in Posiva (2014) shows that, whilst the Forsmark data was used by Posiva for CR to cereal in support of its TURVA-2012 safety case for spent nuclear fuel disposal at Olkiluoto, it was not used for any other type of crop.

It is also noteworthy that none of the site-specific soil to crop transfer data for Forsmark were based on cultivated peat, which is the specific type of soil that is applicable to drained mire farming that forms the focus of the biosphere modelling for SR-Site. The data was collected at sites with clay gyttja, glacial clay and clayey till soils (Sheppard et al., 2011).

### Treatment of C-14 in the biosphere

The representation of C-14 in the biosphere differs from other radionuclides in the SR-Site assessment; for example, it is excluded from the parameter revisions described in SKB (2019b) because a different modelling approach is adopted. Biosphere modelling for C-14 in the SR-PSU assessment was subject to significant update in comparison to the model used in SR-Site. SKB (2019a) does not state that any changes were introduced to the way in which C-14 is assessed in the biosphere. It is, therefore, assumed that the original SR-Site biosphere model for C-14 was used in assessing potential dose consequences for the new robustness calculations.

## 3.2. Implications of changes to biosphere $K_d$ and CRs

In support of SSM's original review of the SR-Site biosphere modelling, biosphere models for the Forsmark system were independently developed for steady-state ecosystems without landscape evolution, but drawing on the dataset used by SKB (including  $K_d$  and CR parameterisations). The independent biosphere models were able to reasonably reproduce the SR-Site LDFs (see Figure 8 in Walke and Limer, 2014).

The implications of the revised biosphere parameter values used in the new robustness calculations presented in SKB (2019a) have been explored by updating the  $K_d$  and CR values used in the independent biosphere models for Forsmark and comparing the resulting equilibrium flux to dose conversion factors. The comparison is shown in Figure 3. The figure shows relatively limited differences for most radionuclides. Of the important radionuclides for the SKB (2019a) robustness calculation, the figure shows a reduction by nearly a factor of three for I-129 and by about a factor of fifty for Se-79.

**Figure 3:** Comparison of equilibrium flux to dose conversion factors with updated  $K_d$  and CR values (based on SKB, 2019b) with the original values based on the model of Walke and Limer (2014)

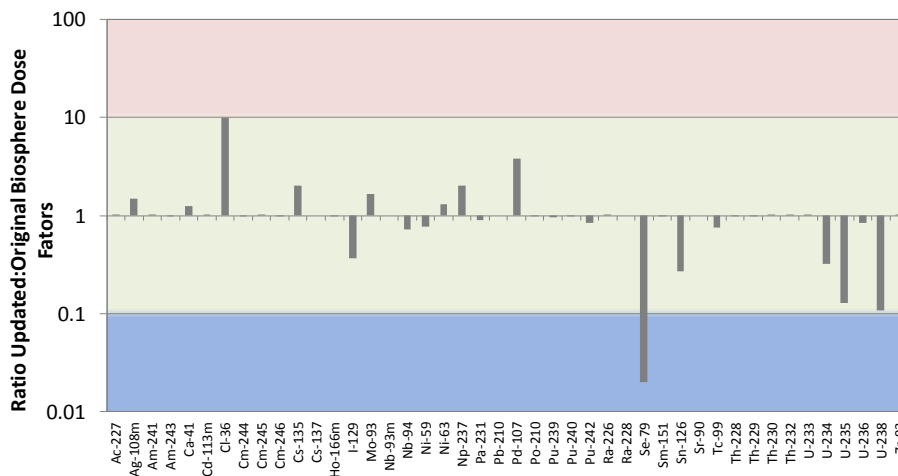


Figure 10-1 of SKB (2014b) indicates<sup>2</sup> that the reductions in biosphere dose factors for I-129 and Se-79 obtained using SKB's biosphere models between SR-Site and the full biosphere model for SR-PSU<sup>3</sup> are even greater than illustrated in Figure 3, with reductions for I-129 of about two orders of magnitude and more than three orders of magnitude for Se-79.

The precise implication of changing assumptions surrounding  $K_d$  and CR on the dose assessment model employed by SKB will likely fall somewhere between the comparison shown in Figure 3 and the change obtained by use of the full SR-PSU biosphere model. This implies significant reductions in consequence analyses for I-129 and Se-79.

### 3.3. Use of time-dependent flux to the biosphere

The doses calculated for the new robustness calculations presented in SKB (2019a) are based on modelling of the time-dependent flux of radionuclides into the biosphere for a million years, rather than the use of LDFs. This is described by SKB as being "considerably more realistic". This assertion holds true for the current interglacial period. The evolving nature of both the radionuclide releases and the landscape means that potential exposures that may arise within any of the biosphere objects considered by SKB may not reach equilibrium. The approach is, however, not realistic for timescales beyond the current interglacial, because a perpetual temperate climate without further glacial periods is not tenable. This is recognised by SKB, who highlight the continued accumulation of Cs-135 in the biosphere within Figure 9-3 and 9-4 of SKB (2019a) as an artefact of this approach.

SKB (2019a) does not state how the fluxes to the biosphere resulting from the new robustness calculations are distributed. The case is based on failure of all of the canisters, with potential fluxes to the biosphere associated with deposition holes that

<sup>2</sup> Reference to Table 4-1 of SKB (2010) enables Se-79 and I-129 to be identified in Figure 10-1 of SKB (2014b).

<sup>3</sup> Note that the full biosphere model for SR-PSU involved more than just changes to  $K_d$  and CR, e.g. different biosphere objects, finer discretisation of the regolith, and a new biosphere model for C-14.

may be associated with advective groundwater pathways. There is, therefore, potential for fluxes to the biosphere to be distributed across several biosphere objects. However, SKB (2019a) give no indication that a distributed release was assessed.

The unusual fluctuations in the C-14 doses evident in Figure 9-3 and 9-4 of SKB (2019a) indicate that SKB take account of potential consequences of release to different biosphere objects. C-14 doses are typically dominated by ingestion of fish from isolated lakes because of the relatively high carbon content in fish relative to the carbon content in water. The fluctuations in the C-14 doses in Figures 9-3 and 9-4 of SKB (2019a) are likely associated with timescales of isolation (a time of C-14 dose increases due to concentrations in newly isolated lakes) and full terrestrialisation (a time of C-14 dose decreases due to the infilling of lakes).

The C-14 dose fluctuations in Figure 9-3 and 9-4 of SKB (2019a) indicate that SKB assessed dynamic biosphere doses for the new robustness calculations by using the highest doses calculated by separately discharging the total calculated flux from the far-field to each biosphere object in turn. If true, this represents a pessimistic approach, given that the releases may occur from separate deposition holes distributed across the landscape.

By the time of the sudden widening of the initially small defects in all of the canisters after 10,000 years, all of the biosphere objects have been fully terrestrialised (biosphere object 105 is the last, which is fully terrestrialised by 11,634 AD). It is notable that the highest C-14 dose consequences occur during slow release from the small canister defects prior to sudden widening. This implies that C-14 doses would be much greater if sudden widening occurred prior to end of full terrestrialisation (requiring only a relatively small change in assumptions regarding timescales of either terrestrialisation or sudden widening).

## 4. Overall conclusions

This technical note describes review of biosphere modelling related aspects of additional compliance and robustness calculations relating to SKB's licence application for construction, possession and operation of a KBS-3 spent nuclear fuel repository at the Forsmark site. SKB has chosen to adopt and present differing approaches to evaluating the potential dose consequences of the new corrosion cases and the additional robustness calculations. The main conclusions from a biosphere assessment perspective are presented separately for each set of calculations below.

### Conclusions relating to the new corrosion calculations

SKB (2019a) uses updated flux to dose conversion factors (LDFs) in assessing the potential dose consequences of new corrosion calculations. The updated LDFs correct for omissions in the original analysis identified in SSM's reviews.

- The analyses correct for omitting a contribution from Po-210 in the groundwater flux to the biosphere in the original SR-Site assessment.
- The analysis also includes a contribution from Rn-222 in groundwater, which was not included in the original SR-Site assessment.

The inclusion of a contribution from Po-210 in groundwater released to the biosphere is well founded. However, the conceptual basis for the inclusion of a dose factor for Rn-222 is not well described.

- The calculation of a dose consequence for Rn-222 in a groundwater flux to the biosphere uses a model that was developed for Rn-222 transport from the repository to the surface in the gas phase; the applicability of this model to the differing context is not discussed or justified by SKB.
- The model used for Rn-222 includes favourable house volumes and ventilation rates compared to other studies (notably UNSCEAR recommendations); the more favourable values are not well justified by SKB.

The Pensado and Stothoff (2019) application of SKB's updated LDFs to independently calculated far-field fluxes has been verified.

### Conclusions relating to the new robustness calculations

In assessment of potential dose consequences of new hypothetical robustness calculations, SKB has chosen to modify the way in which the potential doses are evaluated. The modifications significantly reduce potential doses assessed for key radionuclides in the original analyses, notably C-14, Se-79 and I-129. Using the updated biosphere modelling, SKB presents results that remain below the dose that corresponds to the risk limit (within a factor of about five). The modifications to the biosphere modelling make the analyses inconsistent with all of the other analyses supporting the SR-Site assessment.

The modified representation of the biosphere draws on updated sorption ( $K_d$ ) and equilibrium concentration ratios (CRs) used in the more recent SR-PSU assessment for the SFR facility at Forsmark.

Changes to  $K_d$  values are based on more extensive use of site-specific data and are well justified.

Changes to CR values are presented by SKB as better-representing sorption and uptake at Forsmark, drawing on major sampling campaigns at Forsmark and its vicinity. It is notable that the new dataset includes significant reductions in CR values for Se-79 and I-129. However, the significant changes in CR values for these radionuclides are based on:

- a more favourable interpretation of generic international data that was available at the time of the SR-Site assessment, or
- extrapolation of limited site-specific data for cereals to tubers and vegetables, and
- the limited site data for cereals is based on clay soils rather than the drained mire soils that form the basis of the exposure scenario in SR-Site.

The changes to CR values for Se-79 and I-129 result in very significant (two or three orders of magnitude) reductions in associated dose consequences compared to the original SR-Site assessment.

In the new robustness calculations, SKB explicitly models radionuclide releases to the biosphere using time-dependent fluxes rather than using LDF values. This approach is described in SKB (2019a) as being "considerably more realistic". This

statement is true for timescales up to future cold climate periods, but it is not true thereafter. It is unrealistic to model perpetual temperate conditions to a million years. This approach results in artefacts in the results, such as continued accumulation of very long-lived radionuclides including Cs-135, as noted by SKB in its explanation of the results.

The SR-Site assessment included modelling of radionuclide releases to a single biosphere object as well as modelling of distributed releases, informed by particle tracking of releases from across the repository footprint. The approach adopted for the new robustness calculations is not clearly described by SKB.

Finally, it is notable that the sudden widening of canister defects at 10,000 years occurs relatively shortly after complete terrestrialisation. This is favourable for C-14, for which the most significant exposures arise when lakes remain present in the landscape.

## 5. References

Avila, R. 2006. The ecosystem models used for dose assessments in SR-Can. Svensk Kärnbränslehantering AB (SKB) Report R-06-81.

Benke, R., La Plante, P. 2012. Biosphere Dose Assessment: Review of Dose Consequence of Radionuclides in the Uranium-238 Series Decay Chain. SSM Technical Note 2012:56.

Klos, R., Limer, L., Shaw, G., Wörman, A. 2014. Modelling comparison of alternative biosphere models with LDF models and evaluation of selected parameter values used in the biosphere assessment. Main Review Phase Technical Note 59, SSM 2014:35.

Pensado, O. 2012. Independent radionuclide transport modelling – Reproducing results for main scenario. SSM technical note 2012-142, addendum 1.

Pensado, O., Stothoff, S. 2019. Review of Assignment for the Swedish Radiation Safety Authority: Independent Canister Integrity Modelling and Dose Assessment. Part 3 of this review report.

Posiva. 2014. Safety Case for the Disposal of Spent Nuclear Fuel at Olkiluoto: Data Basis for the Biosphere Assessment BSA-2012. Posiva Oy report 2012:28.

Sheppard, S., Sohlenius, G., Omberg, L-G., Borgiel, M., Grolander, S., Nordén, S. 2011. Solid/liquid partition coefficients ( $K_d$ ) and plant/soil concentration ratios (CR) for selected soils, tills and sediments at Forsmark. Svensk Kärnbränslehantering AB (SKB) Report R-11-24.

SKB. 2010. Landscape dose conversion factors used in the safety assessment SR-Site. Svensk Kärnbränslehantering AB (SKB) Technical Report TR-10-06, Updated August 2013.

SKB. 2011. Long-term safety for the final repository for spent nuclear fuel at Forsmark: Main report of the SR-Site project. Svensk Kärnbränslehantering AB (SKB) Technical Report TR-11-01.

- SKB. 2014a. Safety analysis for SFR Long-term safety: Main report for the safety assessment SR-PSU. Svensk Kärnbränslehantering AB (SKB) Technical Report TR-14-01.
- SKB. 2014b. Biosphere synthesis report for the safety assessment SR-PSU. Svensk Kärnbränslehantering AB (SKB) Technical Report TR-14-06.
- SKB. 2015. Svar till SSM på begäran daterad 2013-02-11 om komplettering rörande radionuklidtransport och dos. Svensk Kärnbränslehantering AB (SKB) document to SSM 1418468, dated 30 April 2015.
- SKB. 2019a. Supplementary information on canister integrity issues. Svensk Kärnbränslehantering AB (SKB) Technical Report TR-19-15, March 2019.
- SKB. 2019b. Uppdatering av Fördelningskoefficienter (Kd) och koncentrationskvoter (CR) i kompletterande biosfärsberäkningar. Svensk Kärnbränslehantering AB (SKB) documents to SSM 1712318 and 1712319, dated January 2019.
- Tröjbom, M., Grolander, S., Nordén, S. 2013. Kd and CR used for transport calculations in the biosphere in SR-PSU. Svensk Kärnbränslehantering AB (SKB) Report R-13-01.
- UNSCEAR. 2000. Sources and effects of ionizing radiation: Report to the General Assembly of the United Nations with Scientific Annexes. Vol. 1. United Nations Scientific Committee on the Effects of Atomic Radiation.
- US EPA. 2011. Exposure Factors Handbook: 2011 Edition. United States (US) Environmental Protection Agency (EPA) report EPA/600/R-090/052F. 2011.
- Walke, R. 2013. Modelling comparison of simple reference biosphere models with LDF models. Main Review Phase Technical Note 58, SSM 2014:34.
- Walke, R., Limer, L. 2014. Further modelling comparison of simple reference biosphere models with the LDF modelling approach. Main Review Phase Technical Note 70, SSM 2014:54.
- Walke, R., Limer, L., Shaw, G. 2017. Review of specific topics relating to the biosphere dose assessment for key radionuclides. Within SSM's external experts' review of SKB's safety assessment SR-PSU - consequence analysis: Main review phase. SSM 2017:30.

## APPENDIX 1

# Coverage of SKB reports

Following reports have been covered in the review.

**Table 1:** Table text

Reviewed report	Reviewed sections	Comments
TR-19-15	9.3. 9.4	Focus on Sections 9.3.3, 9.4.2 and 9.4.4
SKB document 1418468	Discussion of Rn-222 Footnote iii to Figure 0-3 Response 2c Appendix 1	Reviewed a version translated into English
SKB document 1712318 and supporting appendices	Whole document	Reviewed a version translated into English





2019:22

The Swedish Radiation Safety Authority has a comprehensive responsibility to ensure that society is safe from the effects of radiation. The Authority works to achieve radiation safety in a number of areas: nuclear power, medical care as well as commercial products and services. The Authority also works to achieve protection from natural radiation and to increase the level of radiation safety internationally.

The Swedish Radiation Safety Authority works proactively and preventively to protect people and the environment from the harmful effects of radiation, now and in the future. The Authority issues regulations and supervises compliance, while also supporting research, providing training and information, and issuing advice. Often, activities involving radiation require licences issued by the Authority. The Swedish Radiation Safety Authority maintains emergency preparedness around the clock with the aim of limiting the aftermath of radiation accidents and the unintentional spreading of radioactive substances. The Authority participates in international co-operation in order to promote radiation safety and finances projects aiming to raise the level of radiation safety in certain Eastern European countries.

The Authority reports to the Ministry of the Environment and has around 300 employees with competencies in the fields of engineering, natural and behavioural sciences, law, economics and communications. We have received quality, environmental and working environment certification.

**Strålsäkerhetsmyndigheten**  
**Swedish Radiation Safety Authority**

SE-17116 Stockholm

Tel: +46 8 799 40 00

E-mail: [registrator@ssm.se](mailto:registrator@ssm.se)

Web: [stralsakerhetsmyndigheten.se](http://stralsakerhetsmyndigheten.se)